Topology and dimensioning of a maritime MANET coupled with a satellite network

Achraf Kessab

ParisTech
INSTITUT DES SCIENCES ET TECHNOLOGIES
PARIS INSTITUTE OF TECHNOLOGY

TELECOM ParisTech

2017-ENST-0003

EDITE - ED 130

Doctorat ParisTech

T H È S E

pour obtenir le grade de docteur délivré par

TELECOM ParisTech

Spécialité « Informatique et Électronique »

présentée et soutenue publiquement par

Achraf KESSAB

le 3 Février 2017

Topologie et Dimensionnement d'un Réseau Ad hoc Maritime Couplé avec un Réseau Satellitaire

Directeurs de thèse : **Prof. Philippe Martins**, **Dr. Lina Mroueh**
Co-encadrement industriel de la thèse : **M. Serge Héthuin & Mme Isabelle Bucaille**

Jury

M. Loutfi NUAYMI, HDR, Telecom Bretagne	Rapporteur
M. Carlos Faouzi BADER, HDR, Supélec	Rapporteur
M. Mérouane DEBBAH, Professeur, Supélec	Examinateur
M. Michel TERRÉ, Professeur, CNAM	Examinateur
M. Ken CHEN, Professeur, Université Paris 13	Examinateur
Mme Isabelle BUCAILLE, Ingénieur, Thales	Examinateur
M. Philippe MARTINS, Professeur, Télécom ParisTech	Directeur de thèse
Mme Lina Mroueh, Docteur, ISEP	Directeur de thèse

TELECOM ParisTech
école de l'Institut Mines-Télécom - membre de ParisTech
46 rue Barrault 75013 Paris - (+33) 1 45 81 77 77 - www.telecom-paristech.fr

T H È S E

— "Exalted are You; we have no knowledge except what You have taught us. Indeed, it is You who is the Knowing, the Wise." *Quran, Chap. 2 verse 32.*

To my beloved mother Souad...
In honour of my adored and late grandmother Lalla Khadija Bent Salem who passed away the night before the defence of this thesis. May God rest her in His mercy.

Acknowledgements / Remerciements

Je tiens à remercier dans un premier temps mes encadrants académique, le Dr. Emmanuelle Vivier, Dr. Lina Mroueh et Prof. Philippe Martins, pour la confiance qu'ils m'ont accordée ainsi que pour leur soutien dès mon cursus d'ingénieur et jusqu'à ma soutenance de thèse. Je remercie aussi mon encadrant industriel Mr. Serge Héthuin pour accepté l'idée de cette collaboration et s'être impliqué pleinement dans ce projet qui n'aurait pas pu se concrétiser sans lui. Je n'oublie pas Mme. Isabelle Bucaille. Ma gratitude se porte aussi vers mes collaborateurs du laboratoire SITe à l'ISEP Paris, sans eux ces années de thèses n'auraient pas été si agréables. J'insiste sur ma reconnaissance envers le Dr. Lina Mroueh pour son soutien tant sur le plan technique que moral, je tiens à lui exprimer ma plus sincère gratitude et admiration, je n'oublierais pas son investissement inconditionnel dans mon cursus académique et sa pédagogie qui me permis de me dépasser, un grand merci!

Du côté de mes proches, je remercie mes beaux parents Sophie et Christian pour avoir cru en moi et encouragé dans mes études. Mon père et mes sœurs cadettes et particulièrement ma mère Souad, sans elle cet ouvrage n'aurais pas pu voir le jour. C'est elle qui me donna le goût d'étudier dès mon plus jeune âge, qui se surpassa et sacrifia pour me donner la meilleure éducation possible et m'appris à ne jamais relâcher mes efforts. Je lui suis redevable à jamais, Maman, merci.

Et enfin, "last but not least", un mot ému à ma fiancée Margaux. Elle fut à mes côtés tout au long de ce projet, je n'aurais pu avancer sans son soutien infaillible, ses encouragements et son amour. Je t'aime...

Achraf KESSAB

Abstract

Mobile Ad hoc Networks "MANETs" attract nowadays lots of attention in academia and in industry. Due to their infrastructure less nature and their capacity to handle machine to machine communications, MANETs are considered as ideal candidates to interconnect mobile nodes on the fly. However these characteristics imply more challenging issues to face. Their high dynamic, the lack of a central control entity, the unpredictable topologies and the limited ranges and energy, the design of protocols and communication strategies for such networks are ambitious. In the scope of this thesis we emphasis on a group of mobile nodes in a maritime context forming a naval fleet offshore. This study case in an isolated environment as the high seas, legitimates the implementation of a MANET as a solution to this application. At the radio side, mobile nodes are equipped with Long Term Evolution "LTE" devices offering high data throughputs and enhanced technologies. The secluded aspect of the network is removed by the support of a satellite backhaul to ensure either communications with terrestrial equipments or isolated nodes.

In the first part of this thesis, we tackle the initialization of the network in this hierarchical context. We propose a statistical model enabling a network designer to perceive the requirements in terms of equipments, channel bandwidth, antenna configurations, antenna radiation pattern, achievable data rates for instance. In order to guarantee fully connected MANET, we introduce an analytical tool to estimate the required inter-staff-ships and inter-shipmasters coverage radii. Then we study the multi-hop end-to-end communications and we propose several routing protocols to enhance the delays. Afterwards, we focus on the contribution of the satellite backhaul with a comparative study qualifying the needs in Hybrid Stations "HSs" and a strategy to access to these gateways.

In a second part, we emphasis on the radio resource outage occurrence and the dimensioning matter to optimize the allocated bandwidth to the network. We investigate stochastic geometry tools to provide an analytical model enabling to foresee the amount of required radio resources by the active nodes with a certain Quality of Service "QoS" and several Multiple Inputs Multiple Outputs "MIMO" antenna configurations in the maritime context. We consider first the centralized access scheme where all communications are performed via the shipmasters that are in charge of the radio resource management. Then we focus on the distributed access scheme with Aloha Medium Access Control "MAC" protocol where nodes are authorized to access to the shared bandwidth arbitrarily and unilaterally. Simulation and numerical results are provided to evaluate the performances in terms of required bandwidth, aggregate capacity and achievable coverage radii.

List Of Publications

Previously published :

— **Achraf Kessab** Fatima Z. Kaddour, Emmanuelle Vivier, Lina Mroueh, Mylene Pischella and Philippe Martins, **Gain of Multi-Resource Block Allocation and Tuning in the Uplink of LTE Networks**, Proc. of ISWCS 2012, Paris, France, Aug. 2012.

Chapter 3:

— Lina Mroueh, **Achraf Kessab**, Philippe Martins, Serge Héthuin and Isabelle Bucaille. **Topology design of fully connected hierarchical mobile ad hoc networks**. In IEEE International Symposium on Wireless Communication Systems 2016.

— **Achraf Kessab**, Lina Mroueh, Philippe Martins and Isabelle Bucaille. **Optimizing End-to-End Propagation Delays in Hybrid Satellite-Maritime Mobile Ad Hoc Networks**. In the Software Telecommunications and Computer Networks Conference 2016.

Chapter 4:

— Lina Mroueh, **Achraf Kessab**, Philippe Martins, Serge Héthuin and Emmanuelle Vivier. **Radio resource dimensioning in a centralized Ad-Hoc maritime MIMO LTE network**. In 36th IEEE Sarnoff Symposium 2015.

— **Achraf Kessab**, Lina Mroueh, Philippe Martins, Serge Héthuin and Isabelle Bucaille. **Impact of the ITU-R Maritime Propagation on the Dimensioning of a Centralized LTE MANET**. In IEEE Wireless Communications and Networking Conference 2016.

Chapter 5:

— The work lead in this chapter will be subject to future publications.

Abbreviations & Acronyms

3GPP	The 3rd Generation Partnership Project
AF	Amplify and Forward relay
AODV	Ad hoc On Demand Distance Vector
AOMDV	Ad hoc On Demand Multi path Distance Vector
AS	Access Stratum
BCH	Broadcast CHannel
BP	BiPolar receiver model
CC	Carrier Component
CDF	Cumulative Distribution Function
CH	Cluster Head
CQI	Channel Quality Indicator
CSI	Channel State Information
CSI-R	Channel State Information at the Receiver
DF	Decode and Forward relay
eNB	evolved NodeB
EPC	Evolved Packet Core
e.r.p.	Effective radiated power
FFT	Fast Fourier Transform
FSTD	Frequency Switched Transmit Diversity
GEO	Geostationary Earth Orbit
GPRS	General Packet Radio Service
GSM	Global System for Mobile Communications
GW	GateWay node
HMC	Hierarchical MANET Clustering Algorithm
HS	Hybrid Station
HSDPA/HSUPA	High Speed Downlink Packet Access/High Speed Uplink Packet Access
IDFT	Inverse Discrete Fourier Transform
IFFT	Inverse Fast Fourier Transform
i.i.d.	independent and identically distributed
INR	Independent Nearest Receiver model
I-SC-FDMA	Interleaved Single-Carrier Frequency Division Multiple Access
ITU	International Telecommunication Union
ITU-R	ITU Radiocommunication sector

KCMBC	*d*-hops Compound Metric Based Clustering
LOS	Line Of Sight
L-SC-FDMA	Localized Single-Carrier Frequency Division Multiple Access
LTE	Long Term Evolution
LEO	Low Earth Orbit
MAC	Medium Access Control
MAI	Medium Access Indicator
MANET	Mobile Ad hoc NETwork
MCS	Modulation and Coding Scheme
MEO	Medium Earth Orbit
MIMO	Multiple Input Multiple Output
ML	Maximum Likelihood decoder
MME	Mobility Management Entity
MPR	Multi-Point Relay
MRC	Maximum Ratio Combiner
MRC-R	Maximum Ratio Combiner at Receiver
MRC-RS	Maximum Ratio Combiner at Receiver with antenna Selection
NAS	Non Access Stratum
NLOS	Non Line Of Sight
OFDM	Orthogonal Frequency Division Multiplexing
OFDMA	Orthogonal Frequency Division Multiple Access
OLSR	Optimized Link State Routing
PAPR	Peak-to-Average Power Ratio
PCRF	Policy and Charging Rules Function
PCH	Paging CHannel
PDF	Probability Density Function
PEL	Plane Earth Loss model
PGW	Packet GateWay
PHY	OSI Physical Layer
PMI	Precoding Matrix Indicator
PPP	Poisson Point Process
QoS	Quality of Service
RAN	Radio Access Network
RB	Resource Block
RE	Resource Element
REL	Round Earth Loss model
RI	Rank Indicator
RREP	Route REPly
RREQ	Route REQuest
RERR	Route ERRor
RRM	Radio Resource Management
SC-FDMA	Single-Carrier Frequency Division Multiple Access

SFBC	Space Frequency Block Code
SGW	Satellite GateWay
SIC	Successive Interference Cancellation
SINR	Signal to Interference plus Noise Ratio
SMS	Short Message Service
TC	Topology Control
TM	Transmission Mode
UE	User Equipment
USAT	Ultra Small Aperture Terminal
V-BLAST	Vertical-Bell Laboratories Layered Space Time
ZF	Zero Forcing

Contents

List of Figures

List of Tables

French Detailed Summary

Condensé

De nos jours, les réseaux ad hoc mobiles (Mobile ad hoc Network "MANET") représentent un domaine de recherche très actif. L' absence d'infrastructure et la capacité des MANET à gérer les communications pair à pair rend ces réseaux idéaux pour interconnecter des nœuds mobiles. Cependant, leurs caractéristiques impliquent des enjeux plus difficiles à résoudre. Leur dynamique élevée, l' absence d'une entité centrale de contrôle et leurs topologies imprévisibles induisent une conception de protocoles et de stratégies de communication complexe. Dans le cadre de cette thèse, nous considérons un groupe de nœuds mobiles dans un contexte maritime formant une flotte navale hiérarchisée. Ce cas d'étude dans un environnement isolé comme la haute mer, légitime la mise en œuvre d'un MANET comme solution à cette application. Les nœuds mobiles sont équipés de radios Long Term Evolution "LTE" offrant des débits de données élevés. L' aspect isolé du réseau est solutionné par le support d'un réseau d'amenée satellite afin d'assurer soit des communications avec des équipements terrestres soit la connectivité des nœuds isolés. Dans la première partie de cette thèse, nous abordons la topologie du réseau dans ce contexte hiérarchique. Nous proposons un modèle statistique permettant à un concepteur de réseau de percevoir les exigences en termes d'équipements, de largeur de bande de fréquence, de configurations d'antenne, de diagramme de rayonnement d'antenne, de débits de données cibles, par exemple. Afin de garantir un MANET totalement connecté, nous proposons un outil analytique permettant d'estimer les rayons de couverture requis. Ensuite, nous étudions les communications multi-sauts et nous proposons plusieurs protocoles de routage pour améliorer les délais de communications. Puis, nous nous focalisons sur la contribution du réseau satellite en menant une étude comparative qualifiant les besoins en stations hybrides "HS" ainsi qu'une stratégie d'accès à ces passerelles satellite. Dans un deuxième temps, nous traitons l' occurrence du dépassement des ressources radio et le dimensionnement de ces dernières de façon à optimiser la bande passante allouée au réseau. Nous dérivons un modèle analytique en utilisant des résultats issus de la géométrie aléatoire, permettant de prévoir la quantité de ressources radio requises par les nœuds actifs sous une certaine qualité de service "QoS" et plusieurs configurations d'antennes MIMO. Nous considérons tout d'abord un système d'accès centralisé où toutes les communications sont effectuées par l' intermédiaire des nœuds chargés de la gestion des ressources radio. Ensuite, nous

traitons le cas d'un système d'accès distribué sous le protocole d'accès Aloha où les nœuds sont autorisés à accéder à la bande passante partagée aléatoirement et uniformément. Les simulations et les résultats numériques permettent d'évaluer les performances en termes de bande passante requise, de capacité globale et de rayons de couverture.

♦ Introduction

◊ Motivations

Contrairement aux réseaux cellulaires classiques nécessitant des infrastructures préconfigurées telles que les stations de base, les réseaux MANET sont des réseaux où des nœuds équipés de périphériques de communication sont libres de se déplacer et de s'organiser arbitrairement. Ils peuvent être connectés à Internet ou fonctionner de manière autonome. Ces caractéristiques conduisent à des réseaux hautement dynamiques avec des topologies imprévisibles. Cette dernière caractéristique rend le design des stratégies de communication pour les MANET plus difficile que pour les réseaux cellulaires classiques. Les systèmes de communication ad hoc ont été largement abordés dans la littérature où ont été étudiés différents aspects liés aux couches PHYsiques " PHY " et Medium Access Control " MAC " [6]. Un noeud peut communiquer directement avec d' autres si ils sont dans sa portée et, si non, des noeuds intermédiaires qui agissent comme des relais sont par conséquent nécessaires.

La connectivité réseau dépend de manière critique des processus de routage et de la fiabilité des liens, la topologie dynamique peut avoir un impact important sur les performances du réseau en provoquant des pannes de liens. En raison du manque d'entité de gestion centrale, ces comportements ne peuvent être facilement prédits et détectés, ce qui implique une grande complexité dans la conception des protocoles. Ces MANET sont soumis aux contraintes suivantes: i) une gestion non centralisée de l' allocation des ressources radio et du routage, les noeuds interagissent pour configurer le réseau et le rendre fonctionnel; ii) une topologie dynamique, à mesure que les nœuds se déplacent, les liaisons radio devront être mises à jour, la topologie doit s'adapter à ces fluctuations afin d' assurer une fiabilité optimale du flux de données; iii) une portée et une énergie limitées, de manière similaire aux réseaux mobiles traditionnels, les réseaux ad hoc mobiles sont soumis à des contraintes de puissance qui affectent la qualité des liaisons radio, y compris la portée.
Dans le cadre de cette thèse, nous étudions un MANET hybride dans un environnement maritime, où les nœuds du réseau correspondent à des navires et sont équipés de radio Long Term Evolution "LTE" et [4]. Les systèmes LTE sont conçus pour fournir des débits et des éfficacités spectrales élevés ainsi que pour supporter des configurations d' antenne avancées qui répondent aux exigences d'un concepteur de réseau. Une partie des nœuds mobiles sont également équipés de terminaux satellites à ultra faible ouverture "Ultra Small Aperture Terminals" ou encore " USATs " [7]. Ils permettent l'échange de données inter noeuds et/ou avec un hub situé sur la côte par liaisons satellitaires et sont identifiés comme des stations hybrides " HSs ". Les caractéristiques spécifiques induites par l'environnement maritime doivent également être prise en compte, un modèle empirique de propagation du signal maritime que nous dérivrerons de la recommandation de l' Union internationale des télécommunications "UIT" [3], sur les techniques de prévision de la propagation sera explicité et nous servira de modéle de référence.

Nos travaux ont pour objectif de fournir des outils analytiques permettant à un concepteur de réseau de construire des modèles de topologie et des stratégies de communication efficaces afin de plannifier des transmissions fiables avec un certain niveau de performance. Parmi les approches les plus appliquées dans les étude des réseaux ad hoc, la géométrie stochastique semble être un domaine très intéressant permettant de déterminer le comportement statistique moyen du réseau [8, 9], plusieurs travaux ont été proposés dans la littérature [?, 10, 11, 12] et il est apparu que des résultats significatifs peuvent être obtenus. Sur la base de ces observations, il nous a semblé pertinent, motivant et bien justifié d'investiguer ce domaine dans le cadre de cette thèse. En effet, tout au long de nos travaux, nos outils seront dérivés de résultats issus de la géométrie stochastique, la mise en place du réseau par la configuration topologie sera étudié dans un premier temps, ensuite nous centrons les travaux sur le dimensionnement des ressources radio dans les systèmes d'accès centralisés et distribués. Bien que nous nous traitions en particulier le cas de nœuds pourvus d'équipements radio LTE lors de nos études, les modèles analytiques et les algorithmes fournis dans cette thèse peuvent être aisément adaptés à d'autres systèmes de communication.

◊ Contributions

Dans cette dissertation, l'objectif principal est de fournir des algorithmes et des modèles performants permettant à un concepteur de réseau de mettre en place un MANET hybride LTE/Satcom efficient, de la sélection des équipements et de la construction du réseau à la conception des stratégies de communication, conciliant performances et coûts ciblés par le concepteur. Nous nous concentrons d'abord sur l'initialisation du réseau et le partitionnement des nœuds mobiles dans un contexte hiérarchique. Le comportement statistique moyen du réseau est ensuite considéré en étudiant les communications de bout en bout et l'aspect satellitaire du réseau hybride à l'aide des techniques issues de la théorie des graphes [13, 14]. Par la suite, nous nous focalisons sur un cluster circulaire afin d'étudier la probabilité de dépassement des ressources radio et la question du dimensionnement des ressources radio dans un réseau centralisé et distribué en utilisant des outils de la géométrie stochastique [8, 9] pour plusieurs configurations antennaires. Plusieurs objectifs sont identifiés et le travail proposé et développé au cours de ce manuscrit a été conduit de manière à contribuer à leur aboutissement. En résumé, nous visons à:

— Fournir un modèle statistique permettant à un concepteur de réseaux de percevoir les avantages et les inconvénients entre un accès centralisé via des navires maîtres ou un accès distribué. Nous considérons le comportement statistique moyen du réseau pour le cas centralisé, puis nous étudions la théorie des graphes et présentons une solution exhaustive dérivant les rayons de couverture requis dans un schéma d'accès distribué aboutissant à un réseau connecté.

— Caractériser les communications de bout en bout dans le réseau et mener une étude comparative des performances des protocoles de routage envisagés. Nous dérivons d'abord la distribution typique du nombre de sauts via les voisins les plus proches. Nous présentons les algorithmes disponibles dans la littérature et proposons plusieurs protocoles : Recherche progressive de voisins les plus éloignés pour un certain angle

de propagation “Progressive spread angle furthest neighbors search” (Algorithme 3), Soutien du maître de navires “Shipmaster aided” et le protocole de recherche des nœuds passerelles “Gateways search”. Les performances de ces protocoles sont évaluées en termes de délais de bout en bout et comparées à celles des protocoles dits traditionnels.

— Établir un outil statistique aidant un concepteur de réseau à mener une étude comparative, afin de quantifier les besoins en stations hybrides en fonction des délais de bout en bout maximaux tolérés. Dans ce but, nous dérivons analytiquement le nombre moyen de passerelles satellites dans un cluster en fonction de leur distribution spatiale. Ensuite, nous comparons les délais de communication multi-sauts de bout en bout avec l'utilisation de voies terrestres uniquement et hybrides sous plusieurs systèmes satellites.

— Aborder le problème du dimensionnement des ressources radio qui dépend des paramètres du réseau, comme la charge du réseau, la configuration d' antenne et la QoS requise. Ainsi, nous nous focalisons sur le dimensionnement des ressources radio dans un cluster d'un MANET avec un schéma de communication centralisé. En étudiant les outils de la géométrie stochastique, nous fournissons un modèle analytique pour permettre à un concepteur de réseau d' estimer la bande passante requise pour éviter l'événement de dépassement de ressources radio. Pour ce faire, nous dérivons d'abord une borne supérieure de la probabilité de dépassement “Outage” de ressources en considérant les paramètres du réseau. Nous estimons le nombre moyen de blocs de ressources “Ressource Blocks (RBs)” requis par les nœuds mobiles. De cette borne supérieure, nous déterminons le nombre de RBs total requis par le réseau afin que le dépassement de ressources radio ne dépasse pas un certain seuil. Enfin, nous étudions l'impact de la fluctuation de la propagation maritime et aboutissons à un modèle linéaire pour prédire l'impact sur l'estimation de la bande passante.

— Prédire la bande passante requise à allouer dans un réseau ad hoc mobile du type OFDMA MIMO distribué sous le protocole MAC Aloha, afin déviter le dépassement des ressources radio. Nous supposons que la bande passante OFDMA partagée dans le réseau ad hoc est divisée en plusieurs sous-bandes, contenant chacune un nombre prédéfini de RBs en fonction de la QoS. Nous voulons garantir que le nombre de RBs dans une sous-bande donnée est suffisant pour répondre aux exigences d'un certain nombre de nœuds mobiles. A cette intention, nous dérivons l'expression analytique de la probabilité de dépassement des ressources dans une sous-bande pour différents modes de transmission en considérant le comportement statistique moyen du réseau.

◊ Plan

Ci-dessous, nous décrivons succintement l'organisation de cette dissertation et le sujet principal de chaque chapitre:

- **Chapitre 2 - Cadres technique et mathématique**
  Nous présentons dans un premier temps les antécédents et les préliminaires sur les plan technique et mathématique. Nous passons en revue successivement les domaines d'intérêt pour nous travaux et détaillons les éléments étudiés dans le cadre de cette thèse. Nous nous concentrons d'abord sur l'aspect "MANETs" des réseaux ad hoc mobiles, les caractéristiques des composantes radio et satellite envisagées dans ce travail sont ensuite présentées. Il suit une description détaillée de la propagation sans fil maritime et de sa modélisation. Les principes de théorie de l'information essentiels pour calculer la capacité du canal sous différentes configurations multi-antennes sont également abordés. Enfin, nous fournissons une description détaillée des outils de la théorie des graphes et de la géométrie stochastique étudiés afin de modéliser le comportement statistique moyen des nœuds mobiles du réseau.
- **Chapitre 3 - Conception de la topologie d'un réseau hybride Satellite-MANET**
  Ce chapitre vise à introduire un modèle statistique permettant à un concepteur de réseau de percevoir les avantages et les inconvénients des solutions possibles parmi: i) l'utilisation d'un accès centralisé via les navires maîtres ou un accès distribué, ii) les besoins en passerelles satellite dans le réseau et iii) les gains en termes de délais de communication de bout en bout par rapport aux coûts induits par les équipements satellitaires. Pour répondre à ces interrogations, nous commençons par considérer le comportement statistique moyen du réseau pour le cas centralisé, puis nous étudions le domaine de la théorie des graphes et présentons une solution exhaustive pour dériver les rayons de couverture requis dans un schéma d'accès distribué. Plusieurs protocoles de routage sont évalués en termes de délais de communication de bout en bout, nous proposons ensuite une stratégie pour l'accès aux passerelles satellites et aussi une étude comparative pour qualifier les besoins en stations hybrides en fonction des délais de bout en bout tolérés.
- **Chapitre 4 - Dépassement de Ressources radio dans un Réseau Centralisé & Dimensionnement**
  Le Management de Ressource Radio " RRM " est utilisé pour optimiser la bande passante allouée de manière à servir tous les utilisateurs tout en minimisant la probabilité de l'événement qui survient lorsque l'entité de gestion n'a plus de ressources radio à attribuer aux utilisateurs. Cet événement sera désigné comme "événement de dépassement des ressources radio". Ce chapitre se focalise sur le dimensionnement dans un cluster d'un MANET avec un schéma de communication centralisé. Nous utilisons des outils de géométrie stochastique pour fournir un modèle analytique permettant à un concepteur de réseau d'estimer la bande passante requise pour éviter l'événement de dépassement des ressources radio. A cette intention, nous dérivons

d'abord une borne supérieure de la probabilité de dépassement des ressources en considérant les paramètres du réseau. Ensuite, nous estimons le nombre moyen de RBs requis par les membres du cluster "CN" et donc la bande passante nécessaire pour une classe de QoS unique et multiple. En fonction de cette borne supérieure, nous déterminons le nombre de RB requis par le réseau de telle sorte que l'occurence du dépassement des ressources radio soit inférieur à un seuil donné. L'efficacité spectrale moyenne dans le réseau ad hoc est alors déduite. En outre, l'impact de la fluctuation de la propagation maritime est étudié et un modèle linéaire permettant l'estimation de cet impact sur la bande passante est fourni.

- **Chapitre 5 - Dépassement des ressources radio du réseau ad hoc distribué sous Aloha**
  Les systèmes d'accès distribués améliorent l'efficacité des communications en permettant des transmissions pair à pair entre les noeuds mobiles sans le soutien d'une entité de gestion comme dans le schéma centralisé. Les nœuds du réseaux, accédent unilatéralement à la bande partagé. Dans ce chapitre, nous définissons des outils statistiques pour le dimensionnement radio dans un MANET OFDMA MIMO non-coopératif sous le protocole Aloha. Nous supposons que la bande passante OFDMA partagée est divisée en plusieurs sous-bandes, contenant chacune un nombre prédéfini de blocs de ressources radio dépendant de la QoS requise. Notre objectif principal est de trouver la bande passante requise à allouer dans le réseau afin de garantir que le nombre de RBs dans une sous-bande donnée soit suffisant pour satisfaire une quantité acceptable de noeuds transmettant dans cette sous-bande. Pour cela, nous dérivons l'expression analytique de la probabilité de dépassement des ressources dans une sous-bande pour différents modes de transmission compte tenu du comportement statistique moyen du réseau. Nous proposons enfin des résultats numériques pour comparer les performances des différents modes de transmission MIMO en termes de rayon de couverture, de bande passante et de capacité globale.

♦ Introduction

Dans un premier temps nous introduisons les bases et les préliminaires des domaines technique et mathématique impliqués dans nos travaux. Nous traitons des réseaux ad hoc mobiles, puis des éléments des technologies radio et satellitaires. Une description détaillée du canal de propagation maritime et sa modélisation ainsi que les principes de la théorie de l'information essentiels à nos développements. Enfin, nous décrivons précisément les outils issus de la géométrie stochastique et de la théorie des graphes permettant la modélisation statistique de notre réseau.

◊ Mobile Ad hoc Networks "MANETs"

▷ **Algorithme de clustering traditionnels**

◇ k-means algorithm dans $\mathbb{R}^2$
L'algorithme de clustering k-means, connu également sous l'appelation algorithme de Lloyd, est un algorithme de partitionnement itératif minimisant la distance Euclidienne moyenne entre les nœuds d'un réseau. Le choix du nombre de cluster est laissé à la discrétion de l'utilisateur, de plus cet algorithme comprend quatres étapes explicitées ci-dessous.

- **Etape 1:** A un instant $t = 1$, sélection aléatoire de k centroïdes $\mathcal{O}^1 = \{o_1^1, \ldots, o_k^1\}$ sur une aire de simulation $\mathcal{A}$.
- **Etape 2:** Pour $j = \{1, \ldots, n\}$ nœuds $x_j \in \mathcal{N}$, crée les clusters $\mathcal{C}_i^1$ tels que : $\mathcal{C}_i^1 = \left\{x_j : \left\|x_j - o_i^1\right\| \leq \left\|x_j - o_{i*}^1\right\| \forall i* = 1, \ldots, k\right\}$.
- **Etape 3:** Mise à jour des centroïdes, $o_i^{t+1} = \frac{1}{\|\mathcal{C}_i^t\|} \sum_{x_j \in \mathcal{C}_i^t} x_j$.
- **Etape 4:** Itérer les étapes 2 et 3 jusqu'à ce que $\mathcal{O}$ soit fixé i.e. $\mathcal{O}^{t+1} = \mathcal{O}^t$.

Dans nos travaux nous décidons d'élir comme maître de cluster "Cluster Head (CH)" le nœud le plus proche en terme de distance Euclidienne du barycentre du cluster. ◇ Max-Min d-hops cluster formation

Dans [15], un algorithme heuristique où les nœuds sont situés au plus à d-sauts de leur leader est proposé. Les nœuds du cluster maintiennent deux tableaux WINNER et SENDER de taille $2d$ nœuds chacun. Les nœuds procédent à deux étapes fondamentales de "flooding" *Floodmax* et *Floodmin* :

> **Floodmax** : Chaque nœud broadcast sa valeur WINNER (initialement son ID) à ses voisins situés à 1-saut. La nouvelle valeur WINNER est la plus élevée.
>
> **Floodmin** : Idem à **Floodmax** sauf que la valeur WINNER est la plus petite

L'algorithme est composé de 4 étapes décrite dans le Chapitre 2.
◇ d-hops Compound Metric Based Clustering "KCMBC"

Similairement à Max-Min, cet algorithme génére des clusters où les nœuds sont situés au plus à *d*-sauts de leur leader. La différence est que KCMBC propose de prendre en compte la connectivité des nœuds et leur mobilité dans le processus. La description détaillée de cet algorithme est disponible dans le chapitre ??.

▷ **Protocoles de routage**

◇ Protocoles MANET

Les différents protocoles des routage issus de la littérature MANET sont :

- Ad hoc On Demand Distance Vector Protocol "AODV" [16]
- Ad hoc On Demand Multi-path Distance Vector Protocol "AOMDV"[17]
- Optimized Link State Routing Protocol "OLSR"[18]

▷ **Modélisation de la mobilité**

La caractéristique principale des MANETs est leur mobilité nous répertorions ci-après les différents modèles de mobilité utiles à nos travaux [1]. Les modèles utlisés sont :

- Random Walk
- Nomadic Community

◊ Equipements Hybride Satellite-MANET

Cette section présente les technologies mise en œuvre dans nos travaux afin d'établir les liens de communications entre les nœuds du réseaux. Pour la partie terrestre nous introduisons la technologie de radiocommunication LTE et nous présentons par la suite les base des communications par satellite.

▷ **Long Term Evolution "LTE"**

La technologie LTE est standardisée par le consortium 3GPP. Elle dispose d'une architecture simplifiée l' UE (e.g. terminal opérateur) accède plus rapidement au cœur de réseau. Le système LTE est composé de trois entités principales:

- User Equipment "UE": Tout appareil utilisé afin de réaliser des communications de bout en bout,
- Evolved Node B "eNB": la station de base,
- Evolved Packet Core Network "EPC": le cœur de réseau.

◇ Lien descendant : Orthogonal Frequency Division Multiple Access "OFDMA"

Le terme Orthogonal Frequency Division Multiple Access "OFDMA" [6] référe à l'utilisation de l' Orthogonal Frequency Division Multiplexing "OFDM" comme schéma d'accés multiple pour les transmitions simultanées. Cette technologie est utilisée pour la liaison descendante en LTE.

◇ Lien montant : Single Carrier-Frequency Division Multiple Access "SC-FDMA"

Single Carrier - FDMA consiste en une transmission OFDMA linéairement précodée. SC-FDMA permet le multiplexage des utilisateurs avec une attribution inégale de la bande.

◇ Resource Block
L'unité de ressource, la plus petite, en LTE et le "Resource Element (RE)" qui correspond à un symbole OFDM transmis sur un sous-canal. Ces REs sont regroupés en un "Resource Block (RB)", composé de $N_c = 12$ sous-canaux OFDM et ayant pour durée un intervalle de temps $T_{RB} = 0.5$ ms et une largeur de bande totale $W_{RB} = 180$ kHz. ◇ Aggregation de canal
En LTE-A jusqu'à cinq porteuses peuvent ôtre aggrégés, ainsi la largeur de bande totale peut atteindre 100 MHz.

▷ **Satellite component**
Cette partie introduit brièvement les différents systèmes satellites que nous allons mettre en œuvre dans nos travaux.

◇ Orbites satellite
Les orbites géocentriques sont classifiées en trois catégories en fonction de leurs altitudes respectives. Nous résumons dans le tableau ci-aprè les valeurs typiques de temps d'observation, intervalles d'altitudes et délais de propagation pour chaque type d'orbite. L'orbite géostationnaire est la seule permettant une couverture continue avec un satellite,

Orbite	Altitude (km)	Temps d'observation	Délais (ms)
GEO	35 786	24 h	280
MEO	10 000-20 000	1-2 h	80-120
LEO	160-1500	8-10 min	20-60

Propriétés des orbites [5]

mais cette couverture est aussi atteignable avec d'autres types d'orbites en utilisant une constellation de satellites.

♢ Processus de Point de Poisson "PPPs"

Les Processus de Point de Poisson "PPPs" sont des processus stochastiques qui constituent la base de nos développements mathématiques de manière caractériser le dimensionnement des ressources radios dans les chapitres 4 et 5. Plusieurs résultats mathématiques nous permettront de modéliser notre réseau et de fournir des outils statistiques permettant de répondre à la problématique de cette thèse. Ces outils sont décrits de manière détaillée dans la suite du manuscrit.

♦ Topologie d' un réseau hybride Satellite - MANET

L ' étude de la topologie du réseau est essentielle à l' intialisation de ce dernier, cette étape englobe le partitionnement du réseau ainsi que la mise en place des connexions inter-nœuds. Ce chapitre vise à élaborer un modèle statistique permettant à un concepteur de réseau d' évaluer les avantages et les inconvenients parmis les solutions suivantes : i) un réseau d' accés centralisé au niveau du bateau maître, ii)les besoins en passerelles satellites, iii) les gains en termes de délais de bout en bout par rapport aux coûts induits par les équipements satellite. Notre étude débute par la caractérisation du comportement statistique moyen de notre réseau centralisé. Dans un deuxième temps nous présentons une solutions exhaustive en exploitant des résultats de la théorie des graphes permettant de déterminer les rayons de couverture requis pour un accés distribué. Nous évaluons de multiples protocoles de routage en terme de délais de bout en bout et proposons une stratégies d' accés au passerelles satellite. Un étude comparative permettant d' évaluer les besoins en nœuds hybrides en fonction des délais tolérés. Ces travaux ont donné lieu à deux publications [19] et [20].

◊ Introduction

Nous utiliserons au long de ce chapitre des algorithmes dits de clustering. En construisant une organisation locale du réseau, le cluster permet d' obtenir une connectivité rapide, un routage efficient et simplifié ainsi qu'une gestion topologie améliorée. Nos réseaux sont composés de bateaux au large de l' océan, ceux-ci sont classifiés en deux catégories hiérarchiques les bateaux maîtres qui sont les nœuds meneurs "Cluster Heads (CHs)" et les bateaux ordinaires. Nous sélectionnons trois algorithmes de la littérature k-means [21], Max-Min [15] et KCMBC [22]. Dans nos réseaux les bateaux maîtres disposent d' équipements plus performants et sont donc naturellement les nœuds meneurs du réseau, les CHs. Nous introduisons donc un algorithme de partitionnement à convergence rapide basé sur la distance géographique des nœuds ordinaires aux CHs que nous nommons Hierarchical MANET Clustering "HMC".

Le comportement statistique moyen du réseau est considéré, les bateaux ordinaires appartenant à l' ensemble $\mathcal{N}$ et les bateaux maîtres à l' ensemble $\mathcal{H}$ sont distribués de manière aléatoire suivant deux PPP homogènes dans $\mathbb{R}^2$ et d' intensité λ_C et λ_H respectivement. Chaque cluster k est modélisé par un graphe $\mathcal{G}_k = (\mathcal{V}_k, \mathcal{E}_k)$ où $\mathcal{V}_k$ est l' ensemble des sommets correspondant aux positions des nœuds et $\mathcal{E}_k$ l' ensemble des arê tes. Nous définissons une notion de similarité $s_{ij} > 0$ entre une paire de nœuds a (i, j), deux nœuds sont connectés leurs similarité est positive ou supérieure à un certain seuil. Dans nos travaux cette similarité correspond à la distance euclidienne $dist(i, j)$. Nous modélisons aussi le réseau formé par les CHs comme un graphe $\mathcal{G}_h = (\mathcal{H}, \mathcal{E}_h)$

◊ Naval fleet Clustering

▷ Hierarchical MANET Clustering "HMC"

Nous considérons une aire circulaire $\mathcal{A}$ de rayon R. Les bateaux maître ont pleine connaissance des positions des nœuds, ainsi chaque CH détermine quel nœud est plus proche de lui que des autres CHs en distance euclidienne. Par la suite le CH informe les nœuds séléctionnés qu'ils font partie de leur cluster, les nœuds gateway "GWs" sont usuellement situés aux frontières des clusters et peuvent donc ê tre utilisés comme relais de communication avec les cluster voisins.

La figure illustre les clusters formés par HMC et les algorithmes de la littérature pour une même configuration de nœuds.

▷ Estimation de la taille moyenne d' un cluster typique

$\mathcal{C}_o$ cluster typique centré en l' origine $(0,0)$. Soit N_0 le nombre moyen de bateaux $x \in \mathcal{N}$ appartenant à $\mathcal{C}_o$ tel que,

$$N_0 = \mathbb{E}\left[\sum_{x\in\mathcal{N}} \mathbb{1}_{\{|x|\leq r_1\}}\right],$$

où r_1 représente la distance entre un point $x \in \mathcal{N}$ quelconque et son plus proche voisin dans l' ensemble des bateaux maîtres $\mathcal{H} \cup \{o\}$.

En appliquant le théorème de Campbell [8] et la distritibution de la distance au plus proche voisin décrite par Haenggi [23] le nombre moyen de nœud dans le cluster typique C_o est,

$$\begin{aligned} N_0 &= \int_0^R \int_r^\infty 2\pi\lambda_h r_1 e^{-\lambda_h \pi r_1^2} dr_1 (2\pi\lambda_c r) dr \\ &= \int_0^R (2\pi\lambda_c r) e^{-\lambda_h \pi r^2} dr \\ \boxed{N_0 &= \left\lceil \frac{\lambda_c}{\lambda_h}(1 - e^{-\lambda_h \pi R^2}) \right\rceil}. \end{aligned}$$

▷ Rayons de couverture dans un cluster à accès centralisé

Nous calculons les rayons de couverture inter-CHs et intra-cluster de manière à atteindre une connectivité complète du réseau, pour ce faire nous exprimons les événements correspondants :

$$\{\forall h \in \mathcal{H} : dist(0,\ h) \leq \frac{1}{2} d^*_{hh,max}\} \Rightarrow \{\mathcal{G}_h \text{ is fully connected}\},$$

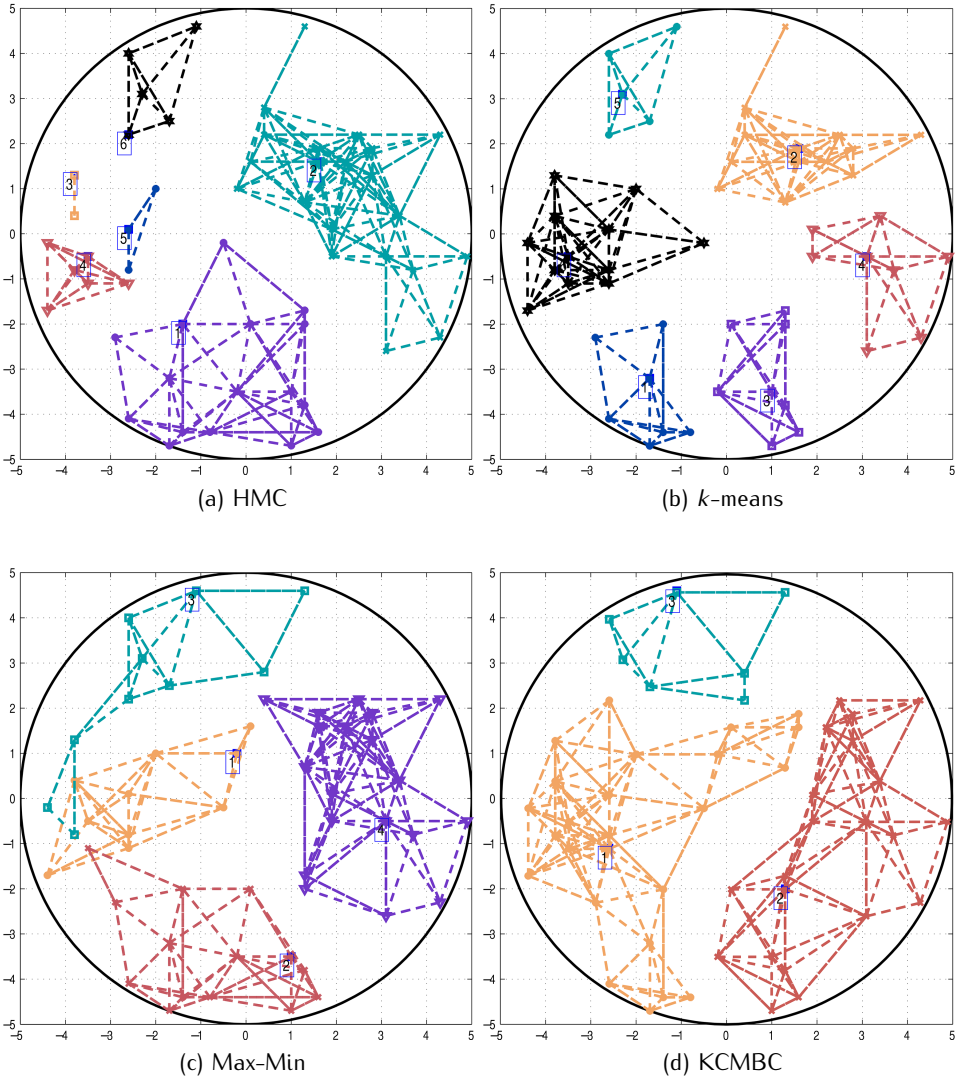

(a) HMC (b) k-means

(c) Max-Min (d) KCMBC

Clusters résultants des algorithmes HMC, k-means, Max-Min and KCMBC

ou $d^*_{hh,max}$ est la borne supérieure sur le rayon de couverture inter-CHs,

$$\{\forall x \in \mathcal{N} : dist(x, h_k) \leq d^*_{sh,k} | h_k \text{ premier voisin de } x\} \Rightarrow \{\mathcal{G}_k \text{ est totalement connecté}\}$$

En exprimant les probabilités de ne pas atteindre une connectivité totale et en paramétrant un seuil de tolérance d'occurence de cet événement p_{th}, nous obtenons les expressions suivantes :

$$d^*_{hh,\max} = \sqrt[2]{4(R^2 + \frac{1}{\pi\lambda_h}\log(1 - p_{th}))}.$$

$$d^*_{sh,\max} = \sqrt[2]{\frac{1}{\pi\lambda_h}\log\left(\frac{\lambda_c \pi R^2}{-\log(1 - p_{th})}\right)}.$$

▷ **Rayons de couverture dans un cluster à accès distribué**

Les rayons de couverture à déterminer pour un réseau à accés distribué sont : le rayon inter-navires d_{ss}, entre un navire ordinaire et maître d_{sh} et inter-maîtres d_{hh}. Nous proposons un algorithme exhaustif permettant de dériver ces métriques en utilisant des les outils de la théorie des graphes, plus précisément les propriétés des matrices Laplaciennes. La figure illustre un MANET distribué totalement connecté avec une topologie résultant de l'algorithme HMC et des rayons de couverture déterminés par notre algortihme.

◊ Communications bout en bout multi-sauts

Nous analysons dans cette partie les délais de communications de bout en bout sous différents protocoles de routage. Nous contribuons avec une évaluation statistique de la distribution typique du nombre de sauts entre une source centrée en l'origine d'un cluster typique $\mathcal{C}_o$ et un destinataire aléatoire. Nous proposons trois protocole de routage adaptés à notre contexte :

- Progressive spread angle furthest neighbors search : recherche le nœud intermédiaire le plus éloigné en direction de la destination,
- Shipmaster aided : s'appuyant sur la connaissance du réseau au niveau des navire maîtres,
- Gateways search : basé sur les positions des nœuds passerelles.

Nous comparons leurs performances en terme de délais à des algorithmes de la littérature. Ceux-ci sont détaillés Chapitre 3, nous décrivons ci-dessous l'algorithme Progressive spread angle furthest neighbors search.

▷ **Focus sur les stations hybrides**

Nous répértorions les navires équipés de terminaux satellites comme des stations hybrides "HSs" $\in \mathcal{S}$. Nous introduisons le paramètre $\beta_{\text{sat}} \leq 1$ permettant d'exprimer l'intensité du

Algorithm 0: Détermination des rayons de couverture en accés distribué

Input : Ensemble des navires maîtres : $\mathcal{H}$, ensemble des navires ordinaires: $\mathcal{N}$, ensemble des clusters: $\mathcal{C}_k$, α.

Output: d^*_{ss}, d^*_{sh}, d^*_{hh}.

1 Calcul du vecteur $\mathbf{d}_{ss}$ contenant les distances euclidiennes ordonnées entre chaque nœuds $x \in \mathcal{N}$
2 $iter_s \leftarrow 1$;
3 $d^*_{ss} \leftarrow \mathbf{d}_{ss}(iter_s)$;
4 $d^*_{sh} \leftarrow \alpha \cdot d^*_{ss}$;
5 Calcul de la matrice d'adjacence $\mathbf{A}_k$, la matrice de degrés $\mathbf{D}_k$ et les matrices Laplcaciennes $\mathbf{L}_k$;
6 Calcul de la multiplicité m^0_k of de la valeur propre 0 de $\mathbf{L}_k$;
7 fullyCoClusters $\leftarrow \sum_{k=1}^{|\mathcal{C}_k|} m^0_k$;
8 **while** *fullyConnectedClusters* $\neq |\mathcal{H}|$ **do**
9 $iter_s \leftarrow iter_s + 1$;
10 $d^*_{ss} \leftarrow \mathbf{d}_{ss}(iter_s)$;
11 $d^*_{sh} \leftarrow \alpha \cdot d^*_{ss}$;
12 Repéter *Etapes* 5 *to* 7;
13 **end**
14 Calcul du vecteur $\mathbf{d}_{hh}$ contenant les distances euclidiennes ordonnées entre chaque nœuds $h \in \mathcal{H}$;
15 $iter_h \leftarrow 1$;
16 $d^*_{hh} \leftarrow \mathbf{d}_{hh}(iter_h)$;
17 Calcul de $\mathbf{A}_h$, $\mathbf{D}_h$ and $\mathbf{L}_h$;
18 Calcul de la multiplicité m^0_h of de la valeur propre 0 d $\mathbf{L}_h$;
19 fullyConnectedCHs $\leftarrow m^0_h$;
20 **while** *fullyConnectedCHs* $\neq 1$; **do**
21 $iter_h \leftarrow iter_h + 1$;
22 $d^*_{hh} \leftarrow \mathbf{d}_{hh}(iter_h)$;
23 Répéter *Etapes* 16 *to* 18;
24 **end**

PPP de ces stations en fonction de λ_c comme : $\lambda_s = \beta_{\text{sat}}\lambda_c$. Ce qui nous permet d'exprimer le nombre moyen de HSs dans un cluster typique $\mathcal{C}_o$:

$$N_s = \left\lceil \frac{\lambda_s}{\lambda_h}(1 - e^{-\lambda_h \pi R^2}) \right\rceil.$$

En finalité, nous voulons estimer l'intensité λ_s permettant d'obtenir des délais de bout en bout par liaison satellite inférieurs à un certain seuil. Dans un deuxième temps nous comparons les délais par voie satellite D_{sat} aux délais terrestres D_{ter} grâce au facteur $\kappa_s \in \mathbb{N}^*$ tel que $D_{sat} = \kappa_s D_{ter}$. En définissant la matrice de coût $\mathbf{C}$ sur les liens du réseau

Algorithm 0: Progressive spread angle furthest neighbors search protocol

Input : Total graph: $\mathcal{G}_{all} = \cup_k \mathcal{G}_k \cup \mathcal{G}_h$, s and d the source and destination ids, spread angle Θ, current delay t and the maximal end-to-end delay t_{max}.

Output: $\mathcal{P}$, the set of intermediates nodes from s to d.

$t \leftarrow 0$;
$\mathcal{NB} \leftarrow \{x \in \mathcal{G}_h \text{ s.t. } |x \rightarrow s| \leq d^*_{ss}\}$; // set of neighbors of s
if $d \in \mathcal{NB}$ **then**
    $\mathcal{P} = \{s, d\}$;
    else
        $\theta_d \leftarrow \angle sOd$; // angle between s and d
        $\mathcal{I} \leftarrow \{x \in \mathcal{NB} \text{ s.t. } \theta_d - \Theta < \angle sOx < \theta_d + \Theta\}$; // set of possible intermediates nodes
    end
end
$Intra \leftarrow 0$; // 1 if s and d are in the same cluster, 0 otherwise
while $d \notin \mathcal{P}$ ***and*** $t < t_{max}$ ***and*** $\mathcal{I} \neq \emptyset$ **do**
    if $\{\exists x \text{ s.t. } x \in \mathcal{S} \cap \mathcal{H}\}$ ***and not*** $Intra$ **then**
        $\mathcal{I} \leftarrow \{x\}$;
        $i \leftarrow x \in \mathcal{I}$ s.t. x is the closer node to d;
        else
            $i \leftarrow x$ s.t. $x \in \mathcal{I}$ **and** $x \in \mathcal{H}$ s.t. x is the closer node to d; // intermediate node
        end
    end
end
$\mathcal{P} \leftarrow \mathcal{P} \cup i$;
$t \leftarrow t + delay$;
$\mathcal{NB} \leftarrow \{x \in \mathcal{G}_h \notin \mathcal{P} \text{ s.t. } |x \rightarrow i| \leq d^*_{ss}\}$; // set of neighbors of i
if $d \in \mathcal{NB}$ **then**
    $\mathcal{P} \leftarrow \mathcal{P} \cup d$;
    else
        $\theta_d \leftarrow \angle iOd$; // angle between i and d
        $\mathcal{I} \leftarrow \{x \in \mathcal{NB} \text{ s.t. } \theta_d - \Theta < \angle iOx < \theta_d + \Theta\}$
    end
end
if $t = t_{max}$ ***or*** $\mathcal{I} = \emptyset$; **then**
    $\mathcal{P} \leftarrow \emptyset$;
end

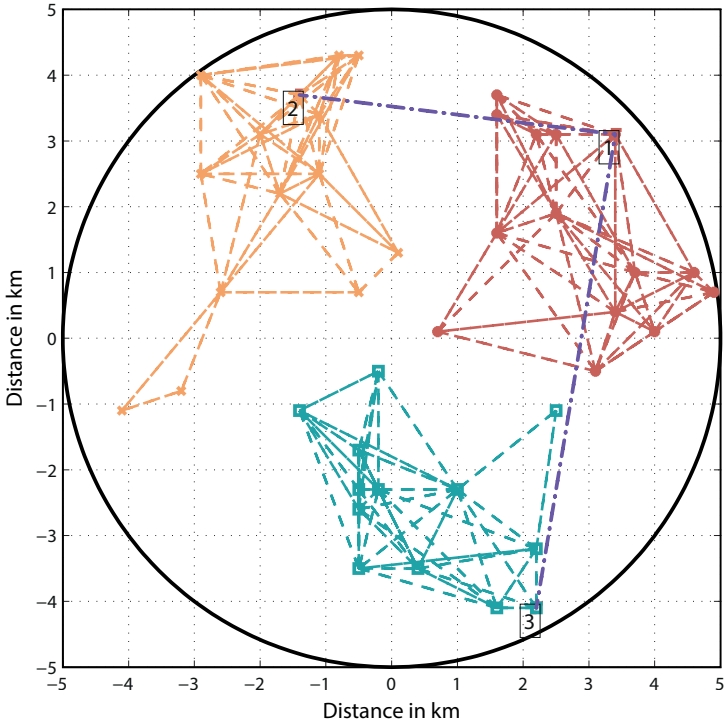

MANET totalement connecté issu de l'algorithme HMC

comme,

$$\mathbf{C} = \begin{cases} dist(i,j) \leq d^*_{ss}, & \forall\ (i,j) \in (\mathcal{N}|\mathcal{H} \times \mathcal{N}|\mathcal{H}) \\ dist(i,j) \leq d^*_{sh}, & \forall\ (i,j) \in (\mathcal{N}|\mathcal{H} \times \mathcal{H}) \cup (\mathcal{H} \times \mathcal{N}|\mathcal{H}) \\ \kappa_s, & \forall\ (i,j) \in \mathcal{S} \times \mathcal{S}. \end{cases}$$

nous pouvons appliquer l'algorithme de Dijkstra [24] qui sélectionnera le trajet le plus court en terme de délais.

◊ Résultats numériques

Pour développer nos résultats numériques nous considérons un MANET où les navires sont distribués, en fonction de leurs catégories respectives, sur une aire circulaire de rayon R selon un PPP d'intensité $\in \mathbb{R}^2$ d'intensité λ_c et λ_h. Nous dérivons les CDFs des rayons de couverture requis sous des algorithmes de clustering de la littérature et notre algorithme HMC. Par la suite, nous déterminons de manière empirique les PDFs des délais de bout en bout dans des réseaux centralisés et distribués. Ces délais sont aussi comparer sous différents protocoles de routage et selon la nature terrestre ou hybride des liens de communications.

▷ Paramètres

Généraux	
Rayon de la surface	$R = 5$ km
Intensité des navires ordinaires	$\lambda_c = 6e^{-1}$
Intensité des navires maîtres	$\lambda_h = 1e^{-1}$
Ratio couverture navires ordinaires → CH	$\alpha = 1, 1.75$
Seuil de tolérance	$p_{th} = 1\%$
Ratio HSs	$\beta_{\text{sat}} = 0, 0.25, 0.5, 0.75$ et 1
Facteur de délais Sat./Ter.	$\kappa_s = 3, 10$ et 14
Clustering	
k-means	$k = \lvert\mathcal{H}\rvert$
Max-Min et KCMBC	$d = 4$

Paramètres de simulation

▷ **Rayons de couverture**

Avec le seuil de couverture considéré, le rayons de couverture avec accès centralisé analytique exprimés plus haut sont $d^*_{hh,\max} = 9.99$ km et $d_{sh,\max} = 5.4$ km .

La figure réprésente les CDFs des rayons de couverture inter-CHs évaluées numériquement pour $\alpha = 1$. Pour le réseau distribué résultant d' un partitionment par l' algorithme HMC le rayon de couverture requis est de 7 km alors qu'en configuration centralisée celui-ci est de 9.9 km pour assurer une connectivité totale dans 99.99% des cas. Nous observons que la sélection non aléatoire du CH imposée le contexte hiérarchique pénalise de manière significative les rayons de couverture, sous k-means nous obtenons des rayons requis de 5.1 km et 9.2 km respectivement en acces distribué et centralisé.

▷ **Distribution des délais aux CHs**

Nous comparons les délais de communications pour atteindre le CH dans un cluster résultant des algorithmes de clustering HMC, k-means, Max-Min et KCMBC. Pour k-means, 88% des noeuds ont accès à leur CH en un saut. Pour le cas distribué avec $\alpha = 1$, seulement 46% des noeuds sont connectés en un saut alors 72% le sont avec $\alpha = 1.75$. Hence, the network designer is can adjust this scaling factor, to find an accurate trade off between the equipments requirements and the achievable coverage radii. Max-Min et KCMBC aboutissent à des délais plus élevés car ils forment des clusters de plus grandes circonférences.

▷ **ICDF des délais de communications de bout en bout multi-sauts**

Nous illustrons l'ICDF des délais de communications de bout en bout multi-sauts le nombre moyen typique de sauts pour atteindre le centre o et l'écart type sont de 27 et 15.9.

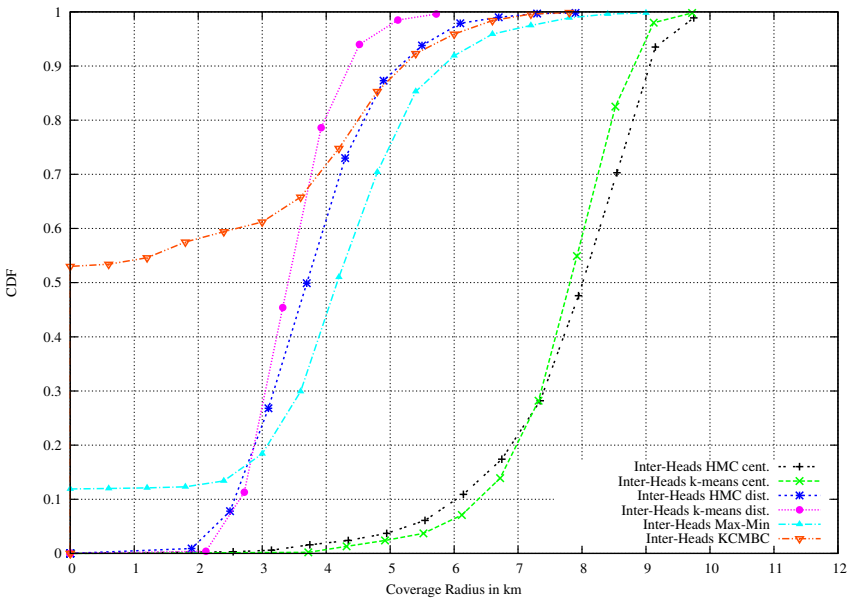

Distribution des rayons de couverture Inter-CHs

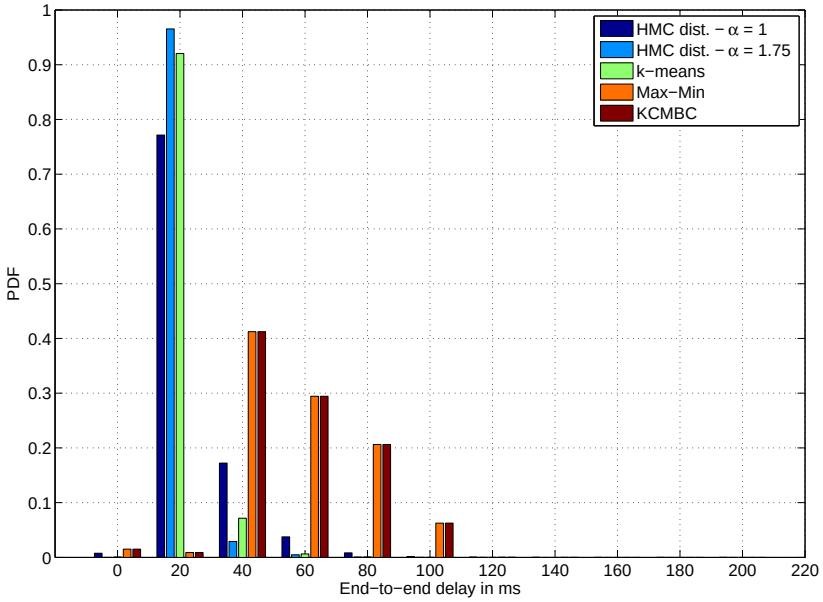

Distribution des sauts au CHs Intra-cluster

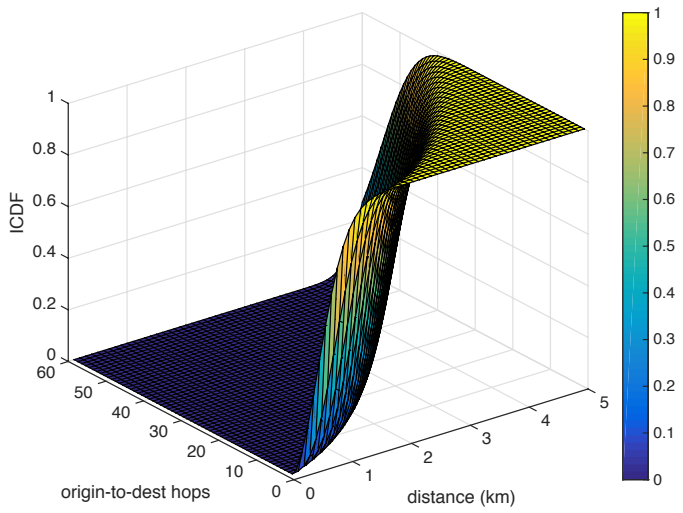

ICDF de la borne supérieure sur le nombre de sauts pour le chemin $o \rightarrow d$

▷ **PDF des délais de communication**

Nous observons que les performances du Progressive furthest point search sont proches de celles de l'algorithme optimale de Dijkstra.Poure les deux algorithmes les délais sont dans presque 100% des cas sous les 160 ms. Pour le shipmaster aided protocol les délais sont au dessus de 3% des cas. L'utilisation des USATs dépend de manière critique sur les délais de bout en bout tolérés. Par exemple avec une faible tolérance de délais de 60 ms, 26% des noeuds pour le shortest path, respectivement 29% et 21% des noeuds pour le progressive search et le gateways search dépassent la barre des 60 ms. Ce pourcentage est significatif et l'emploi des HSs est primordial pour réduire les délais dans le réseau.

▷ **Délais de bout en bout avec des USATs**

Nous considérons que les CHs et un nombre aléatoire de CNs sont pourvus d'USAT. Les intensités des PPP déterminant la distribution des navires HSs est étudiée pour $\beta_{\text{sat}} = 0, 0.25, 0.5, 0.75$ et 1, ce qui correspond à un nombre moyen de HSs $N_s = 0, 2, 3, 5$ et 6. Le réseau est partitionné par l'algorithme HMC, nous considérons des satellites Low Earth Orbit "LEO", correspondant à une valeur de $\kappa_s = 3$.

Nous dérivons la PDF des délais de communications de bout en bout avec l'agorithme de Dijkstra algorithm. Un saut terrestre à pour délai $D_{ter} = 20$ ms, le satellite $D_{sat}^{LEO} = 3 \times 20 = 60$ ms. Le réseau d'amenée satellite est utilisé uniquement lorsque D_{ter}^{LEO} est de 60 ms i.e. D_{sat}. Nous remarquons que 84% des délais sont inférieurs à 60 ms avec $\beta_{\text{sat}} = 0.25$ contre 93% avec $\beta_{\text{sat}} = 0.75$. Un compromis doit être trouvé entre les coûts dus à l'infrastructure satellite et les délais maximum tolérés.

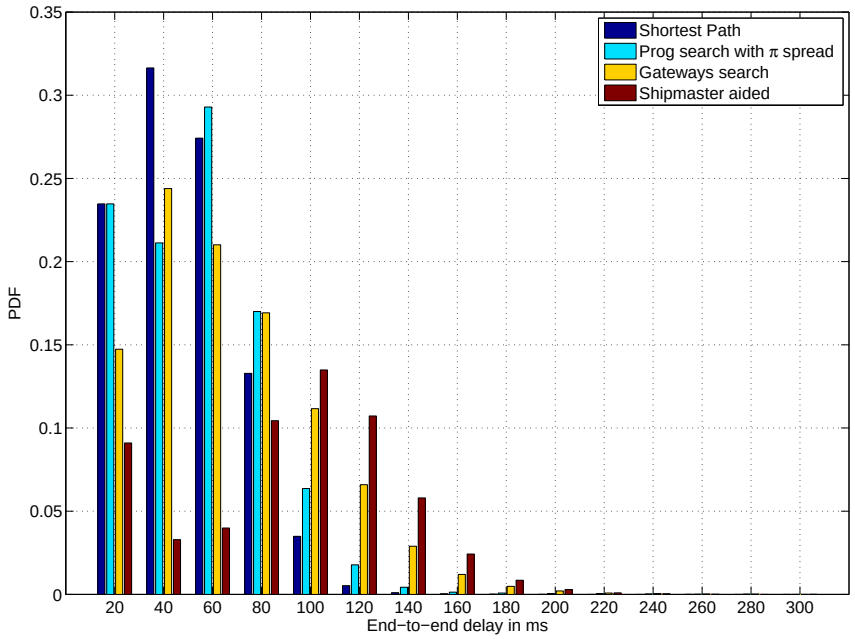

Distributions des délais de communications de bout en bout

◊ Conclusion

Nous avons débuté par considérer le comportement statistique moyen du réseau pour le cas centralisé, puis nous avons étudié le domaine de la théorie des graphes et présenté une solution exhaustive pour dériver les rayons de couverture requis dans un schéma d'accès distribué. Plusieurs protocoles de routage ont été évalués en termes de délais de communication de bout en bout, nous avons proposé une stratégie pour l'accès aux passerelles satellites et aussi une étude comparative pour qualifier les besoins en stations hybrides en fonction des délais de bout en bout tolérés.

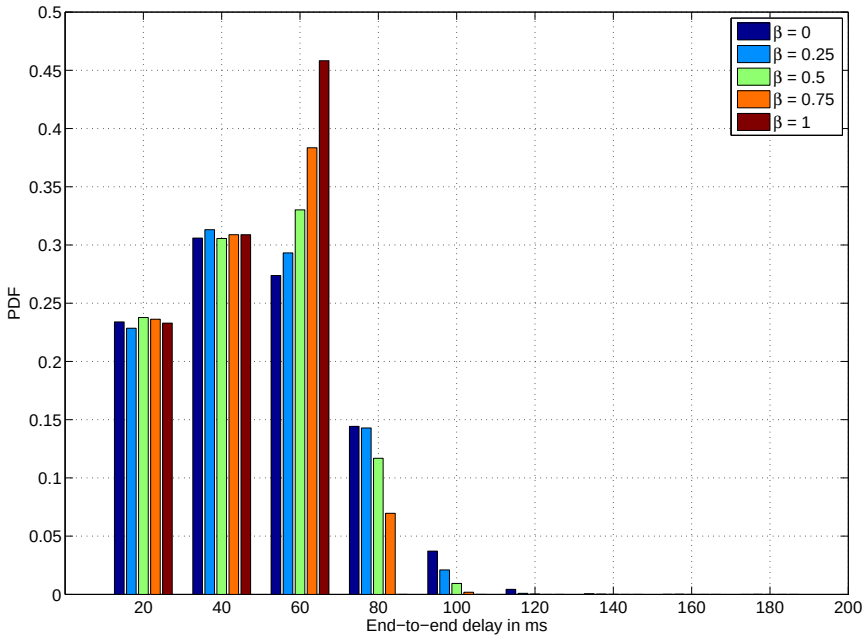

Délais de bout en bout avec des satellites LEO, $\kappa_s = 3$

♦ Dépassement de Ressources radio dans un Réseau Centralisé & Dimensionnement

◊ Introduction

Nous adressons dans ce chapitre les sujets du dimensionnement des ressources radios et la probabilité de dépassement de ces ressources pour un MANET centralisé.

Soit $\mathcal{C}$ un cluster circulaire de diamètre R appartenant à un MANET centralisé. Les navires mis en œuvre sont équipés d'une ou deux antennes à gain omnidirectionnel. Φ_{nodes} est l'ensemble des nœuds actifs dans un cluster. Ces travaux furent publiés dans [25] et [26].

▷ Probabilité de dépassement de ressources

L'ensemble des nœuds actifs est décrit par un PPP marqué :

$$\tilde{\Phi} = \{\tilde{X}_i \in \mathcal{C} \times \mathbb{R}^+ : \tilde{X}_i = (X_i, y_i)\}$$

où x est la position du CN de $\mathcal{C}$ et y le cœfficient d'atténuation aléatoire du trajet entre le CN et le CH. $\tilde{\Phi}$ est caractérisé par son intensité $\Lambda(dx) \otimes p_y(y)dy = \lambda p(y)dxdy$.

Nous exprimons le nombre de RBs requis par un CN dans le cas d'une QoS unique comme :

$$N_{RB}(x, y) = min\left(\sum_{j \in \mathbb{N}^*} j\mathbb{1}_{\{j-1<N_{RB}\leq j\}}, N_{max}\right),$$

et le nombre total de RBs requis :

$$N_{RB,t}(\tilde{\Phi}) = \sum_{\tilde{X} \in \tilde{\Phi}} N_{RB}(\tilde{X}) .$$

La probabilité que le nombre de RBs requis dépasse le nombre de RBs disponible N_{net} est donc :

$$\mathbb{P}_{out}(N_{net}) = Prob\{N_{RB,t}(\tilde{\Phi}) > N_{net}\} .$$

Notre objectif est de déterminer N_{net} tel que la probabilité de dépassement de ressource soit inférieure à un certain seuil p_{th}.

▷ Borne supérieure sur la probabilité de dépassement de ressources

Nous exprimons cette borne supérieure comme

$$\mathbb{P}_{sup}(N_{net}) = exp\left(-\frac{\nu_N}{N_{max}^2} g\left(\frac{(\delta - 1)m_N N_{max}}{\nu_N}\right)\right) .$$

sachant que $g(t) = (1 + t)\log(1 + t) - t$. De plus le premier et le second moment du PPP

sont exprimés tel que :

$$m_N = \lambda \left[\sum_{j=1}^{N_{max}-1} j(A_j - A_{j-1}) + N_{\max}(\pi R^2 - A_{N_{max}-1}) \right]$$

$$v_N = \lambda \left[\sum_{j=1}^{N_{max}-1} j^2(A_j - A_{j-1}) + N_{max}^2(\pi R^2 - A_{N_{max}-1}) \right],$$

où $A_j = \int_{\mathcal{C}} \text{Prob}\{N_{RB}(x,y) \leq j\}\, dx$ est l'aire dans laquelle les nœuds requièrent au plus j RBs. Dans le cas d'une QoS k-multiple la borne supérieure sur la probabilité de dépassement est:

$$\mathbb{P}_{sup}^{mult.}(N_{net}) = exp\left(-\frac{\bar{v}_N}{\bar{N}_{max}^2} g\left(\frac{(\delta-1)\bar{m}_N \bar{N}_{max}}{\bar{v}_N} \right) \right) .$$

où $\bar{m}_N = \sum_{k=1}^{\mathcal{K}} m_{N,k}$, $\bar{v}_N = \sum_{k=1}^{\mathcal{K}} v_{N,k}$ et $\bar{N}_{max} = \max_k N_{max,k}$.

▷ **Efficacité spectrale moyenne & Dimensionnement**

Nous définissons $N_{net} = \delta m_N$, avec $\delta = 1 + \frac{v_N}{m_N N_{max}} g^{-1}\left(-\frac{N_{max}^2}{v_N} \log(p_{th}) \right)$, et dérivons l'efficacité spectrale moyenne dans le réseau :

$$S = \lambda \left[A_{N_{max}} C_0 + \lambda \sum_{j \geq N_{max}+1} (A_j - A_{j-1}) C_j \right] / B .$$

Une fois ces équations obtenues il ne nous reste plus qu'à déterminer les expression des aires A_j pour différentes configurations d'antennes, nous nous focalisons sur les configurations SISO, MIMO avec diversité de gain et avec gain de multiplexage. Après des calculs décrit dans le corps principal du manuscrit nous aboutissons aux équations suivantes :

$$\begin{aligned} A_j^{SISO} = {} & 2\pi \left[\xi_{FS} \Gamma_{inc}\left(a_{FS} d_c^{\gamma_{FS}}, \frac{2}{\gamma_{FS}} \right) \right] \\ & + 2\pi \sum_{i=1}^{2} \left[\xi_{m,i} \Gamma_{inc}\left(a_{\mathrm{m},i} R^{\gamma_{\mathrm{m},i}}, \frac{2}{\gamma_{\mathrm{m},i}} \right) \right. \\ & \left. - \xi_{m,i} \Gamma_{inc}\left(a_{\mathrm{m},i} d_c^{\gamma_{\mathrm{m},i}}, \frac{2}{\gamma_{\mathrm{m},i}} \right) \right], \end{aligned}$$

où :

$$\Gamma(m) = \int_0^\infty e^{-t} t^{m-1} dt$$

$$\Gamma_{inc}(x,m) = \frac{1}{\Gamma(m)} \int_0^x e^{-t} t^{m-1} dt.$$

et,

$$\xi_{FS} = \frac{1}{\gamma_{FS}} \left(\frac{1}{a_{FS}} \right)^{\frac{2}{\gamma_{FS}}} \Gamma \left(\frac{2}{\gamma_{FS}} \right),$$

$$\xi_{m,i} = \frac{1}{\gamma_{\mathrm{m},i}} \left(\frac{1}{a_{\mathrm{m},i}} \right)^{\frac{2}{\gamma_{\mathrm{m},i}}} \Gamma \left(\frac{2}{\gamma_{\mathrm{m},i}} \right).$$

$$A_j^{MIMO,d} = 2\pi \left[\int_{\mathcal{C}_{d_c}} r(1 - \frac{1}{\sigma_f^2} \Gamma_{inc} \left(\frac{1}{\sigma_f^2} \frac{r^{\gamma_{FS}}}{\tilde{\beta_{j,d,FS}}}, 4 \right)) dr \right] + 2\pi \left[\sum_{i=1}^{2} \int_0^{2\pi} \int_{d_{c,i}}^{d_{c,i+1}} r(1 - \frac{1}{\sigma_f^2} \Gamma_{inc} \left(\frac{1}{\sigma_f^2} \frac{r^{\gamma_{\mathrm{m},i}}}{\tilde{\beta}_{j,d,m,i}}, 4 \right)) dr \right],$$

avec $\tilde{\beta_{j,d}} = \frac{P_T \alpha}{2\eta} \frac{1}{\beta_j}$ et $\beta_j = 2^{\frac{C_0}{jW}} - 1$; et enfin,

$$A_j^{MIMO,m} = 2\pi \left[\xi_{FS} \Gamma_{inc} \left(a_{FS} d_c^{\gamma_{FS}}, \frac{2}{\gamma_{FS}} \right) \right] + 2\pi \left[\sum_{i=1}^{2} \xi_{m,i} \Gamma_{inc} \left(a_{\mathrm{m},i} d_{c,i+1}^{\gamma_{\mathrm{m},i}}, \frac{2}{\gamma_{\mathrm{m},i}} \right) - \xi_{m,i} \Gamma_{inc} \left(a_{\mathrm{m},i} d_{c,i}^{\gamma_{\mathrm{m},i}}, \frac{2}{\gamma_{\mathrm{m},i}} \right) \right].$$

◊ Validation du modèle analytique

▷ **Paramètres du système**

Les paramètres de simulation utilisés dans nos travaux sont décrits dans le tableau “Paramètres Système”.

Paramètres Système

Paramètre	Valeur
Fréquence porteuse	800 MHz
Puissance Tx CH	$P_T = 10^{2,3}$ mW
Gain d'antenne eNB	G (dBi) = 0 (omni)
Hauteur Tx & Rx	$h_1 = h_2 = 12$ m
Configuration d'antenne	$n_t = 1, 2$ et $n_r = 1, 2$
Puissance du bruit	$\eta = 7.1 \cdot 10^{-}13$ mW
Affaiblissement en espace libre	$K_{\mathrm{FS}} = 10^{-9.01}$, $\gamma_{FS} = 2$
Rayleigh variance	$\sigma_f = 1$
Seuil SNR	$\beta_{min} = -2.3$ dB

▷ **Classe QoS unique**

Nous dérivons la probabilité de dépassement de ressources pour $N_{RB} = \{50, 65, 75, 90 \text{ et } 100\}$, correspondant aux bandes B = {10, [10; 3], 15, [15; 3] et 20} MHz. En utilisant une simulation de Monte Carlo à 10^7 itérations, nous calculons pour différentes configurations d' antenne $\mathbb{P}_{out}$. Le test log-ratio

$$\Delta = \log_{10}\left(\frac{\mathbb{P}_{sup}}{\mathbb{P}_{out}}\right)$$

compare les valeurs analytiques et numériques des résultats.

◇ SISO

Les valeurs analytiques de la moyenne et la variance obtenues sont :

$$m_{\text{N,SISO}} = 47$$

et

$$v_{\text{N,SISO}} = 76.$$

Le tableau ci-dessous résume les résultats. La borne supérieure calculée s'avère ê tre en adéquation avec la probabilité de dépassement de ressources obtenues par simulation et le log ratio maximum est de 1.9. ◇ MIMO avec diversité de gain

Dimensionnement SISO

Band(MHz)	10	[10,3]	15	[15,3]	20
N_{RB}	50	65	75	90	100
δ	1.06	1.39	1.6	2	2.12
P_{sup}	0.94	0.22	0.04	0.001	$1 \cdot 10^{-4}$
P_{out}	0.3	0.02	0.0016	$1.7 \cdot 10^{-5}$	0
Δ	0.5	1.04	1.39	1.9	$\times$

Les valeurs analytiques de la moyenne et la variance obtenues sont

$$m^{d}_{\text{N,MIMO}} = 38$$

et

$$v^{d}_{\text{N,MIMO}} = 38.$$

Nous remarquons que les probabilité de dépassement de ressources du tableau sont considérablement réduites par rapport au cas SISO, en effet les codes d'Alamouti extraient la totalité du gain de diversité.

◇ MIMO avec gain de multiplexage

Pour ce schéma les valeurs analytiques de la moyenne et la variance du PPP sont :

$$m^{mx}_{\text{N,MIMO}} = 48$$

Dimensionnement en 2×2 MIMO avec gain de diversité

Band(MHz)	10	[10,3]	15	[15,3]	20
N_{RB}	50	65	75	90	100
δ	1.32	1.71	1.97	2.36	2.63
P_{sup}	0.29	0.009	0.0004	$2.5 \cdot 10^{-6}$	$5.3 \cdot 10^{-8}$
P_{out}	0.0235	$1.7 \cdot 10^{-5}$	0	0	0
Δ	1.09	2.72	$\times$	$\times$	$\times$

et

$$v^{mx}_{\text{N,MIMO}} = 89.$$

Les valeurs numériques sont 48 pour la moyenne et 88 pour la variance. On ne constate pas de différence avec la configuration SISO étant donné le partage de puissance entre les deux porteuses qui n'est pas compensé par le gain induit par le multiplexage.

Dimensionnement en 2×2 MIMO avec gain de multiplexage

Band(MHz)	10	[10,3]	15	[15,3]	20
N_{RB}	50	65	75	90	100
δ	1.04	1.35	1.56	1.87	2.08
P_{sup}	0.98	0.29	0.065	0.003	$3 \cdot 10^{-4}$
P_{out}	0.356	0.032	0.0042	$7.1 \cdot 10^{-5}$	$31 \cdot 10^{-6}$
Δ	0.42	0.89	1.18	1.66	2.48

▷ **Multiple QoS en SISO**

Nous dérivons les résultats numériques avec les classes de QOS $C_1 = 600$ kb/s, $C_2 = 800$ kb/s et $C_3 = 1$ Mb/s. Les valeurs analytiques de la moyenne et la variance obtenus sont

$$m^{mx}_{\text{N,MIMO}} = 49$$

et

$$v^{mx}_{\text{N,MIMO}} = 90.$$

Les probabilités de dépassement de ressources sont résumées dans le tableau ci-après. Les probabilités de dépassement sont plus importantes étant donné le niveau de saturation réseau étant élevé.

◊ Conclusion

Nous avons utilisé des outils de géométrie stochastique pour fournir un modèle analytique permettant à un concepteur de réseau d'estimer la bande passante requise pour éviter l'événement de dépassement des ressources radio. A cette intention, nous avons dérivé une borne supérieure de la probabilité de dépassement des ressources en considérant les paramètres du réseau. Ce qui nous a permis de déterminer le nombre moyen de RBs requis par les membres du cluster et donc la bande passante nécessaire pour une classe

Dimensionnement en SISO avec des classes de QoS mutliples

Band(MHz)	10	[10,3]	15	[15,3]	20
N_{RB}	50	65	75	90	100
δ	1.02	1.33	1.54	1.84	2.05
P_{sup}	0.99	0.33	0.08	0.004	$4 \cdot 10^{-4}$
P_{out}	0.4	0.05	0.06	0.0001	$6 \cdot 10^{-6}$
Δ	0.38	0.84	1.13	1.66	1.89

de QoS unique et multiple. Enfin le nombre de RB requis par le réseau de telle sorte que l'occurence du dépassement des ressources radio soit inférieur à un seuil donné en est déduit. L'efficacité spectrale moyenne dans le réseau ad hoc est alors déduite. De plus, l'impact de la fluctuation de la propagation maritime est étudié et un modèle linéaire permettant l'estimation de cet impact sur la bande passante est fourni.

1 Introduction

The expansion of wireless networks introduces new needs and challenges for researchers and industrials. In the past decades wireless terminals proliferate and wireless networks became essential in our societies. As in a military or a civil scope, the demand in applications is diversifying, to respond to these needs researchers continuously provide new solutions to outperform the available technologies. Classical networks rely on their infrastructures that limits the field of applications. A solution to these limitations resides in the field of Mobile Ad hoc Networks "MANETs" [27] that sharply extend the potential to generate wireless communications in a group of mobile nodes.

1 Motivations

Unlike classical cellular wireless networks requiring preconfigured infrastructures as base stations and routers, MANETs are device to device based networks and nodes are free to move and organize themselves arbitrarily. They may be connected to the Internet or operate in a standalone way. These characteristics lead to highly dynamic networks with unpredictable topologies. The latter characteristic makes the design of communications strategies for MANETs more challenging than the classical cellular networks. Ad hoc communication schemes have been widely addressed in literature where different aspects related to the PHYsical "PHY" and Medium Access Control "MAC" layers [6] were studied. A node may communicate with others directly if they are in its range and if not it needs to use intermediate nodes which act like relays consequently.

The network connectivity depends critically on the routing processes and the links reliability, the dynamic topology can have a severe impact on the network performances by causing link failures. Due to the lack of central monitoring, these behaviors cannot be easily predicted and detected which imply a high complexity in the protocols design. These MANETs are subject to the following constraints: i) a non centralized management of the radio resource allocation and the routing, the nodes interact to set up the network and to make it functional; ii) a dynamic topology, as the nodes are moving, the radio links will

have to be updated, the topology must adapt to these fluctuations to ensure an optimal reliability of the data flow; iii) a limited range and energy, similarly to traditional mobile networks, mobile ad hoc networks are subject to power constraints which affect the quality of radio links including the range.

In the framework of this thesis, we study a hybrid MANET in a maritime environment, where the network nodes corresponding to ships are equipped with Long Term Evolution "LTE" [4] radio devices. LTE systems are designed to provide high throughputs and spectral efficiencies and support advanced antenna configurations which reach the network designer requirements. The mobile nodes consisting in ships part of a naval fleet, far from the coast, will be supported by a satellite backhaul network. Thus, a finite number of nodes will be equipped with Ultra small Aperture Terminals "USATs" [7] to exchange data information between nodes and/or with the coast and will be referred as Hybrid Stations "HSs". The maritime environment specific features have also to be considered, an empirical maritime signal propagation model will be derive in this work from the recommendation of the International Telecommunications Union "ITU" [3] on propagation prediction techniques.

We aim in this work to provide analytical tools enabling a network designer to build efficient topology designs and communications strategies to ensure feasible and reliable transmissions and a certain performances level. Among popular approaches involved in the study of ad hoc networks, stochastic geometry appears to be a very interesting field enabling to capture the average statistical behavior of the network [8, 9], several works have been proposed in literature [28, 11, 12] and it came out that significant results can be derived based on available previous works. Based on these observations, it seemed very interesting, motivating and well-justified to us to invoke this field in the scope of this thesis. Indeed, all along stochastic geometry will be used, the network set up via its topology design will first be studied then we emphasis on the radio resource dimensioning in both centralized and distributed access schemes. Although we focus on LTE radio equipments in our derivations the analytical models and algorithms provided in this thesis can be easily adapted to alternative communication systems.

2 Contributions

In this dissertation, the main purpose is to provide efficient algorithms and models enabling a network designer to set up a suitable LTE Hybrid Satellite-MANET, from the selection of the equipments and the network construction to the design of the communications strategies, reaching both the designer targeted performances and costs. We first focus on the network initialization and the partitioning of the mobile nodes in a hierarchical context. The average statistical behavior of the network is then considered to study the end-to-end communications and the satellite aspect of the hybrid network using Graph Theory [13, 14] techniques. Afterwards, we focus on one circular cluster to study the radio resource outage probability and the dimensioning matter in a centralized and distributed network using Stochastic Geometry [8, 9] tools for several antenna configurations. In this thesis several

goals are identified and the proposed work developed along this manuscript has been led to contribute to their achievement. In summary, we aim:

— to provide a statistical model to help a network designer to perceive the advantages and the inconvenients of the possible solutions among the use of centralized access via the shipmasters or a distributed access. We consider the average statistical behavior of the network for the centralized case, we then investigate the Graph Theory field and present an exhaustive solution to derive the required coverage radii in a distributed access scheme.

— to characterize the end-to-end communications within the network and to compare the performances of routing protocols. We first derive the typical distribution of the number of hops through the nearest neighbors. We introduce the algorithms available in literature and propose several protocols: the Progressive spread angle furthest neighbors search (Algorithm 3), the Shipmaster aided and the Gateways search protocol. The performances of these protocols are evaluated in terms of end-to-end delays and compared to traditional ones.

— to establish a statistical tool helping a network designer to lead a comparative study, in order to qualify the needs in hybrid stations in function of the maximal end-to-end tolerated delays. To that aim we analytically derive the average number of satellite gateways in a cluster. Then we compare the end-to-end multi-hops communication delays with the use of terrestrial only and hybrid paths under several satellite systems.

— to tackle the radio dimensioning matter on which depend the network parameters including the network load, the antenna configuration, and the required QoS. Thus, we emphasis on the dimensioning in a cluster of a MANET with a centralized communication scheme. By investigating stochastic geometry tools, we provide an analytical model to help a network designer to estimate the required bandwidth to avoid the radio resource outage event. To this intent, we first derive an upper bound on the resource outage probability considering networks parameters. We estimate the average number of resource blocks requested by the mobile nodes. From this upper-bound, we determine the number of resource blocks required by the network in such that the radio resource outage does not exceed a given threshold. Finally, we study the impact of the maritime propagation fluctuation and a linear model to predict the impact on the bandwidth estimation is furnished.

— to predict the required bandwidth to allocate in a distributed OFDMA MIMO mobile ad hoc network under Aloha MAC protocol, in order to avoid radio resource outage. We assume that the ad-hoc shared OFDMA bandwidth is divided into several sub-mediums, containing each a predefined number of radio resource blocks depending on the QoS. We aim to guarantee that the number of RBs in a given sub-medium is sufficient to fulfill the requirements of a certain amount of mobile nodes. To this intent we derive the analytical expression of the sub-medium resource outage probability for different transmission modes considering the average statistical behavior of the network.

3 Thesis outline

In the following we review briefly the organization of this dissertation and the main subject of each chapter:

- **Chapter 2 - Technical and Mathematical Frameworks**
  We start this dissertation by introducing the background and preliminaries on the technical and mathematical fields involved in this thesis. We successively review the fields of concern and detail the elements investigated in the scope of this work. We first focus on the Mobile Ad hoc Networks "MANETs" framework, the features of the radio and satellite components envisaged in this work are then presented. It follows a detailed description of the maritime wireless channel and its modeling. Information theory principles essential to compute the channel capacity under different multiple antenna techniques are also depicted. Finally, we provide a detailed description of the Stochastic Geometry and Graph theory tools investigated to model the average behavior of the network mobile nodes.
- **Chapter 3 - Topology Design of a Hybrid Satellite-MANET**
  This chapter aims to introduce a statistical model enabling a network designer to perceive the pros and cons of the possible solutions among: i) the use of centralized access via the shipmasters or a distributed access, ii) the needs in satellite gateways in the network and iii) the gains in terms of end-to-end communication delays vs. the costs induced by the satellite equipments. To answer these interrogations we start by considering the average statistical behavior of the network for the centralized case, we then investigate the Graph Theory field and present an exhaustive solution to derive the required coverage radii in a distributed access scheme. Several routing protocols are evaluated in terms of end-to-end communication delays, we then propose a strategy for the access to the satellite gateways and also a comparative study to qualify the needs in hybrid stations in function of the maximal end-to-end tolerated delay.
- **Chapter 4 - Centralized Network Resource Outage & Dimensioning**
  Radio Resource Management "RRM" is used to optimize the allocated bandwidth in such way to serve all users while minimizing the probability of the event that arises when the management entity has no more radio resources to attribute to the users. This event will be denoted as "radio resource outage event". This chapter focuses on the dimensioning in a cluster of a MANET with a centralized communication scheme. We use stochastic geometry tools to provide an analytical model enabling a network designer to estimate the required bandwidth to avoid the radio resource outage event. To this intent, we first derive an upper bound on the resource outage probability considering networks parameters. Then, we estimate the average number of RBs requested by the CNs and thus the necessary bandwidth for the single and multiple class users QoS. Afterwards, based on this upper-bound, we determine the number of

RBs required by the network in such a way that the occurrence of the radio resource outage does not exceed a given threshold. The average spectral efficiency in the ad hoc network is then deduced. Moreover the impact of the maritime propagation fluctuation is studied and an linear model to foresee this impact on the bandwidth estimation is provided.

- **Chapter 5 - Distributed Network Resource Outage in a MANET with Aloha MAC** Distributed access schemes enhance the communications efficiency by enabling pairwise transmissions between the mobile nodes without the support of a management entity as in the centralized scheme. In these networks nodes access the shared medium unilaterally. In this chapter, we define statistical tools for radio dimensioning in a non-cooperative OFDMA Aloha MIMO MANET. We assume that the ad-hoc shared OFDMA bandwidth is divided into several sub-mediums, containing each a predefined number of radio resource blocks that depends on the required QoS. Our main objective is to find the required bandwidth to allocate in the network to guarantee that the number of RBs in a given sub-medium is sufficient to serve an acceptable amount of nodes within the considered sub-medium. For this, we derive the analytical expression of the sub-medium resource outage probability for different transmission modes considering the average statistical behavior of the network. We finally provide numerical results to compare the performances of the different MIMO transmission modes in terms of coverage radius, bandwidth and aggregate capacity.

2 Technical and Mathematical Frameworks

First of all we introduce the background and preliminaries on the technical and mathematical fields involved in this thesis. This chapter is the keystone of our work as it holds the fundamentals on which this thesis relies. We successively review these fields and detail the elements investigated in the scope of this work. We first focus on the Mobile Ad hoc Networks "MANETs" framework, the features of the radio and satellite components envisaged in this work are then presented. It follows a detailed description of the maritime wireless channel and its modeling. Information theory principles essential to model the channel under different antenna techniques are also depicted. Finally, we provide a detailed description of the Stochastic Geometry and Graph theory tools investigated to model the average behavior of the network mobile nodes.

1 Introduction

In the framework of this thesis, we study an hybrid MANET in a maritime environment, where the network nodes are part of a naval fleet offshore. Ships are equipped with LTE radio devices. This ships network, far from the coast, will be supported by a satellite backhaul network. Thus, a finite number of nodes will be equipped with Ultra small Aperture Terminals "USATs" to exchange data information between nodes and/or with the coast, for example.

First MANET applications, in early 70's, were only military oriented and quite limited, however with the huge advances in mobile communications the last few years demand of applications grew considerably. Different research projects were conducted to improve these network performances. It appears that dividing the mobile nodes in subgroups known as clusters [29], has several significant advantages at the MAC layer and the PHY layer for MANETs. Concerning the MAC layer, clustering increases the possibilities of spatial reuse, throughput, scalability and reduces power consumption. At the PHY layer side, clustering helps to reduce the size of routing tables and to reduce the number of table updates as the topology changes. Routing [30] is also a key matter for these networks, several protocols

have been especially designed [16, 17, 18, 31]. These protocols differ by their reactive [32, 33] or pro-active [34] nature and their efficiencies depend on the MANET characteristics and more particularly on nodes mobility and the environment stability. In literature, Graph Theory approach is used to find an optimal path within the network between a source and a destination [13, 14]. This approach will be involved in this thesis in order to compare the strategies performances for instance.

Convergence between satellite and terrestrial networks becomes essential for designing effective communications infrastructure at all points of the globe [35]. Indeed, these two types of networks are subject to the same constraint to provide low flow rates with a limited energy consumption. Moreover, they are complementary: satellite networks extend the very short range of ad hoc networks, and benefit in return of the very dynamic and rapidly reconfigurable topologies of these networks. Potential applications include transmissions in public safety networks ("Public Safety", police, ambulance and first aid, fire, etc.) [36, 37] and defense (military) but also broadband connection of fleets off the coast.

In the following we detail the basics and tools of the different fields introduced above and involved in our work. We first present the basics and challenges of the MANETs, then we present focus on the hybrid satellite-MANET equipments and their characteristics. The maritime wireless channel properties and features follows. Afterwards, we present the information theory principles necessary to model the propagation channel in function of the different antenna techniques. Finally, the last two sections of the chapter focus on the Poisson point processes and the graph theory frameworks used to model the mobile nodes to study the average behavior of our network. .

2 Mobile Ad hoc Networks "MANETs"

The expansion of wireless networks introduces new needs and challenges for academicals and industrials. In the last decades wireless terminals proliferate putting wireless networks in a central place of our societies. The demand in applications is diversifying, to respond to these requirements researchers continuously innovate by providing new solutions to outperform the available technologies. Mobile Ad hoc Networks "MANETs" were developed to overcome the limits of the classical cellular networks requiring high infrastructure. In this section we review the different techniques developed or applied to MANETs. We first study the partitioning of the mobile nodes into subgroups referred as clusters. We then review the different routing schemes enabling to construct links between the cluster nodes. Finally we introduce the mobility model envisaged in this thesis.

2.1 Traditional Clustering Algorithms

In this section we investigate the literature and review the three widely used clustering algorithms of concern in this work. The first one referred as k-means clustering algorithm is only based on the geographical positions of the network nodes. The last two, Max-Min

and KCMBC, are part of the d-hops clustering algorithms, which means that the clusters are formed so that the cluster nodes are situated at most at d-hops from their respective cluster head.

2.1.1 k-means clustering algorithm in $\mathbb{R}^2$

The clustering algorithm k-means, also referred as Lloyd's algorithm, is an iterative partitioning algorithm aiming to minimize the average square distance between the network nodes within a same cluster. The choice of the number of clusters k is left to the user and this algorithm is composed of 4 steps described below:

- **Step 1:** At an instant $t = 1$, randomly select k initial centroids $\mathcal{O}^1 = \{o_1^1, \ldots, o_k^1\}$ over a simulation area $\mathcal{A}$.
- **Step 2:** For $j = \{1, \ldots, n\}$ nodes x_j in $\mathcal{N}$, form the clusters $\mathcal{C}_i^1$ such that: $\mathcal{C}_i^1 = \left\{x_j : \left\|x_j - o_i^1\right\| \leq \left\|x_j - o_{i*}^1\right\| \forall i* = 1, \ldots, k\right\}$.
- **Step 3:** Update the centroids as, $o_i^{t+1} = \frac{1}{\|\mathcal{C}_i^t\|} \sum_{x_j \in \mathcal{C}_i^t} x_j$.
- **Step 4:** Iterate Steps 2 and 3 until $\mathcal{O}$ is fixed i.e. $\mathcal{O}^{t+1} = \mathcal{O}^t$.

k-means algorithm does not deal with the cluster head election during the partitioning of the network, but additional cluster head election protocols available in literature can be used. In this work, we decided to elect as CH the closest node in term of euclidean distance to the cluster barycenter.

2.1.2 Max-Min d-hops cluster formation

In [15] the authors propose a heuristic algorithm where nodes are situated at most d-hops from their leader, the only metric of this algorithm is the nodes ids. Authors showed that this cluster formation is NP-complete and provide an heuristic solution to the problem. The cluster nodes maintain two arrays, WINNER and SENDER of size $2d$ nodes ids each. Initially, nodes set their WINNER value to their id number. Then the nodes proceed to two fundamental steps of flooding, *Floodmax* and *Floodmin* described hereafter.

> **Floodmax**: During this phase, each node broadcasts its WINNER value to its 1-hop neighborhood. Upon receiving all neighbors, WINNER values, the node updates its WINNER value to the largest one between its value and the received ones.
>
> **Floodmin**: It consists in the same process than *Floodmax* except that the nodes updates their WINNER value to the smallest one between its value and the received ones.

The algorithm consists therefore in four steps:

- **Step 1:** *d*-rounds of *Floodmax*.
- **Step 2:** *d*-rounds of *Floodmin* enabling relatively small id nodes to build their clusters which provides load balancing.
- **Step 3:** After these two stages, each node selects its cluster head. The cluster head selection criteria are described below.
- **Step 4:** The last step is the clusters linking. The nodes situated at the periphery of a cluster, send a converge-cast message including its id and all gateways id. This step can highlight that a cluster head is situated between a node and its cluster head, hence the cluster head closest to the node adopts it as a child. This process maximizes the number of gateways which provides enhanced fault tolerance as the backbone results in a multiple paths between the CHs.

The cluster heads election criteria used in Step 3 are composed of 4 rules depicted below:

- **Rule 1:** Each node verifies if its WINNER value after the *d* rounds of *Floodmin* corresponds to its own id. If so the node elects itself has cluster head, otherwise proceed to Rule 2.
- **Rule 2:** The node checks for node pairs, a node pair is the node that occurs as WINNER value for this node at least once in *Floodmax* and *Floodmin*. The node pair with the smallest id is selected as cluster head for this node. In case of lack of node pair proceed to Rule 3.
- **Rule 3:** The maximum node id received in *Floodmax* is elected as cluster head. Moreover during the Step 4 of the algorithm i.e. the converge-cast process, a node can find a cluster head on the path to its own cluster head, if so proceed to Rule 4.
- **Rule 4:** The first cluster head receiving the converge-cast declares the node in its cluster.

After the CHs determination stage, each node broadcasts its elected cluster heads, thus a node receiving more than one CH id knows that it is a gateway node.

2.1.3 *d*-hops Compound Metric Based Clustering "KCMBC"

As Max-Min algorithm described above, this algorithm generates clusters in which each node is situated at most at *d*-hops from the cluster head. For the cluster formation, KCMBC uses the same approach than the Max-Min algorithm which converges in $2d$ rounds of packet exchanges at each node. However, authors remark that the Max-Min strategy for the CHs election produces more clusters than needed and is not well adapted to dynamic environment. Moreover, the algorithm neglects the nodes connectivity criteria during the cluster head election. Thus, KCMBC proposes to take into account the mobility and the

connectivity of nodes in its process.

Indeed this algorithm introduces a mobility metric: the average link expiration. The nodes with highest average link expiration ensure a stability of the network topology and thus are more likely to be elected cluster heads. Periodical Hello packets containing the node position are broadcasted to the neighborhood with a time interval of τ_S. Each node adjusts dynamically the time interval in order to not overhead the network. In a first stage, nodes with a mobility metric T_i above a certain threshold T_{ALT} are selected candidates to the cluster head election. Afterwards, the candidates set up their compound metric $CP_i = (D_i, T_i, i)$, where D_i is the number of 1-hop neighbors of node i, and other nodes set $CP = (0, 0, 0)$. Then each node broadcasts their compound metric and selects the largest on received, this step is similar to Max-Min *Floodmax*. The rest of the process is the same than Max-Min with a WINNER value corresponding to the compound metric. Nodes position $x_i(t)$ at time t are considered and their respective velocity vector $v_i(t)$ calculated by their neighbors. It is assumed that the euclidean distance between a nodes pair i and j is less than a certain coverage radius. The algorithm employs a distance based converge-cast which consist in attaching the number of hops to the corresponding WINNER in the messages exchanged during the two flooding processes. Nodes stocks this number of hops and the SENDER node, afterwards nodes broadcast to its d-neighborhood the number of hops and its CH id. KCMBC was developed for dynamic environment applications a cluster maintenance process is provided.
Two cases of change in the cluster structure are considered:

- **Node or Link Activation**: If an orphan node receives a Hello packet, it tries to join the cluster of the CH which is situated in d-hops. If it senses several CHs the nodes chooses the one with biggest average link expiration. If two CHs are in d-hop range re-clustering is triggered and the CH with the highest average link expiration remains.
- **Node or Link Deactivation**: A cluster node that looses connection within its cluster directly tries to join another cluster. If a cluster looses all its cluster nodes and is only composed of gateway nodes, the cluster is dismissed. Moreover, if a CH wants to deactivate itself it will choose another CH to allocate to its nodes. If some nodes are situated at more than d-hops from the new CH they will select another one.

2.2 Routing Protocols

Routing or path discovery protocols are essential to build communications among the network mobile nodes. These protocols aim to establish an efficient communication path between a pair of nodes without causing overhead and bandwidth wastage. Critical criteria are considered in the design of these schemes: the links have to be reliable and support the targeted QoS, routes discovered must be robust, optimal and loop free and the protocol must be simple and easily implementable. Added to the criteria enumerated above, routing protocols for MANETs should meet new challenges brought by their highly dynamic nature

resulting in frequent and unpredictable topology changes. Thus, the design of routing protocols MANETs specific are widely considered in the literature. Three types of protocols can be highlighted, reactive, proactive and hybrid protocols. The first group discovers routes between a pair of nodes on demand from the sender node. In the second group, nodes maintain route tables to the other nodes of the network and the last one has some elements from both reactive and proactive protocols. In the following we describe three ad hoc routing protocols and compare their performances in a maritime environment.

2.2.1 Literature MANET protocols

■ Ad hoc On Demand Distance Vector Protocol "AODV"

As the name implies AODV [16] is an on demand (i.e. reactive) routing protocol for MANETs. When a source needs to transmit data, it initiates the process by broadcasting to its neighbors a Route REQuest "RREQ" message for the destination. Intermediate nodes retransmit the request if they are not the destination neighbors. In the other case, the node sends a Route REPly "RREP" message on the reverse path until the source node. Each node maintains a route table for future communication. However after a certain period of time the validity of the route is not sure due to the dynamic topology. Thus the node removes the route from its route table after this period. A link may break during a communication, in this case a Route ERRor "RRERR" message is sent to the source and each intermediate node discards the route. AODV enables both unicast and multicast routing and loop free routes. The major drawback of this protocol is that it increases latency during route discovery, but it reduces the control message overhead.

■ Ad hoc On Demand Multi-path Distance Vector Protocol "AOMDV"

AOMDV [17] protocol is the multi-path version of AODV. This algorithm increases the reliability of communications by discovering multiple paths from a source to a destination. Multiple RREP messages are authorized on the reverse paths, AOMDV ensures that the different routes are loop free and disjoint. However, due to the higher number of messages, this protocol has a higher overhead than AODV.

■ Optimized Link State Routing Protocol "OLSR"

This protocol [18] is an optimization of the classic link state algorithm adapted to the requirements of a mobile wireless LAN. The concept of this protocol is the use of MultiPoint Relays "MPRs". Each node broadcasts its HELLO packet containing one-hop neighborhood information to its direct neighbors via one-hop or two-hops neighborhood. Then a node is capable to select a set of neighbors as MPR. Only the MPRs broadcast messages during the flooding process which significantly reduces service messages compared to a classical flooding. MPRs broadcast Topology Control "TC" messages, each node builds topology

tables based on the received TC containing information of the last hop towards a certain destination. Unlike conventional algorithm based on link state, only partial information link state are distributed in the network. Thus routing tables are built in a proactive way. The sending intervals of HELLO and TC messages is a critical parameter in OLSR: if the interval is too high, the protocol will not detect link break. On the other hand, too small interval will result in control overhead and packet loss. The state of information links is only generated by nodes elected as MPRs.

2.3 Mobility Models

An essential component of MANETs is the nodes mobility that imposes some constraints that should be considered in the design of MANETs protocols. In this section we describe the most used mobility models in the field of ad hoc networks [1]. We can identify two different type of models, the entity mobility models where nodes adopt their own mobility schemes and group mobility model where nodes within a group move according to a group pattern.

2.3.1 Random Walk

Several mobility model are described in literature depending on the study case. The Random waypoint mobility model consider that nodes observe a pause time between the change in direction and/or speed while in the Random direction mobile nodes choose a random direction and move toward this direction until it reaches the simulation area border. In our work we consider the Random walk mobility model. This model was created to describe unpredictable movements of the mobile nodes. A node chooses randomly a speed and a direction from pre-defined intervals. The directions and speeds are periodically updated with either a period of time t or a travelled distance d. If a node reaches a simulation boundary, its angle of direction determines a bounce angle that enables it to get away from the border. In our scope, we consider the 2D random walk mobility model although this model is also available for 1D and 3D configurations. Depending on the parameter t or d this model can concentrate nodes in a small part of the simulation area which is not of interest, one have to parameter accurately these constants in order to avoid this phenomena.

2.3.2 Group Mobility Models

We presented entity mobility models where nodes move independently in the above subsection, here we present group mobility models where all nodes within a group or cluster move together in a synchronized manner. Indeed, in some MANETs applications mobile nodes can adopt this kind of moves, for example a military fleet moving toward a target point. Several models have been developed to describe some nodes behaviors as the Column mobility

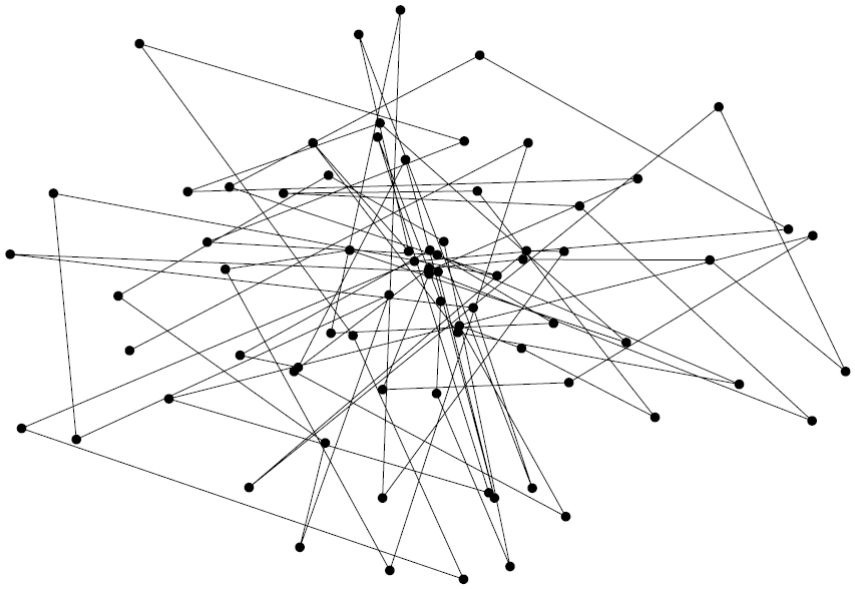

Figure 2.1: Pattern of a mobile node using 2D Random Walk Mobility Model [1]

model [1] represent a line of mobile node moving toward a direction and the Nomadic Community model. In the following, we present the Nomadic Community model that appear to be the more interesting in the scope of this thesis.

■ **Nomadic Community**

This algorithm models a group of mobile nodes moving together from one point to another one. Each node uses an entity model to move around a reference point, when the reference point moves all the nodes follow the reference point and begin again to move around the new position. In this model nodes have a semi-freedom in their moves in the area around the reference point, but one can consider that nodes are immobile once they reach the reference point area. The pattern of this model is depicted in Figure 2.2.

3 Hybrid Satellite-MANET equipments

This section focuses on the radio equipments technologies employed in our networks. We first introduce the LTE technology used for the terrestrial communications and then present the basics of the satellite networks.

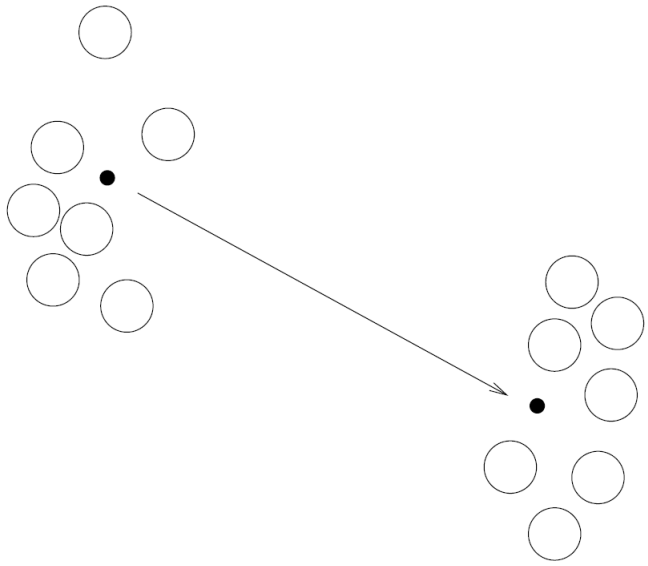

Figure 2.2: Pattern of the 2D Nomadic Community Group Mobility Model [1]

3.1 Long Term Evolution "LTE"

In the past years, mobile communications became an extended technology with a growth of users all around the world. The design of mobile technologies is no longer a matter of states or region, but it is now managed by organizations as the Third Generation Partnership Project "3GPP" with co-workers worldwide. Nowadays we have been through three generations of mobile communications, 1G with the GSM technology [38], 2G with the apparition of data traffic thanks to GPRS/EDGE techniques [38] and the first broadband technology the 3G composed with UMTS enhancement [39]. The next generation, the 4G, is therefore the LTE although some fellows are claiming that the first release of LTE (release 8) is not the real 4G but a "3.9G" and that the 4G comes with the LTE release 10, LTE-A for LTE Advanced. Nevertheless, LTE and LTE-A are not different systems, and LTE-A is not the ending point of the 4G evolution [4]. In this section, we present an overview on the LTE background and the challenges faced by this technology. Then we present a detailed study on the key LTE technologies used in this thesis.

3.1.1 Background of the LTE and challenges

Global System for Mobile communications "GSM" is a telephony system developed in Europe in the 80's based on TDMA and it is the first generation of narrowband standards. The service proposed by this standard is only a voice service with an analogical modulation. With the second generation 2G, the first data service, Short Message Service "SMS", a text messaging service is provided. The 2G is still a GSM standard based system with new services, the modulation is now digital in addition of a vocoder and Roaming which provide

a handover between different network operators. General Packet Radio Services "GPRS" technology to transmit data packets over cellular systems is introduced in the 90's and it is referred as the 2.5 G.

Wideband CDMA is the key feature in the next generation of cellular networks the 3G. UMTS is a WCDMA based standard component of the International Mobile Union (IMT-2000). Developed by the 3GPP consortium, it achieves a better spectral efficiency and provides a greater bandwidth. At the beginning, 3G includes data services over packet-switched and circuited-switched bearers and voice and video services over circuit switched bearers with high data rates. High Speed Downlink Packet Access and High Speed Uplink Packet Access "HSDPA/HSUPA" brought new horizons to 3G and higher data rates, this enhancement of 3G is referred as "3.5G".

The LTE is the successor of the UMTS norm, standardized by the 3GPP consortium. It aims to bring new technology to optimize the radio communications by improving flow rates, latency and spectral efficiency and allow more coverage than previous standards. LTE has a simplified architecture, the UE (e.g. mobile terminal User Equipment) accesses faster to the core network. LTE classical systems distinguish between three principal entities:

- User's Equipment "UE": any device used by an end-user to communicate (mobile phones, laptops etc...),
- Evolved Node B "eNB": the base transceiver station,
- Evolved Packet Core Network "EPC": the core network.

The EPC has no access to the circuit switched domain but only to the packet switched domain, this makes it an important evolution from the core network used for previous standards.
Several entities compose the EPC, as shown in the Figure 2.3 above, we describe some of them in the following:

- The Mobility Management Entity "MME" is responsible of connection/release of bearers to a terminal, handling of IDLE to ACTIVE transitions, and handling of security keys. It is part of the Non-Access Stratum "NAS" meaning that this entity is operating between the EPC and the terminal in comparison of the Access Stratum "AS" which is operating between the terminal and the radio access network "RAN".
- The Serving Gateway "SGW" connects the EPC to the LTE RAN. The SGW acts as a mobility anchor for handover procedures, and also as a mobility anchor for others 3GPP technologies.
- The Packet Data Network Gateway "PGW" connects the EPC to the internet. The PGW is as well in charge of allocating the IP address to a UE, it is also a quality of service "QoS" enforcement according to the policy controlled by the Policy and Charging Rules Function "PCRF". The PGW is as well the mobility anchor for non 3GPP technologies connected to the EPC.

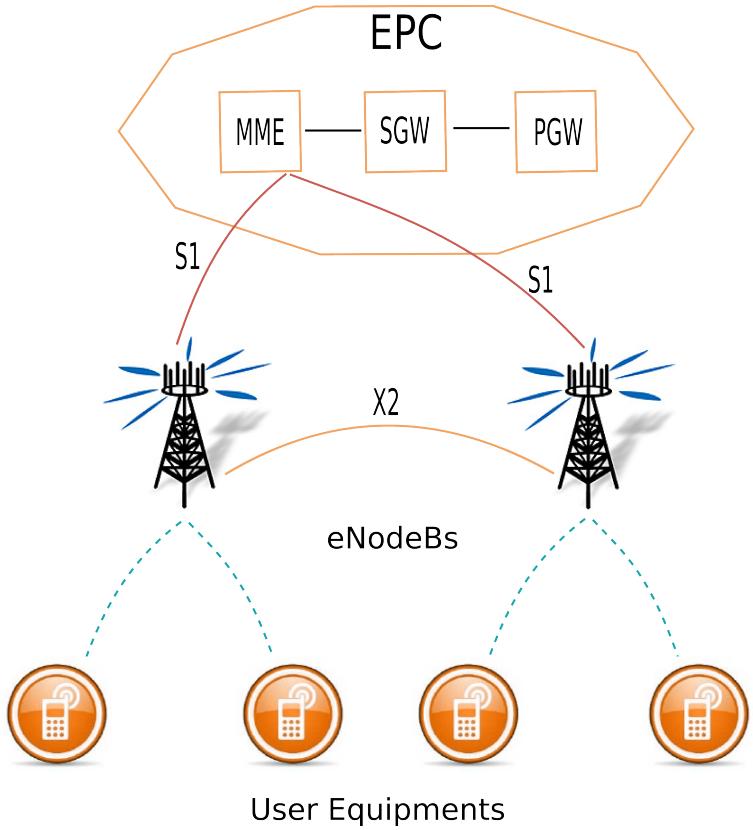

Figure 2.3: LTE system architecture

3.1.2 Downlink : Orthogonal Frequency Division Multiple Access "OFDMA"

The term Orthogonal Frequency Division Multiple Access "OFDMA" refers to the use of Orthogonal Frequency Division Multiplexing "OFDM" as multiple access scheme for simultaneous frequency-separated transmissions between multiple equipments. In LTE, OFDMA is applied on the downlink, thus the overall set of subcarriers available at the eNodeB in each OFDM interval are used for the transmission to different equipments, see Figure 2.4 below. OFDM [6] was first used in the WiMAX standard in 2005. It is a kind of multi-carrier transmission but it differs from basic multi-carrier transmission by the use of a very large number of narrowband subcarriers while straight forward multi-carrier transmissions use a few number of subcarriers with wide bandwidths and a tight subcarrier spacing $\Delta f = 1/T_u$. T_u refers to the subcarrier modulation symbol. A mathematical illustration of a basic OFDM modulator considers a bank of N_c complex modulators, each modulator corresponding to one OFDM subcarrier. Thus an OFDM signal $x(t)$ during a time interval $mT_u \leq t < (m+1)T_u$ can be expressed as:

$$x(t) = \sum_{k=0}^{N_c-1} x_k(t) = \sum_{k=0}^{N_c-1} a_k^{(m)} e^{j2\pi k\Delta f t} \tag{2.1}$$

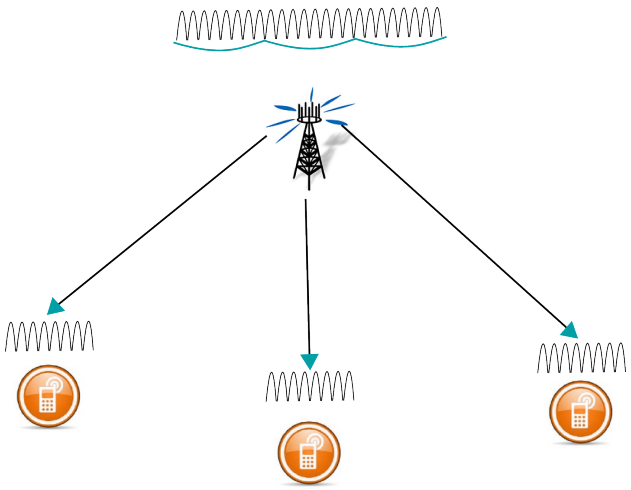

Figure 2.4: OFDMA in a downlink LTE system

where $x_k(t)$ is the k^{th} modulated subcarrier with $f_k = k \cdot \Delta f$ and $a_k^{(m)}$ is the complex modulation symbol of the k th modulated subcarrier the OFDM symbol interval m. In the LTE standard the subcarrier spacing is of 15 kHz. As an example, the order of subcarriers in the case of a bandwidth of 10 MHz is 300 subcarriers. Two modulated OFDM subcarriers are mutually orthogonal over the time interval $m T_u \leq t < (m+1) T_u$, therefore the OFDM transmission is similar to a set of orthogonal functions defined as:

$$\phi_k(t) = \begin{cases} e^{j2\pi k \Delta f t} & 0 \leq t < T_u \\ 0 & \text{otherwise} \end{cases}$$

OFDM enables low complexity implementation by use of Fast Fourier Transform "FFT" [40] processing. We consider a sampled OFDM signal and assume a sampling rate f_s as a multiple of the subcarrier spacing Δf as $f_s = 1/T_s = N \cdot \Delta f$, where T_s is the sampling time interval and N chosen in order to respect the Nyquist-Shannon sampling theorem [40] i.e. N should respect $N \cdot \Delta f > 2 N_c \Delta f$ which implies that N should exceed sufficiently N_c. Therefore the sampled OFDM signal is expressed as:

$$x_n = x(n T_s) = \sum_{k=0}^{N_c-1} a_k \, e^{j2\pi \, k \Delta f n T_s} = \sum_{k=0}^{N_c-1} a_k \, e^{j2\pi k n/N} = \sum_{k=0}^{N-1} a'_k \, e^{j2\pi k n/N} \tag{2.2}$$

where,

$$a'_k = \begin{cases} a_k & 0 \leq k < N_c \\ 0 & N_c \leq k < N \end{cases}$$

As a consequence, the time-discrete OFDM signal is the Inverse Discrete Fourier Transform "IDFT" of size N of the block of modulation symbols $a_0, \ldots, a_{N_c-1}$ is extended with zeros to length N. If N is chosen equal to 2^m with an integer m, the OFDM modulation can been implemented through an Inverse Fast Fourier Transform "IFFT" processing and the

demodulation by an FFT, see Figure 2.6.

3.1.3 Cyclic Prefix

During the signal propagation over a channel, the orthogonality between the subcarriers will be partly lost or even totally lost, the demodulator correlation interval for one path will overlap with the symbol of a previous path resulting in inter-subcarriers interference. Thus, Cyclic Prefix (CP) insertion is used in ODFM in order to deal with this matter, it increases the OFDM symbol's length of T_{CP}, the length of the cyclic prefix. The last part of the OFDM symbol is copied and inserted at the beginning of the symbol. This process makes the OFDM signal resistant to the time-dispersion while the length of the cyclic prefix is greater than the time dispersion. The drawbacks of the cyclic prefix is a power loss in the demodulation and a loss of bandwidth, thus a trade-off should be find while choosing the length of the cyclic prefix. Figure 2.5 illustrates the CP processing.

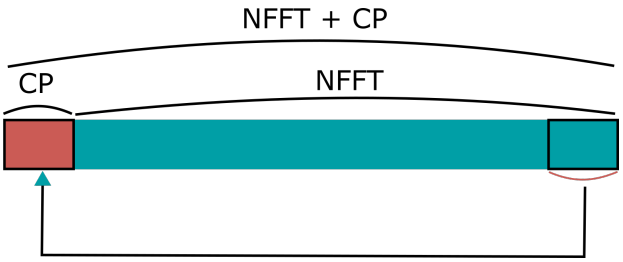

Figure 2.5: Cyclic prefix processing

3.1.4 Uplink : Single Carrier-Frequency Division Multiple Access "SC-FDMA"

Single Carrier - FDMA is linearly precoded OFDMA transmission processing, it differs from OFDMA by an additional FFT/IFFT previously to the OFDMA modulation/demodulation processing. It results in a multiple access among users by assigning different users to different sets of non-overlapping subcarriers. The term "Single Carrier" is due to the fact that SC-FDMA leads to a single carrier transmit signal. Two different subcarrier mappings can be implemented in SC-FDMA, distributed mapping an localized mapping. In distributed mapping, the FFT outputs of the input data are un-continuously assigned to subcarriers over the entire bandwidth and the remaining subcarriers amplitudes are set to zero. Interleaved SC-FDMA "I-SC-FDMA" is a particular case of distributed SC-FDMA, where the occupied subcarriers are equally spaced over the entire bandwidth. Localized SC-FDMA "L-SC-FDMA" maps the FFT outputs to a subset of consecutive subcarriers resulting in a centralization of subcarriers at only one part of the system bandwidth.

In OFDMA the parallel transmission of multiple symbols results in high Peak-to-Average Power Ratio "PAPR". By transmitting the N OFDM symbols in series at N times the rate, the SC-FDMA occupied bandwidth is the same as multi-carrier OFDMA but the PAPR

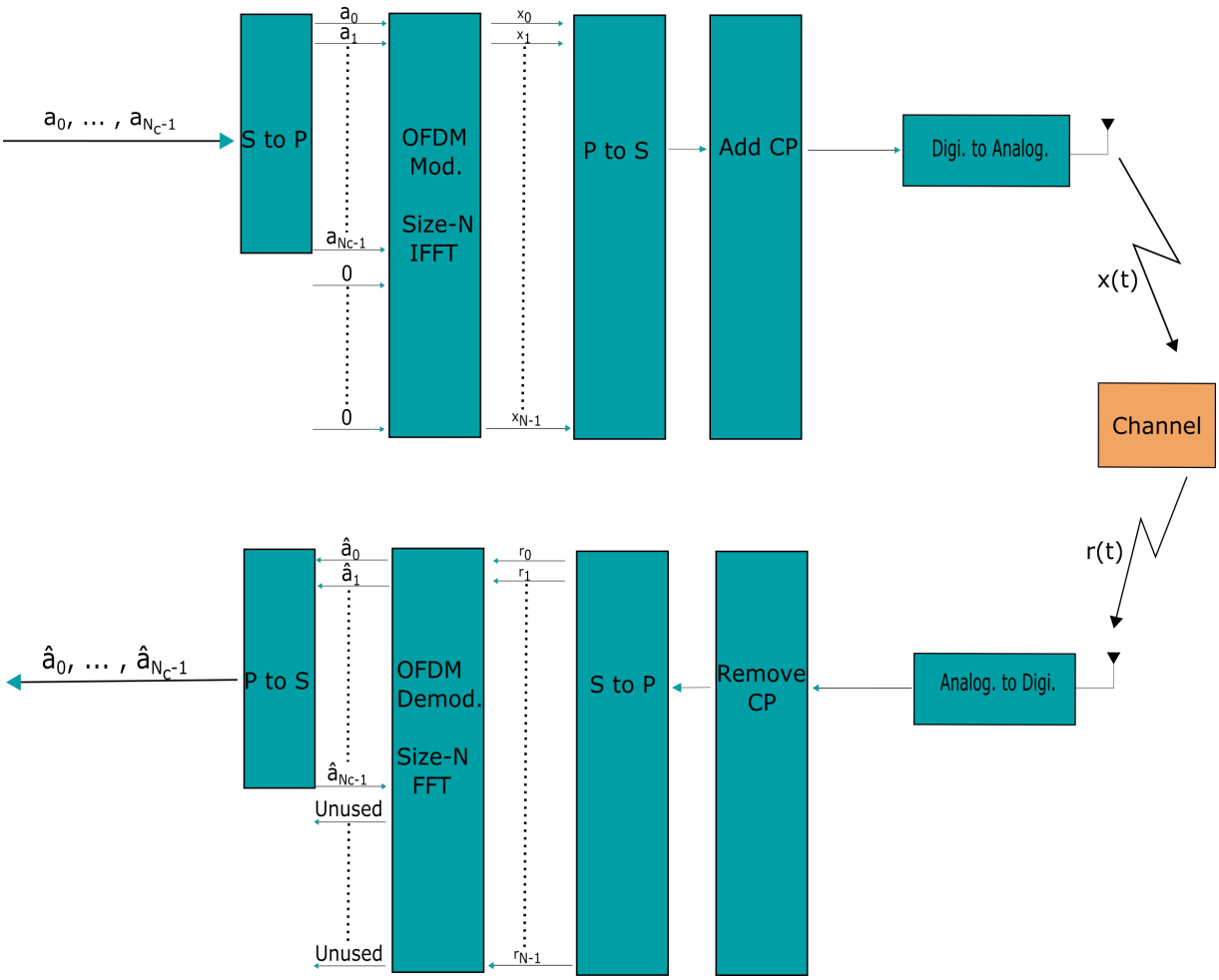

Figure 2.6: OFDM modulation and demodulation by means of IFFT/FFT processing

is the same as that used for the original OFDM symbols. Due to the mobile terminals constraints (energy economy), OFDMA and its high PAPR is not sustainable for the LTE uplink, thus SC-FDMA which reduces the PAPR level is employed. Several studies [41] show that the overall performances in terms of PAPR of L-SC-FDMA are better than I-SC-FDMA, thus the L-SC-FDMA is the mapping that was chosen to be implemented in 3GPP LTE release 8.

SC-FDMA enables multiplexing of users with unequal bandwidth assignment. Figure 2.7 illustrates the case where three users are multiplexed over a single carrier. Each user of respectively a modulation symbols length of M_1, M_2 and M_3 are applied to a $M_2 > M_1 > M_3$ FFT block size.

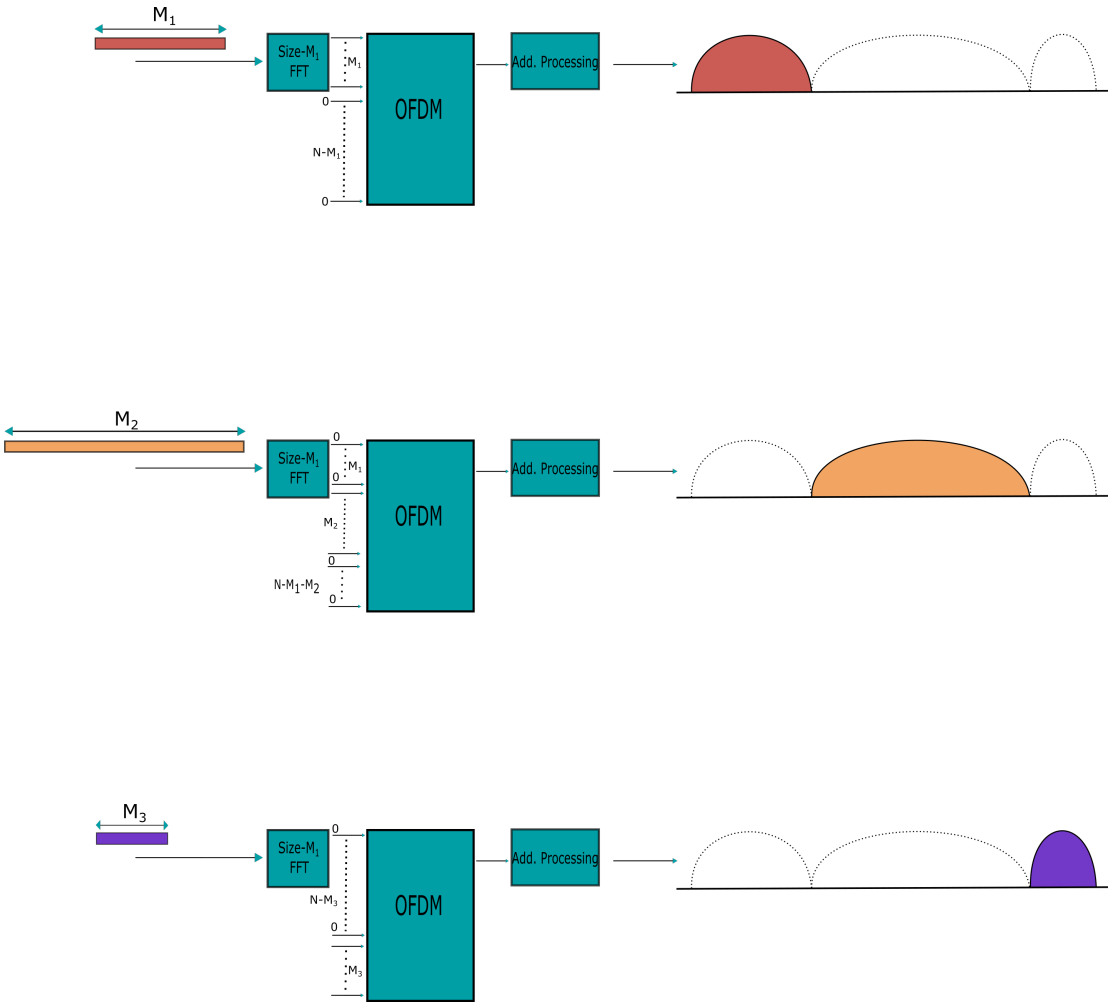

Figure 2.7: Uplink users multiplexing with unequal bandwidth assignment via a L-SC-FDMA processing

3.1.5 Resource Management

One of the main goals of the LTE standard developers is to ensure very high data rates and system performances within the network. Resource management is a key point to enhance the system performances and thus to increase the data rates in order to achieve high system throughput. As we said above, the LTE downlink and uplink transmission schemes are based on OFDM processing. Thanks to this scheme the scheduler has access to the time and frequency domains which ensure shared channel transmission schemes by allocating a specific time instant and frequency region to the best user. This scheduling is known as "Channel-dependent scheduling", the best user is the user experiencing the best channel conditions at a time instant and for a frequency region. Rate adaptation is a functionality of this scheduler, for each transmission it decides the data rate to be used.

In the following we provide on overview of the time-frequency the structure of the LTE

and the resource structure. As we said in the previous sequence the subcarrier spacing is a key factor of the OFDM process, the LTE OFDM subcarrier spacing is $\Delta f_{LTE} = 15$ kHz, this value appeared to be a good trade-off between the overhead from the cyclic prefix and the sensitivity to the Doppler effects constraints. The LTE time domain is divided into radio frames with a duration of $T_{frame} = 10$ ms, each organized in ten subframes of $T_{subframe} = 1$ ms length, consisting in slots of length $T_{slot} = 0.5$ ms and each slot is composed of OFDM symbols (note that the cyclic prefix is included). The LTE frame structure is illustrated in Figure 2.8 below.

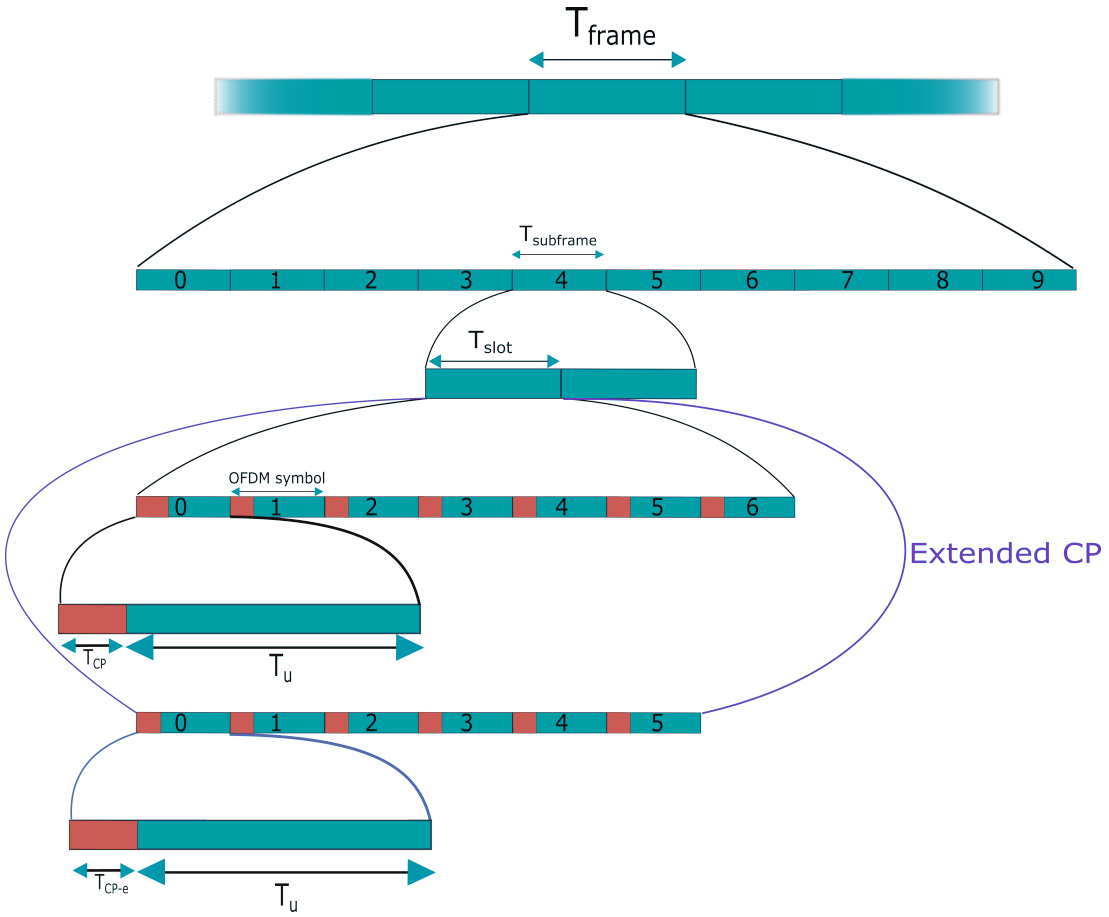

Figure 2.8: LTE time frame structure

3.1.6 Physical Resource Block

In the time-frequency domain the smallest resource in LTE is a resource element "RE" which corresponds to one OFDM symbol transmitted over one subcarrier. These resource elements are regrouped into resource blocks "RBs", illustrated in Figure 2.9, consisting of $N_c = 12$ OFDM contiguous subcarriers and one time slot duration $T_{\text{RB}} = 0.5$ ms with total bandwidth $W_{\text{RB}} = 180$ kHz. The RBs are composed by $N_s = 7$ or $N_s = 6$ OFDM

symbols respectively with normal CP and extended CP corresponding to $7 \times 12 = 84$ or $6 \times 12 = 72$ REs. Each RB carries R_{MCS} information bits. The resulting spectral efficiency in the case of normal CP is expressed as

$$\mathcal{S}_{eff} = \frac{N_s N_c}{W_{RB} T_{RB}} R_{MCS} = \frac{84}{90} R_{MCS} \text{ (b/s/Hz)}. \tag{2.3}$$

Table 2.1 presents the spectral efficiencies associated to the adopted Modulation and Coding Schemes "MCS" in LTE [4].

MCS	Code rate (b/s)	Spectral efficiency (b/s/Hz)
QPSK	1/2	0.93
QPSK	2/3	1.24
QPSK	3/4	1.86
16QAM	1/2	2.48
16QAM	3/4	2.8
64QAM	2/3	3.73
64QAM	3/4	4.2

Table 2.1: Spectral efficiency to Modulation and Coding Schemes mapping

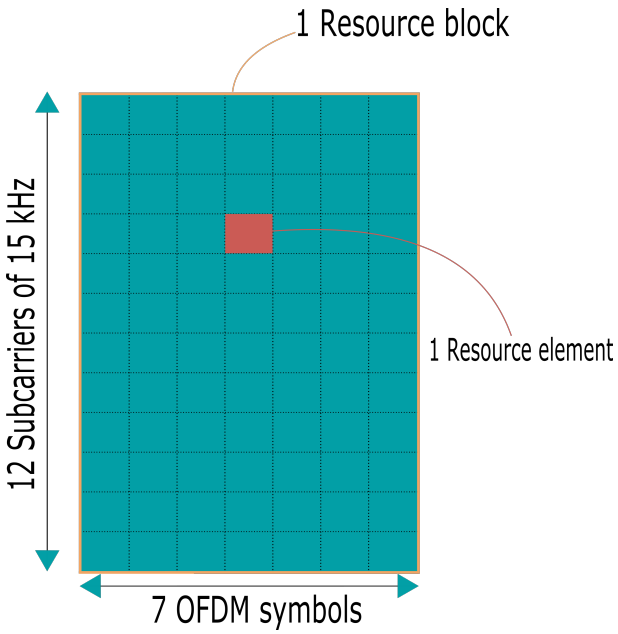

Figure 2.9: LTE resource block with normal CP, time-frequency structure

The number of RBs allowed in the LTE physical layer specification is from 6 RBs up to 100 RBs corresponding respectively to bandwidths from 1.4 MHz up to 20 MHz. Table 2.2 details the number of RBs in function of the total channel bandwidth "B".

Channel Bandwidth B (MHz)	1.4	3	5	10	15	20
Number of RBs	6	15	25	50	75	100
FFT size	128	256	512	1024	1536	2048
Number of occupied subcarriers	72	180	300	600	900	1200
Sample rate (MHz)	1.92	3.84	7.68	15.36	23.04	30.72
Samples per slot	960	1920	3840	7680	11520	15360

Table 2.2: Number of RBs in function of the bandwidth [4]

3.1.7 Carrier aggregation

LTE-A introduces more flexibility in the bandwidth allocation by enabling carrier aggregation up to five carriers, thus the total bandwidth can be as large as 100 MHz. Several Carrier Components "CC" of different width can be contiguously or non-contiguously aggregated. In order to support this aggregation, the mapping adopted in this release is now the I-SC-FDMA which allows frequency selective scheduling. Figure 2.10 illustrates this technique for CCs of 20 MHz.

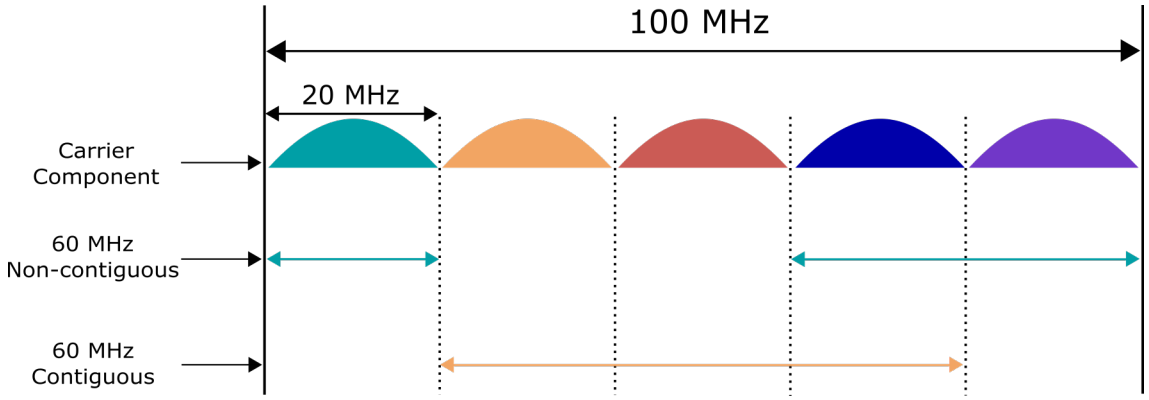

Figure 2.10: Carrier aggregation illustration

3.1.8 Multiple Input Multiple Output "MIMO" antenna scheme

Multiple Input Multiple Output "MIMO" antenna scheme is a part of the multi-antenna techniques field, employing multiple antennas at the transmitter as well as at the receiver, these techniques are used in order to improve the overall system performances as the per user data rates and the system performances. Due to the impact of the antennas spacing over the mutual correlation between the fading experienced by the different channels, the antennas distance has to be set carefully depending on the aim of the use of MIMO schemes, at a terminal side a spacing of $\lambda/2$ is sufficient to ensure uncorrelated fading, where λ is the signal wavelength. Indeed, MIMO can achieve three different goals:

- The antenna gain maximization: MIMO can be used to shape the transmitter/receiver beam in a direction, this technique is known as "Beamforming",
- "Spatial multiplexing" which consists in creating parallel channels in order to increase the spectral efficiency and thus the achievable data rate in a limited bandwidth,
- "Spatial diversity" that increases the system reliability by transmitting the signal over uncorrelated fading MIMO paths.

The different transmission modes and MIMO receivers used in this dissertation are further detailed in Section 5.

3.1.9 Relaying

For MANETs, multi-hop communications are essential to set up communications between nodes out of range. Research addressed this matter and relaying was proposed as solution. In LTE, several mechanisms are available [42].

■ Amplify and Forward "AF" relays

Also known as 'repeaters', these relay nodes amplify the received signal and forward it. The main advantages of AF relays are their simplicity, the low delay and their low cost. However a major drawback is that when the signal is amplified the noise and interferences are also amplified which causes a decrease in the SINR at the output of the repeater. Moreover, authors in [43] claim that these relays are suitable for two hops at most.

■ Decode and Forward "DF" relays

DF relays are more sophisticated relays as the decode the received signal and re-encode it prior to forwarding it. Thus, the noise and interference amplification is not a matter anymore. Furthermore these relay nodes are suitable for more than 2 hops according to [43], which improves their utility. The inconvenient of this mechanism is the larger delay and complexity implied by the decode and re-encode process.

3.1.10 Performances summary

We review in Table 2.3 the performances offered by the LTE systems.

3.2 Satellite component

This subsection presents the performances of satellite communications links and the associated computations necessary to design efficient communication schemes for our hybrid

	Downlink	Uplink
Technology	OFDMA	SC-FDMA
Peak speeds	100 Mb/s	50 Mb/s
User avg. throughput	5-12 Mb/s	2-5 Mb/s
Latency	20 ms	
Bandwidth	1.4-20 MHz	

Table 2.3: Performances of LTE systems [4]

Satellite-MANET. Performances of satellite links are evaluated in the same way than cellular communications links. However these communications links have some specificities, like thermal noise at the receiver and propagation losses, that we will expose in the following.

3.2.1 Budget link and Performances

The following Table 2.4 presents the parameters of our USAT and a satellite station in the Ku band.

■ Uplink performances:

Uplink stands for the link from the USAT to the satellite station. The carrier to noise ratio is defined as follows in function of the figure of merit $(G/T)_{Sat}$ of the satellite station:

$$(C/N_0) = EIRP_{USAT} \cdot 1/L_U \cdot (G/T)_{Sat} \cdot 1/k, \tag{2.4}$$

where $EIRP_{USAT} = P_{USAT} \cdot G_{USAT}/L_T L_{FU}$ is the effective isotropic radiated power of the USAT in W, P_{USAT}, G_{USAT}, L_T and L_{FU} being defined in Table 2.4. $L_U = L_A \cdot L_{\text{FS}}$ are the uplink losses resulting from the atmospheric losses and the free space losses respectively L_A and L_{FS}, and k is the Boltzmann constant $k = -228.6$(dBJ/K). We first compute the EIRP of the USAT: $EIRP_{USAT} = 31.5$ dB. We now compute the path attenuation $L_U = L_{\text{FS}} + L_A = 207.9$ dB. The expression of $(G/T)_{Sat}$ is,

$$(G/T)_{Sat} = \frac{(G_{sat}/L_R L_{FSAT} L_{POL})}{T_A/L_{FSAT} + T_F(1 - 1/L_{FSAT}) + T_{RX}} \ (\text{dB.K}^{-1}), \tag{2.5}$$

where $G_{sat} = \eta(70\pi/\theta_{3dB})^2 = 38.2$ dBi and the reception losses $L_R = 12(\theta_R/\theta_{3dB})^2 = 3$ dB, with $\theta_R = \theta_{2dB}/2$. Assuming $L_{POL} = 0$ dB, we obtain:

$$(G/T)_{Sat} = 38.2 \ \text{dB.K}^{-1},$$

and

$$(C/N_0) = EIRP_{USAT} - L_U + (G/T)_{Sat} - k = 58.81 \ \text{(dBHz)}$$

Satellite	
Carrier frequency	12 GHz
Max Tx power	$P_{TX} = 40$ dBm
Loss between amplifier and antenna	$L_{FSAT} = 1$ dB
Transmitting beam half power angular width	$\theta_{3dB} = 2°$
Antenna efficiency	$\eta = 0.55$
Distance to earth	$R = 40000\ km$
Receiver noise figure	$F = 3\ dB$
USAT	
Carrier frequency	14.25 GHz
Max Tx Power	$P_{USAT} = 23$ dBm
Antenna gain	$G_{USAT} = 39$ dBi
Elevation Angle	$\phi_{USAT} = 30°$
Maximum pointing error	$\theta_T = 0.1°$
Gain/Temperature	16 dB/K
Receiver noise figure	$F = 3$ dB
Ground noise temperature	$T_{GROUND} = 45\ K$
Diameter	$D = 75$ cm
Loss between antenna and receiver	$L_{FU} = 0.5\ dB$
Transmission loss	$L_T = 0.3$ dB
Atmospheric attenuations	
Clear Sky	$L_A = 0.3$ dB
Rain	UL: $L_A = 10.3$ dB; DL: $L_A = 7.3\ dB$

Table 2.4: System Parameters

■ Downlink performances:
Downlink stands for the link from satellite station to the USAT, the carrier to noise ratio becomes:

$$(C/N_0) = EIRP_{Sat} \cdot 1/L_D \cdot (G/T)_{USAT} \cdot 1/k \tag{2.6}$$

where $L_D = L_A + L_{\mathrm{FS}}$ are the total link losses dB.

$$EIRP_{SAT} = G_{USAT} + P_{USAT} - L_T - L_{FSAT} = 47.2 \ \text{(dB)}$$

with $L_T = 3$ dB, $L_{\mathrm{FS}} = 206.1$ dB and $L_D = 206.4$ (dB).
The downlink system noise temperature is $T_{SKY} = 8°$ (K) for f = 12 GHz at 30° elevation, and $T_{GROUND} = 45$ K then $T_A = T_{SKY} + T_{GROUND} = 53$ (K), finally,

$$T_D = T_A/L_{FUSAT} + T_F(1 - 1/L_{FUSAT}) + T_{RX} = 153.9 \ \text{(K)},$$

and,

$$(C/N_0) = EIRP_{SAT} - L_D + (G/T)_{USAT} - k = 58.81 \text{ (dBHz)}.$$

3.2.2 Satellite Orbits

Geocentric orbits refer to orbits around the planet Earth, these orbits are commonly classified in function of their altitudes in three types enumerated below and illustrated in Figure 2.11, Geostationary Earth Orbits "GEO", Medium Earth Orbits "MEO" and Low Earth Orbits "LEO". The satellite orbit determines the observation time for an earth terminal at

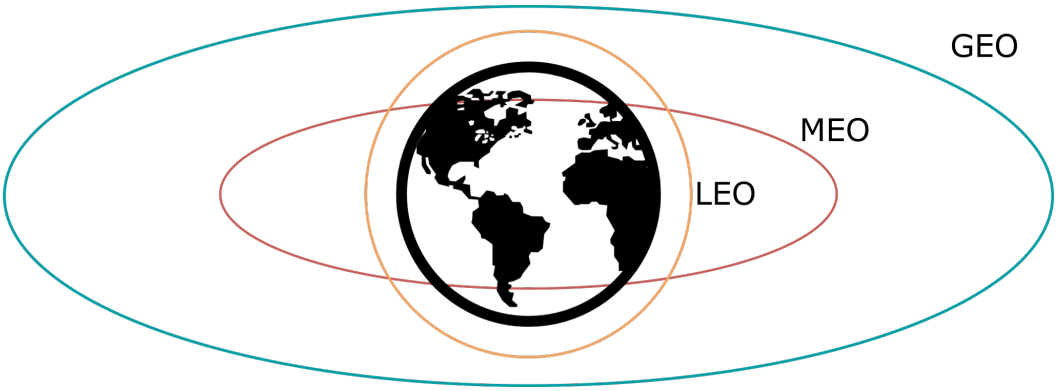

Figure 2.11: Types of satellite orbits

a fixed location and the end-to-end delays for GEO, MEO and LEO satellites [44]. We summarize in Table 2.5 the typical values of the observation time, the altitude intervals and the propagation delays for each orbit type. Hence GEO satellites are the only equipments

Orbit	Orbit altitude (km)	Observation time	Maximum delay (ms)
GEO	35 786	24 h	280
MEO	10 000-20 000	1-2 h	80-120
LEO	160-1500	8-10 min	20-60

Table 2.5: Orbits properties [5]

enabling an operability of 24 hours. If continuous coverage is required, a constellation of multiple satellites is needed, with links between the satellites. For example, Figure 2.12 shows the Iridium satellite system [2] composed of a 66 LEO satellites constellation.

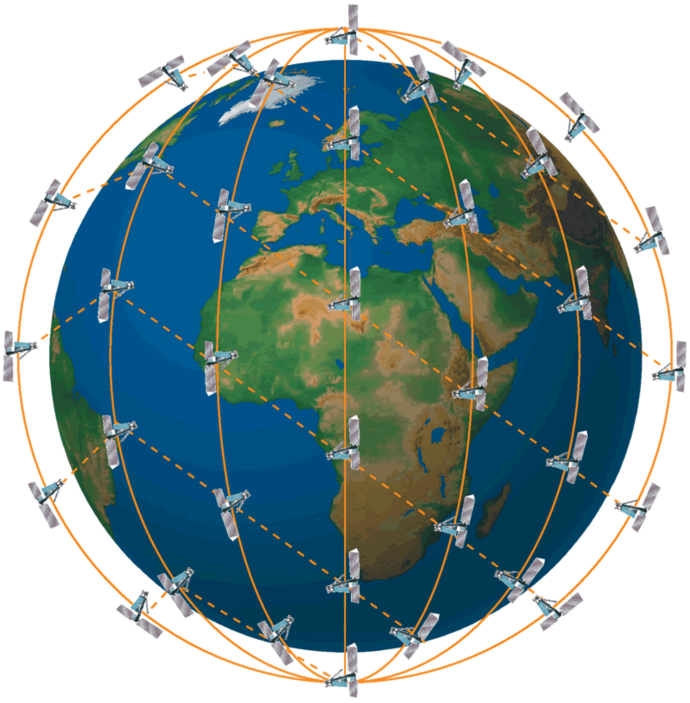

Figure 2.12: Iridium LEO satellites constellation [2]

4 Maritime wireless channel and Cellular networks

In this section we focus on the channel variation in a maritime context and introduce the maritime path loss model used in this thesis, finally we review briefly the modeling of random channel variations experienced during the signal propagation.

4.1 Maritime Propagation: ITU-R recommendation path loss model

Maritime communication paths are subject to different types of losses during the signal propagation. The complexity in the design of a model propagation for this context resides in the large amount of elements to consider. Path loss propagation models can be classified in two types: empirical and deterministic model. The first group are models derived after measurements taken in a particular environment, like Okumura-Hata's [45] model proposed for an urban environment, the second group is based on mathematical expressions taking into account some events and states without any random parameter. Usually, researchers use a deterministic model when there is one available and compares it to the measures in order to evaluate the accuracy of the model. In the case of maritime propagation, two deterministic models are available in literature in order to estimate the attenuation of the signal in an open sea environment the Plane Earth Loss "PEL" model and the Round Earth Loss "REL" model. The PEL [46] is a model designed for the case where the transmitter and the receiver are above a plane reflective ground, which shares similarities with a

maritime environment, while the REL [47] is a more complex geometrical model considering the geometric aspects of the earth surface and their impact on the signal propagation for long distances. An empirical model for maritime propagation path loss determination is introduced by the International Telecommunication Union "ITU" [3] which consists in a method to interpolate/extrapolate the path loss from empirically derived field-strength curves as functions of distance, antenna height and frequency. In this dissertation we opted for the use of the ITU-R model for its accuracy, we first review the general model and then we introduce the linear path loss expression derived from this model.

4.1.1 ITU-R recommendation on maritime propagation path loss

The International Telecommunication Union sector responsible of radio-communications "ITU-R" delivers in its recommendation a method based on interpolation/extrapolation from empirically derived field-strength curves as functions of distance, antenna heights and frequency for point to area radio propagation predictions for terrestrial communications. The field measures curves statistically capture the behavior of the field strength for fields exceeded for 50%, 10% and 1% percentage of time. The measurements parameters are:

- Frequency range: 30 MHz to 3000 MHz
- Effective antenna heights: Up to 3 000 m
- Path length: Up to 1000 km

Figure 2.13 is an example of the available curves in [3] for a frequency of 600 MHz and for fields exceeded for 50% of time in a temperate sea environment.
The provided propagation curves represent field-strength values for 1 kW effective radiated power "e.r.p." at frequencies of 100, 600 and 2 000 MHz, respectively, as a function of sea paths. Interpolation or extrapolation of the values obtained at these frequencies should be used to obtain field-strength values for any given required frequency using the provided method. The sea-path curves were derived from measured data obtained mainly from the Mediterranean and the North Sea regions. We express the basic transmission path loss in function of the transmitted and received power, respectively P_t and P_r in W, as

$$\ell_{\text{ITU}}(h, f, d) = \frac{P_t}{P_r}, \tag{2.7}$$

where is the transmitted power in dB and $\ell_{\text{ITU}}(h, f, d)$ is the basic transmission loss. This received power can also be expressed in function of Z_m the characteristic impedance in a maritime environment and empirically derived in Ohms, $E_r(h, f, d)$ the field strength in $\mu V/m$ as,

$$P_r = \frac{E_r^2(h, f, d)}{Z_m} A_r \quad (W), \tag{2.8}$$

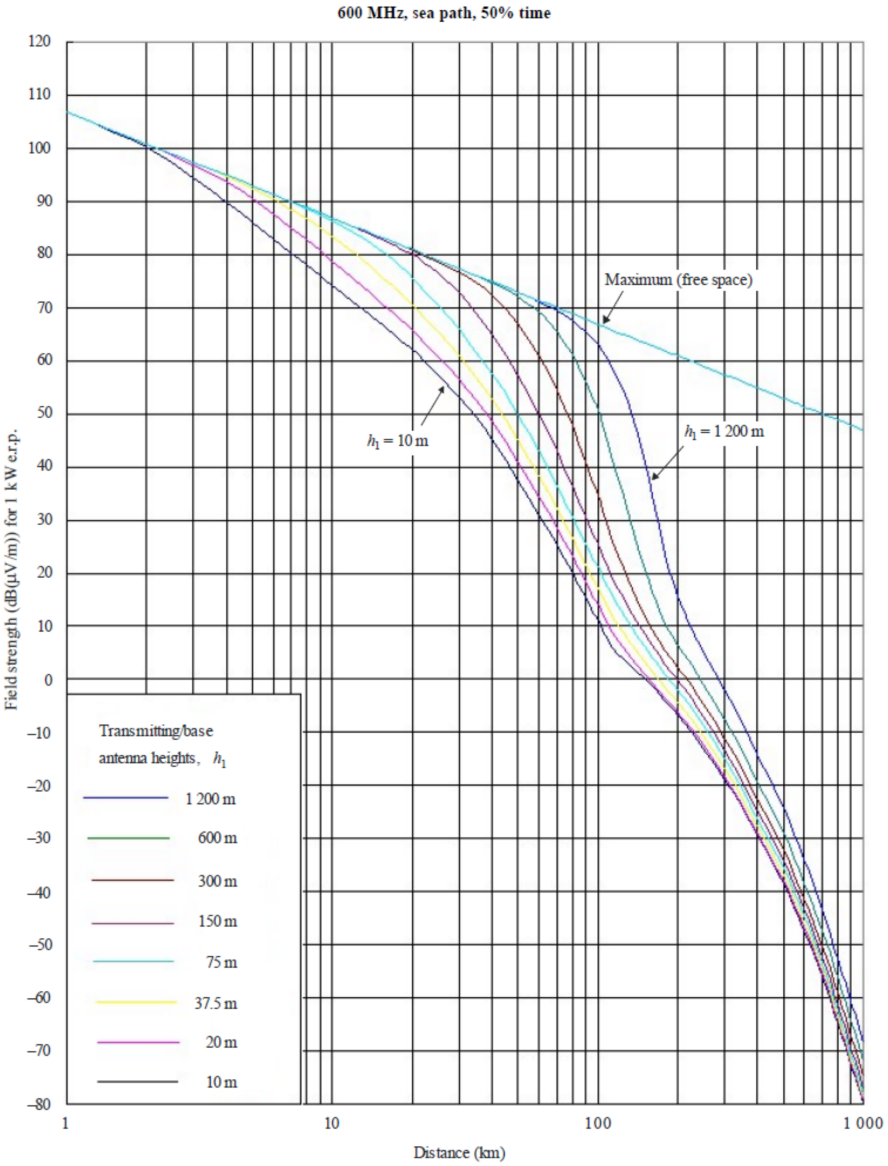

Figure 2.13: Field strength curves example [3]

where $A_r = \frac{\lambda^2}{4\pi}$ m^2 is the antenna effective cross section with λ is the signal wavelength (m). Hence, by replacing P_r in (2.7) by its expression in (2.8) the basic transmission loss equivalent to a given measured field strength is given by,

$$\ell_{\text{ITU}}(h, f, d) = \frac{P_t Z_m}{E_r^2(h, f, d) A_r} = \frac{P_t Z_m 4\pi}{c^2} \cdot \frac{f^2}{E_r^2(h, f, d)},$$

finally in logarithmic scale the final expression of the basic transmission path loss for $P_t = 1kW$ e.r.p is,

$$\ell_{\text{ITU}}(h, f, d) = 139 - E_r(h, f, d) + 20 \log_{10}(f) \ \text{(dB)}, \tag{2.9}$$

where E_r field strength (dB($\mu V/m$)) for 1 kW e.r.p. To find the values of the field strength for the figures we follow the interpolation/extrapolation method below proposed within the recommendation. If the value of h_1 coincides with one of the eight heights for which curves are provided, the required field strength can be obtained directly from the plotted curves Otherwise the required field strength should be interpolated or extrapolated from field strengths obtained from two curves as follows:

$$E_r(h, f_n, d) = E_r(h_{\text{inf}}, f_n, d) + \Big(E_{r,\text{sup}}(h_{\text{sup}}, f_n, d) - E_r(h_{r,\text{inf}}, f_n, d)\Big) \frac{\log_{10}(h/h_{\text{inf}})}{\log_{10}(h_{\text{sup}}/h_{\text{inf}})},$$

where $E_r(h_{\text{inf}}, f_n, d)$ and $E_r(h_{\text{sup}}, f_n, d)$ are respectively the empirical field-strength values for h_{inf} and h_{sup} at nominal frequencies $f_n = f_{\text{inf}}$ and $f_n = f_{\text{sup}}$ given in Figure 1 of [3].

- h_{inf}: 600 m if h1 $>$ 1 200 m,
- h_{sup}: 1200 m if h1 $>$ 1 200 m,
- $E_r(h, f_{\text{inf}}, d)$: field-strength value for h_{inf} at the required distance,
- $E_r(h, f_{\text{sup}}, d)$: field-strength value for h_{sup} at the required distance.

Field-strength values for the required frequency should be obtained by interpolating between the values for the nominal frequency values of 100, 600 and 2000 MHz. In the case of frequencies below 100 MHz or above 2 000 MHz, the interpolation must be replaced by an extrapolation from the two nearer nominal frequency values. For sea paths where the required frequency f is the range $f_{\text{inf}} \leq f \leq f_{\text{sup}}$, the field strength is calculated by interpolation and extrapolation as follows:

$$E_r(h, f, d) = E_r(h, f_{\text{inf}}, d) + \Big(E_r(h, f_{\text{sup}}, d) - E_r(h, f_{\text{inf}}, d)\Big) \frac{\log_{10}(f/f_{\text{inf}})}{\log_{10}(f_{\text{sup}}/f_{\text{inf}})}.$$

- f: frequency for which the prediction is required (MHz)
- f_{inf}: lower nominal frequency (100 MHz if f $<$ 600 MHz, 600 MHz otherwise)

- f_{sup}: higher nominal frequency (600 MHz if f $<$ 600 MHz, 2000 MHz otherwise)
- $E_r(h, f_{\text{inf}}, d)$: field-strength value for f_{inf}
- $E_r(h, f_{\text{sup}}, d)$: field-strength value for f_{sup}.

4.1.2 Linear model resulting from the interpolation of the field strength measures

Finally, the linear path loss model, for a circular area of radius R, is expressed in function of the distance d and the percentage of time p as

$$\ell(h, f, d) = \ell_{\text{FS}} \mathbb{1}_{\{d \leq d_{c,0}\}} + \ell_{\text{m}}^{p} \mathbb{1}_{\{d_{c,0} \leq d \leq R\}}, \tag{2.10}$$

where $\ell_{\text{FS}} = \alpha_{\text{FS}} d^{\gamma_{\text{FS}}}$ is the free space path loss, $d_{c,0}$ is the critical distance expressed in km defined in [47], the limit distance above which the free space path loss model become invalid, in function of the transmitter and receiver heights h_t and h_r, and the wavelength λ as,

$$d_{c,0} = \frac{4 h_t h_r}{\lambda} \text{ (km)},$$

and $\ell_{\text{m}}^{p}(h, f, d)$ is the the maritime path-loss propagation given by:

$$\ell_{\text{m}}^{p}(h, f, d) = \alpha_{m,1}^{p} d^{-\gamma_{m,1}^{p}} \mathbb{1}_{\{d_{c,0} \leq d \leq d_{c,1}\}} + \alpha_{m,2}^{p} d^{-\gamma_{m,2}^{p}} \mathbb{1}_{\{d_{c,1} \leq d \leq 2R\}}, \tag{2.11}$$

with $d_{c,1} = 5$ km. The following Table 2.6 resumes the attenuation factors and the distance exponents for the free space and the maritime propagation models with different percentage of time p, a frequency of 800 MHz and antenna heights as $h_t = h_r = 12$ m.

Maritime			
	ITU-R 50%	**ITU-R 10%**	**ITU-R 1%**
$\alpha_{m,1}$	1.28×10^{-9}	1.23×10^{-9}	1.11×10^{-9}
$\gamma_{m,1}$	2.9	2.8	2.53
$\alpha_{m,2}$	6×10^{-9}	4.38×10^{-9}	3.17×10^{-9}
$\gamma_{m,2}$	3.9	3.57	3.23
Free space			
α_{FS}	0.89×10^{-9}		
γ_{FS}	2		

Table 2.6: Propagation coefficients

Figure 2.14 represents the path loss in a maritime environment computed for $h_t = h_r = 12$ m and a frequency $f = 800$ MHz. It can be seen that the free space propagation path loss is lower than the maritime one above the critical distance as expected. We notice also that the maritime propagation path loss increases with the percentage of time p, thus the reference model as to be chosen with accuracy by the network designer in function of the

context. We discuss in Chapter 4 the impact of this fluctuation on the network resource dimensioning.

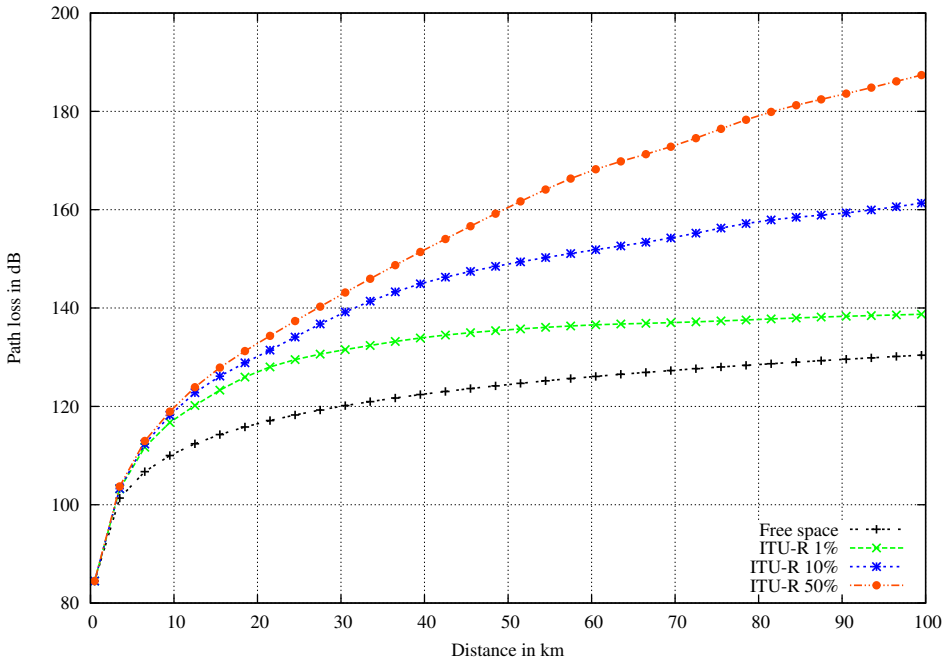

Figure 2.14: Path losses as a function of distances

4.2 Random channel variation

In wireless communications, the signal is subject to several random fluctuations due to the propagation environment. These fluctuations are divided in two categories, the first one is the log-normal shadowing resulting from the distortion experienced by the signal due to random obstacles encountered on the propagation path. In a maritime environment, these obstacles are quasi non-existent and thus the shadowing effects will be neglected in this dissertation. The second category of fluctuations that affects the signal is the so calling multi-path fading resulting from multi-path propagation. At the receiver side, the signal arriving results from a superposition of signals due to the scatters and reflectors encountered. This superposition of several signals experiencing different paths may be constructive or destructive. In literature, several stochastic models for fading coefficients are available depending on the propagation context. The channel coefficients are considered as independent and identically "i.i.d." distributed Gaussian random variables.

4.2.1 Fading model

In case of line of sight "LOS" path between the transmitter and the receiver, the amplitude of the received signal is modeled following a Rician [48] distribution with PDF expressed as,

$$f(x) = \frac{2x(K+1)}{\Omega} \exp\left(-K - \frac{(K+1)x^2}{\Omega}\right) I_0\left(2x\sqrt{\frac{K(K+1)}{\Omega}}\right), \; x \geq 0, \tag{2.12}$$

where $I_0(x) = \frac{1}{2\pi}\int_0^{2\pi} e^{x\cos\theta} d\theta$ is the zero-order modified Bessel function [49], Ω is the average received power and K is the Rician factor [50].

At the contrary when the propagation path is non LOS, the channel coefficients are still assumed i.i.d. Gaussian random variables, but with zero-mean. The amplitude of the received signal in this case is modeled by a Rayleigh distribution [51] with PDF expressed as,

$$f(x) = \frac{2x}{\Omega} \exp\left(-\frac{x^2}{\Omega}\right), \; x \geq 0, \tag{2.13}$$

Note that this distribution corresponds to the case where the Rician factor K is null in (2.12) which is also the worst case. We plot in Figure 2.15 the CDFs of the Rice distribution for different values of K including the Rayleigh case ($K = 0$). At a first glance, propagation

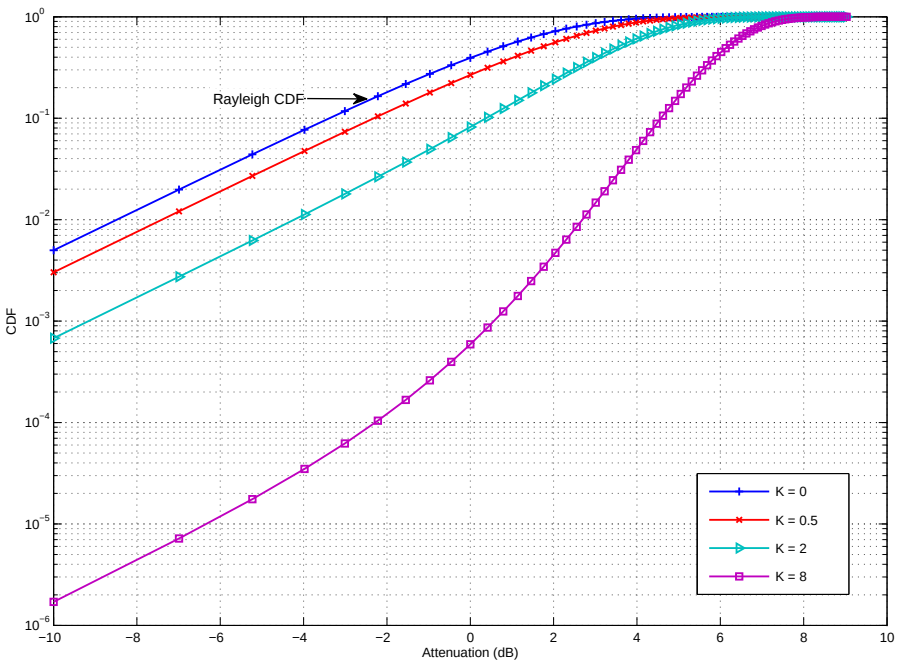

Figure 2.15: Rice distributions for different values of K

on a maritime environment seems to be in a line of sight. However, as we are targeting long propagation distance between ships (in the order of 10 km), the first Fresnel zone [40] delimited by $r = \frac{\sqrt{\lambda d}}{2} = 21.65$ m (λ being the wavelength) is obstructed for antenna heights of 12 m and a frequency of 800 MHz, as illustrated in Figure 2.16. This results in a non line of sight propagation path and thus the multi-path fading will be modeled as a Rayleigh random variable in the scope of this work.

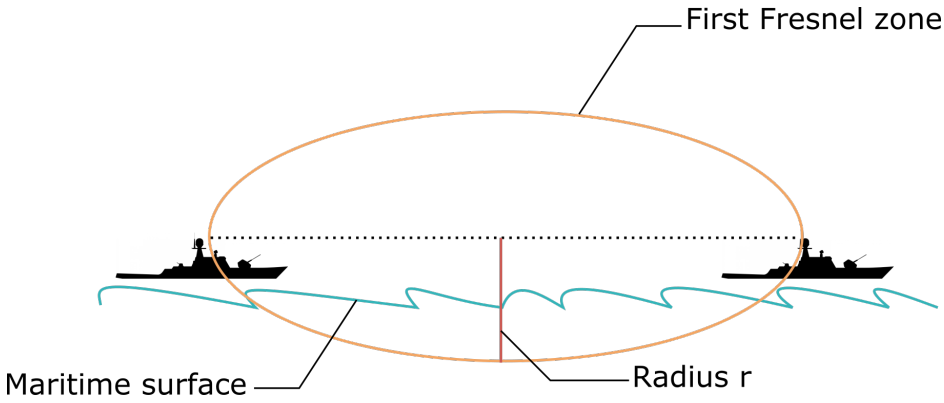

Figure 2.16: First Fresnel zone obturation

5 Information Theory Principles

In this section we present the information theory principles used in this dissertation to model the channel and its performances.

5.1 Single Input Single Output schemes

5.1.1 Channel Modeling

As we said earlier in Section 4, the multi-path fading is modeled by a complex Gaussian random variable as,

$$h = re^{j\theta} \sim \mathcal{CN}(0, \sigma_f^2),$$

where r is Rayleigh distributed with PDF,

$$p(r) = \frac{r}{\sigma_f^2} e^{-\frac{r^2}{2\sigma_f^2}}. \tag{2.14}$$

and θ the phase of h is uniformly distributed over the range $[0, 2\pi]$. The received signal y is expressed in function of the emitted signal s as,

$$y = hs + \eta \tag{2.15}$$

where $\eta \sim \mathcal{CN}(0, N_0)$ is the additive noise also modeled as a complex Gaussian random variable with variance N_0. Claude Shannon in 1948 showed that the maximal data rate R_d over a radio channel is upper-bounded by a certain capacity referred as Shannon capacity [6] defined below. Above this capacity the communication is no longer reliable.

$$C_{SISO} = \log_2(1 + SNR|h|^2), \tag{2.16}$$

where $SNR = \frac{P_t}{N_0}$ is the signal to noise ratio in function of the transmission power P_t. In the following we introduce the multiplexing gain corresponding to the maximal number of symbols transmitted simultaneously over a channel and defined as,

$$r = \lim_{SNR \to \infty} \frac{C}{\log_2 SNR}. \tag{2.17}$$

5.2 Multiple Input Multiple Output schemes

5.2.1 Channel State information

Four types of Channel State Information "CSI" knowledge are available:

- CSI at the receiver only "CSIR",
- CSI at the transmitter only "CSIT",
- CSI at both transmitter and receiver referred as full CSI.

CSIT is obtained by feedback or channel estimation in case of reciprocity while training sequences are used to estimate the CSIR. CSI is a critical factor for the characterization of a fading channel, hereinafter, we focus on the CSIR case. We present the MIMO architecture, then define the channel capacity in this case and focus on the diverse receivers designs available to estimate the signal.

5.2.2 MIMO architecture

Figure 2.17 illustrates a MIMO communication scheme [52] for n_t transmission antennas and n_r reception antennas, $h_{n_t n_r}$ represents the respective channel coefficients on the link $n_t \to n_r$ and η_{n_r} the additive noise at the receiver. Hence the received signal is mathematically expressed as,

$$\begin{bmatrix} y_1 \\ y_2 \\ \vdots \\ y_{n_r} \end{bmatrix} = \begin{bmatrix} h_{11} & h_{12} & \dots & h_{1n_t} \\ h_{21} & h_{22} & \dots & h_{2n_t} \\ \vdots & \vdots & \ddots & \vdots \\ h_{n_r 1} & h_{n_r 2} & \dots & h_{n_t n_r} \end{bmatrix} \cdot \begin{bmatrix} s_1 \\ s_2 \\ \vdots \\ s_{n_r} \end{bmatrix} + \begin{bmatrix} \eta_1 \\ \eta_2 \\ \vdots \\ \eta_{n_t n_r} \end{bmatrix} \tag{2.18a}$$

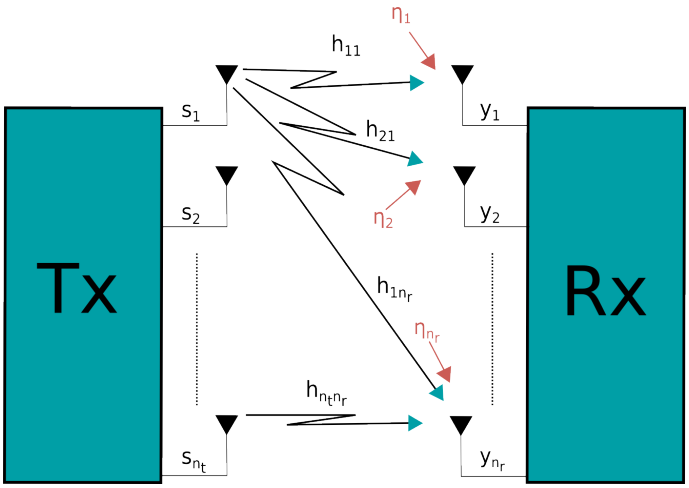

Figure 2.17: $n_t \times n_r$ MIMO antennas configuration

$$\mathbf{y} = \mathbf{H}\mathbf{s} + \eta \tag{2.18b}$$

The Shannon capacity of this MIMO channel is expressed as:

$$C_{MIMO} = \max_{\mathbf{K}_s : Tr(\mathbf{K}_s) \leq P_t} \log_2 \det \left(\mathbf{I} + \frac{1}{N_0} \mathbf{H}\mathbf{K}_s\mathbf{H}^* \right), \tag{2.19}$$

where $\mathbf{H}^*$ is the Hermitian matrix of $\mathbf{H}$ and $\mathbf{K}_s = \mathbb{E}[\mathbf{s}\mathbf{s}^*]$ is the covariance matrix of the signal $\mathbf{s}$ transmitted with a maximal power Pt. In the particular no CSIT case, the power is uniformly allocated over the n_t antenna, thus for the covariance matrix is,

$$\mathbf{K}_s = \left(\frac{P_t}{n_t} \right) \mathbf{I},$$

and the capacity can be expressed as,

$$C_{MIMO} = \log_2 \det \left(\mathbf{I} + \frac{SNR}{n_t} \mathbf{H}\mathbf{H}^* \right). \tag{2.20}$$

Moreover, at high SNR [40] regime this capacity can be approximated as follows,

$$C_{MIMO} \sim \min(n_t, n_r) \log_2 SNR. \tag{2.21}$$

5.2.3 Outage event and diversity gain

The outage stands for the event that arises when the transmitted rate R_d exceeds the channel Shannon capacity and is defined as,

$$\mathcal{E}_{out} = \left\{ \mathbf{H} : \log_2 \det \left(\mathbf{I} + \frac{SNR}{n_t} \mathbf{H}\mathbf{H}^* \right) < R_d \right\},$$

and the resulting outage probability P_{out} is then,

$$P_{out}(R_d) = Prob(\mathcal{E}_{out}). \tag{2.22}$$

It has been shown [6] that the outage probability at high SNR regime scales as,

$$P_{out} \sim SNR^{-d}, \tag{2.23}$$

where $d = n_t \times n_r$ is the diversity gain.

5.2.4 Spatial diversity gain schemes

■ **Antenna selection**

The transmit antenna selection scheme [53] enables to extract the full MIMO diversity gain by selecting the antenna maximizing the total received power. Several algorithms [54, 55, 56, 57] are available in literature to determine the optimal antenna maximizing the performances. In this case the channel capacity is:

$$C = log_2(1 + SNR|h^*|^2), \tag{2.24}$$

where $h^* = \underset{1\leq i\leq n_t}{max}\ \underset{1\leq j\leq n_r}{max} h_{ij}$. For i.i.d channel coefficients the equivalent fading F_i is the maximum between $n_t n_r$ random variables and its CDF is,

$$F_{F_i}(t) = \left(1 - e^{-\frac{t}{\sigma_f^2}}\right)^{n_t n_r}. \tag{2.25}$$

■ **Maximum ratio combining** at the receiver side

Maximum ratio combining at the receiver side "MRC-R" [58, 59, 60] at the transmitter side is a technique used to increase the signal strength toward a direction, generally the signal strength can be n_t time duplicated, where n_t is the number of transmitters. In case of insufficiently spaced antennas and thus high mutual antenna correlation, the transmitter form a beam by shifting the phases of the signals in order to obtain a common beam steered in the direction of the receiver. But in low mutual antenna correlation configuration, not only the phase may differ but also the channels gain. Thus, complex weights are applied to the antennas in order to adapt both the signals phases and amplitudes, which results in applying a precoding vector $\mathbf{p}$ to the vector of the signal $\mathbf{s}$ as,

$$\tilde{\mathbf{s}} = \mathbf{p} \cdot \mathbf{s}.$$

As LTE is based on OFDM transmissions, subcarriers are experiencing non frequency selective channels, [42] shows that the precoding weights should be selected as follows:

$$p_i = \frac{h_i^*}{\sqrt{\sum_{j=1}^{n_t} |h_j|^2}} \tag{2.26}$$

where h_i^* is the conjugate of the channel coefficient which is normalized to obtain a fixed transmit power. For this scheme, the equivalent fading is distributed following a chis-squared random variable with $2n_r$ degrees of freedom $\chi^2_{2n_r}$ with CDF,

$$F_{F_i}(t) = \frac{1}{(n_r-1)!}\,\gamma\left(n_r, \frac{t}{\sigma_f^2}\right), \tag{2.27}$$

where $\gamma(n_r, t) = (n_r-1)!\left(1 - g(n_r, t)\, e^{-t}\right)$ and $g(n_r, x) = \sum_{k=0}^{n_r-1} \frac{1}{k!}\, x^k$.

■ **Transmit antenna selection with MRC "MRC-RS"**

This scheme is the combination of the transmit antenna selection and maximal ratio combining at the receiver schemes presented above and traditionally referred as MRC-RS [61]. It enables significant amelioration of the performances of MIMO communications with a low complexity level. Thus, in this case the equivalent fading is the maximum between n_t chi-squared random variables with $2n_t$ degrees of freedom $\chi^2_{2n_t}$ and its CDF is,

$$F_{F_i}(t) = \left(F_{\chi^2_{2n_r}}(t)\right)^{n_t} = \left(1 - g\left(n_r, \frac{t}{\sigma_f^2}\right) e^{-\frac{t}{\sigma_f^2}}\right)^{n_t}. \tag{2.28}$$

5.2.5 Spatial multiplexing gain schemes

■ **V-BLAST architecture**

Vertical Bell Labs Space-Time "V-BLAST" architecture [62], was specially designed for transmissions where no knowledge of the channel $\mathbf{H}$ is available at the transmitter. The n_t data streams are independently, arbitrary multiplexed and decoded jointly at the reception. Maximum multiplexing gain corresponding to $\min(n_t, n_r)$ is achievable while only receive diversity is obtained. Following Figure 2.18 illustrates this architecture, where Q is a unitary matrix depending on the CSI. Each stream $s_.$ is codes at rate $R_.$ such that $\sum_{i=1}^{n_t} R_i = R$.

■ **V-BLAST with successive interference cancellation**

Successive Interference Cancellation "SIC" [63, 64] is a decoding scheme applicable in the case where the signals multiplexed are not jointly coded but separately coded before the transmission. This scheme consists first in demodulating and decoding one of the

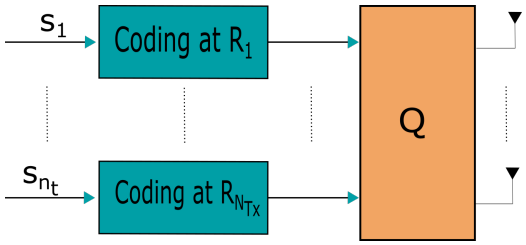

Figure 2.18: V-BLAST architecture for MIMO communications

signals and then re-encode it before subtracting it from the other signals. Then the receiver repeats the same operation until all signals are decoded. Figure 2.19 below illustrates the SIC processing for two parallel multiplexed channels: We denote by $n_s \triangleq \min(n_t, n_r)$

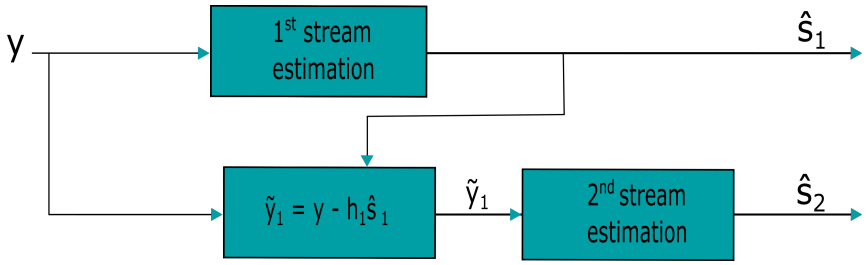

Figure 2.19: SIC receiver in a 2×2 MIMO spatial multiplexing scheme

the maximal number of spatial layers in a $n_t \times n_r$ MIMO scheme where the total power is uniformly distributed across the transmitting antennas. Consider a sub-optimal decoder in which the n_s streams are individually decoding. The maximal achieved spectral efficiency by the individual decoding for each sub-stream is,

$$C_s(r, X_i, \tilde{\Phi}^+) = \log_2\left(1 + \frac{P_a\ F_{s,i}}{n_s \ell(r)(\omega + I(y_i, \tilde{\Phi}^+|\tilde{X}_i))}\right), \quad 1 \leq s \leq n_s.$$

where P_a/n_s is the normalized transmission power per RB and per stream and $F_{s,i}$ is the the fading coefficient for each stream. ω is the exponential power of the noise, $\ell(r)$ is the propagation path loss and $I(y_i, \tilde{\Phi}^+|\tilde{X}_i^{(k)})$ is the interference introduced by the nodes transmitting on the same radio resource block. Therefore the fading coefficient corresponds to the minimal coefficient experienced by the n_s sub-streams, $F_i = \min_{1 \leq s \leq n_s} F_{s,i}$. With a SIC decoder, the first sub-stream is decoded on a fading coefficient $F_{1,i}$ chi-squared randomly distributed with $2(n_r - n_s + 1)$ degrees of freedom. The contribution of this first sub-stream is subtracted from the received signal and the second sub-stream is decoded over a chi-squared random variable with $2(n_r - n_s + 2)$ degrees of freedom. Similarly, the s^{th} sub-stream is decoded over a chi-squared random variable with $2(n_r - (n_s - (s-1)) + 1)$ degrees of freedom. The resulting equivalent fading as therefore distributed following

$\chi^2_{2(n_r-n_s+1)}$ with a CDF,

$$F_{F_i}(t) = 1 - g\left((n_r - n_s + 1), \frac{t}{\sigma_f^2}\right) e^{-\frac{t}{\sigma_f^2}}. \tag{2.29}$$

6 Poisson Point Processes "PPPs"

This section introduces the mathematical tools involved in this dissertation. More precisely the stochastic geometry tools and Poisson Point Processes "PPPs" properties used to model the network behaviors. We review the fundamental definitions and theorems that will be used for network dimensioning in chapters 4 and 5.

6.1 Stochastic geometry

Stochastic geometry is an efficient mathematical tool to model wireless networks [8, 9]. It is widely used in literature [28, ?, 11, 12] to model the network nodes locations and to analytically characterize the network metrics as the bandwidth, the capacity, the connectivity, the delays, etc. Poisson point processes appear to be the most suiting for the point process modeling in mobile ad hoc networks [65]. In this dissertation these tools will be used in Chapters 3 to 5 to model the nodes distribution and to provide statistical tools to derive the end-to-end delay distributions, the resource outage probability and the required bandwidth in the network.

6.1.1 Definitions

A spatial point process Φ over the d-dimensional Euclidean space $\mathbb{R}^d$ is a random combination of points. A realization ϕ of a point process can be considered as a discrete subset $\phi = \{x_i\} \subset \mathbb{R}^d$ and expressed as:

$$\phi = \sum_i \epsilon_{x_i},$$

where ϵ_x is the Dirac measure at x i.e. if $x \in A$, $\epsilon_x(A) = 1$, 0 otherwise. Thus, the number of point of ϕ in A is given by $\phi(A)$ and for f a real function on $\mathbb{R}^d$,

$$\sum_i f(x_i) = \int_{\mathbb{R}^d} f(x)\phi(dx),$$

and finally for $A \in \mathcal{B}$, the bounded Borel subsets of $\mathbb{R}^d$, the point process can be considered as a stochastic process

$$\Phi = \{\Phi(A)\}_{A\in\mathcal{B}} \in \mathbb{N}.$$

Additionally, the point process distribution is characterized by the collection of finite dimensional distributions $(\phi(A_1), \ldots, \phi(A_k))$, $A_k \in \mathbb{R}^d$.

Thus a Poisson point process is nothing but a particular case among point processes defined as:

Definition 2.1. *Let Φ a Poisson point process with intensity measure Λ, by means of its finite-dimensional distribution Φ is defined as:*

$$\mathbb{P}\{\Phi(A_1) = n_1, \ldots, \Phi(A_k) = n_k\} = \prod_{i=1}^{k} \exp\left(-\Lambda(A_i)\frac{\Lambda(A_i)^{n_i}}{n_i!}\right),$$

where $k \in \mathbb{N}^*$ and bounded, mutually disjoint set $A_i \ \ \forall i = 1, \ldots, k$ and $n_1, \ldots, n_k \in \mathbb{N}$. Φ is referred as an homogeneous PPP with intensity parameter λ, if $\Lambda(dx) = \lambda dx$ is a multiple of Lebesgue [66] measure in $\mathbb{R}^d$.

From Definition 2.1, it follows that Φ is a poisson point process if and only if: $\forall k \in \mathbb{N}^*$ and all mutually disjoint and bounded $A_i \subset \mathbb{R}^d$, $i = 1, \ldots, k$, $\Phi(A_1), \ldots, \Phi(A_k)$ are independent Poisson random variable with respective intensities $\Lambda(A_i), \ldots, \Lambda(A_k)$. Moreover $\mathbb{E}(\Phi(A)) = \Lambda(A)$. For wireless networks it is possible to characterize the active network nodes locations distribution through the following proposition,

Proposition 2.1. *Let assume that the network nodes localizations are i.i.d, the service time is exponentially distributed with mean ν^{-1} and the time between two consecutive demands for service is also exponentially distributed with a surface density $\rho(x)$. The point process of active nodes location is then a Poisson point process with intensity $d\Lambda(x) = \rho(x) \cdot \nu^{-1} dx$.*

6.1.2 Operations preserving the PPP

Definition 2.2. *The superposition of point processes Φ_k is the point process $\Phi = \sum_k \Phi_k$.*

Proposition 2.2. *'Superposition' For k independent Poisson point processes Φ_k with intensities Λ_k, the point process $\Phi = \sum_k \Phi_k$ is a Poisson point process with intensity $\Lambda = \sum_k \Lambda_k$ if and only if Λ is a locally finite measure.*

We know focus on the thinning of a PPP, which is the inverse operation of the above described superposition.

Proposition 2.3. *'Thinning' Considering a Poisson point process with intensity Λ, the thinning of this PPP with the retention function $p : \mathbb{R}^d \to [0, 1]$, is a Poisson point process with intensity $p\Lambda$ such that $p\Lambda(A) = \int_A p(x)\Lambda(dx)$.*

This means that a realization of a Poisson point process can be constructed from a Poisson point process Φ by independently and randomly remove some points with a probability that a node localized at x is not removed equals to $p(x)$. We know consider random transformation of points, let $p(x, B)$ be a probability kernel from $\mathbb{R}^d$ to $\mathbb{R}^{d'}$, $d' \geq 1$. The above theorem known as the "Displacement Theorem" states,

Theorem 2.1. *'Displacement' For a Poisson point process with intensity Λ, the transformation by a probability kernel p yields to a Poisson point process with intensity $\Lambda'(A) = \int_{\mathbb{R}^d} p(x, A)\Lambda(dx)$, $A \subset \mathbb{R}^{d'}$.*

The proofs of the above propositions and theorems are all available in [8].

6.2 Useful theorems

Hereafter we present some useful stochastic geometry theorems involved in the scope of this thesis. Campbell formula's theorem [67] enables the computation of the expectation of a random sum and is defined as following:

Theorem 2.2. *'Campbell's formula' Let Φ a Poisson point process on $\mathbb{R}^d$ with intensity Λ and $f : \Phi \to \mathbb{R}$ a measurable function. The random sum $F = \sum_{x\in\Phi} f(x)$ is a random variable with expectation:*

$$\mathbb{E}\left[\sum_{x\in\Phi} f(x)\right] = \int_{\mathbb{R}^d} f(x)\Lambda(dx) \tag{2.30}$$

The next theorem referred as Bennett's concentration inequality [68] enables to obtain an upper-bound on the sum of independent randomly distributed bounded variables.

Theorem 2.3. *'Bennett's concentration inequality' Let X_i be a bounded independent random variable $X_i < a$ with an average $m_x = \sum_{i=1}^{N} \mathbb{E}(X_i)$ and let $v_x = \sum_{i=1}^{N} \mathbb{E}(X_i^2)$. For $\alpha \geq 1$, the complementary cumulative distribution function of $X = \sum_{i=1}^{N} X_i$ is such that:*

$$Prob\{X > \alpha m_x\} \leq exp\left(-\frac{v_x}{a^2} g\left(\frac{(\alpha - 1)m_x a}{v_x}\right)\right) \tag{2.31}$$

with $g(t) = (1 + t)\log(1 + t) - t$.

6.3 Marked Poisson Point Process

In this subsection we start by defining marked point processes and then present their useful properties.

Definition 2.3. *Consider a point process in $\mathbb{R}^d$, $d \geq 1$ and $\mathbb{R}^l$, $l \geq 1$ the space of the marks. A marked point process is defined as the collection of pairs $\tilde{\Phi} = \{(x_i, m_i)\}_i$, where $\{x_i\}$ is the set of points and $\{m_i\}$ the set of marks. $\tilde{\Phi}$ is a point process in $\mathbb{R}^d \times \mathbb{R}^l$.*

A particular case of marked point process is the independently marked point process.

Definition 2.4. *An independently marked point process is a marked point process $\Phi = \{x_i\}$ where the marks are mutually independent random vectors in $\mathbb{R}^l$ and with a conditional*

distribution of a mark m of a point $x \in \Phi$ depending only on the location of the point x:

$$\mathbb{P}\{m \in \cdot | \Phi\} = \mathbb{P}\{m \in \cdot | x\} = F_x(dm),$$

where $F_\cdot(\cdot) : \mathbb{R}^d \to \mathbb{R}^l$ is the marks probability kernel.

It results from the above definition the following corollary characterizing an independently marked Poisson point process.

Corollary 2.1. *Let $\tilde{\Phi}$ an independently marked Poisson point process with intensity Λ on $\mathbb{R}^d$ and marks with distributions $F_x(dm)$ on $\mathbb{R}^l$. $\tilde{\Phi}$ is a Poisson point process with intensity*

$$\tilde{\Lambda}(A \times K) = \int_A \tilde{p}(x, K)\Lambda(dx), \; A \subset \mathbb{R}^d, K \subset \mathbb{R}^l, \tag{2.32}$$

with $\tilde{p}(x, K) = \int_K F_x(dm)$.

Consequently, the first moment of the independently marked Poisson point process is derived in the following theorem:

Theorem 2.4. *For $f : \mathbb{R}^d \to \mathbb{R}^l$ a measurable positive function and $F = \int f d\tilde{\Phi}$ the sum of realizations of f over $\tilde{\Phi}$, the first moment of F is derived as,*

$$\mathbb{E}(F) = \int_{\mathbb{R}^d \times \mathbb{R}^l} f(x, m) F_x(dm) d\Lambda(x), \tag{2.33}$$

using the Campbell formula in theorem 2.2.

7 Basics from Graph Theory

Spectral clustering is based on graph theory and eigen-structure of a similarity matrix derived from a weighted similarity graph $G = G(V, E)$ where V is the vertex set describing the data points and E the edge set and weighted similarity matrix is referred as W. Two nodes are connected if the similarity factor between them is positive or greater than a certain threshold. In the following we describe the three types of similarity graphs and the properties used in our work.

7.1 Similarity graphs

As we said earlier, several similarity graphs are available in the literature to build a graph from nodes similarities. The k-nearest neighbor graph which connects two vertices v_i and v_j if v_j is in the k-neighborhood of v_i. The ϵ-neighborhood graph were connected nodes are at most at a distance ϵ apart. The Fully connected graph where all points with a positive similarity factor $s_{ij}$are connected together.

In the scope of this thesis we focus on the 1-neighborhood graph where nodes are connected if they are direct neighbors and consider unweighted edges.

7.2 Laplacian graph

The unnormalized Laplacian graph is determined by the degree matrix $\mathbf{D}$ and the weighted adjacency matrix $\mathbf{W} = (w_{ij})_{i,j=1,\dots,n}$ ($w_{ij} = 1$ if $s_{ij} > 0$) as,

$$\mathbf{L} = \mathbf{D} - \mathbf{W}.$$

where $\mathbf{D}$ is a diagonal matrix with $d_i = \sum_{j=1}^{n} w_{ij}$. Its most important properties are:

- For every vector $\mathbf{v} \in \mathbb{R}^n$:

$$\mathbf{v}'\mathbf{L}\mathbf{v} = \frac{1}{2}\sum_{i=1}^{n}\sum_{j=1}^{n} w_{ij}(v_i - v_j)^2 \tag{2.34}$$

- L is symmetric and positive,
- The smallest eigenvalue of L is 0 and the corresponding eigenvector is the constant on vector $\mathbb{1}$,
- L has n non-negative and real eigenvalues.

In our work in Chapter 3, we use the following property to state if a graph is fully connected or not [69],

Proposition 2.4. *'Number of connected components' $\mathcal{G}$ is fully connected if the multiplicity of the smallest eigenvalue of* $\mathbf{L}$ *(equal to 0), is equal to 1.*

The proof of this proposition is provided in [69].

7.3 Dijkstra's algorithm

Dijkstra's shortest path algorithm [24] is a greedy algorithm proposed by Edsger Wybe Dijkstra and detailed below in Algorithm 1. It is a solution to the single source shortest path problem in graph theory. It assumes full knowledge of the graph and works on undirected or directed graphs either, with non negative edge weights. This algorithm will be used in Chapter 3 to study the multi-hop end-to-end communications.

Algorithm 1: Dijkstra single source shortest path algorithm

Input : Weighted graph $\mathcal{G} = \mathcal{E}, \mathcal{V}$ and source vertex $v \in \mathcal{V}$, s.t all edge weights are non negative

Output: Vector **dist** Shortest paths from a given source vertex $v \in \mathcal{V}$ to all other vertices

```
1  for v ∈ V\{s} do
2      dist[v] ← ∞;                          // Distances to s are set to infinity
3  end
4  S_v ← ∅;                                  // Visited vertices set is initially empty
5  Q_v ← V;                                  // Queue contains all vertices initially
6  while Q_v ≠ ∅ do
7      u ← min(distance(Q_v, dist));         // Element of Q_v with the minimal distance
8      S ← S ∪ {u};
9      if dist[v] > dist[u] + w(u, v) then
10         dist[v] ← dist[u] + w(u, v);      // w(u, v) being the weight of the u → v egde
11     end
12 end
```

8 Conclusion

In this chapter we focused on the technical and mathematical frameworks being the basics of this thesis. We introduced the mobile ad hoc, LTE and satellite networks fundamentals which are the envisaged technologies in our studies. The mathematical background and especially the stochastic geometry tools are used throughout this dissertation. Stochastic geometry is involved in Chapters 4 and 5 for the radio resource dimensioning of a centralized and a distributed LTE MANET under SISO and several MIMO antenna configurations. In the following Chapter 3, we address the topology design challenges, we provide an analytical model based on stochastic geometry and graph theory in order to enable a user to estimate the required network characteristics to achieve the necessary coverage radii enabling full connection of the network nodes. Routing protocols performances and the contribution of the satellite backhaul are also addressed.

3 Topology Design of Hybrid Satellite - MANET

Topology design focuses on the network initialization phase i.e. the partitioning of the nodes followed by the network connection. In the considered Mobile Ad hoc Network "MANET", the mobile nodes are part of a hierarchical naval fleet offshore. This network will be supported by a satellite backhaul, thus some of the mobile nodes will be provided with Satellite GateWays "SGWs" and will be referred as Hybrid Stations "HSs". This chapter aims to provide a statistical model to help a network designer to perceive the pros and cons of the possible solutions among: i) the use of centralized access via the shipmasters or a distributed access, ii) the needs in satellite gateways in the network and iii) the gains in terms of end-to-end communication delays vs. the costs induced by the satellite equipments. To answer these interrogations we start by considering the average statistical behavior of the network for the centralized case, we then investigate the Graph Theory field and present an exhaustive solution to derive the required coverage radii in a distributed access scheme. Several routing protocols are evaluated in terms of end-to-end communication delays, we then propose a strategy for the access to the satellite gateways and also a comparative study to qualify the needs in hybrid stations in function of the maximal end-to-end tolerated delay. Part of this work is published in [19] and in [20].

1 Introduction

In this chapter, we investigate the clustering algorithms [29] that divide the whole network into multiple subgroups. By setting up a local organization of the nodes, clustering provides a fast network connection, easier and more efficient routing and a better topology management. In these clusters the mobile nodes will be divided in two types, the leading nodes referred as cluster heads "CHs" and the ordinary nodes. Several clustering algorithms are available in the literature, in this work we focus on three well known ones: k-means algorithm [21], Max-Min algorithm [15] and KCMBC algorithm [22]. The main objective of these algorithms is to optimize the number of hops to the CH and the size of the clusters to provide load balancing and reduce the amount of handovers resulting from nodes mobility. In these

algorithms, the cluster heads have to be elected, the election protocol is left to the user for k-means while the two latter include an election protocol based on the nodes characteristics as the id number, the geographical proximity, the energy consumption, the mobility, etc.

In this thesis, we consider a maritime Mobile Ad-hoc Network "MANET" studied in an hierarchical context. The network nodes correspond to ships and are part of a naval fleet offshore. The ships are equipped with either terrestrial LTE radio devices [4] or hybrid terrestrial and satellite Ultra Small Aperture Terminals "USATs". We distinguish between two classes of nodes the shipmasters and the staff-ships nodes. The shipmasters have the advantage to be equipped with more advanced and performant materials than the staff-ships. For the distributed access scheme, non transmitting staff-ships act as decode and forward (see Chapter 2) relay nodes [43]. The shipmasters are a priori elected CHs, thus the staff-ships are divided in function of their geographical proximity to the shipmasters. We introduce in the following an efficient and fast converging method to manage the clustering of the staff ships referred as Hierarchical MANET Clustering "HMC".

The fundamental requirement in a clustered MANET is to obtain fully connected clusters. We aim to provide a statistical model enabling network designers to predict the necessary ranges to achieve this requirement. To this intent, the average statistical behavior of the network is considered, staff-ships in the set $\mathcal{N}$ and shipmasters in the set $\mathcal{H}$ are assumed to be randomly distributed according to two homogeneous Poisson Point Process "PPP" in $\mathbb{R}^2$ of intensity λ_C and λ_H respectively. Each cluster k is modeled by an undirected graph $\mathcal{G}_k = (\mathcal{V}_k, \mathcal{E}_k)$ where $\mathcal{V}_k$ is the vertices set describing the cluster nodes positions and $\mathcal{E}_k$ the edges set. We define a similarity notion $s_{ij} > 0$ between a nodes pair (i, j), two nodes are connected if the similarity factor between them is positive or greater than a certain threshold. Here the similarity factor corresponds to the euclidean distance $dist(i, j)$ between the network nodes. Moreover, we also target to form a network backbone by connecting the shipmasters together. Thus, this backbone is also represented as an undirected graph $\mathcal{G}_h = (\mathcal{H}, \mathcal{E}_h)$, similarly the minimal threshold distance: d^*_{hh} between CHs in order to obtain a fully connected CH backbone will be determined.

In the remaining of this chapter, we first introduce the HMC algorithm. Then, we consider a typical cluster and focus on the centralized case, where all cluster nodes have to be situated at 1-hop from their respective CH and communicates through it. Afterwards we derive the inter-CHs and the intra-cluster communications coverage radii for this access scheme. We focus then on the distributed access scheme where pairwise communications are enabled. We investigate the field of Spectral Graph Clustering which is a performant technique easy to implement based on Graph Theory. By deriving the Laplacian matrices [69] of these graphs we bring out the optimization problems determining the upper-bound on intra-cluster coverage radii between staff-ships: d^*_{ss} and between nodes and their respective CH: d^*_{sh}, to obtain fully connected clusters. Moreover, we derive the end-to-end propagation delays distributions during communications for several path discovery protocols, enlightening the strategy minimizing them. Cumulative Distribution Functions "CDFs" of the threshold distances and the end-to-end delays Probability Density Functions "PDFs" are derived under HMC algorithm and the reference clustering algorithms cited above. Finally, we

consider the satellite component and derive the end-to-end delays PDFs in function of the amount of HSs available in the network, enabling to enlighten the gain induced by the satellite backhaul and its efficiency.

2 Naval fleet Clustering

This section first introduces the hierarchical MANET clustering algorithm. Then we focus on a typical cluster $\mathcal{C}_o$ centered at the origin and study its statistical behavior. The centralized and distributed access schemes are studied. In the centralized case all cluster nodes have to be situated at 1-hop from their respective CH and all communications are made through this latter. While in distributed access pairwise communications are enabled and no restrictions in hops number to the CH are considered. In the following we derive the optimal inter-nodes coverage radii ensuring fully connected clusters for the two access schemes. To do so, we consider a circular area $\mathcal{A}$ of radius R and assume that the shipmasters in $\mathcal{H}$ and the staff-ships in $\mathcal{N}$ are randomly distributed following two random PPPs with respective intensities λ_h and λ_c.

2.1 Hierarchical MANET Clustering "HMC"

Hierarchical MANET Clustering "HMC" is a clustering algorithm with fast convergence designed to fulfill the requirements of a MANET composed of two types of nodes: staff-ships and shipmasters forming a naval fleet offshore. The shipmasters are a priori elected CHs and are assumed to have full knowledge on the network nodes positions. Thus each CH is enabled to determine which staff-ships are closest to it rather to another CH in terms of euclidean distance. Afterwards, the CHs advertises its selected staff-ships that they belong to its cluster. The Gateway Nodes "GWs" are cluster nodes able to communicate with neighboring clusters. These nodes are usually situated at the clusters edges, and may be used has relay nodes to establish inter-cluster communication links.

We model nodes mobility according to the nomadic mobility model [1] detailed in Chapter 2. Staff-ships are allowed to move separately in the reference point area which is the CH. Once the CH moves toward a new destination all the staff-ships follow it, upon arrival of the CH, nodes can again independently move around the CH area. However, a staff-ship may be closer to another CH than it initial one after a certain amount of time. Shipmasters periodically check if a new staff-ship is closer to them, if it appears that a staff-ship should update its membership, the candidate CH informs through the cluster heads backbone the initial CH of the node to release the node. The staff-ship is informed by its initial and future CH about the handover procedure. Figure 3.1 illustrates the clusters resulting from HMC and the literature algorithms reviewed in Chapter 2, performed on the same nodes configuration.

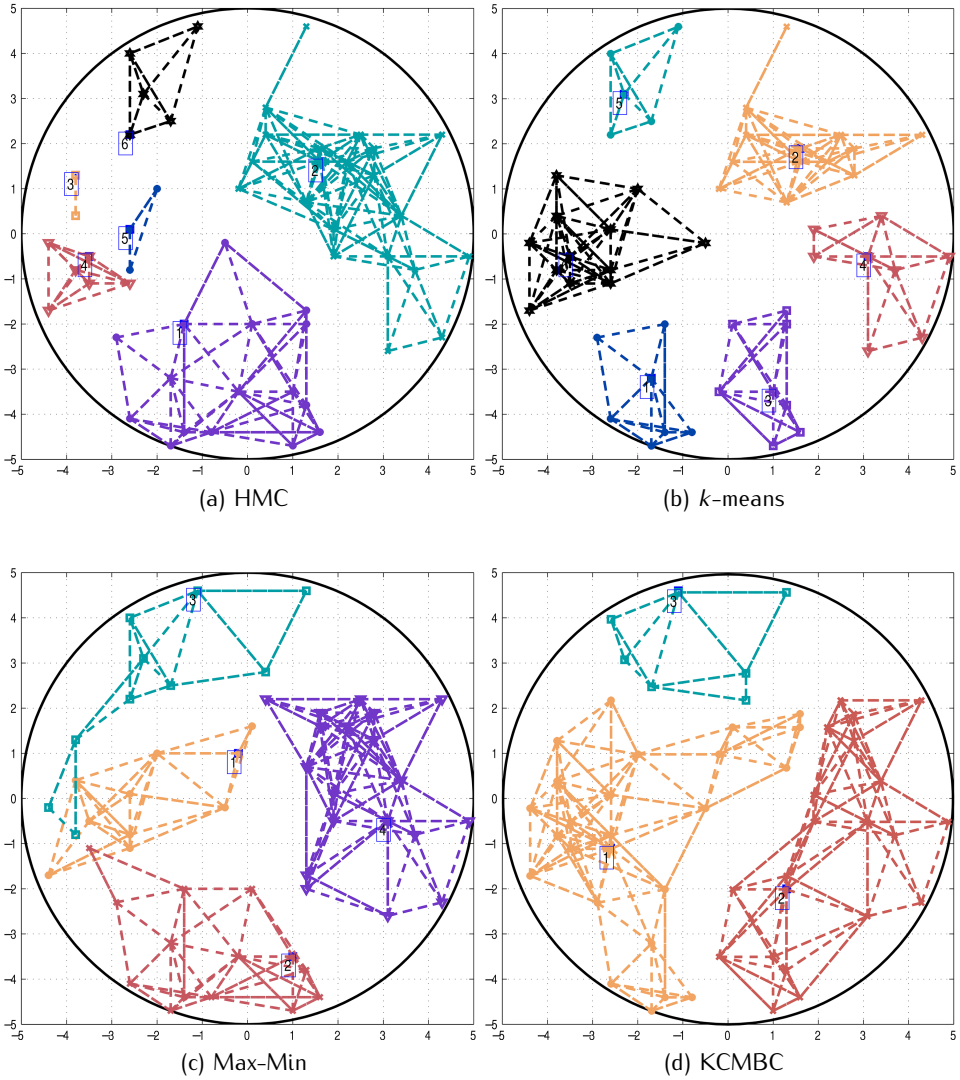

(a) HMC (b) *k*-means

(c) Max-Min (d) KCMBC

Figure 3.1: Resulting clusters from HMC, *k*-means, Max-Min and KCMBC algorithms

2.2 Typical cluster average size estimation

Assuming $\mathcal{C}_o$ a typical cluster centered at the origin $(0,0)$. Let $\mathcal{N}_0$ be the average number of staff-ships $x \in \mathcal{N}$ belonging to $\mathcal{C}_o$ and expressed as

$$\mathcal{N}_0 = \mathbb{E}\left[\sum_{x\in\mathcal{N}} \mathbb{1}_{\{|x|\leq r_1\}}\right],$$

where r_1 is the distance between any point $x \in \mathcal{N}$ and its closest neighbor in the set of shipmasters $\mathcal{H} \cup \{o\}$. From Campbell Theorem [8] in Chapter 2, the average cluster size is given by

$$\mathcal{N}_0 = \int_0^R \int_r^\infty f(r_1)dr_1(2\pi\lambda_c r)dr.$$

Haenggi proved in [23] that the distribution of the Euclidean distance to n^{th} neighbor in a PPP can be described as in the following theorem:

Theorem 3.1. (Distribution of Euclidean Distance to n^{th} Neighbor) *In a Poisson point process in $\mathbb{R}^m$ of intensity λ_h, the distance between a point and its n^{th} neighbor is distributed as:*

$$f(r_n) = \frac{2\lambda_h c_m r_n}{r_n \Gamma(n)} e^{-\lambda_h c_m r_n^m}. \tag{3.1}$$

where $c_m r^m$ is the volume of the m-dimensional ball of radius r_n, where c_m is given by:

$$c_m = \begin{cases} \frac{1}{(m/2)!}\pi^{m/2} & \text{for even } m \\ \\ \frac{2^m\left(\frac{m-1}{2}\right)}{m!}\pi^{(m-1)/2} & \text{for odd } m. \end{cases} \tag{3.2}$$

Hence $f(r_1) = 2\pi\lambda_h r_1 e^{-\lambda_h \pi r_1^2}$ and the average number of nodes in $\mathcal{C}_o$ is

$$\begin{aligned} \mathcal{N}_0 &= \int_0^R \int_r^\infty 2\pi\lambda_h r_1 e^{-\lambda_h \pi r_1^2} dr_1 (2\pi\lambda_c r)dr \\ &= \int_0^R (2\pi\lambda_c r) e^{-\lambda_h \pi r^2} dr \\ \boxed{\mathcal{N}_0 &= \left\lceil \frac{\lambda_c}{\lambda_h}(1 - e^{-\lambda_h \pi R^2}) \right\rceil}. \end{aligned} \tag{3.3a}$$

2.3 Coverage radii in a centralized network

We derive here the inter-CHs and the intra-cluster communications coverage radii in a centralized network. As we said earlier, in a centralized access cluster we aim to connect all the members to the CH within one hop. Note that these radii also provide an upper-bound

on the coverage ranges in a distributed scheme. Figure 3.2 illustrates the two access schemes, the CH is represented by the node 9.

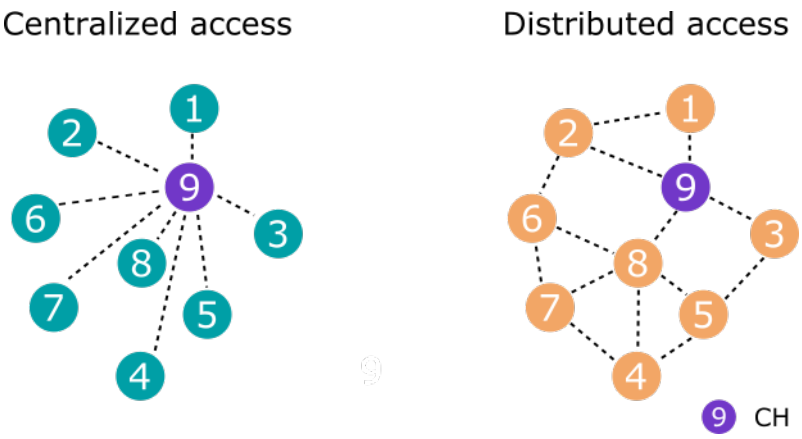

Figure 3.2: Illustration of a centralized and a distributed cluster

2.3.1 Inter-CHs coverage radius outer bound

In the following we present an outer bound on the inter-CHs coverage radius that ensures a fully connected CHs backbone i.e. a fully connected shipmaster graph $\mathcal{G}_h$. Connect pairwise each shipmasters together is a sufficient condition but not necessary to ensure a fully connected shipmaster graph. It corresponds to the event that arises when all CHs are incircle in the disk of radius $\frac{1}{2}d^*_{hh}$:

$$\{\forall h \in \mathcal{H} : dist(0,\ h) \leq \frac{1}{2}d^*_{hh,max}\} \Rightarrow \{\mathcal{G}_h \text{ is fully connected}\},$$

where $d^*_{hh,max}$ is the inter-CHs coverage radius upper-bound. This means that each shipmaster is connected to the other ones within one hop and that the inter-CHs distance is at most equal to $d^*_{hh,max}$. Considering that the probability that the region corresponding to the ring delimited by the area radius R and d^*_{hh} is empty as: Prob$\{\forall h \in \mathcal{H} :$ dist $(o,\ h) \leq \frac{1}{2}d^*_{hh}\}$, the upper bound on the probability to get a non fully connected graph $\mathcal{G}_h$ is expressed as:

$$\text{Prob}\{\mathcal{G}_h \text{ is not fully connected}\} \leq 1 - \text{Prob}\{\forall h \in \mathcal{H} : dist(o,h) \leq \frac{1}{2}d^*_{hh}\}$$

Moreover, the probability to get an empty region is as follows:

$$\begin{aligned}\text{Prob}\{\forall h \in \mathcal{H} : dist(0,h) \leq \frac{1}{2}d^*_{hh}\} &= \exp\left(-\lambda_h \int_{\frac{1}{2}d^*_{hh}}^{R}\int_0^{2\pi} r dr d\theta\right) \\ &= \exp\left(-\pi\lambda_h\left(R^2 - \frac{1}{4}d^{*2}_{hh}\right)\right),\end{aligned}$$

By setting a threshold p_{th} on this upper-bound the inter-CHs coverage radius is determined as:

$$d^*_{hh,\max} = \sqrt[2]{4(R^2 + \frac{1}{\pi\lambda_h}\log(1-p_{th}))}. \tag{3.4}$$

2.3.2 Outer bound on intra-cluster coverage radius

We focus here on the coverage radius $d^*_{sh,k}$ necessary to connect all staff-ships to their respective CH denoted h_k. This is a sufficient condition to obtain a fully connected cluster $\mathcal{C}_k$ mathematically expressed as:

$$\{\forall x \in \mathcal{N} : dist(x, h_k) \leq d^*_{sh,k} | h_k \text{ is the first neighbor of } x\} \Rightarrow \{\mathcal{G}_k \text{ is fully connected}\}$$

and it is equivalent to: $\{r_1 \leq d^*_{sh,k}\}$. The probability that $\mathcal{G}_k$ is not connected is upper-bounded as follows:

$$\text{Prob}\{\exists k : \mathcal{G}_k \text{ is not fully connected}\} \leq 1 - \text{Prob}\{\max_{x_i \in \mathcal{N}} r_{1,i} \leq d^*_{sh,k}\}.$$

The probability distribution function $f(r_1)$ of r_1 was derived above and its CDF is $F_{r_1}(d^*_{sh,k}) = 1 - e^{-\lambda_h \pi d^{*2}_{sh}}$. Thus,

$$\begin{aligned}\text{Prob}\{\max_{x_i \in \mathcal{N}} r_{1,i} \leq d^*_{sh,k}\} &= \sum_{n=0}^{\infty} \left[F_{r_1}(d^*_{sh,k})\right]^n \text{Prob}\{|\mathcal{N}| = n\} \\ &= \exp(-\lambda_c \pi R^2 (1 - F_{r_1}(d^*_{sh,k})),\end{aligned}$$

and the staff-ship → shipmaster coverage radius is then determined by setting an acceptable threshold p_{th} on the upper-bound,

$$d^*_{sh,\max} = \sqrt[2]{\frac{1}{\pi\lambda_h}\log\left(\frac{\lambda_c \pi R^2}{-\log(1-p_{th})}\right)}. \tag{3.5}$$

2.4 Coverage radii in a distributed network

We consider here a distributed network, three coverage radii are of concern, the inter staff-ships one: d_{ss}, the staff-ships→shipmaster one: d_{sh} and the inter shipmasters one d_{hh}. We propose an exhaustive method to compute the coverage radius to fully interconnect the network CHs and to ensure full connection in each cluster. We focus first on the inter-CHs connection then present the derivations for the intra cluster connections.

2.4.1 Inter-CHs connection

We model the shipmasters by an undirected graph $\mathcal{G}_h$ where the edges availability is conditioned by the shipmasters connectivity. We denote by d^*_{hh} the threshold distance ensuring the graph $\mathcal{G}_h$ full connection. We define the following Boolean adjacency matrix resulting from $\mathcal{G}_h$:

$$\mathsf{A}_h = dist(i,j) \leq d^*_{hh},\ \forall (i,j) \in (\mathcal{H} \times \mathcal{H}) \tag{3.6}$$

The threshold distance is then determined as a solution of the following optimization problem

$$d^*_{hh} = \min(dist(i,j)),\ \forall (i,j) \in (\mathcal{H} \times \mathcal{H}) \tag{3.7}$$

such that $\mathcal{G}_h$ is fully connected.

2.5 Intra-cluster coverage radius

We assume here that the staff-ship→shipmaster communication range is advantaged in comparison to the inter staff-ships one by using different frequency bands or powerful MIMO receiver at the shipmaster. This advantage is modeled by the scaling factor α. Similarly we model the staff-ships nodes belonging to a given cluster C_k by an undirected graph $\mathcal{G}_k$ in which the availability of edges is conditioned by the nodes connectivity. The threshold staff-ships interconnection distance $d^*_{ss,k}$ and the staff-ships→shipmasters threshold distance $d^*_{sh,k}$ are computed at the CH side which uses its knowledge of all nodes positions. We define also the Boolean and symmetric adjacency matrix of a graph $\mathcal{G}_k$ as,

$$\mathsf{A}_k = \begin{cases} dist(i,j) \leq d^*_{ss,k}, & \forall\ (i,j) \in (\mathcal{C}_k|\mathcal{H} \times \mathcal{C}_k|\mathcal{H}) \\ dist(i,j) \leq d^*_{sh,k}, & \forall\ (i,j) \in (\mathcal{C}_k|\mathcal{H} \times \mathcal{H}) \cup (\mathcal{H} \times \mathcal{C}_k|\mathcal{H}) \end{cases} \tag{3.8}$$

with $dist(i,j)$ being the Euclidean distance between two nodes i and j. The main objective is to find jointly the minimal values of $d^*_{ss,k}$ and $d^*_{sh,k}$ for which the cluster is fully connected. This can be computed as a solution of the optimization problem:

$$\begin{aligned} d^*_{ss,k} &= \min\Big(d_{ss,\max}; \min(dist(i,j))\Big), \forall\ (i,j) \in (\mathcal{C}_k|\mathcal{H} \times \mathcal{C}_k|\mathcal{H}) \\ d^*_{sh,k} &= \min\Big(d_{sh,\max}; \min(dist(i,j))\Big), \forall\ (i,j) \in (\mathcal{C}_k|\mathcal{H} \times \mathcal{H}) \cup (\mathcal{H} \times \mathcal{C}_k|\mathcal{H}) \end{aligned} \tag{3.9}$$

such that $\mathcal{G}_k$ is fully connected.

2.5.1 Exhaustive solution of the optimization problems

The problem in (3.7) and in (3.9) is iteratively solved by increasing progressively the threshold distance to ensure that the cluster is fully connected. For each threshold value, the adjacency matrix in (3.6) or in (3.8) is computed. The fully connectivity of the graph is

then verified using Proposition 3.1.

Proposition 3.1. *Given a graph $\mathcal{G}$ and its corresponding unnormalized Laplacian matrix* $\mathbf{L}$*, $\mathcal{G}$ is fully connected if the multiplicity of the smallest eigenvalue of* $\mathbf{L}$*: 0, is equal to one. .*

The unnormalized Laplacian matrix is defined as:

$$\mathbf{L} = \mathbf{D} - \mathbf{A}. \tag{3.10}$$

where $\mathbf{D}$ is a diagonal matrix referred as the Degree matrix such that $d_i = \sum_{j=1}^{n} \mathbf{A}(i,j)$. Algorithm 2 describes the proposed method to derive simultaneously the upper-bounds on the inter-CHs and inter staff-ships coverage radii in a distributed access scheme.

Algorithm 2: Distributed coverage radii derivation

Input : Set of shipmasters: $\mathcal{H}$, set of staff-ships: $\mathcal{N}$, set of clusters: $\mathcal{C}_k$, α.
Output: d^*_{ss}, d^*_{sh}, d^*_{hh}.

1 Compute the vector $\mathbf{d}_{ss}$ containing the ordered euclidean distances between each nodes $x \in \mathcal{N}$
2 $iter_s \leftarrow 1$;
3 $d^*_{ss} \leftarrow \mathbf{d}_{ss}(iter_s)$;
4 $d^*_{sh} \leftarrow \alpha \cdot d^*_{ss}$;
5 Compute the adjacency matrices $\mathbf{A}_k$, the degree matrices $\mathbf{D}_k$ and the Laplacian matrices $\mathbf{L}_k$;
6 Compute the multiplicity m^0_k of the eigenvalue 0 of $\mathbf{L}_k$;
7 fullyCoClusters $\leftarrow \sum_{k=1}^{|\mathcal{C}_k|} m^0_k$;
8 **while** *fullyConnectedClusters* $\neq |\mathcal{H}|$ **do**
9 $iter_s \leftarrow iter_s + 1$;
10 $d^*_{ss} \leftarrow \mathbf{d}_{ss}(iter_s)$;
11 $d^*_{sh} \leftarrow \alpha \cdot d^*_{ss}$;
12 Repeat *Steps* 5 *to* 7;
13 **end**
14 Compute the vector $\mathbf{d}_{hh}$ containing the ordered euclidean distances between each nodes $h \in \mathcal{H}$;
15 $iter_h \leftarrow 1$;
16 $d^*_{hh} \leftarrow \mathbf{d}_{hh}(iter_h)$;
17 Compute $\mathbf{A}_h$, $\mathbf{D}_h$ and $\mathbf{L}_h$;
18 Compute the multiplicity m^0_h of the eigenvalue 0 of $\mathbf{L}_h$;
19 fullyConnectedCHs $\leftarrow m^0_h$;
20 **while** *fullyConnectedCHs* $\neq 1$; **do**
21 $iter_h \leftarrow iter_h + 1$;
22 $d^*_{hh} \leftarrow \mathbf{d}_{hh}(iter_h)$;
23 Repeat *Steps* 16 *to* 18;
24 **end**

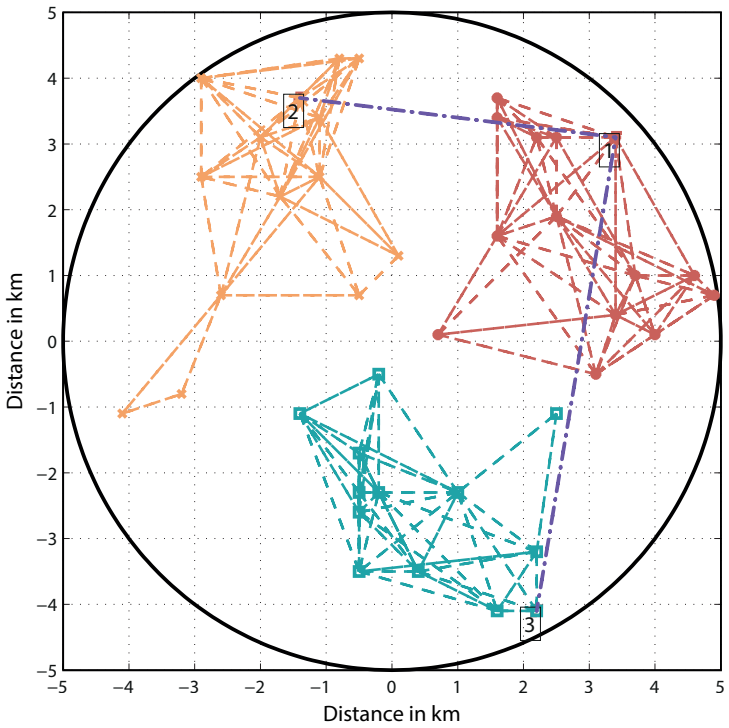

Figure 3.3: Fully Connected MANET formed with HMC algorithm

The resulting clusters with HMC algorithm, in which nodes are randomly distributed according to a PPP in a circular area of radius $R = 5$ km, are illustrated in Figure 3.3. The hierarchical MANET fleet clustering algorithm partitions this network into $N_c = 3$ clusters that are led by the shipmasters. The dashed edges in Figure 1 represent connected points. For inter-cluster communication, cluster gates are identified to route the information. The nodes at the edge of two clusters are considered as gates if there exists nodes in the neighboring cluster that are situated in their communication ranges.

3 Multi-hop end-to-end communications

This section focuses on the end-to-end communication path between two network nodes. We provide here a statistical evaluation of the typical distribution of the number of hops between a source centered at the origin of a typical cluster $\mathcal{C}_o$ and a random destination node, using the nearest neighbor search. We then introduce the multi-hop path discovery protocols of interest in our work.

3.1 Typical distribution of hops through the nearest neighbors

We denote by d a random destination node, $|o \rightarrow d|$ the number of hops required for origin-to-destination communication and $\delta = dist(o,\ d)$ the euclidean distance between o and d. We perform the nearest point search considering the whole network $\mathcal{N} \cup \mathcal{H}$. The union of these two independents Poisson point processes is also a PPP with intensity $\lambda = \lambda_c + \lambda_h$. We describe by the event $\mathcal{V}_n$ the sufficient condition to ensure that $|o \rightarrow d|$ is at most equal to n hops. The event $\mathcal{V}_n$ is defined as: i) d as the n^{th} nearest point to o; and that ii) all neighbors points are connected with inter-distance lower than the maximal inter-nodes coverage radius d_{ss} and mathematically expressed as:

$$\mathcal{V}_n \triangleq \bigcap_{i=1}^{n} \{r_{1,i} \leq d_s\} \cap \{d \equiv n^{th} \text{nearest point to } o\} \Rightarrow \{|o \rightarrow d| \leq n\} \tag{3.11}$$

where $r_{1,i}$ is the distance between two nearest neighbors.

From this sufficient condition, we can deduce the upper-bound on the Inverse Cumulative Distribution Function (ICDF) of the hops number as,

$$\mathbb{P}^0_{hops}(n|\delta) = \text{Prob}\{|o \rightarrow d| > n | dist(o,\ d) = \delta\} \leq 1 - \text{Prob}\{\mathcal{V}_n | dist(o,\ d) = \delta\},$$

with $\mathbb{P}^0\{\mathcal{V}_n|$ dist $(o,\ d) = \delta\} = \text{Prob}\delta \leq r_n\}$ Prob $\{r_1 \leq d_s\}^n$. Let r_n denote the euclidean distance from an arbitrary node to its n^{th} neighbor with pdf given in (3.1) by,

$$f(r_n) = \frac{2(\pi\lambda)^n}{(n-1)!} r_n^{2n-1} e^{-\pi\lambda r_n^2}.$$

Then,

$$\mathbb{P}^0_{hops}(n|\delta) \leq 1 - (1 - e^{-\lambda\pi d_s^2})^n \times \Gamma_{inc}(n,\ \lambda\pi\delta^2) \tag{3.12}$$

where

$$\Gamma_{inc}(n,\ \lambda\pi\delta^2) = \frac{1}{\Gamma(n)} \int_{\lambda\pi\delta^2}^{\infty} t^{n-1} e^{-t} dt,$$

is the upper-incomplete gamma function that is nothing but Prob $\{|C(\delta)| < n\}$ with $C(\delta)$ being the disk with radius δ. From this conditional probability we deduce the probability distribution function of the number of hops as,

$$p^0_{hops}(n) = \int_0^R [\mathbb{P}^0_{hops}(n-1|\delta) - \mathbb{P}^0_{hops}(n|\delta)] p(\delta) d\delta, \tag{3.13}$$

with $p(\delta)$ being the distribution of δ. By numerically computing this distribution, we are enabled to derive the mean and the standard deviation of the typical hops number from the origin o to a random destination.

3.2 Multi-hop routing protocols

We focus, in this subsection, on the multi-hop routing protocols used to set up end-to-end communications between two network nodes. Depending on the nodes positions knowledge we distinguish between two types of routing protocols, the optimal and sub-optimal ones.

3.2.1 Optimal Shortest Path routing protocol

This protocol is based on Dijkstra's shortest path algorithm [24] applied to the whole network graph including cluster nodes and cluster heads $\mathcal{N} \cup \mathcal{H}$. This protocol is considered as optimal because it assumes full knowledge at any node of all the network paths, which enables a source to find the optimal path in term of number of hops to the destination. However, a substantial drawback of this protocol is its unfeasible need of a large amount of feedback, Figure 3.4 illustrates this algorithm.

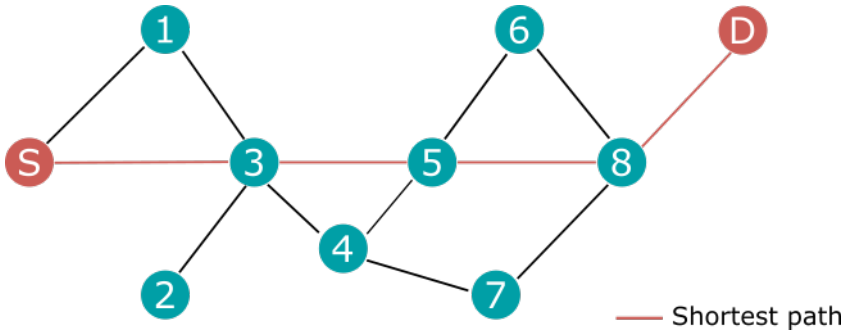

Figure 3.4: Shortest path algorithm

3.2.2 Sub-optimal Progressive spread angle furthest neighbors search

Sub-optimal Progressive spread angle furthest neighbors search protocol discovers a feasible path discovery for multi-hop end-to-end communications. The source node searches the furthest intermediate neighbors within a spreading angle toward the destination. Figure 3.5 illustrates this path discovery protocol and the detailed algorithm is depicted below in Algorithm 3.

3.2.3 Shipmaster aided protocol

The source node forwards first its message to its CH. This latter uses the shortest path algorithm to compute the route in its cluster and indicates the path to the source and informs the nodes in its cluster to relay the information. The CH uses the CH backbone graph $\mathcal{G}_h$ to localize the destination and to send the message to the concerned destination CH via the shortest path. Finally, the message is relayed in the destination cluster via the

Algorithm 3: Progressive spread angle furthest neighbors search protocol

Input : Total graph: $\mathcal{G}_{all} = \cup_k \mathcal{G}_k \cup \mathcal{G}_h$, s and d the source and destination ids, spread angle Θ, current delay t and the maximal end-to-end delay t_{max}.

Output: $\mathcal{P}$, the set of intermediates nodes from s to d.

$t \leftarrow 0$;
$\mathcal{NB} \leftarrow \{x \in \mathcal{G}_h \text{ s.t. } |x \rightarrow s| \leq d^*_{ss}\}$; // set of neighbors of s
if $d \in \mathcal{NB}$ **then**
    $\mathcal{P} = \{s, d\}$;
    else
        $\theta_d \leftarrow \angle sOd$; // angle between s and d
        $\mathcal{I} \leftarrow \{x \in \mathcal{NB} \text{ s.t. } \theta_d - \Theta < \angle sOx < \theta_d + \Theta\}$; // set of possible intermediates nodes
    end
end
$Intra \leftarrow 0$; // 1 if s and d are in the same cluster, 0 otherwise
while $d \notin \mathcal{P}$ ***and*** $t < t_{max}$ ***and*** $\mathcal{I} \neq \emptyset$ **do**
    if $\{\exists x \text{ s.t. } x \in \mathcal{S} \cap \mathcal{H}\}$ ***and not*** $Intra$ **then**
        $\mathcal{I} \leftarrow \{x\}$;
        $i \leftarrow x \in \mathcal{I}$ s.t. x is the closer node to d;
        else
            $i \leftarrow x$ s.t. $x \in \mathcal{I}$ **and** $x \in \mathcal{H}$ s.t. x is the closer node to d; // intermediate node
        end
    end
end
$\mathcal{P} \leftarrow \mathcal{P} \cup i$;
$t \leftarrow t + delay$;
$\mathcal{NB} \leftarrow \{x \in \mathcal{G}_h \notin \mathcal{P} \text{ s.t. } |x \rightarrow i| \leq d^*_{ss}\}$; // set of neighbors of i
if $d \in \mathcal{NB}$ **then**
    $\mathcal{P} \leftarrow \mathcal{P} \cup d$;
    else
        $\theta_d \leftarrow \angle iOd$; // angle between i and d
        $\mathcal{I} \leftarrow \{x \in \mathcal{NB} \text{ s.t. } \theta_d - \Theta < \angle iOx < \theta_d + \Theta\}$
    end
end
if $t = t_{max}$ ***or*** $\mathcal{I} = \emptyset$; **then**
    $\mathcal{P} \leftarrow \emptyset$;
end

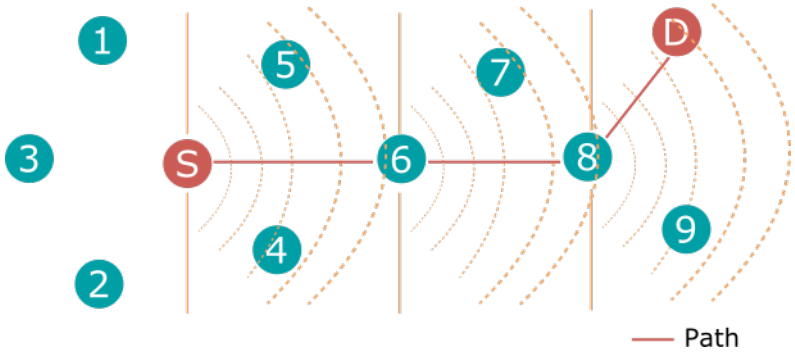

Figure 3.5: Progressive π-spread angle furthest neighbors search

staff-ships from the CH to the final destination using the shortest path algorithm.

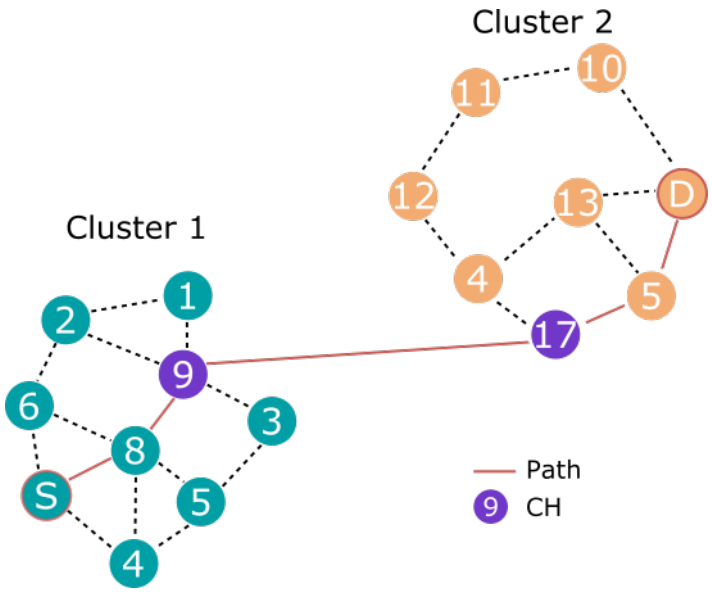

Figure 3.6: Inter-cluster Shipmaster aided routing protocol

3.2.4 Gateways Search

As we said earlier, the gateway nodes are cluster nodes able to communicate with neighboring clusters. These nodes are usually situated at the cluster edges, and may be used has relay nodes to establish inter-cluster communication links. The set of GWs is defined as:

$$\mathcal{GW}_k = \left\{ x \in \mathcal{C}_k : \exists\, y_j \in \mathcal{C}_k / \text{dist}(x_i, y_j) \leq d^*_{ss} \right\} \tag{3.14}$$

The source node s searches the nearest gateway node in its cluster to the destination d cluster using the shortest path algorithm. Once the destination gateway is reached, path

discovery to the destination node is done with the shortest path algorithm on the graph $\mathcal{G}_k / d \in \mathcal{C}_k$

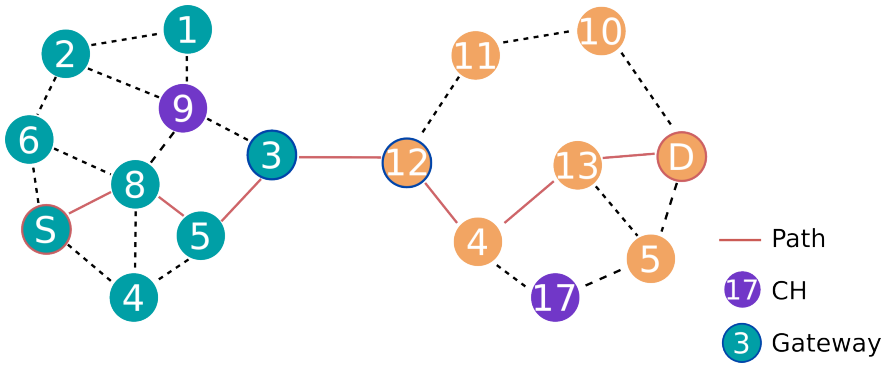

Figure 3.7: Inter-cluster Gateways search protocol

3.3 Hybrid stations strategy

Henceforward, we consider that all the CHs are provided with Ultra Small Aperture Terminals "USATs" satellite gateways as well as a random number of staff-ships, from now referred as hybrid stations "HSs" grouped in the set $\mathcal{S}$. We introduce the parameter $\beta_{\text{sat}} \leq 1$ describing the PPP intensity of the hybrid stations in function of the PPP intensity of the cluster nodes λ_c as:

$$\lambda_s = \beta_{\text{sat}} \lambda_c.$$

From (3.3a), we can easily express the average number of HSs N_s in the typical cluster $\mathcal{C}_o$ as:

$$N_s = \left\lceil \frac{\lambda_s}{\lambda_h} (1 - e^{-\lambda_h \pi R^2}) \right\rceil.$$

We aim to empirically estimate the intensity λ_s e.g. the parameter β_{sat} to ensure that the end-to-end delay through the satellite backhaul is less than a certain threshold. Thus, in the following we present a satellite path discovery protocol and an exhaustive solution to estimate β_{sat}.

3.3.1 Terrestrial versus Satellite path

During the communication path discovery, a source node s attempting to join a destination d may find a terrestrial path with an end-to-end delay greater than the tolerated one. In this case the satellite backhaul appears as an alternative. However we notice that the transmission delay differs between terrestrial and satellite networks [70]. Indeed, due to the large distance between a satellite ground station and the satellite end-to-end delays are larger in satellite networks as one could expect, moreover the satellite end-to-end delay depends on the satellite orbits. Thus we introduce the parameter $\kappa_s \in \mathbb{N}^*$ determining a

rough estimate between the satellite link end-to-end delay D_{sat} and the terrestrial one: D_{ter} as

$$D_{sat} = \kappa_s D_{ter}.$$

We define the cost matrix $\mathbf{C}$ of the network links weights as:

$$\mathbf{C} = \begin{cases} dist(i,j) \leq d^*_{ss}, & \forall\ (i,j) \in (\mathcal{N}|\mathcal{H} \times \mathcal{N}|\mathcal{H}) \\ dist(i,j) \leq d^*_{sh}, & \forall\ (i,j) \in (\mathcal{N}|\mathcal{H} \times \mathcal{H}) \cup (\mathcal{H} \times \mathcal{N}|\mathcal{H}) \\ \kappa_s, & \forall\ (i,j) \in \mathcal{S} \times \mathcal{S}. \end{cases} \tag{3.15}$$

Hence, during the path discovery, the accurate delay cost of a path can be computed using the Dijkstra's [24] algorithm and the one with the minimal cost is selected. We describe below the satellite path discovery protocol.

3.3.2 Satellite path discovery

We propose a strategy enabling s to find the shortest path to d through the satellite backhaul considering that the CHs periodically broadcasts the HSs positions to the cluster nodes:

- **Step 1:** The source node s forwards its message to the closest HS (HS_s) using the shortest path routing protocol.
- **Step 2:** HS_s uses the satellite backhaul to find HS_d the closest hybrid station to the dest.
- **Step 3:** HS_d forwards the message to d using the shortest path routing protocol.

4 Numerical results

In this section we first consider a MANET where the staff-ships and the shipmasters are randomly distributed in a circular area of radius R, according to a PPP in $\mathbb{R}^2$ with intensity λ_c and λ_h respectively. We derive the CDFs of the inter-CHs and inter staff-ships coverage radii in a centralized and distributed access schemes using literature and HMC clustering algorithms. We also empirically derive the PDFs of the delays to head in a distributed scheme. Then, we focus on the end-to-end delays and compare the performances for the path discovery protocols discussed above. Secondly, we investigate the hybrid aspect of the MANET where the CHs and a random number of staff-ships are equipped with satellite gateways consisting in Ultra Small Aperture Terminals "USATs". We consider that the staff-ships provided with USATs are randomly distributed according to a PPP with intensity $\beta_{\text{sat}}\lambda_c$ ($\beta_{\text{sat}} \leq 1$).

4.1 Simulation parameters

We resume in the following Table 3.1 the parameters considered in this study:

General Parameters	
Area radius	$R = 5$ km
Staff-ships intensity	$\lambda_c = 6e^{-1}$
Shipmasters intensity	$\lambda_h = 1e^{-1}$
Staff-ships → CH ratio	$\alpha = 1, 1.75$
Upper-bound threshold	$p_{th} = 1\%$
USAT ratio	$\beta_{\text{sat}} = 0, 0.25, 0.5, 0.75$ and 1
Sat./Ter. delays scaling factor	$\kappa_s = 3, 10$ and 14
Clustering Algorithms Parameters	
k-means	$k = \lvert\mathcal{H}\rvert$
Max-Min and KCMBC	$d = 4$

Table 3.1: Simulation parameters

4.2 Coverage radii

We recall that the staff-ship → shipmaster coverage radius is assumed to possibly be higher than the inter staff-ships one, meaning $d_{sh,\max} = \alpha d^*_{ss,\max}$ with $\alpha \geq 1$. We set a connectivity threshold to $p_{th} = 1\%$. With this threshold, the centralized inter-shipmasters and intra-cluster coverage radii analytically computed in (3.4) and (3.5) are $d^*_{hh,\max} = 9.99$ km and $d_{sh,\max} = 5.4$ km .

In Figure 3.8, we numerically evaluate the CDFs of the inter-shipmasters coverage

radii assuming that $\alpha = 1$ for the centralized and distributed access schemes of HMC, and k-means algorithm where the closest node to the centroid is elected as CH. We also provide these CDFs for Max-Min and KCMBC algorithms. Note that even if the number of clusters is not initially limited in the case of Max-Min and KCMBC algorithms, we choose to limit the number of clusters for fair comparison. For the distributed HMC network, the coverage radius is equal to 7 km while for the centralized scheme the coverage radius is equal to 9.9 km to ensure inter-heads communications in 99.99% of the cases. It can be seen that the random choice of the CH imposed by the hierarchical context significantly increases the inter-heads coverage radius in the network. Indeed for k-means algorithm the inter-shipmasters coverage radius for the distributed access scheme (respectively centralized) is equal to 5.1 km (respectively 9.2 km). The d-hops algorithms require shortest coverage radius than HMC, however we notice that the restriction of the CH number discussed above lead to less clusters, explaining these improvements. For instance, KCMBC leads to a unique cluster in 53% of the cases.

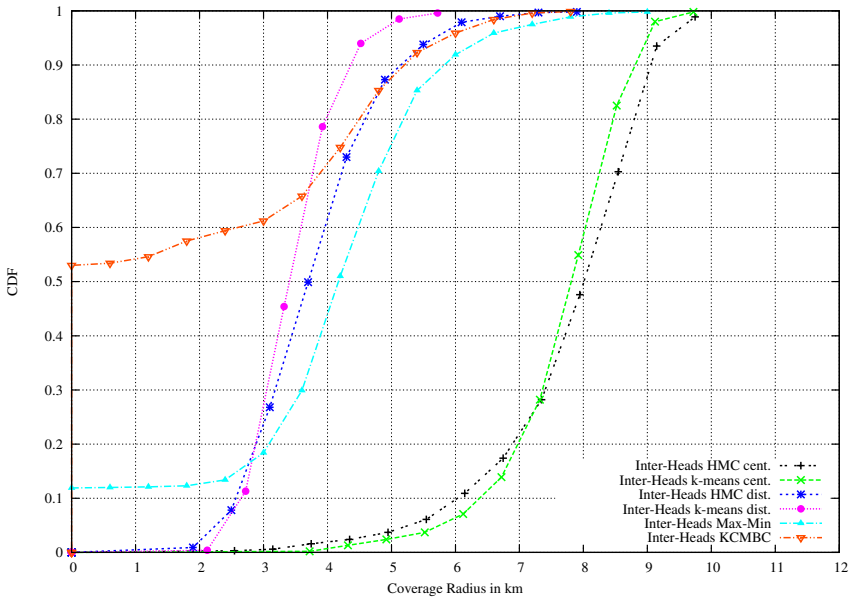

Figure 3.8: Inter-shipmasters coverage radii distributions

We evaluate in Figure 3.9 the CDFs of intra-cluster coverage radii. The hierarchical context penalizes more the intra-cluster coverage radius than the inter-shipmasters one, we observe that for the distributed access scheme in HMC and k-means the coverage radius is of 3.9 and 3.2 km respectively, in 99.99% of the cases. Max-Min and KCMBC have quite similar requirements than the HMC distributed. From Figure 3.8 we notice that the d-hops algorithms lead to less clusters than the HMC algorithm which explains the coverage radius distribution for intra-cluster communications. One can remark that as k-means optimally sets the positions of the CHs at the nearest point to the staff-ships barycenter, the CDF of the intra-cluster coverage radius is the lowest one among the other clustering algorithms.

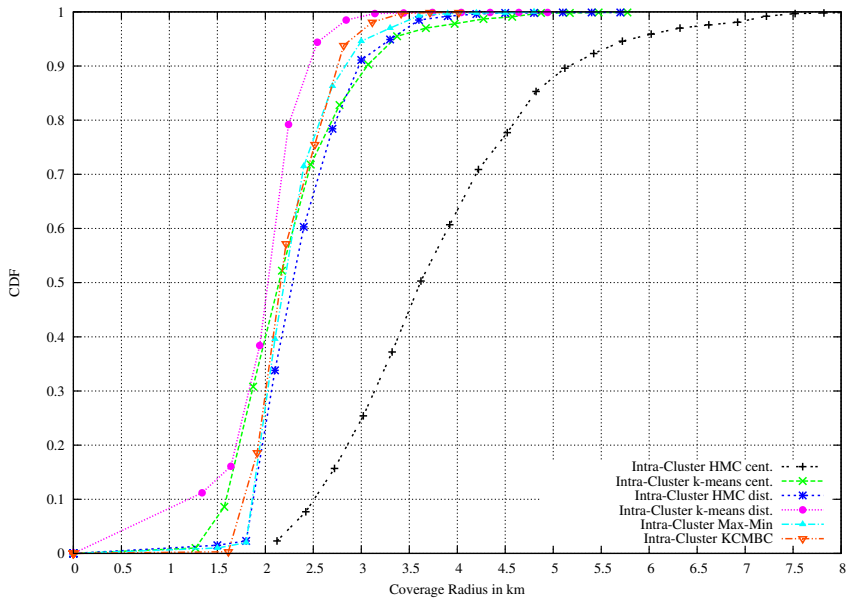

Figure 3.9: Intra-cluster coverage radii distributions

4.3 Delays to shipmaster distribution

Figure 3.10 compares the delays to head within one cluster for the HMC distributed, k-means, Max-Min and KCMBC algorithms. For the k-means, the CH is elected at the center of the cluster and 88% of the nodes have access within 1-hop to their CH. By adequately adjusting the scaling α-parameters, the delays to the head is minimized: For the distributed case with $\alpha = 1$, only 46% of nodes are connected within 1-hop with the CH compared to 72% with $\alpha = 1.75$. Hence, the network designer is can adjust this scaling factor, to find an accurate trade off between the equipments requirements and the achievable coverage radii. Max-Min and KCMBC have the same behavior, they provide higher delays than the other algorithms as they lead to clusters with bigger size.

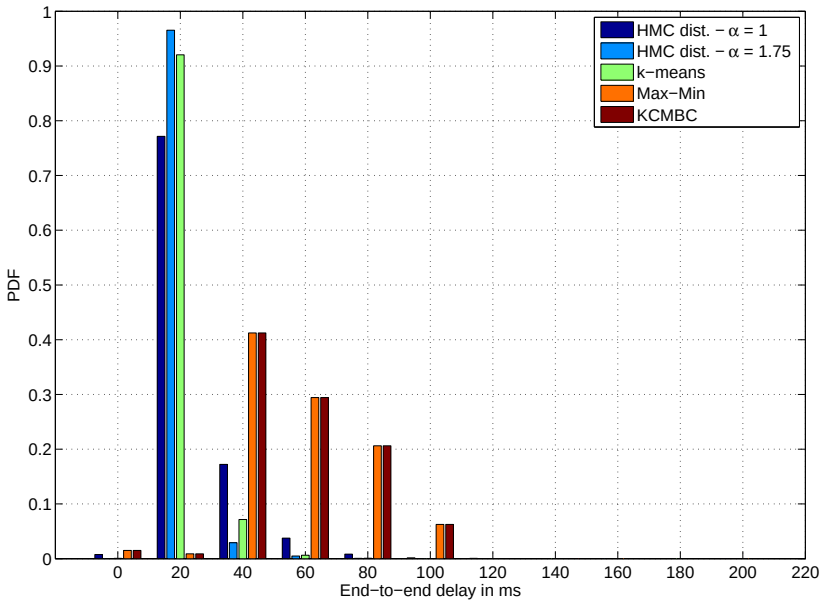

Figure 3.10: Intra-cluster hops to shipmaster distribution

4.4 Multi-hop end-to-end communications ICDF

Figure 3.11 illustrates the upper-bound in (3.12) on the ICDF of the number of hops for different source-destination distance ranges computed for $d_s \to \infty$. Naturally, the number of required hops becomes more significant for large distance ranges. At a given distance range and using the nearest point search, the number of hops is relatively high when the density of close neighbors around the nodes is high and this induces high redundancy in the message transmission. Based on the numerical evaluation of distance to the origin $p(\delta)$ in (3.13), the typical mean number of hops to o and the standard deviation are 27 and 15.9. Although the nearest point search protocol optimizes the power consumption, it is not efficient in terms of end-to-end delay due to the transmission redundancy in the network and results in a large number of required end-to-end hops.

4.5 Probability distribution function of end-to-end delays

The probability distribution function of the end-to-end communication delays using the above mentioned routing protocols are evaluated in Figure 3.12. We can see that the performance of the Progressive furthest point search with an angle spread of π protocol is close to the optimal Dijkstra shortest path. For both algorithms, the end-to-end delays are less than 160 ms almost surely. However, for the shipmaster aided protocol the delays are higher than 160 ms for almost 3% of the cases. The gateways search protocol appears to slightly less perform than the progressive search protocol. The use of USAT at the staff-ships depends critically on the end-to-end delay tolerance that will dictate the maximal

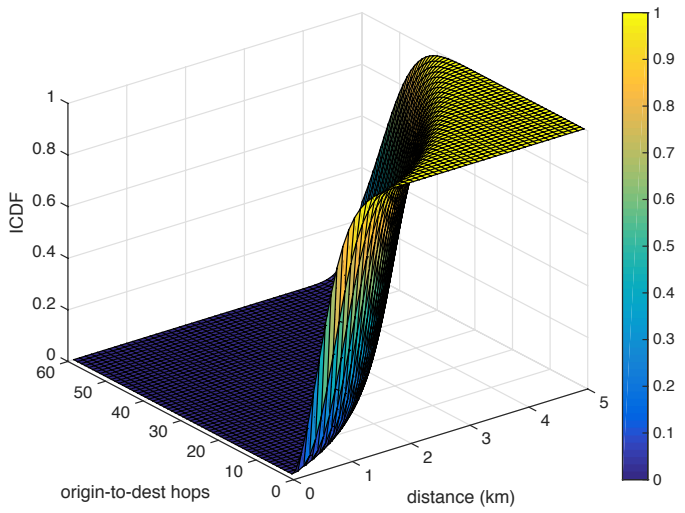

Figure 3.11: Typical ICDF upper-bound on $o \rightarrow d$ hops number

authorized number of hops in the network. For example, by setting a short end-to-end delay tolerance corresponding to 60 ms, the percentage of communications requiring more than 60 ms is equal to 26% for the shortest path, respectively 29% and 21% for the progressive search and the gateways search. This percentage is significant and the deployment of USATs at all staff-ships is then required. However, for flexible tolerance corresponding to 140 ms, less than 0.1% of communications requires a number of hops greater than this value with the shortest path or the progressive search protocols, and 5.5% with the shipmaster aided protocol. The multi-hop terrestrial communications are then sufficient to establish all end-to-end communications.

4.6 End-to-end delays with USATs probability density function

Hereafter, we consider that the shipmasters and a random number of staff-ships are equipped with satellite gateways. The intensities of the PPP determining the distribution of the staff-ships provided with USAT are derived for $\beta_{\text{sat}} = 0, 0.25, 0.5, 0.75$ and 1, which corresponds to an average number of staff-ships USATs per cluster equal to $N_s = 0, 2, 3, 5$ and 6. We assume that the partitioning of the network is done through HMC algorithm with a distributed access scheme. The case where β_{sat} is null implies that only the shipmasters are equipped with satellite gateways. Moreover, the end-to-end delay scaling factor κ_s between the terrestrial and the satellite communication link depends on the satellite orbits. Indeed the more the orbits are elevated the more the propagation delays are long. Thus, in this work, we study the cases where Low Earth Orbit "LEO", Medium Earth Orbit "MEO"and Geostationary Earth Orbit "GEO" satellites [7] support the MANET, respectively corresponding to $\kappa_s = 3, 10$ and 14.

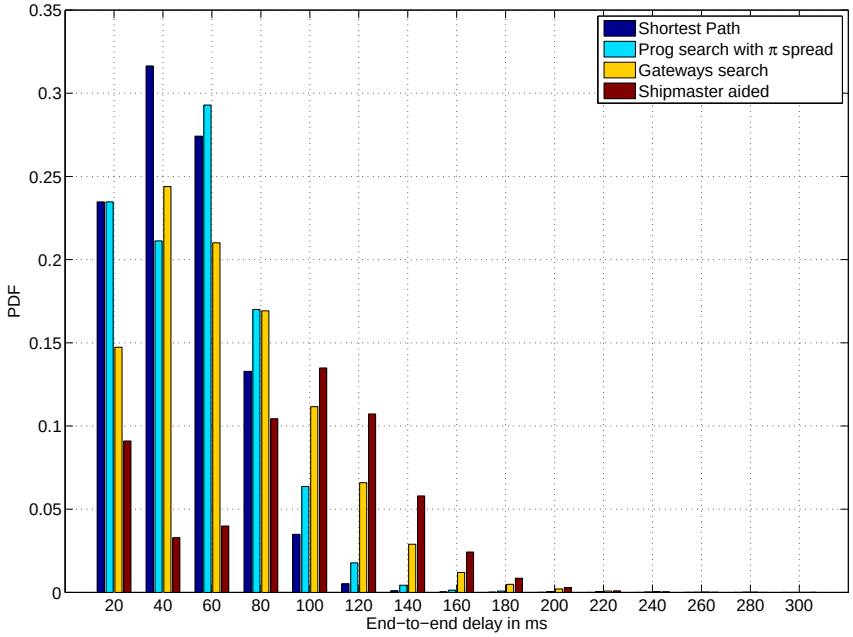

Figure 3.12: End-to-end delays distributions

In Figure 3.13, we numerically derive the PDF of the end-to-end delays, through Dijkstra algorithm, in the network where the MANET is coupled with a LEO satellite network. Thus, when a terrestrial hop is assumed to have a delay $D_{ter} = 20$ ms, the satellite end-to-end delay is assumed to $D_{sat}^{LEO} = 3 \times 20 = 60$ ms. It can be seen that the satellite backhaul is only used when D_{ter}^{LEO} is equal to 60 ms i.e. to D_{sat}. We notice that, as expected, the more the number of USATs, the more the end-to-end delays are of 60 ms. Indeed, when the shipmasters are the only satellite gateways, 27% of the cases have a propagation delay of 60 ms while 46% when all staff-ships are provided with USATs. Moreover, with the latter configuration the end-to-end delays are upper-bounded by 60 ms as all communications are made within one hop through the satellite backhaul.

Figures 3.14 and 3.15 represent the PDF of the end-to-end delays with a MEO and GEO satellite backhauls respectively. The satellite link end-to-end propagation delay corresponds here to $D_{sat}^{MEO} = 10 \times 20 = 200$ ms and $D_{sat}^{GEO} = 14 \times 20 = 280$ ms. One can observe that with these configurations the satellite backhaul is useless, whatever the number of USATs in the network, the terrestrial link remain the more advantageous in terms of end-to-end delays. However the satellite backhaul can be necessary for inter-MANETs communications or to join a land station.

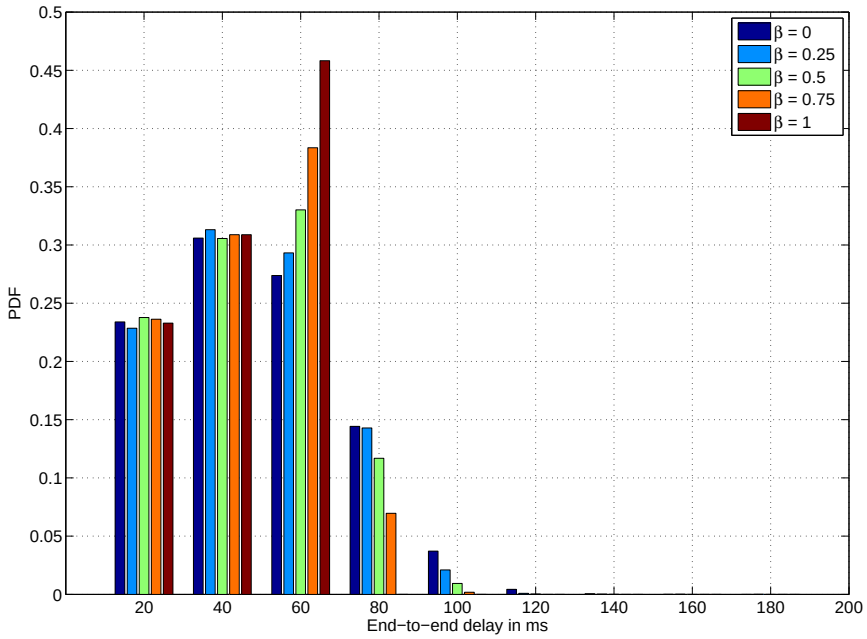

Figure 3.13: End-to-end delays with LEO satellite systems, $\kappa_s = 3$

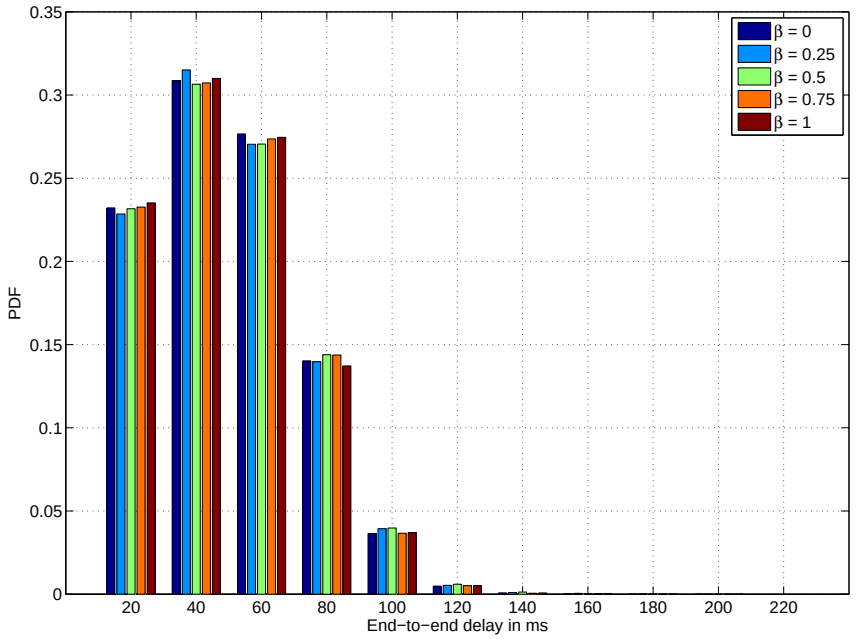

Figure 3.14: End-to-end delays with MEO satellite systems, $\kappa_s = 10$

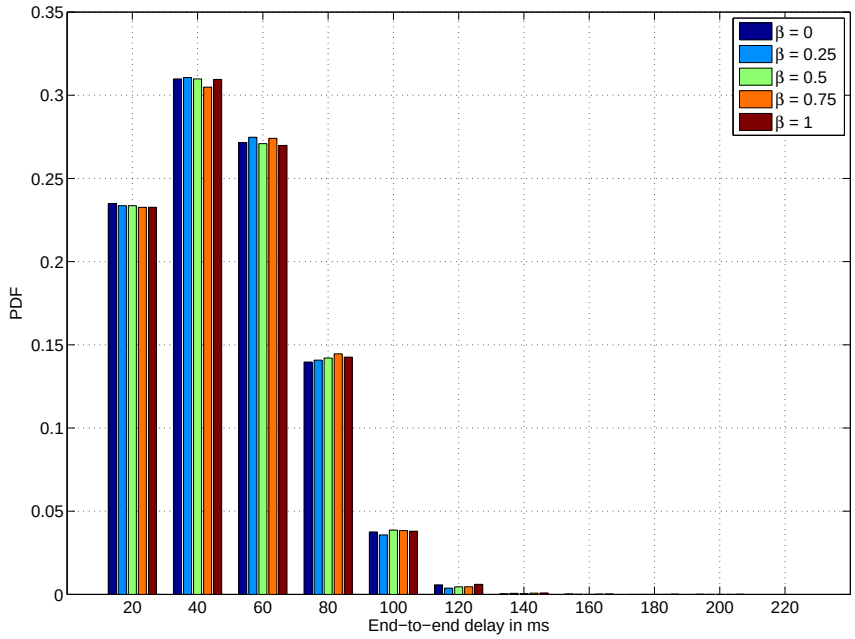

Figure 3.15: End-to-end delays with GEO satellite systems, $\kappa_s = 14$

We study in Figure 3.16 the improvements induced by the LEO satellite backhaul i.e. $\kappa_s = 0.75$. To do so, we numerically derive the PDF of the end-to-end delays using the optimal Dijkstra algorithm with the cost matrix $\mathbf{C}$ in (3.15). The two cases considered are the case where only terrestrial communications links are available in the MANET i.e. no shipmasters are provided with USATs and $\beta_{sat} = 0$, the second case is the one where shipmasters and 75% ($\beta_{sat} = 0.75$) of staff-ships are equipped with satellite gateways. It can be see that the proportion of nodes connected within 40 and 60 ms of end-to-end delay is 42% with only terrestrial communications, the satellite backhaul with 75% of hybrid stations increases by 24% this proportion to achieve 66% of connected nodes within an en-to-end delay of 40 and 60 ms.

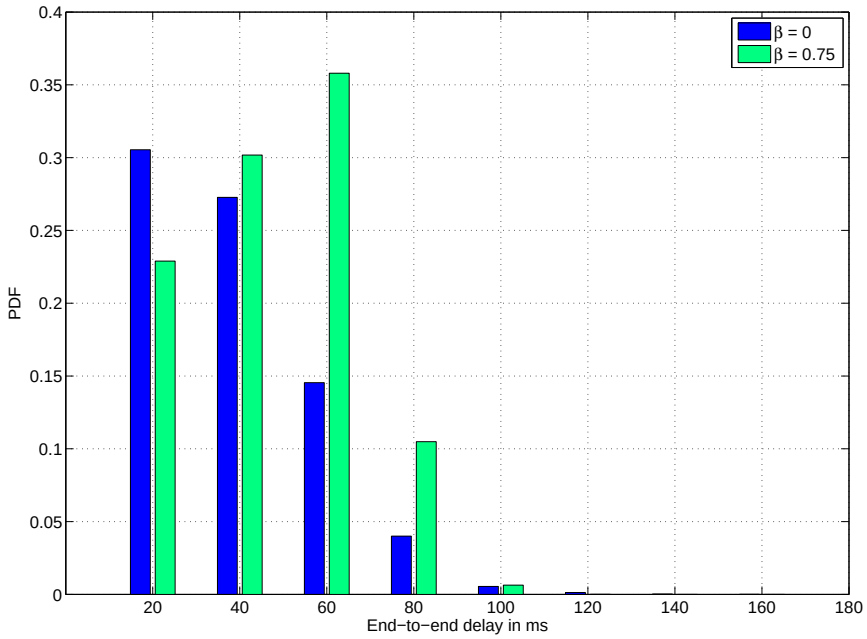

Figure 3.16: Terrestrial end-to-end delays comparison with LEO satellite systems

5 Conclusion

This chapter addressed the topology design in a maritime hybrid Satellite-MANET where nodes are either terrestrial stations with LTE radio devices or hybrid satellite-terrestrial stations, also equipped with satellite gateways. We aimed to provide a solution for a network designer to estimate the required equipment characteristics and network parameters such that the antenna configuration, the power at the transmitter, the bandwidth, the routing protocol and the gain induced by the satellite component. We first focused on the network partitioning and introduced an algorithm, referred as Hierarchical MANET Clustering, suiting the restrictions imposed by the context characteristics. We then developed a statistical model to evaluate the required inter-shipmasters and intra-cluster coverage radii, $d^*_{sh,max}$ and $d^*_{hh,max}$, to ensure fully connected clusters and thus full connection in the network. Two access schemes were envisaged: i) the centralized case where all staff-ships have to be situated at one hop from their respective cluster head, ii) the distributed access schemes with pairwise communications in which the intermediate nodes act as decode and forward relays. For the first one we provided an analytical solution to derive the upper-bounds on the coverage radii, and an exhaustive algorithm was proposed for the latter. By computing the cumulative distribution of this coverage radii, we showed by comparing the clusters resulting from the literature algorithms and HMC one, that the constraining hierarchical context slightly penalizes the coverage range for intra-cluster communication but has a greater impact on the inter-shipmasters required ranges.

Additionally, we evaluated the statistical behavior of the end-to-end communications delays. We introduced several path discovery protocol and showed that for the distributed access the protocol optimizing the nodes distribution in the network is the progressive search with π-spread angle. Numerical results show that this latter has close performances to the optimal shortest path algorithm one. Finally we introduced a strategy for optimizing the number of HSs and to determine when the satellite backhaul optimizes the end-to-end communications delays. We considered three types of satellite backhauls: LEO, MEO and GEO, and showed that the propagation delays with the two latter are too elevated in our study case. Thus, terrestrial communications links are sufficient for intra-network communications. With the LEO satellite backhaul, we demonstrated that the end-to-end delays can be efficiently reduced by the deployment of HSs. The end-to-end delays distributions in function of the number of HSs in the network were computed, enabling the network designer to perceive a trade-off between the cost and the contributions of these structures.

In keeping with this work, the following chapter focuses on the resource outage probability and the dimensioning in a cluster with a centralized access scheme. We aim to provide an analytical model for the network designer to estimate the required bandwidth for different antenna configurations and transmission modes, considering the maritime propagation fluctuation impact.

4 Centralized Network Resource Outage & Dimensioning

Resource outage is a main issue in the design of a network and more particularly in MANETs. Radio Resource Management "RRM" is used to optimize the allocated bandwidth in such way to serve all users while minimizing the probability of the event that arises when the management entity has no more radio resources to attribute to the users. This event will be denoted as "radio resource outage event". The radio dimensioning problem depends critically on the network parameters including the network load, the antenna configuration, and the required Quality of Service "QoS". This chapter focuses on the dimensioning in a cluster of a MANET with a centralized communication scheme. We use stochastic geometry tools to provide an analytical model enabling a network designer to estimate the required bandwidth to avoid the radio resource outage event. To this intent, we first derive an upper bound on the resource outage probability considering networks parameters. Then, we estimate the average number of RBs requested by the CNs and thus the necessary bandwidth for the single and multiple class users QoS. Afterwards, based on this upper-bound, we determine the number of RBs required by the network in such a way that the occurrence of the radio resource outage does not exceed a given threshold. The average spectral efficiency in the ad hoc network is then deduced. Moreover the impact of the maritime propagation fluctuation is studied and a linear model to foresee this impact on the bandwidth estimation is provided.

1 Introduction

In this chapter, we address the radio resource outage probability and the dimensioning matters in a cluster of a MANET with a centralized access scheme. The radio resource management is an essential aspect of the network. A network planner has to provide the necessary resources i.e. the required bandwidth to serve all the network users with a certain quality of service. The entity in charge of the RRM, here the shipmaster, allocates a determined number of resources to a user in function of its channel conditions and its required QoS. In this work, the channel conditions are described by the multi-path fading

experienced by the signal during its propagation additional to the propagation path loss in a maritime environment.

We consider a circular cluster $\mathcal{C}$ of radius R belonging to a centralized MANET in which communications transit via the CH. We assume that the nodes are equipped with 1 or 2 transmit and receive antennas with omnidirectional gains. We define Φ_{nodes} the set of active nodes in the cluster. The radio resources considered in this chapter correspond to the LTE radio Resource Blocks "RBs" (see Chapter 2). The total bandwidth is divided into several RBs. The users still correspond to ships and form a navy fleet that is led by a shipmaster. In this chapter we consider that two antenna configurations are available for the $CN \rightarrow CH$ (uplink) transmission, the SISO mode and the 2×2 MIMO one; note that unlike the cellular network UEs, the considered CNs are evolved transmitters and advanced open loop transmission modes "TMs" can be defined. The 2×2 MIMO configuration is compliant with the LTE standard [4] and is studied for two TMs introduced in Chapter 2: the first one extracts the full diversity gain of the MIMO using an Alamouti [71] scheme and the second one multiplexes different streams on the same RB using a Successive Interference Cancellation "SIC" decoder. The average statistical behavior of the network will be considered, nodes arriving to a given area are assumed to be randomly distributed around the CH according to a random Poisson Point Process "PPP". The randomness of the wireless channel will be considered as a mark of the Poisson position and results from stochastic geometry using marked Poisson Point Process will be invoked. This tools were investigated in [?] to compute the resource outage probability in a cellular network considering random Poisson Point Process marked by the random shadowing.

In the following, fundamental assumptions used in our derivations are introduced, we then derive the radio resource outage probability upper-bound for the different antenna configurations and deduce the average spectral efficiency expression. The maritime propagation fluctuation and its impact on the radio resource dimensioning is also discussed. Finally, the numerical results enabling our analytical model validation are derived at the end of the chapter. Parts of this are published in [25] and [26].

2 Fundamental Assumptions

The cluster considered in this work is denoted by $\mathcal{C}$, of radius $R = 20$ km and belongs to a centralized MANET in which communications transit via the CH. The mobile nodes are assumed to be equipped with 1 or 2 transmit and receive antennas with omnidirectional gains. We define ϕ_{nodes} the set of active nodes in the cluster. Each node at position $x \in \mathcal{C}$ request $N_{RB}(x)$ RBs to achieve its target throughput C_0. The total requested RBs number N_{total} can be expressed as $N_{\text{total}} = \sum_{x \in \phi_{\text{nodes}}} N_{RB}(x)$. Here follow the basics fundamental assumptions on the network essential in our future derivations:

- **Assumption 1**: The surface density of inter-arrival time in $min^{-1}km^{-2}$ is defined by ρ.

- **Assumption 2**: For all nodes, the mean service time in min^{-1} is exponentially distributed with mean μ^{-1}.
- **Assumption 3**: The active nodes are randomly distributed according to an homogeneous PPP of intensity $\Lambda(\mathrm{dx}) = \lambda(dx)$ with $\lambda = \rho v^{-1}\ Tx/km^2$.
- **Assumption 4**: The channel gain depends on three components: the path loss, the Rayleigh random fading attenuation and the log-normal shadowing attenuation. In a maritime context the shadowing effect resulting from the presence of obstacles on the propagation path can be neglected. Moreover, the fading coefficients between transmitting antennas are assumed to be Rayleigh distributed due to NLOS transmission induced by long range communication distances.
- **Assumption 5**: The outer interferers are neglected and we consider that the MANET is noise limited. Indeed, due to the centralized cluster communication, there is no intra-cluster interference. The CHs coordinate the choice of the frequency reuse pattern to guarantee that the inter-cluster interference induced by the remote clusters is negligible compared to the thermal noise power.
- **Assumption 6**: The $CH \rightarrow CN$ communication is established if the SNR is higher than a threshold β_{min}.

The following Figure 4.1 illustrates the cluster configuration, its components and specificities:

3 Analytical model definition

In this section, we review from [28] the statistical tools used in our derivations to provide the upper bound $\mathbb{P}_{sup}$ on the resource outage probability $\mathbb{P}_{out}$. We define the radio resource outage probability and review from [72] the use of the Bennett's concentration inequality in the computation of an upper-bound on the resource outage probability. We show how to make use of this upper-bound to find the adequate bandwidth to be allocated at the CH and the average total achieved spectral efficiency in the network. We finally present the annex tools and the network parameters involved in this study.

3.1 Radio resource outage probability

The set of active CNs is describes by a Marked PPP as follows:

$$\tilde{\Phi} = \{\tilde{X}_i \in \mathcal{C} \times \mathbb{R}^+ : \tilde{X}_i = (X_i, y_i)\}$$

where x is the CN position in the circular cluster $\mathcal{C}$ of radius R and y the random fading coefficient of the path between the CN and the CH. $\tilde{\Phi}$ is characterized by its intensity $\Lambda(dx) \otimes p_y(y)dy = \lambda p(y)dxdy$. We first consider a single class users traffic which means

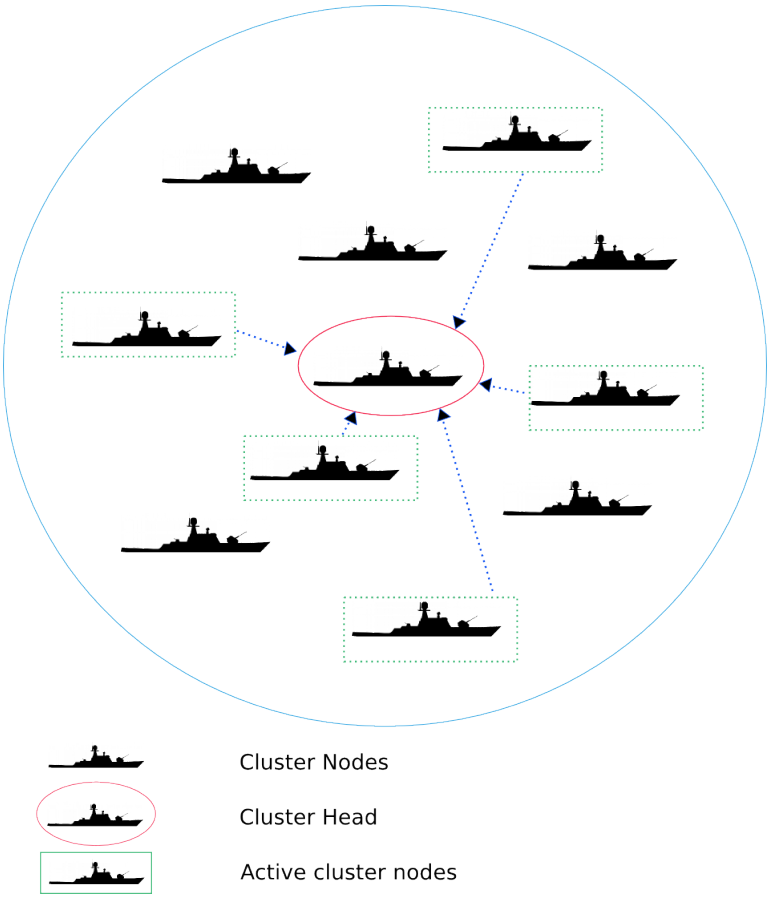

Figure 4.1: Cluster illustration

that all active CNs target the same rate C_0. Let $N_{RB}(x, y)$ denote the random number of required RBs by a given CN positioned at $x \in \mathcal{C}$ and subject to a random fading y, such that:

$$N_{RB}(x, y) = \left\lceil \frac{C_0}{W \times C_{\text{Shannon}}(x, y)} \right\rceil \tag{4.1}$$

where W = 180 kHz is the bandwidth of one RB and $C_{\text{Shannon}}(x, y)$ is the Shannon spectral efficiency that depends on the antenna configuration. The distribution of the fading depends also on the considered antenna configuration and will be further detailed. From **Assumption 6** discussed above, the number of required RBs by a user is upper-bounded by a certain number N_{max} as follows: $N_{RB}(x, y) \leq N_{max}$, where:

$$N_{max} = \left\lceil \frac{C_0}{W \log_2(1 + \beta min)} \right\rceil. \tag{4.2}$$

We can know express the number of RBs required by a CN at position x and subject to a fading y as:

$$N_{RB}(x,y) = min\left(\sum_{j\in\mathbb{N}^*} j\mathbb{1}_{\{j-1<N_{RB}\leq j\}}, N_{max}\right), \tag{4.3}$$

and the total number of required RBs by the active CNs in $\tilde{\Phi}$ as:

$$N_{RB,t}(\tilde{\Phi}) = \sum_{\tilde{X}\in\tilde{\Phi}} N_{RB}(\tilde{X}) . \tag{4.4}$$

The radio resource outage event occurs when the total number of RBs required by all active CNs exceeds N_{net}, the number of available RBs at the CH i.e.

$$\mathbb{P}_{out}(N_{net}) = Prob\{N_{RB,t}(\tilde{\Phi}) > N_{net}\} . \tag{4.5}$$

Our main objective is to find the optimal number of required RBs N_{net} at the CH to guarantee that the outage probability does not exceed a given threshold p_{th}

3.2 Outage probability upper-bound

3.2.1 Single QoS users class target capacity

It is assumed here that all active network users target the same capacity C_0. The Bennett's concentration inequality theorem (Theorem 2.3) from Chapter 2 is an efficient statistical tool to find an upper-bound on the sum of independent randomly distributed bounded variables. The derivation of the resource outage probability upper-bound is based on this theorem. Indeed, in our study the total number of required RBs $N_{RB,t}(\tilde{\Phi})$ appears to be the sum of $N_{RB}(\tilde{X})\ \forall\tilde{X}\in\tilde{\Phi}$, which are independent bounded random variables. Therefore, by setting the expressions of the first and the second moments of the marked PPP as:

$$\begin{aligned} m_N &= \mathbb{E}\left[\sum_{\tilde{x}\in\tilde{\Phi}} N_{RB}(x,y)\right], \\ v_N &= \mathbb{E}\left[\sum_{\tilde{x}\in\tilde{\Phi}} N_{RB}^2(x,y)\right], \end{aligned} \tag{4.6}$$

the upper-bound $\mathbb{P}_{sup}(N_{net})$ on the resource outage probability $\mathbb{P}_{out}(N_{net})$ for $N_{net} = \delta m_N$ is computed as:

$$\mathbb{P}_{sup}(N_{net}) = exp\left(-\frac{v_N}{N_{max}^2} g\left(\frac{(\delta-1)m_N N_{max}}{v_N}\right)\right) . \tag{4.7}$$

with $g(t) = (1+t)\log(1+t) - t$. Moreover, for a marked point process, the expectation of a given function $f(\tilde{X})$ is defined by:

$$\mathbb{E}[f(\tilde{X})] = \int_{\mathcal{C}\times\mathbb{R}^+} f(x,y)p(y)d(y)\lambda dx, \tag{4.8}$$

thus by applying this property to the expression of m_N and v_N we obtain:

$$m_N = \sum_{j=1}^{N_{max}-1} j \int_{\mathcal{C}} \text{Prob}\left\{j-1 < N_{RB}(x,y) \leq j\right\} \lambda \, dx + N_{max} \int_{\mathcal{C}} \text{Prob}\left\{N_{RB}(x,y) > N_{max}-1\right\} \lambda \, dx.$$

Therefore,

$$m_N = \lambda \left[\sum_{j=1}^{N_{max}-1} j(A_j - A_{j-1}) + N_{\max}(\pi R^2 - A_{N_{max}-1}) \right] \tag{4.9}$$

and similarly,

$$v_N = \lambda \left[\sum_{j=1}^{N_{max}-1} j^2(A_j - A_{j-1}) + N_{max}^2(\pi R^2 - A_{N_{max}-1}) \right], \tag{4.10}$$

where A_j is the area of the region in which nodes require at most j RBs illustrated in Figure 4.2 and defined as follows:

$$A_j = \int_{\mathcal{C}} \text{Prob}\{N_{RB}(x,y) \leq j\} \; dx \; . \tag{4.11}$$

3.2.2 Muliple QoS users class target capacity

For the multiple QoS class case, nodes are divided into $\mathcal{K}$ classes and the target capacity in each class is denoted as C_k. As in the single class case, the point process in each class is a marked PPP on $\mathbb{R}^2 \times \mathbb{R}^+$ of intensity $d\Lambda_k(x) \otimes p_u(y)dy$, where $d\Lambda_k(x) = \rho_k(x)v_k^{-1}$. The Poisson point process is independent from each class to an other class, thus the overall point process is a superposition of Poisson point processes with intensity $\sum_{k=1}^{\mathcal{K}} d\Lambda_k(x) \otimes p_u(y)dy$. The number of RBs required by a node in each class is also bounded by $N_{max,k}$ computed in a similar way as in (4.2) due to the threshold SNR β_{min} introduced earlier in **Assumption 6** as follows,

$$N_{max,k} = \left\lceil \frac{C_k}{W \log_2(1+\beta min)} \right\rceil .$$

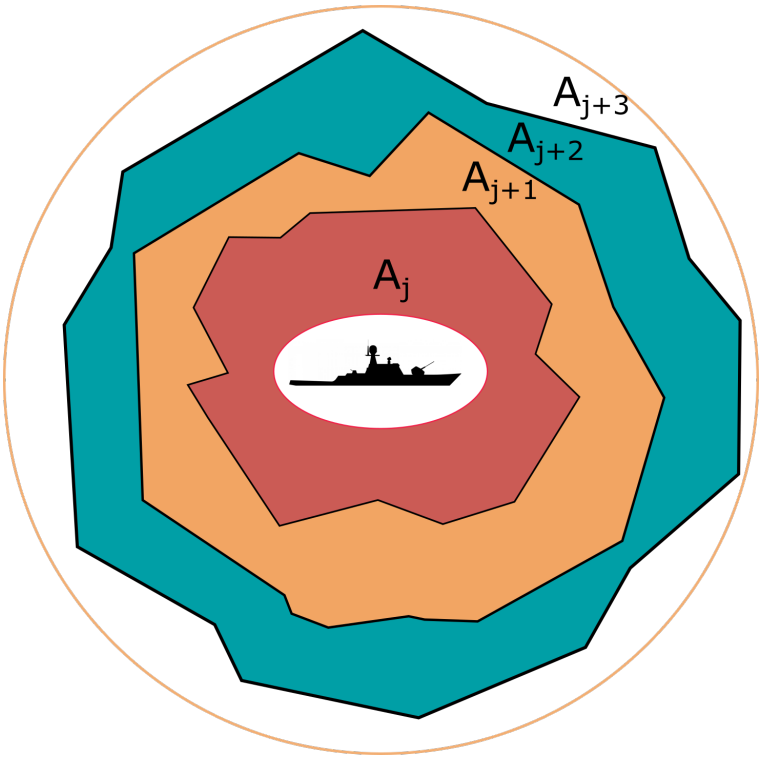

Figure 4.2: Illustration of the areas $A_j s$

The first and second moments of the Poisson point process are thus:

$$\begin{aligned} \bar{m}_N &= \sum_{k=1}^{\mathcal{K}} m_{N,k} \\ \bar{v}_N &= \sum_{k=1}^{\mathcal{K}} v_{N,k}. \end{aligned} \tag{4.12}$$

Finally the resource outage probability upper bound is obtained by replacing $\bar{m}_N$ and $\bar{v}_N$ by their values in (4.7),

$$\mathbb{P}_{sup}^{mult.}(N_{net}) = exp\left(-\frac{\bar{v}_N}{\bar{N}_{max}^2} g\left(\frac{(\delta-1)\bar{m}_N \bar{N}_{max}}{\bar{v}_N}\right)\right). \tag{4.13}$$

where $\bar{N}_{max}$ is the upper-bound on the number of allocated RBs in all QoS classes and defined as $\bar{N}_{max} = \underset{k}{max}\ N_{max,k}$.

3.3 Average spectral efficiency & Dimensioning

The expression of the radio resource outage probability upper-bound $\mathbb{P}_{sup}$ enables to deduce the required number of RBs in the network N_{net} guarantying that the outage probability is less than a certain resource outage probability threshold p_{th}, i.e. $\mathbb{P}_{out}(N_{net}) \leq p_{th}$. The required number of RBs N_{net} is expressed in function of the first moment of the marked PPP as,

$$N_{net} = \delta m_N \,, \tag{4.14}$$

where the scaling factor δ is therefore defined as,

$$\delta = 1 + \frac{v_N}{m_N N_{max}} g^{-1}\left(-\frac{N_{max}^2}{v_N}\log(p_{th})\right). \tag{4.15}$$

The required bandwidth B is deduced according to the value of N_{net} within the normalized LTE bandwidth set {1.4, 3, 5, 10, 15, 20 MHz} or within an aggregated carrier bandwidth. Afterwards, the total average achieved rate in the network is expressed as follows:

$$\bar{C}_t = \mathbb{E}\left[\sum_{\tilde{X}\in\tilde{\Phi}}\left(C_0 \mathbb{1}_{\{N_{RB}(\tilde{X})\leq N_{max}\}} + \sum_{j\geq N_{max}+1} C_j \mathbb{1}_{\{(j-1)<N_{RB}(\tilde{X})\leq j\}}\right)\right],$$

C_j being the achieved rate over N_{max} RBs, provided that C_0 requires j RBs to be achieved and hence C_j satisfies $jC_j = C_0 N_{max}$. Applying the marked PPP property described in (4.8) we can derive a simplified expression of the average total rate $\bar{C}_t$ in function of A_j as defined in (4.11):

$$\bar{C}_t = \lambda\left[A_{N_{max}} C_0 + \lambda \sum_{j\geq N_{max}+1}(A_j - A_{j-1})C_j\right]. \tag{4.16}$$

Finally, we can deduce the average total spectral efficiency of the network in (b/s/Hz) defined as:

$$S = \bar{C}_t / B \,. \tag{4.17}$$

4 Resource Outage in different antenna configurations

In this section we derive an upper-bound on the resource outage probability for three different antenna schemes. We consider the SISO and 2×2 MIMO antenna schemes. Moreover the 2×2 MIMO scheme is studied for two LTE transmission modes (3.1):

- TM_1 which extracts the full diversity using Alamouti [71] space-time codes,
- TM_2 which multiplexes the two different streams on the same radio resource.

To derive this upper-bound, we will derive the expressions of the Shannon capacities and the

cumulative distribution functions of the multi-path fading component for each configurations in order to compute the expression of the corresponding areas of the region A_j.

4.1 SISO communication schemes

For a SISO communication, the Shannon spectral efficiency that will be invoked is expressed in function of the path loss attenuation $\alpha \|x\|^{-\gamma}$ as,

$$C_{SISO}(x, y) = \log_2 \left(1 + \frac{P_T \alpha}{\eta \|x\|^{\gamma}} y\right) \tag{4.18}$$

where η is the thermal noise and y is the random Rayleigh fading exponentially distributed with a cumulative distribution function F described by,

$$F(y) = 1 - e^{-\frac{y}{\sigma_f^2}} \tag{4.19}$$

and σ_f^2 being the fading variance. We define $\tilde{\beta}_j = \frac{P_T \alpha}{\eta} \frac{1}{\beta_j}$ and $\beta_j = 2^{\frac{C_0}{iW}} - 1$. The area of the region A_j in (4.11) in which nodes require at most j RBs is:

$$\begin{aligned} A_j^{SISO} &= 2\pi \left[\xi_{FS} \Gamma_{inc}\left(a_{FS} d_c^{\gamma_{FS}}, \frac{2}{\gamma_{FS}}\right)\right] \\ &+ 2\pi \sum_{i=1}^{2} \left[\xi_{m,i} \Gamma_{inc}\left(a_{\mathrm{m},i} R^{\gamma_{\mathrm{m},i}}, \frac{2}{\gamma_{\mathrm{m},i}}\right)\right. \\ &\left. - \xi_{m,i} \Gamma_{inc}\left(a_{\mathrm{m},i} d_c^{\gamma_{\mathrm{m},i}}, \frac{2}{\gamma_{\mathrm{m},i}}\right)\right], \end{aligned} \tag{4.20}$$

using the gamma and the incomplete gamma functions defined as:

$$\Gamma(m) = \int_0^{\infty} e^{-t} t^{m-1} dt$$

$$\Gamma_{inc}(x, m) = \frac{1}{\Gamma(m)} \int_0^{x} e^{-t} t^{m-1} dt.$$

and the following constants,

$$\xi_{FS} = \frac{1}{\gamma_{FS}} \left(\frac{1}{a_{FS}}\right)^{\frac{2}{\gamma_{FS}}} \Gamma\left(\frac{2}{\gamma_{FS}}\right),$$

$$\xi_{m,i} = \frac{1}{\gamma_{\mathrm{m},i}} \left(\frac{1}{a_{\mathrm{m},i}}\right)^{\frac{2}{\gamma_{\mathrm{m},i}}} \Gamma\left(\frac{2}{\gamma_{\mathrm{m},i}}\right).$$

Detailed computational steps are depicted in Appendix 4.A. The first moment and second moments for the SISO scheme can be therefore computed using (4.9) and (4.10), and consequently the upper-bound can be derived from (4.7).

4.2 MIMO communications with diversity gain

In this subsection we consider that the CH and the CN have 2 transmit and receive antenna each. For a 2×2 MIMO communication, the LTE devices extract the full diversity using an Alamouti code. In this case, symbols are decoded over an equivalent fading y that is distributed according to a chi-squared random variable with 2×4 degrees of freedom and CDF,

$$F(y) = \frac{1}{\sigma_f^2}\Gamma_{inc}\left(\frac{1}{\sigma_f^2}y, 4\right)$$

Using the Alamouti code for the 2×2 MIMO transmission, the spectral efficiency is:

$$C^d_{MIMO}(x, y) = \log_2\left(1 + \frac{P_T\alpha}{2\eta\,||x||^\gamma}y\right)$$

We define $\tilde{\beta_{j,d}} = \frac{P_T\alpha}{2\eta}\frac{1}{\beta_j}$ and $\beta_j = 2^{\frac{C_0}{jW}} - 1$. From (4.11), the area of the region in which nodes require at most j RBs is obtained after computations derived in Appendix 4.B as follows:

$$A_j^{MIMO,d} = 2\pi\left[\int_{\mathcal{C}_{d_c}} r(1 - \frac{1}{\sigma_f^2}\Gamma_{inc}\left(\frac{1}{\sigma_f^2}\frac{r^{\gamma_{FS}}}{\tilde{\beta}_{j,d,FS}}, 4\right))dr\right] + 2\pi\left[\sum_{i=1}^{2}\int_0^{2\pi}\int_{d_{c,i}}^{d_{c,i+1}} r(1 - \frac{1}{\sigma_f^2}\Gamma_{inc}\left(\frac{1}{\sigma_f^2}\frac{r^{\gamma_{m,i}}}{\tilde{\beta}_{j,d,m,i}}, 4\right))dr\right],$$

and it can be numerically computed using the Riemann approximation sum. Once again, the first moment and second moment for this MIMO scheme can be deduced by replacing $A_j^{MIMO,d}$ in (4.9) and (4.10) and consequently the upper-bound can be derived from (4.7).

4.3 MIMO communications with multiplexing gain

In this case, the 2×2 MIMO antenna configuration is used to multiplex on each resource element of the radio RB two data streams. The total rate C_0 is sub-divided into two streams that are spatially multiplexed over the two transmitting antennas. The channel state information is only available at the receiver of the CN and not at the CH transmitter. The CN uses a Successive Interference Cancellation "SIC" decoder (Chapter 5) to cancel the inter-antenna interference. The first stream is first decoded by nulling out the second stream. The second stream is then decoded by subtracting the contribution of the first stream from the observed signal. Two degrees of freedom are left to decode the second stream compared to only one degree for the first stream. The equivalent fading y_1 on which the first stream is decoded is an exponential random variable. Whereas, the second one y_2 is a chi-squared random variable with 4 degrees of freedom. The required number of RBs

by each stream s is then,

$$N_{RB}^{s}(x, y_s) = \left\lceil \frac{C_0/2}{W \min_{s} C_s(x, y_s)} \right\rceil$$

where $\min_{s} C_s(x, y_s) = \log_2\left(1 + \frac{P_t \alpha}{2\eta x^{\gamma}}\, y_s\right)$ and $y_s = min(y_1, y_2) = y_1$ which is exponentially distributed. After some straightforward derivations depicted in Appendix 4.C we obtain:

$$A_j^{MIMO,m} = 2\pi\left[\xi_{FS}\Gamma_{inc}\left(a_{FS} d_c^{\gamma_{FS}}, \frac{2}{\gamma_{FS}}\right)\right] + 2\pi\left[\sum_{i=1}^{2} \xi_{m,i}\Gamma_{inc}\left(a_{\mathrm{m},i} d_{c,i+1}^{\gamma_{\mathrm{m},i}}, \frac{2}{\gamma_{\mathrm{m},i}}\right) - \xi_{m,i}\Gamma_{inc}\left(a_{\mathrm{m},i} d_{c,i}^{\gamma_{\mathrm{m},i}}, \frac{2}{\gamma_{\mathrm{m},i}}\right)\right]$$

From this equation, the first and the second moment in (4.9) and (4.10) can be deduced and consequently the upper-bound can be derived from (4.7).

5 Impact of maritime propagation fluctuation on the dimensioning

The ITU-R propagation model in [3] establishes a relationship between the maritime path-loss and the measured electrical field strength. This latter is empirically measured for different distance ranges at two references min/max frequencies and min/max antenna heights. The ITU recommendation specifies interpolation and extrapolation methods to compute the field-strength values for any frequency and antenna height in the min/max reference range. The field measures were performed in the Mediterranean and the North Sea under different weather conditions cold, temperate or warm sea/ocean. The field measures curves statistically capture the behavior for fields exceeded for 50%, 10% and 1% percentage of time. As discussed in Chapter 2, the maritime propagation path-loss is subject to different fluctuations that affect the dimensioning and therefore may cause resource outage in the network.

To overcome this situation we assume that $\alpha_{\mathrm{m},i}$ and $\gamma_{\mathrm{m},i}$ have respectively a variation of $\Delta\alpha_{\mathrm{m},i}$ and $\Delta\gamma_{\mathrm{m},i}$. We aim to express analytically the variation in the required number of RBs in function of the channel variations. To express ΔN_{net} we base our computations on Taylor's theorem for multivariate functions. The computation of the mean number of required RBs and the resource outage probability upper-bound are based on a partitioning of the cluster into different regions containing the set of CNs that request the same number of RBs. The areas of these regions depend critically on the path-loss exponent and the attenuation factor and should be recomputed for each channel fluctuation. These straightforward calculations require high computational complexity and are not practical in a real scenario.

We recall that the ITU-R maritime propagation path-loss is a piecewise model with two discontinuity points $d_{c,0}$ and $d_{c,1}$. The free-space path-loss is a deterministic model and remains unchanged for the three considered models. As it can be seen from Table 4.1,

both variations of path-loss for distance ranges between $d_{c,0} \leq d \leq d_{c,1}$ and $d_{c,1} \leq d \leq R$ should be considered. We denote by $\overrightarrow{\alpha_{\mathrm{m}}^{0}} = (\alpha_{\mathrm{m},1}^{0}, \alpha_{\mathrm{m},2}^{0})$ and $\overrightarrow{\gamma}_{\mathrm{m}}^{0} = (\gamma_{m,0}^{0}, \gamma_{m,1}^{0})$ the vectors containing the attenuation factors and distance exponents in these two distance ranges.

Our main objective is to provide a linear model to help a network designer to foresee the variation ΔN_{net} in the number of required RBs that will be required to achieve nearly the same target outage probability. We show how to linearly adjust the number of required RBs in function of these fluctuations based on a reference path-loss model that we set, without loss of generality, as the path-loss with 10% of time in a cold sea region. To illustrate this, we propose to predict the variation in the number of RBs considering first a cold sea with 1% of time and then a temperate climate region with 50% of the time. We derive then, the analytical expression that relates the variation in the number of RBs to the channel fluctuations with respect to the reference path-loss model. Based on this analytical model, MANET designers can base the radio dimensioning on a reference path-loss and instantaneously adjust the number of RBs for any path-loss fluctuation induced by weather conditions, salinity, etc.

5.1 Maritime propagation fluctuation

The maritime propagation path-loss defined in Chapter 2 is a piecewise model with two discontinuity points $d_{c,0}$ and $d_{c,1}$. The free-space path-loss is a deterministic model and remains unchanged for the three considered models. Figure 2.14 shows the different maritime propagation path-losses derived from the ITU-R model respectively at 50%, 10% and 1% of time. For distances below 10 km there is no significant change but for long distance signal propagation we observe a significant variation. Our objective is to linearize this variation and to estimate its impact on the network dimensioning. The values of the respective attenuation factors $\alpha_{\mathrm{m},i}$ and distance exponents $\gamma_{\mathrm{m},i}$ are summarized in Table 4.1 below:

Maritime			
	ITU-R 50%	**ITU-R 10%**	**ITU-R 1%**
$\alpha_{\mathrm{m},1}$	1.28×10^{-9}	1.23×10^{-9}	1.11×10^{-9}
$\gamma_{\mathrm{m},1}$	2.9	2.8	2.53
$\alpha_{\mathrm{m},2}$	6×10^{-9}	4.38×10^{-9}	3.17×10^{-9}
$\gamma_{\mathrm{m},2}$	3.9	3.57	3.23
Free space			
α_{FS}	0.89×10^{-9}		
γ_{FS}	2		

Table 4.1: Propagation coefficients

5.2 Variation of the required RBs number

Our main objective is to find the variation ΔN_{net} in the number of required RBs that will be required to achieve nearly the same target outage probability. For this, we consider the expression in (4.7) of the resource outage probability upper-bound and set:

$$f(\alpha_{\mathrm{m}}, \gamma_{\mathrm{m}}, \alpha) = \frac{v_N}{N_{\max}^2} g\left(\frac{(\alpha-1)m_N N_{\max}}{v_N}\right)$$

with $f(\vec{\alpha}_{\mathrm{m}}^0, \vec{\gamma}_{\mathrm{m}}^0, \delta^0) = -\log(p_{th})$. For notation simplification, we let $\vec{h}_0 = (\vec{\alpha}_{\mathrm{m}}^0, \vec{\gamma}_{\mathrm{m}}^0, \delta^0)$ be respectively the reference values of the path-loss attenuation factor, distance exponent and the weight of the required number of RBs $N_{\mathrm{net}}^0 = \delta^0 \times m_N(\vec{\alpha}_{\mathrm{m}}^0, \vec{\gamma}^0)$. For a given vector $\vec{h} = (\vec{\alpha}_{\mathrm{m}}, \vec{\gamma}, \alpha) = \vec{h}_0 + \Delta\vec{h}$ with $\Delta\vec{h} = (\Delta\vec{\alpha}_{\mathrm{m}}, \Delta\vec{\gamma}_{\mathrm{m}}, \Delta\delta)$, the first order of the Taylor expansion for multivariate functions to $f(\vec{\alpha}_{\mathrm{m}}, \vec{\gamma}_{\mathrm{m}}, \delta)$ gives:

$$f(\vec{\alpha}_{\mathrm{m}}, \vec{\gamma}_{\mathrm{m}}, \delta) = f(\vec{\alpha}_{\mathrm{m}}^0, \vec{\gamma}_{\mathrm{m}}^0, \delta^0) + \sum_{i=0}^{1}\left[\Delta\alpha_{\mathrm{m},i}\frac{\partial f}{\partial \alpha_{\mathrm{m},i}}\bigg|_{\vec{h}_0} + \Delta\gamma_{\mathrm{m},i}\frac{\partial f}{\partial \gamma_{\mathrm{m},i}}\bigg|_{\vec{h}_0}\right] + \Delta\delta\frac{\partial f}{\partial \delta}\bigg|_{\vec{h}_0} + o(\Delta\vec{h})$$

with $o(\Delta\vec{h}) \to 0$. Our goal is to obtain the variation $\Delta\delta$, that guarantees that the upper bound on the outage probability is in the same order as the target one, such that,

$$\left| f(\alpha_{\mathrm{m}}, \gamma_{\mathrm{m}}, \delta) + \log(p_{th}) \right| \to o(\Delta\vec{h}),$$

consequently,

$$\Delta\delta = -\frac{\sum_{i=0}^{1}\left(\Delta\alpha_{\mathrm{m},i}\frac{\partial f}{\partial \alpha_{\mathrm{m},i}}|_{\vec{h}_0} + \Delta\gamma_{\mathrm{m},i}\frac{\partial f}{\partial \gamma_{\mathrm{m},i}}|_{\vec{h}_0}\right)}{\frac{\partial f}{\partial \delta}|_{\vec{h}_0}}. \tag{4.21}$$

In order to compute the value of $\Delta\delta$ we derive the expressions of the partial derivatives of $f(.)$ in function of $\alpha_{\mathrm{m},i}$, $\gamma_{\mathrm{m},i}$ and δ as following:

$$\frac{\partial f(\vec{\alpha}_{\mathrm{m}}, \vec{\gamma}_{\mathrm{m}}, \delta)}{\partial \alpha_{\mathrm{m},i}} = \frac{1}{N_{\max}^2}\frac{\partial v_N}{\partial \alpha_{\mathrm{m},i}}(g \circ u)(\vec{\alpha}_{\mathrm{m}}, \vec{\gamma}_{\mathrm{m}}, \delta)) + \frac{v_N}{N_{\max}^2}\frac{\partial g}{\partial \alpha_{\mathrm{m},i}}\left(u(\vec{\alpha}_{\mathrm{m}}, \vec{\gamma}_{\mathrm{m}}, \delta)\right)\frac{\partial u}{\partial \alpha_{\mathrm{m},i}}(\vec{\alpha}_{\mathrm{m}}, \vec{\gamma}_{\mathrm{m}}, \delta),$$

where

$$u(\vec{\alpha}_{\mathrm{m}}, \vec{\gamma}_{\mathrm{m}}, \delta) = (\delta-1)N_{\max}\frac{m_N(\vec{\alpha}_{\mathrm{m}}, \vec{\gamma}_{\mathrm{m}})}{v_N(\vec{\alpha}_{\mathrm{m}}, \vec{\gamma}_{\mathrm{m}})}$$

The derivatives of $g(.)$ and $u(.)$ are such that

$$\frac{\partial g}{\partial \alpha_{\mathrm{m},i}}\left(u(\vec{\alpha}_{\mathrm{m}}, \vec{\gamma}_{\mathrm{m}}, \delta)\right) = \log\left(1 + u(\vec{\alpha}_{\mathrm{m}}, \vec{\gamma}_{\mathrm{m}}, \delta)\right)$$

and

$$\frac{\partial u(\vec{\alpha}_{\mathrm{m}}, \vec{\gamma}_{\mathrm{m}}, \delta)}{\partial \alpha_{\mathrm{m},i}} = (\delta - 1) N_{\max} \frac{\frac{\partial m_N}{\partial \alpha_{\mathrm{m},i}} v_N - m_N \frac{\partial v_N}{\partial \alpha_{\mathrm{m},i}}}{v_N^2},$$

with

$$\frac{\partial m_N(\vec{\alpha}_{\mathrm{m},i}, \vec{\gamma}_{\mathrm{m}})}{\partial \alpha_{\mathrm{m},i}} = \lambda \left[\sum_{j=1}^{N_{\max}-1} j \left(\frac{\partial A_j}{\partial \alpha_{\mathrm{m},i}} - \frac{\partial A_{j-1}}{\partial \alpha_{\mathrm{m},i}} \right) + N_{\max} \left(- \frac{\partial A_{N_{\max}-1}}{\partial \alpha_{\mathrm{m},i}} \right) \right], \tag{4.22}$$

and

$$\frac{\partial v_N(\vec{\alpha_{\mathrm{m}}}, \vec{\gamma}_{\mathrm{m}})}{\partial \alpha_{\mathrm{m},i}} = \lambda \left[\sum_{j=1}^{N_{\max}-1} j^2 \left(\frac{\partial A_j}{\partial \alpha_{\mathrm{m},i}} - \frac{\partial A_{j-1}}{\partial \alpha_{\mathrm{m},i}} \right) + N_{\max}^2 \left(- \frac{\partial A_{N_{\max}-1}}{\partial \alpha_{\mathrm{m},i}} \right) \right]. \tag{4.23}$$

The partial derivative of $f(.)$ in function of γ_{m} is obtained by simply replacing $\partial \alpha_{\mathrm{m},i}$ by $\partial \gamma_{\mathrm{m},i}$. Then, we express the partial derivative of $f(.)$ in function of δ

$$\frac{\partial f(\vec{\alpha}_{\mathrm{m}}, \vec{\gamma}_{\mathrm{m}}, \delta)}{\partial \delta} = \frac{m_N}{N_{\max}} \log \left(1 + \frac{(\delta - 1) m_N N_{\max}}{v_N} \right).$$

The variation in the number of required RBs considering the channel fluctuation can be then expressed as:

$$\Delta N_{net} = \Delta\delta \times m_N(\vec{\alpha_{\mathrm{m}}^0}, \vec{\gamma}_{\mathrm{m}}^0) + \delta_0 \sum_{i=0}^{1} \left[\Delta\alpha_{\mathrm{m},i} \frac{\partial m_N}{\partial \alpha_{\mathrm{m},i}} + \Delta\gamma_{\mathrm{m},i} \frac{\partial m_N}{\partial \gamma_{\mathrm{m},i}} \right] \Bigg|_{(\vec{\alpha}_{\mathrm{m},i}^0, \vec{\gamma}_{\mathrm{m},i}^0)}. \tag{4.24}$$

To obtain the final result we derive in the next subsection the expressions of the A_j areas partial derivatives in function of $\alpha_{\mathrm{m},i}$ and $\gamma_{\mathrm{m},i}$ for the SISO case in the following.

5.3 Focus on the SISO configuration

The next step to obtain the final expression of the variation in the required number of RBs N_{net} is to derive the partial derivatives of the areas of the regions where users request at most j RBs. After straightforward computations detailed in Appendix 4.D, we first express

the partial derivative of the area A_j^{SISO} in (4.20) with respect to $\alpha_{\text{m},i}$ as follows:

$$\begin{aligned}\frac{\partial}{\partial \alpha_{\text{m},i}} A_j^{\text{SISO}} = Z_i \frac{2}{\gamma_{\text{m},i}} \alpha_{\text{m},i}^{\frac{2}{\gamma_{\text{m},i}}-1} \left(\Gamma_{inc}\left(a_{\text{m},i} d_{c,i+1}^{\gamma_{\text{m},i}}, \frac{2}{\gamma_{\text{m},i}} \right) - \Gamma_{inc}\left(a_{\text{m},i} d_{c,i}^{\gamma_{\text{m},i}}, \frac{2}{\gamma_{\text{m},i}} \right) \right) \\ + \frac{Z_i \alpha_{\text{m},i}^{\frac{2}{\gamma_{\text{m},i}}}}{\Gamma\left(\frac{2}{\gamma_{\text{m},i}}\right)} \frac{\partial a_{\text{m},i}}{\partial \alpha_{\text{m},i}} \, d_{c,i+1}^{\gamma_{\text{m},i}} \exp\left(-a_{\text{m},i} d_{c,i+1}^{\gamma_{\text{m},i}}\right) \left(a_{\text{m},i} d_{c,i+1}^{\gamma_{\text{m},i}}\right)^{\frac{2}{\gamma_{\text{m},i}}-1} \\ - \frac{Z_i \alpha_{\text{m},i}^{\frac{2}{\gamma_{\text{m},i}}}}{\Gamma\left(\frac{2}{\gamma_{\text{m},i}}\right)} \frac{\partial a_{\text{m},i}}{\partial \alpha_{\text{m},i}} \, d_{c,i}^{\gamma_{\text{m},i}} \exp\left(-a_{\text{m},i} d_{c,i}^{\gamma_{\text{m},i}}\right) \left(a_{\text{m},i} d_{c,i}^{\gamma_{\text{m},i}}\right)^{\frac{2}{\gamma_{\text{m},i}}-1}, \end{aligned} \tag{4.25}$$

where

$$Z_i = \frac{2\pi}{\gamma_{\text{m},i}} \left(\frac{P_t \sigma_f^2}{\beta_j \eta} \right)^{\frac{2}{\gamma_{\text{m},i}}} \Gamma\left(\frac{2}{\gamma_{\text{m},i}}\right),$$

$$\frac{\partial}{\partial \alpha_{\text{m},i}} \Gamma_{inc}\left(a_{\text{m},i} d_{c,i}^{\gamma_{\text{m},i}}, \frac{2}{\gamma_{\text{m},i}} \right) = \frac{\partial (a_{\text{m},i} d_{c,i}^{\gamma_{\text{m},i}})}{\partial \alpha_{\text{m},i}} \frac{\exp\left(-a_{\text{m},i} d_{c,i}^{\gamma_{\text{m},i}}\right) \left(a_{\text{m},i} d_{c,i}^{\gamma_{\text{m},i}}\right)^{\frac{2}{\gamma_{\text{m},i}}-1}}{\Gamma\left(\frac{2}{\gamma_{\text{m},i}}\right)},$$

and

$$\frac{\partial}{\partial \alpha_{\text{m},i}} a_{\text{m},i} = -\frac{\beta_j \eta}{\sigma_f^2 P_t} \frac{1}{\alpha_{\text{m},i}^2}.$$

The partial derivative of the area A_j^{SISO} with respect to $\gamma_{\text{m},i}$ is similarly, after some computations detailed in Appendix 4.D, expressed as follows:

$$\begin{aligned}&\frac{\partial}{\partial \gamma_{\text{m},i}} A_j^{\text{SISO}} = \\ &2\pi \frac{\zeta_{\text{m},i}^{\frac{2}{\gamma_{\text{m},i}}}}{\gamma_{\text{m},i}} \frac{\partial}{\partial \gamma_{\text{m},i}} \left[\Gamma\left(\frac{2}{\gamma_{\text{m},i}}\right) \Gamma_{inc}\left(a_{\text{m},i} d_{c,i+1}^{\gamma_{\text{m},i}}, \frac{2}{\gamma_{\text{m},i}} \right) - \Gamma\left(\frac{2}{\gamma_{\text{m},i}}\right) \Gamma_{inc}\left(a_{\text{m},i} d_{c,i}^{\gamma_{\text{m},i}}, \frac{2}{\gamma_{\text{m},i}} \right) \right] \\ &- 2\pi \frac{\zeta_{\text{m},i}^{\frac{2}{\gamma_{\text{m},i}}} \Gamma\left(\frac{2}{\gamma_{\text{m},i}}\right)}{\gamma_{\text{m},i}^2} \left(1 + \frac{2}{\gamma_{\text{m},i}} \log(\zeta_{\text{m},i})\right) \left[\Gamma_{inc}\left(a_{\text{m},i} d_{c,i+1}^{\gamma_{\text{m},i}}, \frac{2}{\gamma_{\text{m},i}} \right) - \Gamma_{inc}\left(a_{\text{m},i} d_{c,i}^{\gamma_{\text{m},i}}, \frac{2}{\gamma_{\text{m},i}} \right) \right], \end{aligned}$$

where the constant $\zeta_{\text{m},i}$ is set below,

$$\zeta_{\text{m},i} = \frac{P_t \sigma_f^2 \alpha_{\text{m},i}}{\beta_j \eta},$$

6 Analytical model validation

6.1 System parameters

Table 4.2 presents the different parameters values used in our calculation and simulation:

Table 4.2: System parameters

Parameters	Value
Carrier frequency	800 MHz
CH Tx power	$P_T = 10^{2,3}$ mW
eNB antenna gain	G (dBi) = 0 (omni)
Tx and Rx height	$h_1 = h_2 = 12$ m
Antenna configuration	$n_t = 1, 2$ and $n_r = 1, 2$
Noise power	$\eta = 7.1 \cdot 10^{-}13$ mW
Free space path loss	$K_{\text{FS}} = 10^{-9.01}$, $\gamma_{FS} = 2$
Rayleigh variance	$\sigma_f = 1$
Threshold SNR	$\beta_{min} = -2.3$ dB

6.2 Single QoS users class target capacity

Using the expression of the area A_j in (9), (11) and (13), we find the first and the second moment in (6) and (7) for a target rate of $C_0 = 600$ kb/s and a network load defined by parameters of inter-arrival surface density $\rho = 1 \cdot 10^{-3} s^{-1} km^{-2}$ and mean service time $\nu^{-1} = 30\ min^{-1}$. Then, we deduce the outage probability upper-bound in (5). Using the threshold SNR value of -2,3 dB, the number of RBs is limited to 6 RBs per node. This resource outage probability is computed for different values of total RBs $N_{RB} = \{50, 65, 75, 90 \text{ and } 100\}$. These numbers of RBs correspond in LTE to respective values of bandwidth and aggregated bandwidth (denoted in the following by [CC, CA] where CC is the carrier component and CA is the aggregated one) such that B = {10, [10; 3], 15, [15; 3] and 20} MHz. Using Monte Carlo simulation with 10^7 iterations, we compute for the different antenna configurations and transmission modes, the mean number of RBs required by this network and the resource outage probability for the above mentioned bandwidth values. The log-ratio test

$$\Delta = \log_{10}\left(\frac{\mathbb{P}_{sup}}{\mathbb{P}_{out}}\right)$$

compares the analytical and the numerical results.

6.2.1 SISO scheme

For the SISO antenna configuration, the numerical and analytical mean number of RBs and the numerical and analytical variance are

$$m_{\mathrm{N,SISO}} = 47$$

and

$$v_{\mathrm{N,SISO}} = 76.$$

The analytical and numerical outage probability corresponding to the different values of RBs is given in Table 4.3. It can be noticed that the resource outage probability decreases when more RBs are available at the CH. We remark that the derived upper-bound is adequate to the outage probability obtained after simulations as its value is always higher than the latter and the maximum log-ratio is of 1.9.

Table 4.3: Dimensioning in a SISO scheme

Band(MHz)	10	[10,3]	15	[15,3]	20
N_{RB}	50	65	75	90	100
δ	1.06	1.39	1.6	2	2.12
P_{sup}	0.94	0.22	0.04	0.001	$1 \cdot 10^{-4}$
P_{out}	0.3	0.02	0.0016	$1.7 \cdot 10^{-5}$	0
Δ	0.5	1.04	1.39	1.9	$\times$

6.2.2 MIMO scheme with diversity gain

In this case, the mean and the variance of RBs number computed analytically and numerically are

$$m^{d}_{\mathrm{N,MIMO}} = 38$$

and

$$v^{d}_{\mathrm{N,MIMO}} = 38.$$

The first and second moments are almost equal as for the given target data rate, only one RB is required to be allocated. Remark that the resource outage probability in Table 4.4 is considerably reduced using this diversity transmission mode compared to the SISO configuration.

Table 4.4: Dimensioning in a 2×2 MIMO scheme with diversity gain

Band(MHz)	10	[10,3]	15	[15,3]	20
N_{RB}	50	65	75	90	100
δ	1.32	1.71	1.97	2.36	2.63
P_{sup}	0.29	0.009	0.0004	$2.5 \cdot 10^{-6}$	$5.3 \cdot 10^{-8}$
P_{out}	0.0235	$1.7 \cdot 10^{-5}$	0	0	0
Δ	1.09	2.72	$\times$	$\times$	$\times$

6.2.3 MIMO scheme with multiplexing gain

Table 4.5 contains the resource outage probability 2×2 MIMO configuration with multiplexing gain. The mean number of RBs computed analytically is

$$m^{mx}_{\text{N,MIMO}} = 48$$

and

$$v^{mx}_{\text{N,MIMO}} = 89.$$

The average number of RBs computed with Monte-Carlo simulation is equal to 48 and the variance is equal to 88. As it can be seen, there is no improvement in terms of resource outage probability compared to SISO case. Actually, splitting the power over the two spatial dimensional provides no enhancement on the dimensioning of bandwidth. Moreover, the use of the same MCS corresponding to the one imposed by the worst fading channel experienced by these two spatial dimensions will penalize the MIMO system. The MIMO multiplexing gain will not compensate the loss incurred by the half allocated on each spatial dimension and the same MCS constraint.

Table 4.5: Dimensioning in a 2×2 MIMO scheme with multiplexing gain

Band(MHz)	10	[10,3]	15	[15,3]	20
N_{RB}	50	65	75	90	100
δ	1.04	1.35	1.56	1.87	2.08
P_{sup}	0.98	0.29	0.065	0.003	$3 \cdot 10^{-4}$
P_{out}	0.356	0.032	0.0042	$7.1 \cdot 10^{-5}$	$31 \cdot 10^{-6}$
Δ	0.42	0.89	1.18	1.66	2.48

6.3 Multiple QoS users class target capacity

6.3.1 Muliple class users with SISO scheme

We finally the case of a multi-class services where nodes target three different rate $C_1 = 600$ kb/s, $C_2 = 800$ kb/s and $C_3 = 1$ Mb/s. We consider the following surface densities of

inter-arrival time $\rho_1 = \rho 2 = 1 \cdot 10^{-3} min^{-1} km^{-2}$ and $\rho_3 = 3 \cdot 10^{-3} min^{-1} km^{-2}$ and the mean service times $\mu_1^{-1} = 10 min^{-1}$, $\mu_2^{-1} = 5 min^{-1}$ and $\mu_3^{-1} = 2.5 min^{-1}$. The analytical and numerical average number of required RBs for this scenario and the numerical and analytical variance are.

$$m^{mx}_{\text{N,MIMO}} = 49$$

and

$$v^{mx}_{\text{N,MIMO}} = 90.$$

The resource outage probabilities are evaluated in Table for the case of SISO system. Compared to the single class case, the network is more loaded, which explain the higher resource outage probability that is obtained.

Table 4.6: Dimensioning in a SISO scheme with multiple QoS classes

Band(MHz)	10	[10,3]	15	[15,3]	20
N_{RB}	50	65	75	90	100
δ	1.02	1.33	1.54	1.84	2.05
P_{sup}	0.99	0.33	0.08	0.004	$4 \cdot 10^{-4}$
P_{out}	0.4	0.05	0.06	0.0001	$6 \cdot 10^{-6}$
Δ	0.38	0.84	1.13	1.66	1.89

6.4 Numerical results for the impact of the maritime propagation on SISO scheme

We consider the MANET with parameters described in Table 4.2. We assume that the radio resource dimensioning is performed with a reference maritime propagation path-loss with 10% of time. The required bandwidth is computed assuming that $\mathbb{P}_{sup}$ is less than a certain threshold $p_{th} = 0.01\%$. We propose here to find the required bandwidth when the maritime propagation fluctuates, considering the variations that occurs for 50% and 1% of time. The impact of these channel fluctuations is captured by the variations

$$\begin{aligned} \Delta\alpha^{50\%}_{\text{m},1} &= \alpha^{50\%}_{\text{m},1} - \alpha^{10\%}_{\text{m},1}, \quad \Delta\gamma^{50\%}_{\text{m},1} = \gamma^{50\%}_{\text{m},1} - \gamma^{10\%}_{\text{m},1}, \\ \Delta\alpha^{1\%}_{\text{m},2} &= \alpha^{1\%}_{\text{m},2} - \alpha^{10\%}_{\text{m},2}, \quad \Delta\gamma^{1\%}_{\text{m},2} = \gamma^{10\%}_{\text{m},2} - \gamma^{1\%}_{\text{m},2}. \end{aligned}$$

Based on (4.24) we compute the variation in the number of RBs that ensures that the same target resource outage probability is nearly achieved.

We first notice that when the path-loss attenuation factor α_{m} increases compared to a reference path-loss model, the radio propagation conditions are improved and nodes require less RBs to satisfy their QoS. The areas of the regions A_j^{SISO} in which nodes require at most j RBs increase. This means that A_j^{SISO} is an increasing function of α_{m} and its derivative is positive. Moreover, the mean number of RBs decreases in this case and this means that m_N

is a decreasing function of α_{m} and its derivative with respect to α_{m} is negative. The increase of the path-loss exponent γ_m, compared to a reference path-loss, degrades the quality of the radio propagation. As a consequence, the areas of the regions A_j^{SISO} decrease and the mean number of required RBs m_N increases. This means that the derivative of m_N with respect to γ_m is positive. For the considered reference path-loss model, we compute using the statistical dimensioning model the average number of required RBs is $m_{\text{N}}^{\text{SISO,10\%}} = 44$ and the required number of RBs is $N_{net}^{10\%} = 95$. To deduce the required number of RBs required by the two models defined above, we compute the variation of N_{net} in (4.24) by computing the numerical values of the derivatives as:

$$\Delta N_{net} = -6 \times 10^6 \, \Delta\alpha_{\text{m},1} - 1.15 \times 10^{10} \, \Delta\alpha_{\text{m},2} + 0.04 \, \Delta\gamma_{\text{m},1} + 38.72 \, \Delta\gamma_{\text{m},2}. \tag{4.26}$$

Once again, we can see that when the radio propagation condition decays meaning that $\Delta\alpha_m < 0$, and $\Delta\gamma_m > 0$, the network requires more radio RB and hence $\Delta\delta > 0$. We compare in Table 4.7 the required number of RBs and the bandwidth computed with this linear adjustment and the straightforward computation.

Table 4.7: Maritime propagation model impact on SISO configuration

Linear model			
Path-Loss	10% cold	50% temperate	1% cold
N_{net}	95	110	89
B (MHz)	20	[20; 3]	[15; 3]
$\mathbb{P}_{\text{sup}}$	10^{-4}	$2.3\ 10^{-5}$	$7\ 10^{-5}$
Direct computation			
N_{net}	95	105	88
B (MHz)	20	[20; 3]	[15; 3]
$\mathbb{P}_{\text{sup}}$	10^{-4}	10^{-4}	10^{-4}

We can see from Table 4.7 that the linear model provides approximatively the same number of RBs as the direct computation. We can notice with the linear model, the values of $\mathbb{P}_{\text{sup}}$ are less than the target outage $p_{th} = 10^{-4}$ as this latter is equal to $p_{th} \exp(-o(\Delta h))$ with $o(\Delta h) \to 0^+$ for the studied path-loss models. Based on the reference maritime ITU path-loss loss, the number of required RBs can be linearly adjusted using (4.26). The direct computation of the required number for each channel fluctuation requires high computational complexity as it requires to compute all the areas A_j^{SISO} to compute the corresponding m_N and v_N parameters. The linear model has low complexity and enables the dynamic adjustment of the required number of RBs in function of the channel fluctuation.

7 Conclusion

This chapter focused on the radio resource outage probability in a circular cluster of a centralized MANET. We aimed to provide an analytical model to enable a network designer to estimate properly the required total bandwidth in the network. To this purpose, we investigated advanced stochastic geometry tools and derived an upper-bound on the probability of the event that arises when the RRM entity has no more radio resources to serve all the active users. We envisaged two antennas configurations the SISO and the 2×2 MIMO extracting diversity and multiplexing gain. By setting up a tolerated threshold on the radio resource outage probability we estimate the required bandwidth and the average achieved spectral efficiency in a typical cluster. Moreover we considered both cases where all active users target the same/different QoS class. Numerical results enlighten the fact that the MIMO configuration with extraction of the full diversity gain decreases considerably the radio resource outage occurrence and efficiently increases the achieved average spectral efficiently compared to the SISO and the MIMO with spatial multiplexing for long range communications. Moreover, these results also demonstrated that our analytical approach provides an accurate estimation of the required bandwidth. The maritime aspect of the MANET was also studied, the maritime propagation specificities were considered and more precisely the impact of fluctuation of the propagation path-loss. We provided an rapid linear model enabling the tuning of the allocated bandwidth in function of the attenuation/amplification of the path-loss. A comparative study was lead with straightforward computation where the developed linear model appeared to be an efficient tool to foresee this fluctuation impact on the MANET dimensioning. The next chapter follows on from this work, we consider this time a cluster with a distributed access scheme i.e. users transmit simultaneously in the same medium using the Aloha medium access control protocol. The same problematic on radio resource outage and dimensioning is tackled under different MIMO techniques and different receiver models using stochastic geometry field.

Appendix

4.A Derivation of the area A_j expression with SISO scheme

This appendix provides the detailed computation steps of the expression of A_j^{SISO}. From (4.11) we obtain:

$$\begin{aligned} A_j^{SISO} &= \int_{\mathcal{C}} Prob\left\{\frac{||x||^{\gamma}}{\tilde{\beta}_j} \leq y\right\} dx \\ &= \int_{\mathcal{C}} 1 - F\left(\frac{||x||^{\gamma}}{\tilde{\beta}_j}\right) dx \\ &= \int_{\mathcal{C}} e^{-\frac{||x||^{\gamma}}{\sigma_f^2}\frac{1}{\tilde{\beta}_j}} dx \end{aligned}$$

Applying the maritime propagation path loss described in (4), our study area is thus divided in two parts and we express A_j^{SISO} as,

$$A_j^{SISO} = \int_{\mathcal{C}_{d_{c,0}}} e^{-a_{FS}|x|^{\gamma_{FS}}} dx + \sum_{i=1}^{2} \int_{\mathcal{C}_{d_{c,i}}/\mathcal{C}_{d_{c,i+1}}} e^{-a_{\mathrm{m},i}|x|^{\gamma_{\mathrm{m},i}}} dx \tag{4.27}$$

where,

$$\begin{aligned} a_{FS} &= \frac{1}{\tilde{\beta}_{j,FS}}\frac{1}{\sigma_f^2}, \\ a_{\mathrm{m},i} &= \frac{1}{\tilde{\beta}_{j,m,i}}\frac{1}{\sigma_f^2}, \\ \mathcal{C}_{d_c} &= \{x \in \mathcal{C} : |x| \leq d_c\}, \\ \mathcal{C}_{d_{c,i}}/\mathcal{C}_{d_{c,i+1}} &= \{x \in \mathcal{C} \;\&\; d_{c,i} < |x| \leq d_{c,i+1}\}, d_{c,2} = R. \end{aligned}$$

By employing the two dimensional polar coordinates system the area A_j^{SISO} is of the form,

$$A_j^{SISO} = \int_0^{2\pi}\int_0^{d_c} re^{-a_{FS}r^{\gamma_{FS}}} drd\theta + \sum_{i=1}^{2}\int_0^{2\pi}\int_{d_{c,i}}^{d_{c,i+1}} re^{-a_{\mathrm{m},i}r^{\gamma_{\mathrm{m},i}}} drd\theta, \tag{4.28}$$

and we retrieve the final expression,

$$A_j^{SISO} = 2\pi \left[\xi_{FS} \Gamma_{inc} \left(a_{FS} d_c^{\gamma_{FS}}, \frac{2}{\gamma_{FS}} \right) \right] + 2\pi \sum_{i=1}^{2} \left[\xi_{m,i} \Gamma_{inc} \left(a_{\mathrm{m},i} R^{\gamma_{\mathrm{m},i}}, \frac{2}{\gamma_{\mathrm{m},i}} \right) - \xi_{m,i} \Gamma_{inc} \left(a_{\mathrm{m},i} d_c^{\gamma_{\mathrm{m},i}}, \frac{2}{\gamma_{\mathrm{m},i}} \right) \right].$$

4.B Derivation of the area A_j expression with diversity gain MIMO scheme

Similarly to the SISO case, from the definition of the area A_j and using the multi-path fading distribution the MIMO scheme with extraction of full diversity gain we obtain:

$$\begin{aligned} A_j^{MIMO,d} &= \int_{\mathcal{C}} Prob \left\{ \frac{||x||^{\gamma}}{\tilde{\beta}_{j,d}} \leq y \right\} dx \\ &= \int_{\mathcal{C}} (1 - F \left(\frac{||x||^{\gamma}}{\tilde{\beta}_{j,d}} \right) dx \\ &= \int_{\mathcal{C}} (1 - \frac{1}{\sigma_f^2} \Gamma_{inc} \left(\frac{1}{\sigma_f^2} \frac{||x||^{\gamma}}{\tilde{\beta}_{j,d}}, 4 \right) dx \end{aligned}$$

This area can be decomposed with respect to the path loss model as,

$$A_j^{MIMO,d} = \int_{\mathcal{C}_{d_c}} (1 - \frac{1}{\sigma_f^2} \Gamma_{inc} \left(\frac{1}{\sigma_f^2} \frac{||x||^{\gamma_{FS}}}{\tilde{\beta_{j,d,FS}}}, 4 \right) dx + \int_{\mathcal{C}/\mathcal{C}_{d_{c,0}}} (1 - \frac{1}{\sigma_f^2} \Gamma_{inc} \left(\frac{1}{\sigma_f^2} \frac{||x||^{\gamma_{\mathrm{m}}}}{\tilde{\beta}_{j,d,m}}, 4 \right) dx$$

and finally in polar coordinates,

$$\begin{aligned} A_j^{MIMO,d} = 2\pi \left[\int_{\mathcal{C}_{d_c}} r(1 - \frac{1}{\sigma_f^2} \Gamma_{inc} \left(\frac{1}{\sigma_f^2} \frac{r^{\gamma_{FS}}}{\tilde{\beta_{j,d,FS}}}, 4 \right) dr \right] \\ + 2\pi \left[\sum_{i=1}^{2} \int_0^{2\pi} \int_{d_{c,i}}^{d_{c,i+1}} r(1 - \frac{1}{\sigma_f^2} \Gamma_{inc} \left(\frac{1}{\sigma_f^2} \frac{r^{\gamma_{\mathrm{m},i}}}{\tilde{\beta}_{j,d,m,i}}, 4 \right) dr \right], \end{aligned}$$

4.C Derivation of the area A_j expression with multiplexing gain MIMO scheme

The multi-path fading coefficients with the MIMO scheme with multiplexing gain is also exponentially distributed thus the area A_j is derived as follows, with $\beta_{j,mx} = 2^{\frac{C_0}{2jW}} - 1$ and

$\tilde{\beta}_{j,mx} = \frac{P_T \alpha}{2\eta} \frac{1}{\beta_{j,mx}}$:

$$\begin{aligned} A_j^{MIMO,m} &= \int_{\mathcal{C}} Prob\left\{ \frac{||x||^{\gamma}}{\tilde{\beta}_{j,mx}} \leq y \right\} dx \\ &= \int_{\mathcal{C}} 1 - F\left(\frac{||x||^{\gamma}}{\tilde{\beta}_{j,mx}} \right) dx \\ &= \int_{\mathcal{C}} e^{-\frac{||x||^{\gamma}}{\sigma_f^2} \frac{1}{\tilde{\beta}_{j,mx}}} dx \end{aligned}$$

Applying the maritime propagation path loss described in (4), our study area is thus divided in two parts and we express A_j^{SISO} as,

$$A_j^{MIMO,m} = \int_{\mathcal{C}_{d_{c,0}}} e^{-a_{FS}|x|^{\gamma_{FS}}} dx + \sum_{i=1}^{2} \int_{\mathcal{C}_{d_{c,i}}/\mathcal{C}_{d_{c,i+1}}} e^{-a_{\mathrm{m},i}|x|^{\gamma_{\mathrm{m},i}}} dx \tag{4.29}$$

and finally,

$$\begin{aligned} A_j^{MIMO,m} = 2\pi \left[\xi_{FS} \Gamma_{inc}\left(a_{FS} d_c^{\gamma_{FS}}, \frac{2}{\gamma_{FS}} \right) \right] + 2\pi \left[\sum_{i=1}^{2} \xi_{m,i} \Gamma_{inc}\left(a_{\mathrm{m},i} d_{c,i+1}^{\gamma_{\mathrm{m},i}}, \frac{2}{\gamma_{\mathrm{m},i}} \right) \right. \\ \left. - \xi_{m,i} \Gamma_{inc}\left(a_{\mathrm{m},i} d_{c,i}^{\gamma_{\mathrm{m},i}}, \frac{2}{\gamma_{\mathrm{m},i}} \right) \right] \end{aligned}$$

4.D Derivatives of the area A_j expression in a SISO scheme

This appendix presents the step by step derivations to obtain the partial derivatives of the area A_j^{SISO} in function of $\alpha_{\mathrm{m},i}$ first and $\gamma_{\mathrm{m},i}$ afterwards.

$$\begin{aligned} \frac{\partial}{\partial \alpha_{\mathrm{m},i}} A_j^{SISO} &= 2\pi \frac{\partial}{\partial \alpha_{\mathrm{m},i}} \left[\xi_{\mathrm{m},i} \Gamma_{inc}\left(a_{\mathrm{m},i} R^{\gamma_{\mathrm{m},i}}, \frac{2}{\gamma_{\mathrm{m},i}} \right) - \xi_{m,i} \Gamma_{inc}\left(a_{\mathrm{m},i} d_c^{\gamma_{\mathrm{m},i}}, \frac{2}{\gamma_{\mathrm{m},i}} \right) \right] \\ &= \frac{2\pi}{\gamma_{\mathrm{m},i}} \left(\frac{1}{a_{\mathrm{m},i}} \right)^{\frac{2}{\gamma_{\mathrm{m},i}}} \Gamma\left(\frac{2}{\gamma_{\mathrm{m},i}} \right) \frac{\partial}{\partial \alpha_{\mathrm{m},i}} \left[\Gamma_{inc}\left(a_{\mathrm{m},i} R^{\gamma_{\mathrm{m},i}}, \frac{2}{\gamma_{\mathrm{m},i}} \right) - \Gamma_{inc}\left(a_{\mathrm{m},i} d_c^{\gamma_{\mathrm{m},i}}, \frac{2}{\gamma_{\mathrm{m},i}} \right) \right] \\ &= \frac{2\pi}{\gamma_{\mathrm{m},i}} \left(\frac{P_T \sigma_f^2}{\beta_j \eta} \right)^{\frac{2}{\gamma_{\mathrm{m},i}}} \Gamma\left(\frac{2}{\gamma_{\mathrm{m},i}} \right) \frac{\partial}{\partial \alpha_{\mathrm{m},i}} \left(\alpha_{\mathrm{m},i}^{\frac{2}{\gamma_{\mathrm{m},i}}} \left(\Gamma_{inc}\left(a_{\mathrm{m},i} R^{\gamma_{\mathrm{m},i}}, \frac{2}{\gamma_{\mathrm{m},i}} \right) \right. \right. \\ &\left. \left. - \Gamma_{inc}\left(a_{\mathrm{m},i} d_c^{\gamma_{\mathrm{m},i}}, \frac{2}{\gamma_{\mathrm{m},i}} \right) \right) \right). \end{aligned}$$

Setting the following constant Z_i as,

$$Z_i = \frac{2\pi}{\gamma_{\mathrm{m},i}} \left(\frac{P_t \sigma_f^2}{\beta_j \eta} \right)^{\frac{2}{\gamma_{\mathrm{m},i}}} \Gamma\left(\frac{2}{\gamma_{\mathrm{m},i}} \right),$$

the partial derivative of A_j^{SISO} in function $\alpha_{\mathrm{m},i}$ is therefore expressed as:

$$\begin{aligned}\frac{\partial}{\partial \alpha_{\mathrm{m},i}} A_j^{\mathrm{SISO}} = Z_i \frac{2}{\gamma_{\mathrm{m},i}} \alpha_{\mathrm{m},i}^{\frac{2}{\gamma_{\mathrm{m},i}}-1} \left(\Gamma_{inc}\left(a_{\mathrm{m},i} d_{c,i+1}^{\gamma_{\mathrm{m},i}}, \frac{2}{\gamma_{\mathrm{m},i}} \right) - \Gamma_{inc}\left(a_{\mathrm{m},i} d_{c,i}^{\gamma_{\mathrm{m},i}}, \frac{2}{\gamma_{\mathrm{m},i}} \right) \right) \\ + \frac{Z_i \alpha_{\mathrm{m},i}^{\frac{2}{\gamma_{\mathrm{m},i}}}}{\Gamma\left(\frac{2}{\gamma_{\mathrm{m},i}}\right)} \frac{\partial a_{\mathrm{m},i}}{\partial \alpha_{\mathrm{m},i}} \, d_{c,i+1}^{\gamma_{\mathrm{m},i}} \exp\left(-a_{\mathrm{m},i} d_{c,i+1}^{\gamma_{\mathrm{m},i}}\right) \left(a_{\mathrm{m},i} d_{c,i+1}^{\gamma_{\mathrm{m},i}}\right)^{\frac{2}{\gamma_{\mathrm{m},i}}-1} \\ - \frac{Z_i \alpha_{\mathrm{m},i}^{\frac{2}{\gamma_{\mathrm{m},i}}}}{\Gamma\left(\frac{2}{\gamma_{\mathrm{m},i}}\right)} \frac{\partial a_{\mathrm{m},i}}{\partial \alpha_{\mathrm{m},i}} \, d_{c,i}^{\gamma_{\mathrm{m},i}} \exp\left(-a_{\mathrm{m},i} d_{c,i}^{\gamma_{\mathrm{m},i}}\right) \left(a_{\mathrm{m},i} d_{c,i}^{\gamma_{\mathrm{m},i}}\right)^{\frac{2}{\gamma_{\mathrm{m},i}}-1},\end{aligned}$$

where

$$\frac{\partial}{\partial \alpha_{\mathrm{m},i}} \Gamma_{inc}\left(a_{\mathrm{m},i} d_{c,i}^{\gamma_{\mathrm{m},i}}, \frac{2}{\gamma_{\mathrm{m},i}} \right) = \frac{\partial (a_{\mathrm{m},i} d_{c,i}^{\gamma_{\mathrm{m},i}})}{\partial \alpha_{\mathrm{m},i}} \frac{\exp\left(-a_{\mathrm{m},i} d_{c,i}^{\gamma_{\mathrm{m},i}}\right) \left(a_{\mathrm{m},i} d_{c,i}^{\gamma_{\mathrm{m},i}}\right)^{\frac{2}{\gamma_{\mathrm{m},i}}-1}}{\Gamma\left(\frac{2}{\gamma_{\mathrm{m},i}}\right)},$$

and

$$\frac{\partial}{\partial \alpha_{\mathrm{m},i}} a_{\mathrm{m},i} = -\frac{\beta_j \eta}{\sigma_f^2 P_t} \frac{1}{\alpha_{\mathrm{m},i}^2}.$$

Moreover, the partial derivative of the area $A_j^{SISO}(\alpha_{\mathrm{m},i}, \gamma_{\mathrm{m},i})$ with respect to $\gamma_{\mathrm{m},i}$ is expressed as follows:

$$\begin{aligned}\frac{\partial}{\partial \gamma_{\mathrm{m},i}} A_j^{SISO} = \frac{2\pi}{\gamma_{\mathrm{m},i}} \left(\frac{P_T \sigma_f^2 \alpha_{\mathrm{m},i}}{\beta_j \eta} \right)^{\frac{2}{\gamma_{\mathrm{m},i}}} \frac{\partial}{\partial \gamma_{\mathrm{m},i}} \Gamma\left(\frac{2}{\gamma_{\mathrm{m},i}}\right) \left(K^{\frac{2}{\gamma_{\mathrm{m},i}}} \left(\Gamma_{inc}\left(a_{\mathrm{m},i} R^{\gamma_{\mathrm{m},i}}, \frac{2}{\gamma_{\mathrm{m},i}} \right) \right.\right. \\ \left.\left. - \Gamma_{inc}\left(a_{\mathrm{m},i} d_c^{\gamma_{\mathrm{m},i}}, \frac{2}{\gamma_{\mathrm{m},i}} \right) \right) \right).\end{aligned}$$

Setting the constant $\zeta_{\mathrm{m},i}$ below,

$$\zeta_{\mathrm{m},i} = \frac{P_t \sigma_f^2 \alpha_{\mathrm{m},i}}{\beta_j \eta},$$

we derive the final expression of $\frac{\partial}{\partial \gamma_{\mathrm{m},i}} A_j^{\mathrm{SISO}}(\alpha_{\mathrm{m},i}, \gamma_{\mathrm{m},i})$:

$$\begin{aligned}&\frac{\partial}{\partial \gamma_{\mathrm{m},i}} A_j^{\mathrm{SISO}} = \\ &2\pi \frac{\zeta_{\mathrm{m},i}^{\frac{2}{\gamma_{\mathrm{m},i}}}}{\gamma_{\mathrm{m},i}} \frac{\partial}{\partial \gamma_{\mathrm{m},i}} \left[\Gamma\left(\frac{2}{\gamma_{\mathrm{m},i}}\right) \Gamma_{inc}\left(a_{\mathrm{m},i} d_{c,i+1}^{\gamma_{\mathrm{m},i}}, \frac{2}{\gamma_{\mathrm{m},i}} \right) - \Gamma\left(\frac{2}{\gamma_{\mathrm{m},i}}\right) \Gamma_{inc}\left(a_{\mathrm{m},i} d_{c,i}^{\gamma_{\mathrm{m},i}}, \frac{2}{\gamma_{\mathrm{m},i}} \right) \right] \\ &- 2\pi \frac{\zeta_{\mathrm{m},i}^{\frac{2}{\gamma_{\mathrm{m},i}}} \Gamma\left(\frac{2}{\gamma_{\mathrm{m},i}}\right)}{\gamma_{\mathrm{m},i}^2} \left(1 + \frac{2}{\gamma_{\mathrm{m},i}} \log(\zeta_{\mathrm{m},i})\right) \left[\Gamma_{inc}\left(a_{\mathrm{m},i} d_{c,i+1}^{\gamma_{\mathrm{m},i}}, \frac{2}{\gamma_{\mathrm{m},i}} \right) - \Gamma_{inc}\left(a_{\mathrm{m},i} d_{c,i}^{\gamma_{\mathrm{m},i}}, \frac{2}{\gamma_{\mathrm{m},i}} \right) \right],\end{aligned}$$

where

$$\frac{\partial}{\partial \gamma_{\mathrm{m},i}}\left[\Gamma\left(\frac{2}{\gamma_{\mathrm{m},i}}\right)\Gamma_{inc}\left(a_{\mathrm{m},i}d_{c,i}^{\gamma_{\mathrm{m},i}},\frac{2}{\gamma_{\mathrm{m},i}}\right)\right] = \log(d_{c,i})(a_{\mathrm{m},i}d_{c,i}^{\gamma_{\mathrm{m},i}})^{\frac{2}{\gamma_{\mathrm{m},i}}}e^{-a_{\mathrm{m},i}}d_{c,i}^{\gamma_{\mathrm{m},i}} - \frac{2}{\gamma_{\mathrm{m},i}^2}\int_0^{a_{\mathrm{m},i}} d_{c,i}^{\gamma_{\mathrm{m},i}}\log t\; e^{-t}\; t^{\frac{2}{\gamma_{\mathrm{m},i}}-1}dt.$$

5 Distributed Network Resource Outage in a MANET with Aloha MAC

DISTRIBUTED networks enhance the communications efficiency by enabling pairwise transmissions between the mobile nodes without the support of a management entity as in the centralized scheme. In these networks, nodes access the shared medium unilaterally. Several Medium Access Control "MAC" protocols are available in literature to provide an efficient use of the medium and to ensure reliable transmissions. In this chapter, we define statistical tools for radio dimensioning in a non-cooperative OFDMA Aloha MIMO MANET. We assume that the ad-hoc shared OFDMA bandwidth is divided into several sub-mediums, containing each a predefined number of radio resource blocks that depends on the required QoS. The active nodes are spatially distributed according to a random Poisson point process, and select in a uniform way the sub-medium in which the transmission occurs. Our main objective is to find the required bandwidth to allocate in the network to guarantee that the number of RBs in a given sub-medium is sufficient to serve an acceptable amount of nodes within the considered sub-medium. For this, we derive the analytical expression of the sub-medium resource outage probability for different transmission modes considering the average statistical behavior of the network. We finally provide numerical results to compare the performances of the different MIMO transmission modes in terms of coverage radius, bandwidth and aggregate capacity.

1 Introduction

This chapter considers a MANET where pairs of non-cooperative OFDMA-MIMO nodes communicate, these nodes correspond to ships and form a naval fleet offshore. The smallest OFDMA unit on which data exchange occurs is the physical radio resource block introduced in Chapter 2. For a given rate, the minimal spectral efficiency adopted in the LTE standard [4] limits the maximal number of authorized RBs per communication to N_{max} RBs per node. We assume that the access to the shared medium is managed by an Aloha MAC protocol [73, 74] where the total OFDMA bandwidth is sub-divided into different sub-mediums containing N_{max} RBs each. Each node selects randomly and in a uniform way a Medium

Access Indicator "MAI" referring to the the sub-medium in which transmission occurs. Due to the absence of coordination between nodes, collision occurs between two nodes transmitting in the same sub-medium and this results in a significant interference at the non-intended receivers. As long as the Signal to Interference and Noise Ratio "SINR" is above than a given threshold, the minimal spectral efficiency can be successfully decoded.

One of the main challenges of the RRM is to optimize the allocated bandwidth in such a way to support the traffic of each node within N_{max} RBs. This radio dimensioning problem depends on the network parameters including the network load, the antenna configuration, and the required QoS. On one hand, the choice of the optimal size of the bandwidth should guarantee that the number of sub-mediums is sufficiently large to decrease the collision between nodes and consequently the interference level. On the other hand, the bandwidth should match with the network load to prevent an over-dimensioned bandwidth. The main objective of this paper is to study the impact of MIMO antenna configuration and the transmission modes on the radio dimensioning parameters.

The average statistical behavior of the network is considered: active nodes arriving to a given area are randomly distributed according to a random PPP. The randomness of the wireless channel, the position of the receiver as well as the random Aloha MAI are considered as a mark of the PPP. Unlike the centralized radio resource management considered in our previous works [28, ?, 75, 25, 26], this paper studies the radio dimensioning problem when no coordination between nodes is considered. The application of the marked PPP in ad-hoc networks was extensively addressed in literature in the last decades [8, 9, 12, 76, 77, 78, 79]. Baccelli and Blaszczyszyn provide in [8, 9] a complete survey on the classical stochastic geometry and their applications in cellular and in ad-hoc networks. We base our statistical development on the first part of [8] where the stochastic geometry mathematical tools are defined. The use of the stochastic geometry in the characterization of the signal to interference and noise distribution in cellular network with marked point process distribution was studied in [8]. The statistical behavior of the interference in a PPP ad-hoc network was completely characterized in the work of Haenggi *et al.* in [12] and references therein. In decentralized ad-hoc networks, the randomness aspects of the network (the node locations, the interference, the medium access protocol and the channel fading) are not predictable at the transmitter side. Nodes cannot adjust their transmission and an outage occurs when the transmitted rate exceeds the Shannon capacity between the transmitter and the intended receiver. The characterization of the outage and the single throughput in this type of network was extensively addressed in literature considering randomly placed points distributed according to an homogeneous PPP [9, 76, 77, 78, 79]. The analytical expressions of the outage probability depends on the MAC protocol: close expressions of the outage are obtained with an ALOHA protocol as the set of transmitting points remains Poisson distributed in this case.

We provide in the following, statistical tools to estimate the total bandwidth required by an ALOHA ad-hoc OFDMA network to handle the traffic of non cooperative transmitting nodes. The total available bandwidth is sub-divided into N_m sub-mediums containing each N_{max} RBs. Nodes are equipped with one or multiple transmit and receiver antennas,

and access to the shared OFDMA bandwidth by selecting uniformly a sub-medium among the N_m available ones. We define the sub-medium outage event as the event that occurs when the maximal number of RBs required by nodes transmitting in a given sub-medium is higher than the $N_{\max}$ available ones. Our main objective is to determine the minimal number of sub-medium in order to minimize the occurrence of the sub-medium outage event. For this, we first establish a relationship between the typical coverage outage probability considered in [9] and the sub-medium outage probability. Next, we study the impact of the multi-antenna configuration and the diversity, multiplexing transmission modes on the dimensioning.

2 Background

2.1 Slotted Aloha MAC Protocols

In the absence of a centralized control in the network, the simultaneous access of transmitting nodes to the shared bandwidth induces significant interference at the receiver node. Each node receives in addition to its desired signal the interference from all other nodes transmitting on the same RBs. In the ad hoc OFDMA context, we propose to subdivide the OFDMA bandwidth into N_m sub-mediums where each sub-medium contains exactly $N_{\max}$ RBs. Each sub-medium is labelled by an integer between 1 and N_m as illustrated in Figure 5.1. In the absence of coordination between nodes and in order to avoid the inter-sub-medium interferences, we pre-limit the size of each sub-medium a priori. The optimal

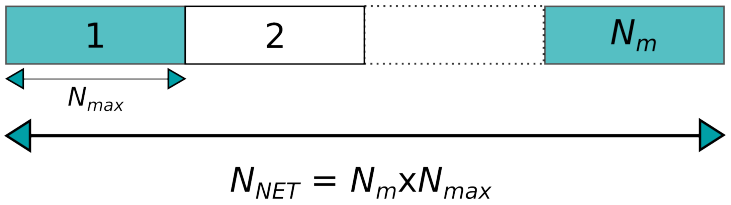

Figure 5.1: The total bandwidth is divided into N_m sub-medium of size $N_{\max}$ each. Nodes have an access to a given sub-medium k with a probability p_k.

size of each sub-medium as well as the choice of N_m and $N_{\max}$ will be further discussed in Section 3. The nodes select randomly, before transmission, a random MAI e from the set $\mathcal{M} = \{0, 1, \ldots, N_m\}$; the transmitter accesses to the shared medium if $e > 0$ and it delays its transmission if $e = 0$. The authorized nodes transmit their information within the sub-medium labelled by the medium access indicator $e > 0$. The intra-sub-medium interference is induced by nodes that select the same sub-medium for transmission. Each

sub-medium is accessible with a probability:

$$p_k = \text{Prob}\{e_k = k\} \tag{5.1}$$

$$p_0 = \text{Prob}\{e_k = 0\} = 1 - \sum_{k=1}^{N_m} p_k. \tag{5.2}$$

For high priority and sensitive information, the value of p_k is small and vice-versa. In the following, we assume without loss of generality that all the sub-mediums are accessible with the same probability i.e. $p_1 = \ldots = p_{N_m} = p = \frac{1-p_0}{N_m}$. By the thinning operation (Proposition 2.3), the authorized transmitting nodes in a given sub-medium k form an homogeneous PPP with intensity λp_k.

2.1.1 BiPolar "BP" receiver model

The bipolar receiver model corresponds to the network in which the receiver is located at the distance r from its associated transmitter, and in an i.i.d. direction. For a given position $X_i \in \Phi$ of a transmitting node, the associated receiver $y_i \in \mathcal{B}(X_i, r)$ in the bipolar receiver model is located at distance r from the transmitter and the random vectors $\{X_i - y_i\}$ are i.i.d. In the bipolar model nodes belonging to a circular region transmit to receiver situated in a range of 1 km.

2.1.2 Independent Nearest Receiver "INR" model

The INR model corresponds to the case in which each transmitting nodes choose the closest node in an independent homogeneous PPP of intensity λ_0. For a given position of a transmitting node $X_i \in \Phi$, the associated receiver y_i in the INR model is located at distance r from the transmitter such that

$$r = \arg \min_{y_i \in \phi_r} |X_i - y_i|.$$

From [11], it is known that the distribution of r is

$$p(r) = 2\pi\lambda_0 r \exp(-\lambda_0 \pi r^2).$$

Note that there is a non-negligible probability that two different nodes choose the same receiver. In this case, the receiver decodes each useful information considering all the others as interference.

3 Radio resource outage in the bipolar receiver model

In this section, we characterize the statistical distribution of the number of sub-medium that guarantees that the traffic of the node is supported by the limited size of each sub-medium. For this, we start first in Subsection 3.1 by defining, in the context of a bipolar receiver model, the number of radio resources required by both the individual node and by the sub-medium. We review in Subsection 3.2 the definition of individual and sub-medium outage events. Next, we compute in Subsection 4 the relationship between these two events. The dimensioning parameters and the spectral efficiency are then defined in Subsection 4.3. Finally, we extend these results to the INR model in Subsection 4.5.

3.1 Target rate and required number of RBs

Let X_i be a random transmitter position, y_i its associated receiver located at distance r from the transmitter, e_i be the medium access indicator with $0 \leq e_i \leq N_m$ and F_i is the random channel fading of the path between the transmitter and the receiver. This MANET network can be represented by a Marked Poisson Point Process

$$\tilde{\Phi} = \{\tilde{X}_i \in (\mathbb{R}^2 \times \mathcal{B}(X_i, r) \times \mathcal{M} \times \mathbb{R}^+) : \tilde{X}_i = (X_i, y_i, e_i, F_i)\}$$

and $\mathcal{B}(X_i, r)$ is the disk of radius r centered at X_i. Let Φ_k be the set of the transmitting nodes in a given sub-medium k i.e. $\Phi_k = \{X_i : e(X_i) = k\}$ and $\Phi^+ = \{X_i : e(X_i) > 0\}$ the set of transmitting nodes that constitutes an homogeneous PPP with intensity $\lambda(1 - p_0)$. The associated marked Point Process $\tilde{\Phi}_k$ is defined as:

$$\tilde{\Phi}_k = \{\tilde{X}_i^{(k)} = (X_i, y_i, e_i = k, F_i) \in \mathbb{R}^2 \times \mathcal{B}(X_i, r) \times \mathcal{M} \times \mathbb{R}^+\}$$

For a single QoS with target rate R_0 (b/s), the number of required RBs for the transmission on a radio link subject to a fading F_i from X_i to y_i is

$$N_{\text{RB}}(r, X_i, \tilde{\Phi}^+) = \left\lceil \frac{R_0}{W_{\text{RB}} \times C(r, X_i, \tilde{\Phi}^+)} \right\rceil \tag{5.3}$$

where $C(r, X_i, \tilde{\Phi}^+)$ is the Shannon spectral efficiency,

$$C(r, X_i, \tilde{\Phi}^+) = \log_2(1 + \text{SINR}(r, X_i, \tilde{\Phi}^+)) \ \ (b/s/Hz)$$

and SINR is the signal to noise and interference ratio that will be specified in Section 5 for different antenna configurations. The level of interference is introduced by the nodes transmitting on the same radio resource block that form an homongeneous Poisson Point Process $\tilde{\Phi}_k$ with intensity $\lambda_k = \lambda p_k = \lambda(1 - p_0)/N_m$. For each group of nodes transmitting in the same medium, the maximal number of requested RB in the given medium labelled by $1 \leq k \leq N_m$, is the maximal number of RBs required by all the nodes transmitting in the

same medium,

$$N^*_{\mathrm{RB}}(r,\tilde{\Phi}_k) = \max_{e(X_i)=k} N_{\mathrm{RB}}(r,X_i,\tilde{\Phi}^+). \tag{5.4}$$

For a given target rate R_0, the maximal number of allocated RBs per node and consequently per sub-medium is related to the minimal spectral efficiency $C_{0,\min}$ in b/s/Hz by

$$N_{\max} = \left\lceil \frac{R_0}{W_{\mathrm{RB}} \times C_{0,\min}} \right\rceil, \tag{5.5}$$

where $W_{\mathrm{RB}} = 180$ KHz is the RB bandwidth. Due to the absence of coordination between the nodes and in order to avoid the interference between nodes transmitting in different sub-mediums, the size of each sub-medium is fixed to $N_{\max}$ independently of the value of $N^*_{\mathrm{RB}}(r,\tilde{\Phi}_k)$. The total number of required RBs in a network sub-divided into N_m sub-medium is therefore a multiple of $N_{\max}$ with

$$N_{\mathrm{RB},t}(r) = N_m(r) \times N_{\max}. \tag{5.6}$$

3.2 Individual resource outage probability

Assuming that the total bandwidth is sub-divided into N^*_m sub-mediums, the individual resource outage event occurs when the number of radio resources required for transmission between two nodes in a given sub-medium exceeds the maximal number of RBs attributed to this latter. For symmetrical sub-medium access, the individual resource outage probability is independent from the sub-medium i.e.

$$\mathbb{P}^{\mathrm{ind}}_{\mathrm{out}}(r,N^*_m) = 1 - F^{(\mathrm{BP})}_{N_{\mathrm{RB}}}(r,N_{\max},N^*_m) \tag{5.7}$$

where

$$F^{(\mathrm{BP})}_{N_{\mathrm{RB}}}(r,n,N^*_m) = \mathrm{Prob}\{N_{\mathrm{RB}}(r,X_i,\tilde{\Phi}^+) \leq n \Big| N_m = N^*_m\},\ \forall n \in \mathbb{N}$$

is the CDF of N_{RB} conditioned by the division of the total bandwidth into N^*_m sub-mediums and corresponds to the coverage probability in the Baccelli *et al.* terminology.

3.3 Non-empty sub-medium resource outage probability

The sub-medium resource outage event occurs when the total number of required RBs by a given sub-medium k exceeds the maximal size in RBs $N_{\max}$ of a given sub-medium i.e.

$$\mathbb{P}^{\mathrm{med},k}_{\mathrm{out}}(r,N^*_m) = \mathrm{Prob}\left\{N^*_{\mathrm{RB}}(r,\tilde{\phi}_k) > N_{\max} \Big| N_m = N^*_m\right\}, \quad \forall\, 1 \leq k \leq N^*_m. \tag{5.8}$$

In each sub-medium, the level of the interference and consequently the resource outage probability, depend both on the percentage of nodes p simultaneously active in the sub-medium k. In the symmetrical sub-medium access case, the sub-medium outage probability

is the same for all sub-mediums and can be written as,

$$\mathbb{P}_{\text{out}}^{\text{med},k}(r, N_m^*) = \mathbb{P}_{\text{out}}^{\text{med}}(r, N_m^*) = 1 - F_{N_{\text{RB}}^*}^{(\text{BP})}(r, N_{\max}, N_m^*) \tag{5.9}$$

where

$$F_{N_{\text{RB}}^*}^{(\text{BP})}(r, N_{\max}, N_m^*) = \text{Prob}\{N_{\text{RB}}^*(r, \tilde{\phi}_j) \leq N_{\max} \Big| N_m = N_m^*\} \tag{5.10}$$

is the CDF of N_{RB}^* conditioned by the division of the total bandwidth into N_m^* sub-mediums.

4 Coverage events

4.1 Typical individual coverage probability

To find the individual coverage probability of nodes located in a given region $\mathcal{R}$, one should find:

$$F_{N_{\text{RB}}}^{(\text{BP})}(r, n, N_m^*) = \frac{1}{\lambda(1-p_0)|\mathcal{R}|}\mathbb{E}\left[\sum_{X_i \in \mathcal{R}} \mathbb{1}_{\{N_{\text{RB}}(r, X_i, \tilde{\Phi}^+) \leq n\}}\right].$$

By the stationarity of the PPP, this is equivalent to find,

$$F_{N_{\text{RB}}}^{(\text{BP})}(r, n, N_m^*) = \frac{1}{\lambda(1-p_0)|\mathcal{R}|}\mathbb{E}\left[\sum_{X_i \in \mathcal{R}} \mathbb{1}_{\{N_{\text{RB}}(r, 0, \tilde{\Phi}^+) \leq n\}}\right].$$

Using again the same terminology as in Baccelli *et al.* [8, 9], this corresponds to the Palm probability associated to the stationary point process $\tilde{\Phi}^+$ i.e.

$$F_{N_{\text{RB}}}^{(\text{BP})}(r, n, N_m^*) = \text{Prob}\{N_{\text{RB}}(r, 0, \tilde{\Phi}^+) \leq n\}.$$

By adding the origin with its associated mark $\tilde{X}_0 = (0, e_0, F_0, y_0)$ to the original marked PPP $\tilde{\Phi}$ and using Slivnyak's theorem, this probability is

$$F_{N_{\text{RB}}}^{(\text{BP})}(r, n, N_m^*) = \text{Prob}\{N_{\text{RB}}(r, 0, \tilde{\Phi}^+ \cup \tilde{X}_0) \leq n | e_0 > 0\}.$$

4.2 Typical sub-medium coverage probability

As stated in (5.4), the number of RBs required by a sub-medium is the maximal number of individual RBs required by nodes in a given sub-medium. The following lemma gives the relationship between the sub-medium and individual coverage events:

Lemma 5.1. *In a bipolar model, the CDF $F_{N_{\text{RB}}^*}^{(BP)}(r, n, N_m^*)$ of the number of required RBs per non-empty sub-medium is related to the CDF of required number of RBs per individual node transmitting in this sub-medium by*

$$F_{N_{\text{RB}}^*}^{(BP)}(r, N_{\max}, N_m^*) = \frac{P_0}{1-P_0}\left(\exp\left(\lambda p |\mathcal{R}| F_{N_{\text{RB}}}^{(BP)}(r, N_{\max}, N_m^*)\right) - 1\right) \tag{5.11}$$

with $P_0 = \exp(-\lambda p|\mathcal{R}|)$.

Proof. The proof of this lemma is detailed in Appendix 5.A. □

4.3 Dimensioning in the bipolar receiver model

4.4 Parameters

Although the allocation of more sub-mediums decreases the probability of collision between nodes, this increases the probability of getting an over-dimensioned bandwidth in which several sub-mediums are left empty. The optimal choice of the sub-medium should not only guarantee that the outage in a sub-medium is less than a given threshold p_{th} but also that the percentage of empty sub-medium is small enough to prevent bandwidth wastage. On one hand, the number of sub-medium N_m^* is chosen to ensure that for a given range r, the outage probability is less than a given threshold i.e.

$$N_{m,r} = \arg_{N_m}\{F^{(\text{BP})}_{N^*_{\text{RB}}}(r, N_{\max}, N_m) \geq 1 - p_{\text{th}}\}. \tag{5.12}$$

On the other hand, the probability that any sub-medium k is not-empty should be higher than a given threshold p_{w} i.e.

$$\text{Prob}\{|\Phi_k| > 0\} = 1 - \exp(-\lambda p|\mathcal{R}|) \geq p_{\text{w}}, \tag{5.13}$$

and consequently,

$$N_m \leq \left\lceil \frac{\lambda|\mathcal{R}|(1-p_0)}{\log(\frac{1}{1-p_{\text{w}}})} \right\rceil \triangleq N_{m,\max}.$$

Then, the OFDMA Bandwidth B is chosen to guarantee that the bandwidth contains at least

$$N_{\text{RB,req}} = \min(N_{m,r}, N_{m,\max}) \times N_{\max} \text{ RBs}.$$

The total achieved rate in the network is,

$$\bar{C}_t(r, \Phi) = \sum_{X_i \in \mathcal{R}} R_0 \, \mathbb{1}_{\{N_{\text{RB}}(r, X_i, \tilde{\Phi}^+) \leq N_{\max}\}}.$$

The average total capacity is therefore

$$\bar{C}_t = \lambda|\mathcal{R}|(1-p_0)R_0 F_{N_{\text{RB}}}(r, N_{\max}, N_m^*). \tag{5.14}$$

This total rate is transmitted within the bandwidth B and the corresponding average total spectral efficiency of the network in b/s/Hz is obtained as $\mathcal{S}_{eff} = \bar{C}_t/B$.

4.5 Extension to the INR model

In the INR model, the CDF probability of the required individual resources by each node, belonging to a given sub-medium, can be deduced from the bipolar receiver model by averaging over all possible nearest independent position of the receiver i.e.

$$F^{(\mathrm{INR})}_{N_{\mathrm{RB}}}(N_{\max}, N^*_m) = \int_0^{\infty} F^{(\mathrm{BP})}_{N_{\mathrm{RB}}}(r, N_{\max}, N^*_m)\, p(r)\, dr. \tag{5.15}$$

In a similar way, the sub-medium coverage probability is

$$F^{(\mathrm{INR})}_{N^*_{\mathrm{RB}}}(N_{\max}, N^*_m) = \frac{P_0}{1-P_0}\left(\exp\left(\lambda p\, |\mathcal{R}| F^{(\mathrm{INR})}_{N_{\mathrm{RB}}}(N_{\max}, N^*_m)\right) - 1 \right). \tag{5.16}$$

5 Typical coverage Probability for different transmission modes

Characterizing the sub-medium outage probability depends on the individual coverage probability as stated in Lemma 5.1. In the following, we compute for the *bipolar receiver model* the individual coverage probability considering different antenna configurations. This latter can be extended to the INR model from (5.15) and (5.16). We consider first the SISO system and then we generalize the results to the $n_t \times n_r$ MIMO configuration introduced in Chapter 2 with different transmission modes: (i) the single layer diversity transmission; (ii) the full multiplexing gain; (iii) the optimal MIMO Maximum Ratio Combiner "MRC" with full CSIT for low SINR regime.

5.1 SISO communications schemes

For a SISO communication studied in the bipolar receiver model, the spectral efficiency between a transmitting node X_i belonging to a sub-medium k and its associated receiver y_i located at distance r is

$$C(r, X_i, \tilde{\Phi}^+) = \log_2\left(1 + \frac{P_a\, F_i}{\ell(r)(\omega + I(y_i, \tilde{\Phi}_i | \tilde{X}_i))}\right) \tag{5.17}$$

where P_a is the transmission power per RB, F_i is the exponential fading, ω is the exponential power of the noise, $\ell(r)$ is the propagation path loss and

$$I(y_i, \tilde{\Phi}^+ | \tilde{X}_i) = \sum_{X_j \in \Phi\,:\, e(X_j)=e(X_i), i\neq j} \frac{P_a\, F^i_j}{\ell(|X_j - y_i|)} \tag{5.18}$$

is the shot noise interference introduced by the nodes transmitting on the same sub-medium as the node i.

Proposition 5.1 (Bipolar model, SISO). *In a SISO case, the typical coverage probability is*

$$F_{N_{\mathrm{RB}}}^{(BP,\ SISO)}(r,n,N_m^*) = \mathcal{L}_\omega\Big(\kappa\,\beta_n\,\ell(r)\Big)\mathcal{L}_I\Big(\kappa\,\beta_n\,\ell(r)\Big) \tag{5.19}$$

where

$$\beta_n \triangleq \left(2^{\frac{R_0}{nW_{\mathrm{RB}}}}-1\right), \qquad \kappa \triangleq \frac{1}{P_a\sigma_f^2} \tag{5.20}$$

and $\mathcal{L}_\omega(s)$ and $\mathcal{L}_I(s)$ are respectively the Laplacian function of the noise and the sub-medium interference such that:

$$\mathcal{L}_\omega(s) = \frac{1}{sN_0+1}, \tag{5.21}$$

$$\mathcal{L}_I(s) = \exp\left\{-2\pi\lambda p\int_0^\infty \frac{s\,t}{s+\kappa\,\ell(t)}dt\right\}. \tag{5.22}$$

with $p=(1-p_0)/N_m^*$.

Proof. The SISO individual coverage probability is

$$F_{N_{\mathrm{RB}}}^{(\mathrm{BP,\ SISO})}(r,n,N_m^*) = \mathrm{Prob}\left\{N_{\mathrm{RB}}(r,\tilde{X}_i^{(k)})<n)\right\}$$

where $N_{\mathrm{RB}}(r,\tilde{X}_i^{(k)},\tilde{\Phi}^+)$ is defined in (5.3) and the expression of $C(r,X_i,\tilde{\Phi}^+)$ is given in (5.17). It follows then,

$$F_{N_{\mathrm{RB}}}^{(\mathrm{BP,\ SISO})}(r,n,N_m^*) = \mathbb{E}\left[\mathrm{Prob}\left\{F_i > \frac{1}{P_a}\,\beta_n\,\ell(r)(\omega+I)\right\}\right]. \tag{5.23}$$

with β_n defined in (5.20) and F_i is an exponentially distributed fading variable with parameter $1/\sigma_f^2$. Then,

$$F_{N_{\mathrm{RB}}}^{(\mathrm{BP,\ SISO})}(r,n,N_m^*) = \mathbb{E}\left[\exp\Big(-\kappa\beta_n\ell(r)(\omega+I)\Big)\right]. \tag{5.24}$$

The expression of the CDF in (5.19) follows from the independence of the noise power ω and the interference I. The Laplacian of the exponential random noise ω with parameter N_0 is

$$\mathcal{L}_\omega(s) = \mathbb{E}[e^{-s\omega}] = \frac{1}{sN_0+1}.$$

For stationary homogeneous PPP, the total interference power measured at any point has the same distribution as the one measured at the origin. The Laplacian of the interference

is derived in [9, 12] and is such that

$$\begin{aligned}\mathcal{L}_I(s) &= \exp\Big\{-2\pi\lambda p\int_0^\infty t\Big(1-\mathcal{L}_F(sP_a/\ell(t))\Big)dt\Big\}\\ &= \exp\Big\{-2\pi\lambda p\int_0^\infty \frac{t}{1+\ell(t)/(sP_a\sigma_f^2)}dt\Big\}.\end{aligned}$$

□

5.2 Single-layer MIMO communication with diversity gain

In this subsection, we consider the $n_t \times n_r$ MIMO configuration studied with different single-layer diversity schemes: (i) the first one extracts the full MIMO diversity using an antenna selection where the full power is transmitted on the best path; (ii) the second one extracts the full MIMO receiver diversity using a Receiver Maximum Ratio Combiner "MRC-R"; (iii) the third scheme is a combination of antenna selection and MRC at the receiver side "MRC-RS". In this case, the spectral efficiency between a transmitting node X_i in a sub-medium k and its associated receiver y_i located at distance r has the same expression as the SISO case given in (5.17), but with a different distribution of the fading coefficients between the transmitter and the intended receiver. Note that the, the fading on which interfering signals arise to the non intended receiver are exponentially distributed. The beamforming and the signal equalization modify only the distribution of the fading on which useful signal information is carried.

5.2.1 MIMO antenna selection

A simple method to extract the full diversity of the $n_t \times n_r$ MIMO scheme consists to select the path on which the signal experiences the lowest fading attenuation among the $n_t n_r$ possible ones. In this case, the fading F_i in (5.17) is the maximum between $n_t n_r$ exponential random variables with CDF,

$$F_{F_i}(t) = \left(1-e^{-\frac{t}{\sigma_f^2}}\right)^{n_t n_r}. \tag{5.25}$$

Proposition 5.2 (MIMO diversity with antenna selection). *In the $n_t \times n_r$ MIMO communication using antenna selection, the typical coverage probability is*

$$F_{N_{\mathrm{RB}}}^{(BP,\ MIMO,\ sel)}(r,n,N_m^*) = \sum_{k=1}^{n_t n_r}(-1)^{k+1}\binom{n_t n_r}{k}\,\mathcal{L}_\omega\Big(k\times s\Big)\mathcal{L}_I\Big(k\times s\Big), \tag{5.26}$$

with $s=\kappa\beta_n\ell(r)$ with β_n and κ being defined in (5.20). The respective expression of the noise and interference Laplacian are given in (5.21) and (5.22).

Proof. The proof of this proposition is deduced from the SISO case by considering in (5.23) a fading that is distributed according to (5.25). Hence,

$$F_{N_{\text{RB}}}^{(\text{BP, MIMO, sel})}(r, n, N_m^*) = \sum_{k=1}^{n_t n_r} (-1)^{k+1} \binom{n_t n_r}{i} \mathbb{E}\left[\exp\left(- k\, \kappa\, \beta_n \ell(r)(\omega + I)\right)\right]. \tag{5.27}$$

which leads to the CDF expression in (5.26). □

5.2.2 Maximum Ratio Combiner Receiver "MRC-R"

The MRC-R extracts the full receiver diversity of the MIMO scheme by combining the different received observations using the conjugate of the fading coefficients. There is no transmission diversity in this case as information are transmitted over a randomly chosen antenna. In this case, equivalent fading F_i in (5.17) is a chi-squared randomly distributed fading with $2n_r$ degrees of freedom $\chi^2_{2n_r}$ and its CDF is,

$$F_{F_i}(t) = \frac{1}{(n_r - 1)!}\, \gamma\left(n_r, \frac{t}{\sigma_f^2}\right),$$

with $\gamma(n_r, t) = (n_r - 1)!\left(1 - g(n_r, t)\, e^{-t}\right)$ and

$$g(n_r, x) = \sum_{k=0}^{n_r - 1} \frac{1}{k!}\, x^k. \tag{5.28}$$

Proposition 5.3 (MIMO with MRC-R). *In the $n_t \times n_r$ MIMO communication using a MRC-R, the typical coverage probability is*

$$F_{N_{\text{RB}}}^{(\text{BP, MIMO, MRC-R})}(r, n, N_m^*) = \sum_{i=0}^{n_r - 1} \frac{1}{i!}\, \Xi_i(s), \tag{5.29}$$

with $s = \kappa \beta_n \ell(r)$ with β_n and κ being defined in (5.20), and

$$\Xi_i(s) = (-1)^i \sum_{j=0}^{i} s^i \binom{i}{j} \frac{\partial^j \mathcal{L}_\omega(s)}{\partial\, s^j} \frac{\partial^{i-j} \mathcal{L}_I(s)}{\partial\, s^{i-j}}. \tag{5.30}$$

The respective expression of the noise and interference Laplacian are given in (5.21) and (5.22).

Proof. The proof of this proposition is the same as in the SISO case by considering a

chi-squared random fading instead the exponential one. In this case,

$$F_{N_{\text{RB}}}^{(\text{BP, MIMO, MRC})}(r, n, N_m^*) = \sum_{i=0}^{n_r-1} \frac{1}{i!}\ \mathbb{E}\Big[\ s^i(\omega + I)^i e^{-s(\omega+I)}\Big]. \tag{5.31}$$

To compute the above expectation, we invoke Lemma 5.2:

Lemma 5.2. *Let* $\Xi_i(s) = \mathbb{E}\left[s^i(\omega + I)^i e^{-s(\omega+I)}\right]$ *Then,*

$$\Xi_i(s) = (-1)^i \sum_{j=0}^{i} s^i \binom{i}{j} \frac{\partial^j \mathcal{L}_\omega(s)}{\partial\, s^j} \frac{\partial^{i-j} \mathcal{L}_I(s)}{\partial\, s^{i-j}}$$

where $\frac{\partial^j f(s)}{\partial s^j}$ *is the derivative of order* j *of the function* $f(s)$ *for* $j \in \mathbb{N}^*$ *and* $\frac{\partial^0 f(s)}{\partial s^0} = f(s)$. *The proof of this Lemma is detailed in Appendix 5.B.*

□

We note that $\mathcal{L}_I(s)$ is an exponential function $\mathcal{L}_I(s) = \exp(-a h(s))$ or $h(s) = -\frac{1}{a}\log\Big(\mathcal{L}_I(s)\Big)$ with $a = 2\pi\lambda p$ and

$$h(s) = \int_0^\infty \frac{s\, t}{s + \kappa\, \ell(t)} dt.$$

The successive derivation of $\mathcal{L}_I(s)$ can be deduced from $\frac{\partial^n h(s)}{\partial s^n} = -\frac{1}{a}\frac{\partial^n \log(\mathcal{L}_I(s))}{\partial s^n}$ with

$$\frac{\partial^n h(s)}{\partial s^n} = (-1)^{n+1}\, n!\, \kappa \int_0^R \frac{t\, \ell(t)}{(\kappa\, \ell(t) + s)^{n+1}}\, dt.$$

Remark 1 ($2 \times n_r$ MIMO using an Alamouti code [71]). *For the particular case of* $n_t = 2$, *the spatial-frequency Alamouti code transmits two symbols carved from a QAM constellation within two consecutive sub-carriers where the channel is assumed to be constant. The power is uniformly distributed among the two transmitting antennas. The equalization of this code at the receiver side transforms the MIMO channel into two parallel channels. Each symbol is decoded on an equivalent fading channel that is chi-squared distributed* $\chi^2_{2n_t n_r}$. *Considering the degrees of freedom of* $\chi^2_{2n_t n_r}$ *and the normalized power, one can easily deduce from Proposition 5.3 the CDF of the individual node required RB with the Alamouti code as,*

$$F_{N_{\text{RB}}}^{(\textit{BP, MIMO, Alamouti})}(r, n, N_m^*) = \sum_{m=0}^{2n_r-1} \frac{1}{m!} \Xi_m(2 \times s), \tag{5.32}$$

with $s = \kappa\beta_n \ell(r)$ *and*

$$\Xi_m(s) = (-1)^m \sum_{j=0}^{m} s^m \binom{m}{j} \frac{\partial^j \mathcal{L}_\omega(s)}{\partial s^j} \frac{\partial^{m-j} \mathcal{L}_I(s)}{\partial s^{i-j}}.$$

5.2.3 Combined antenna selection and MRC-R decoder "MRC-RS"

When combining antenna selection with a MRC-R, the transmitting antenna is the one that maximizes the signal to noise ratio at the receiver side. The fading coefficient in this case is the maximum between n_t chi-squared random variables $\chi^2_{2n_t}$ and its CDF is

$$F_{F_t}(t) = \left(F_{\chi^2_{2n_r}}(t)\right)^{n_t} = \left(1 - g\left(n_r, \frac{t}{\sigma_f^2}\right) e^{-\frac{t}{\sigma_f^2}}\right)^{n_t}. \tag{5.33}$$

Proposition 5.4 (MIMO with MRC-RS). *In the* $n_t \times n_r$ *MIMO communication using a combination of MRC and antenna selection, the typical coverage probability is*

$$F^{(BP,\ MIMO,\ sel\ \&\ MRC\text{-}R)}_{N_{RB}}(r, n, N^*_m) = \sum_{p=1}^{n_t} (-1)^{p+1} \binom{n_t}{p} \sum_{m=0}^{p(n_r-1)} \frac{1}{p^m} a_{(m,p)} \Xi_m\left(p \times s\right) \tag{5.34}$$

with $s = \kappa\beta_n \ell(r)$*, the constant* β_n *and* κ *being defined in (5.20) and*

$$\Xi_m(s) = (-1)^m s^m \sum_{j=0}^{m} \binom{m}{j} \frac{\partial^j \mathcal{L}_\omega(s)}{\partial s^j} \frac{\partial^{m-j} \mathcal{L}_I(s)}{\partial s^{m-j}}. \tag{5.35}$$

Finally, the constants $a_{(m,p)}$ *are the coefficients of the polynomial*

$$\left(g(n_r, x)\right)^p = \sum_{m=0}^{p(n_r-1)} a_{(m,p)} x^m \tag{5.36}$$

where $g(n_r, x)$ *is defined in (5.28) and coefficients* $a_{(m,p)}$ *are computed as:*

$$a_{(m,p)} = \lim_{x \to 0} \frac{\partial^m \left(\left[g(n_r, x)\right]^p\right)}{\partial x^m}$$

The respective expressions of the noise and interference Laplacian are given in (5.21) and (5.22).

Proof. The proof of this proposition is obtained by applying the CDF of the fading coefficient

in (5.33) to (5.23). It follows then,

$$F_{N_{\text{RB}}}^{(\text{BP, MIMO, sel \& MRC-R})}(r, n, N_m^*) = \mathbb{E}\left[\sum_{p=1}^{n_t}(-1)^{p+1}\binom{n_t}{p}\left(e^{-t_0}g(n_r, t_0)\right)^p\right]$$

with $t_0 = \kappa\beta_n\ell(r)(\omega + I)$. Next, by replacing $\left(g(n_r, x)\right)^p$ by its polynomial expansion in (5.36), we get:

$$F_{N_{\text{RB}}}^{(\text{BP, MIMO, sel \& MRC-R})}(r, n, N_m^*) = \sum_{p=1}^{n_t}(-1)^{p+1}\binom{n_t}{p}\mathbb{E}\left[e^{-p\,t_0}\sum_{m=0}^{p(n_r-1)}a_{m,p}\,t_0^m\right].$$

By letting,

$$\Xi_m(p \times s) \triangleq \mathbb{E}\left[e^{-p\,t_0}(p\,t_0)^m\right]$$

we can rewrite $F_{N_{\text{RB}}}^{(\text{BP, MIMO, sel \& MRC})}(r, n, N_m^*)$ as in (5.34). The expression of $\Xi_m(s)$ can be deduced from the independence of ω and I and in the same way as in Proposition 5.6 by applying Lemma 5.2. □

5.3 MIMO communication with full multiplexing gain

The maximal number of spatial layers in a $n_t \times n_r$ MIMO configuration is $n_s \triangleq \min(n_t, n_r)$. In the following, we derive the coverage probability for spatial division multiplexing schemes using a VBLAST code at the transmitter side and a Successive Interference Cancellation "SIC" decoder (see Chapter 2). The total rate of R_0 is sub-divided into $n_s = \min(n_t, n_r)$ sub-streams spatially transmitted on the different antennas, with rate equal to R_0/n_s each. The total power is also uniformly distributed across the transmitting antennas in this case. We consider a sub-optimal decoder in which the n_s streams are individually decoding. Unlike joint stream decoding, the individual decoding penalizes the mutual information between the received signal and the transmitted one. Although both streams are subject to the same interferers, the individual stream decoding restricts the information exchange about the interferers, and results in a loss of mutual information. The maximal achieved spectral efficiency by the individual decoding for each sub-stream is,

$$C_s(r, X_i, \tilde{\Phi}^+) = \log_2\left(1 + \frac{P_a\ F_{s,i}}{n_s\ell(r)(\omega + I(y_i, \tilde{\Phi}^+|\tilde{X}_i))}\right), \quad 1 \leq s \leq n_s.$$

where P_a/n_s is the normalized transmission power per RB and per stream and $F_{s,i}$ is the the fading coefficient for each stream. ω is the exponential power of the noise, $\ell(r)$ is the propagation path loss and $I(y_i, \tilde{\Phi}^+|\tilde{X}_i^{(k)})$ is the interference introduced by the nodes transmitting on the same radio resource block. The $n_s = \min(n_t, n_r)$ sub-streams are transmitted in parallel on the same RBs, and the total number of RBs required for the

transmission of both streams is the one of the slow-rate sub-stream,

$$N_{\mathrm{RB}}(r, X_i, \tilde{\Phi}^+) = \left\lceil \frac{R_0}{n_s \times W_{\mathrm{RB}} \times \min_s C_s(r, \tilde{X}_i^{(k)})} \right\rceil .$$

The fading coefficient that dictates the RB number corresponds therefore to the minimal coefficient experienced by the n_s sub-streams i.e. $F_i = \min_{1 \le s \le n_s} F_{s,i}$. When using a SIC decoder, the receiver decodes the first sub-stream by nulling out all the others. The first sub-stream is decoded on a fading coefficient $F_{1,i}$ that is chi-squared distributed with $2(n_r - n_s + 1)$ degrees of freedom. In order to decode the second sub-stream, the contribution of this sub-stream is subtracted from the received signal and the second sub-stream is decoded over a chi-squared random variable with $2(n_r - n_s + 2)$ degrees of freedom. The s^{th} sub-stream is decoded over a chi-squared random variable with $2(n_r - (n_s - (s-1)) + 1)$ degrees of freedom. In this case,

$$F_i = \min_{1 \le s \le n_s} \chi^2_{2(n_r - n_s + s)} = \chi^2_{2(n_r - n_s + 1)}$$

Proposition 5.5 (VBLAST code and SIC decoder). *In the $n_t \times n_r$ MIMO communication using a VBLAST code and a SIC decoder, the typical coverage probability is*

$$F^{(BP,\ MIMO,\ SIC)}_{N_{\mathrm{RB}}}(r, n, N^*_m) = \sum_{i=0}^{n_r - n_s} \frac{1}{i!} \Xi_i(n_s \tilde{s}), \tag{5.37}$$

where

$$\Xi_i(s) = (-1)^i s^i \sum_{j=0}^{i} \binom{i}{j} \frac{\partial^j \mathcal{L}_W(s)}{\partial s^j} \frac{\partial^{i-j} \mathcal{L}_I(s)}{\partial s^{i-j}},$$

and $\tilde{s} = \kappa \tilde{\beta}_n \ell(r)$ with

$$\tilde{\beta}_n = (2^{\frac{R_0}{n_s n W_{\mathrm{RB}}}} - 1). \tag{5.38}$$

Proof. The proof of this proposition is a straightforward consequence of Proposition 5.6 by replacing the power P_a by the normalized one P_a/n_s. □

5.4 Optimal low SINR outage with full CSIT and MIMO MRC

In the low SINR regime, the optimal power allocation consists to allocate the whole power on the strongest eigen-mode. With full CSIT, the signal information is projected on the right singular vector corresponding to the maximal singular value of the fading channel matrix. At the receiver side, the received signal is projected onto the left singular vector of

the channel matrix. The maximal achieved spectral efficiency is

$$C_s(r, X_i, \tilde{\Phi}^+) = \log_2\left(1 + \frac{P_a\ \lambda_{\max,i}}{\ell(r)(\omega + I(y_i, \tilde{\Phi}^+|\tilde{X}_i))}\right).$$

where $\lambda_{\max}$ is the maximal eigen-value of the Wishart MIMO matrix. The coverage probability depends on the largest eigen-value distribution that is given in Lemma 5.3.

Lemma 5.3 (Largest eigen-value CDF, [60]). *Let* $\mathbf{H}$ *be the* $n_r \times n_t$ *MIMO channel containing the fading coefficients and let* $n_s = \min(n_t, n_r)$ *and* $n_p = \max(n_t, n_r)$. *The CDF of the largest eigen-value of a Wishart matrix* $\mathbf{H}\mathbf{H}^\dagger$ *is:*

$$\text{Prob}\left\{\lambda_{\max} \leq t\right\} = C_{(n_s,n_p)} \left|\Psi_c(t)\right|$$

where

$$C_{(n_s,n_p)} = \frac{1}{\prod_{k=1}^{n_s}(n_s - k)!\,(n_s - k)!}$$

and $\Psi_c(t)$ *is an* $n_s \times n_s$ *Hankel matrix function of* $t > 0$ *with entries given as*

$$\{\Psi_c(t)\}_{(i,j)} = \gamma(n_p - n_s + i + j - 1, t)$$

and $\gamma(k, x) = (k-1)!\left(1 - g(k, x)e^{-x}\right)$, $\forall\, k \in \mathbb{N}$.

By expanding the determinant of the Hankel matrix, the CDF of the maximal eigen-value can be rewritten as,

$$\text{Prob}\left\{\lambda_{\max} \leq t\right\} = 1 - C_{(n_s,n_p)} \sum_{p=1}^{n_s} E_p(t)\, e^{-pt}$$

with $E_p(t) = \sum_{m=1}^{d_p} \xi_{(p,m)}\, t^m$ are polynomial with coefficients $\xi_{(p,m)}$ and with degree d_p are computed by expanding the determinant of the $n_s \times n_s$ Hankel matrix $\Psi_c(t)$.

Proposition 5.6 (MIMO-MRC). *In the* $n_t \times n_r$ *MIMO communication using a MIMO MRC, the typical coverage probability is*

$$F_{N_{\text{RB}}}^{(BP,\ MIMO,\ MRC)}(r, n, N_m^*) = C_{(n_s,n_p)} \sum_{p=1}^{n_s} \sum_{m=1}^{d_p} \frac{1}{p^m}\, \xi_{(m,p)}\, \Xi_m\left(p \times s\right) \tag{5.39}$$

with $s = \kappa\beta_n \ell(r)$, *the constant* β_n *and* κ *being defined in (5.20) and*

$$\Xi_m(s) = (-1)^m\, s^m \sum_{j=0}^{m} \binom{m}{j} \frac{\partial^j \mathcal{L}_\omega(s)}{\partial\, s^j} \frac{\partial^{m-j} \mathcal{L}_I(s)}{\partial\, s^{m-j}}. \tag{5.40}$$

The respective expressions of the noise and interference Laplacian are given in (5.21) and (5.22).

Proof. The proof of this proposition is identical to the previous ones using the distribution of $\lambda_{\max}$ in Lemma 5.3. □

6 Numerical results

We consider an OFDMA maritime ad-hoc network operating at a frequency $f = 800$ MHz in which omnidirectional nodes communicate in a circular area with radius $R = 5$ km. The set of active nodes forms an homogeneous PPP with intensity $\lambda = 0.36$ Tx/km^2 corresponding to an inter-arrival surface density $\rho = 0.003\,\text{min}^{-1}\,\text{km}^{-2}$ and a mean service time $1/\nu = 1.2$ min. The average number of nodes in this circular region is $\lambda\pi R^2 = 29$ nodes. The transmission power is $P_e = 46$ dBm and the transmitter and receiver antennas heights are fixed to $h_t = h_r = 12$ m. We propose to evaluate the above mentioned dimensioning parameters for a target rate $R_0 = 600$ kbps. We adopt $C_{0,\min} = 0.93$ b/s/Hz as the minimal spectral efficiency for all the considered transmission modes corresponding to a maximal number of RBs of $N_{\max} = 4$ RBs in each sub-medium. The percentage of non-transmitting nodes in (5.2) is set to $p_0 = 0$, the non-wastage threshold in (5.13) to $p_w = 70\%$ and the acceptable sub-medium outage threshold in (5.12) is fixed to $p_{\text{th}} = 2.5\%$. Based on these thresholds, the maximal number of sub-medium is limited by (5.13) to $N_m \leq 23$ and the closest bandwidth containing $N_m \times N_{\max} = 92$ RBs is the aggregated bandwidth with carrier components $B = 15 + 3 = 18$ MHz. The maritime propagation model presented in Chapter 2 is interpolated using the ITU reference path-loss model for a frequency carrier $f_c = 800$ MHz and for antenna transmit and receive heights $h_t = h_r = 10$ m in [3].

Due to this maritime path loss model, the most powerful interferers are situated in a disk of radius 5 km around each receiver. We finally note that, due to long range communication distances (in the order of 1 to 1.5 km) and to the limited antenna height, there is a high probability that the first Fresnel zone with radius (in the order of 10 to 12 m) to be obstructed. The transmission occurs then on Non-Line of Sight "NLOS" paths and this justifies the Rayleigh fading distribution assumption.

6.1 Bipolar receiver model

We study first the maritime 2×2 MIMO OFDMA network with a bipolar receiver model with a coverage radius of $r = 1$ km. Considering different values of aggregated OFDMA bandwidth, we compare in Figure 5.1, for the different transmission modes, the analytical expressions of the typical individual and sub-medium resource outage probabilities in Figures 5.1a and 5.1b with the numerical probabilities in Figures 5.1c and 5.1d computed using Monte-Carlo simulations with 5000 iterations. The analytical expressions of the typical individual coverage probability developed in this paper are summarized in Table 5.1.

The numerical and analytical typical outage curves reflect the same behavior of the transmission modes of the 2×2 MIMO configuration. For the evaluation of the analytical expression, we approximate the interference Laplacian using the Riemann summation.

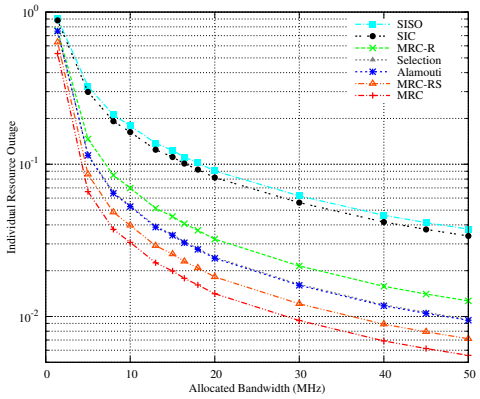

(a) Analytical Individual Outage

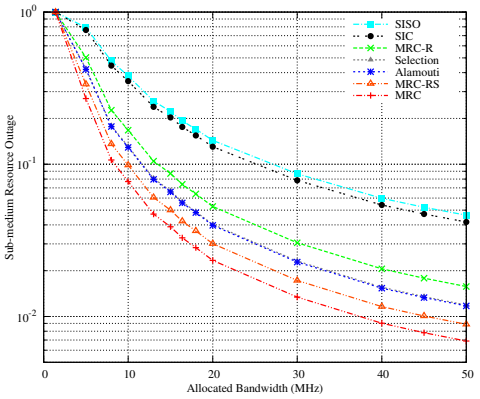

(b) Analytical Sub-Medium Outage

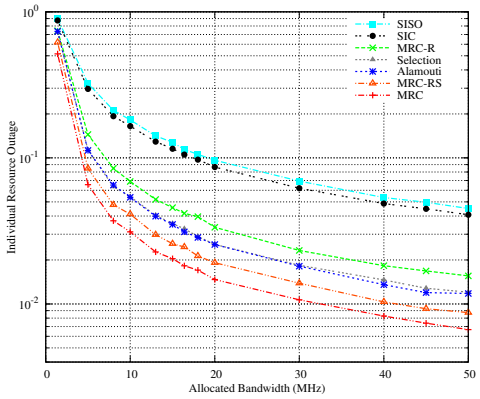

(c) Numerical Individual Outage

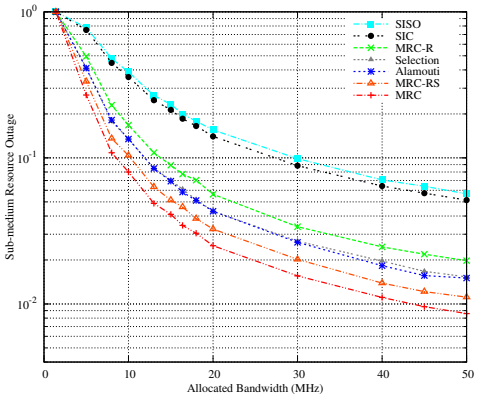

(d) Numerical Sub-Medium Outage

Figure 5.1: Bipolar model with transmission range of $r = 1$ km: Analytical and Numerical Individual and Sub-medium resource outage probabilities for a 2×2 MIMO scheme with different transmission

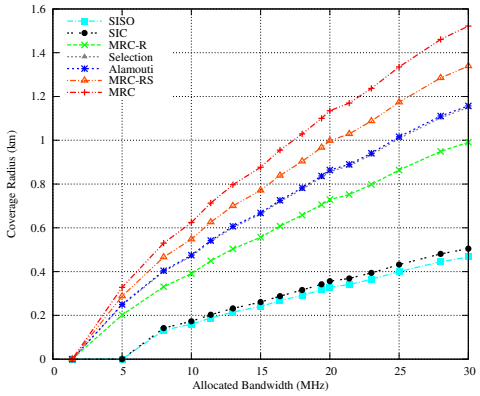

(a) Coverage Radius

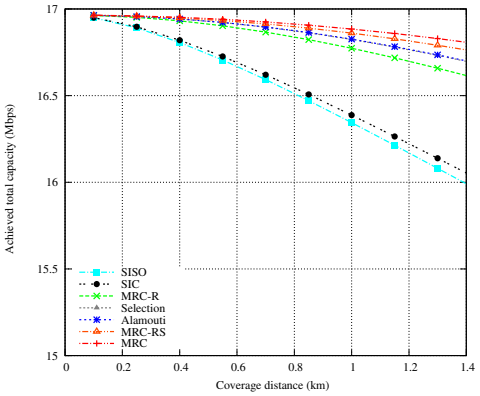

(b) Achieved Total Capacity

Figure 5.2: Coverage radius and achieved total capacity in 2×2 MIMO

Mode	Typical coverage probability
SISO	$\Xi_0(s)$
Selection	$4\,\Xi_0(s) - 6\,\Xi_0(2s) + 4\,\Xi_0(3s) - \Xi_0(4s)$
MRC-R	$\Xi_0(s) + \Xi_1(s)$
Alamouti	$\Xi_0(2s) + \Xi_1(2s) + \frac{1}{2!}\,\Xi_2(2s) + \frac{1}{3!}\,\Xi_3(2s)$
MRC-RS	$2\left(\Xi_0(s) + \Xi_1(s)\right) - \left(\Xi_0(2s) + \Xi_1(2s) + \frac{1}{4}\Xi_2(2s)\right)$
SIC	$\Xi_0(2\,\tilde{s})$
MIMO MRC	$2\,\Xi_0(s) + \Xi_2(s) - \Xi_0(2s)$
$\Xi_0(s)$	$\mathcal{L}_\omega(s)\mathcal{L}_I(s)$
$\Xi_1(s)$	$-s\left(\mathcal{L}_\omega(s)\mathcal{L}'_I(s) + \mathcal{L}_I(s)\mathcal{L}'_\omega(s)\right)$
$\Xi_2(s)$	$s^2\left(\mathcal{L}_\omega(s)\mathcal{L}''_I(s) + 2\mathcal{L}'_\omega(s)\mathcal{L}'_I(s) + \mathcal{L}_I(s)\mathcal{L}''_\omega(s)\right)$
$\Xi_3(s)$	$-s^3\Big(\mathcal{L}_\omega(s)\mathcal{L}'''_I(s) + 3\mathcal{L}''_\omega(s)\mathcal{L}'_I(s) + 3\mathcal{L}'_\omega(s)\mathcal{L}''_I(s) + \mathcal{L}_I(s)\mathcal{L}'''_\omega(s)\Big)$
$\mathcal{L}_I(s)$	$\exp\left(-ah(s)\right)$
$\mathcal{L}'_I(s)$	$-ah'(s)\mathcal{L}_I(s)$
$\mathcal{L}''_I(s)$	$(-ah''(s) + a^2h'^2(s))\mathcal{L}_I(s)$
$\mathcal{L}'''_I(s)$	$(-ah'''(s) + 3a^2h''(s)h'(s) - a^3h'^3(s))\mathcal{L}_I(s)$

Table 5.1: Typical coverage probability for 2×2 MIMO configuration with different transmission modes

When narrow-bands are used, the number of sub-mediums is limited and the level of interference is consequently very high. However, for very wide bandwidths, there is a high probability that the node is the only transmitting one on the considered sub-medium and the network is then noise limited. The sub-medium outage converges toward the individual ones for very large bandwidth. For the 2×2 MIMO configuration, the antenna selection

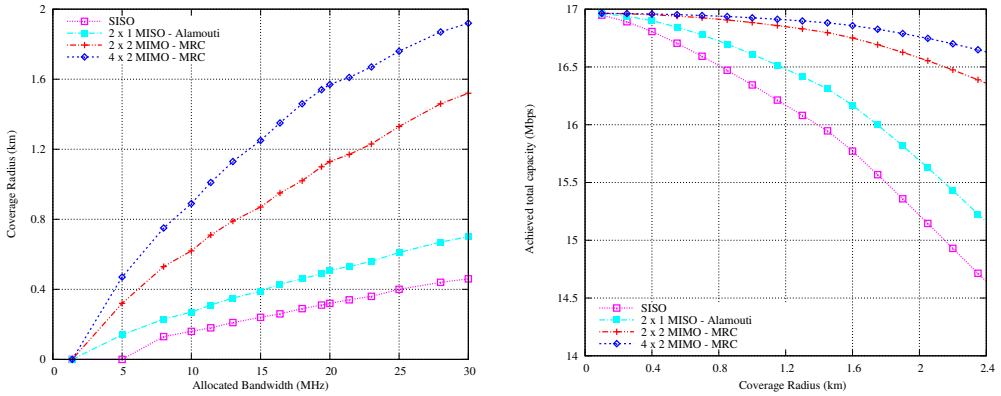

(a) Coverage Radius

(b) Achieved total capacity

Figure 5.3: Coverage radius and achieved total capacity for different MIMO configurations

and the Alamouti code extract the full diversity order of 4 and induces lower outage than the SISO mode without diversity and the MRC-R with diversity order of 2. The outage performance of MRC-R is significantly enhanced when combining this mode with an antenna selection. In this case, the fading mark distributed as the maximum of a two chi-squared distribution is much more stronger than a maximum of four exponentials or a chi-squared mark distribution. When nodes operate with multiplexing transmission modes, the full power is distributed among the two useful data streams. Although the spatial multiplexing reduces the target SINR threshold from $\beta_n = -1$ dB to $\tilde{\beta}_n = -4.75$ dB, this does not compensate the high level of interference arising from both stream of each node transmitting in the same sub-medium and the low signal level transmitted with half power. In the low SINR regime focalizing the power on the strongest eigen-mode reduces significantly the occurrence of the outage event compared to all the other transmission modes. For the coverage range $r = 1$ km, the required bandwidth to achieve an individual rate of 600 kbps with a reliability of 97.5% is respectively 18 MHz for the MRC, 20 MHz for the antenna selection and the Alamouti code and 30 MHz for the MRC-R.

In Figure 5.2, we evaluate the coverage radius, corresponding to different aggregated OFDMA bandwidths. This coverage radius guarantees that the 4 RBs per sub-medium are sufficient to offer a data rate of 600 kbps for 97.5 % of the nodes transmitting in this sub-medium. For 10 MHz of bandwidth, the coverage radius with diversity modes is $0.4 \leq r \leq 0.6$ km and is approximatively 0.2 km for SISO and multiplexing transmission modes. In Figure 5.2a, we evaluate the total capacity achieved in the network. We can observe that as long as the coverage radius increases, the total capacity decreases. The

spectral efficiency for a given coverage radius can be then deduced using the two plots of Figure 5.2b. For a coverage radius of 0.4 km, the respective required bandwidth are respectively 6.4 MHz for MRC, 8 MHz for transmission modes with diversity order of four, 10 MHz for transmission modes with diversity order of two, 23 MHz for the SIC decoder, 25 MHz for the SISO. For the range of 0.4 km, the achieved capacity is nearly 16.9 Mbps for diversity transmission modes and 16.8 Mbps for the SISO and SIC. The achieved spectral efficiency is therefore 2.64 b/s/Hz for MRC and 2.11 b/s/Hz for MRC-RS, Alamouti and the selection, 1.69 b/s/Hz for the MRC-R and 0.73 b/s/Hz for the SIC and 0.672 b/s/Hz for the SISO case. Note that the use of bandwidth above 18 MHz is over-dimensioned as $\exp(-\lambda\pi R^2) = 46.5\%$ of the sub-mediums are left empty.

Figure 5.3 compares the coverage radius and the capacity achieved by different antennas configurations: SISO, 2×1 MISO, 2×2 MIMO and 4×2 MIMO system with optimal transmission modes extracting the full MIMO diversity. We can notice from Figure 5.3a, that the coverage radius is significantly enhanced when adding more antennas at the transmitter side. For a coverage radius of 0.4 km, the required bandwidth by the 4×2 MIMO configuration is 5 MHz instead of 6.4 MHz required by the 2×2 MIMO configuration, 15 MHz required by the MISO and 25 MHz required by the SISO. The respective achieved total spectral efficiency for this coverage range is then deduced from Figure 5.3b and is 3.4 b/s/Hz for the 4×2 MIMO configuration, 2.64 b/s/Hz for the 2×2 MIMO, 1.12 b/s/Hz for the 2×1 MISO and 0.67 b/s/Hz for the SISO.

6.2 INR receiver model

As in the bipolar case, we compare in Figure 5.4, the analytical results in Figures 5.4a and 5.4b in Figures 5.4c and 5.4d with the analytical ones considering the different transmission modes of the 2×2 MIMO and without loss of generality a PPP for the receivers with the same intensity 0.36 Rx/km^2 as the transmitters. The same observations concerning the different transmission modes as the bipolar model holds also for the INR receiver model. Compared to the bipolar model, the individual outage is averaged over all distance weighted by the PDF of the nearest distance between the transmitter and the receiver distance. We note that, for the considered receiver PPP intensity, 70% of the distances are less than $r = 1$ km and the others 30% distances are between 1 km and 2 km. The analytical curves are slightly lower than the bipolar case with a coverage range of $r = 1$ km.

In Figure 5.5a, we evaluate the intensity of the PPP receiver as a function of the available OFDMA bandwidth. We can see when using narrow-bands, the receiver process should be very dense to ensure the presence of receiver in a small coverage range around the transmitter. However, when using wide-bands, this constraint is relaxed and the intensity of the receiver PPP is reduced. For example when pre-allocating a bandwidth of 10 MHz, the PPP receiver intensity should be $\lambda_0 = 2.5$ Rx/km^2 for MRC-R, $\lambda_0 = 1.6$ Rx/km^2 for the selection and for the Alamouti, $\lambda_0 = 1.2$ Rx/km^2 for the MRC-RS and $\lambda_0 = 1$ Rx/km^2 for MRC. Once again, using both plots of Figures 5.5a and 5.5b, one can deduce for a given receiver intensity the corresponding spectral efficiency. For an intensity of $\lambda_0 = 1.5$ Rx/km^2,

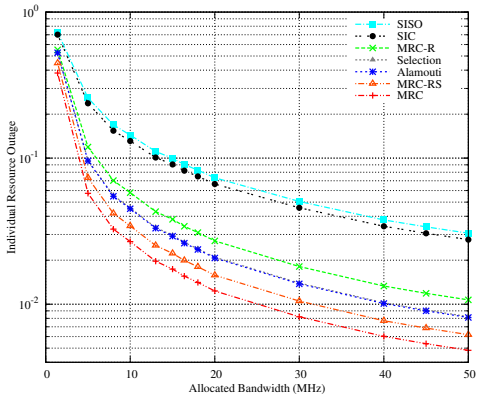

(a) Analytical Individual Outage

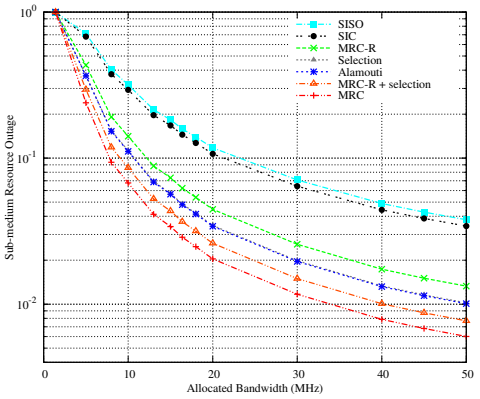

(b) Analytical Sub-Medium Outage

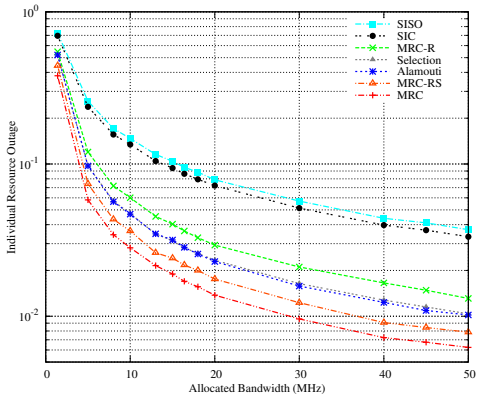

(c) Numerical Individual Outage

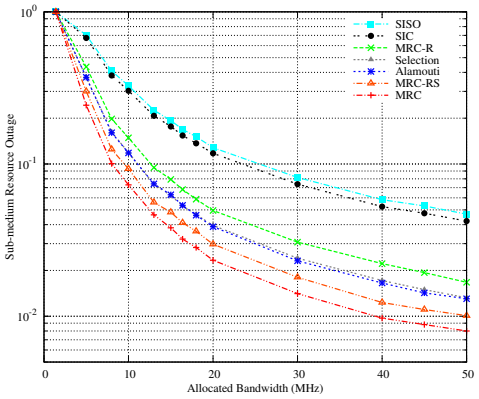

(d) Numerical Sub-Medium Outage

Figure 5.4: Independent Nearest Receiver model: Analytical Individual and Sub-medium resource outage probabilities for a 2×2 MIMO scheme with different transmission

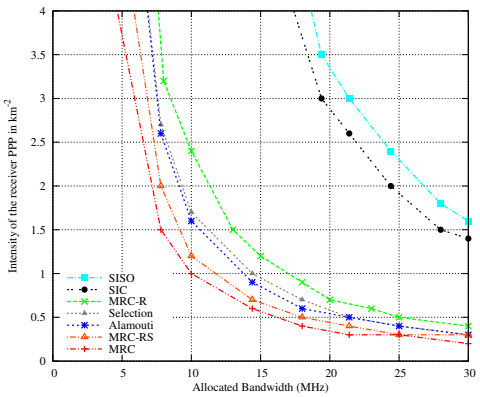

(a) Receiver PPP intensity

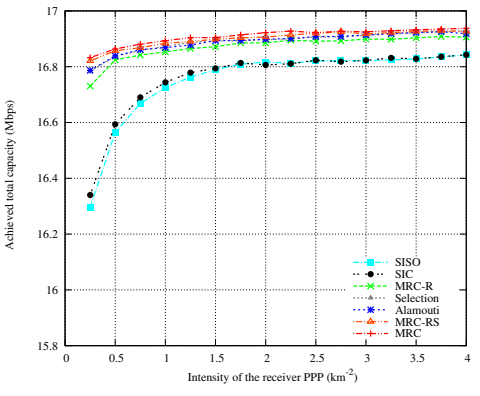

(b) Achieved total capacity

Figure 5.5: Receiver PPP intensity and achieved total capacity with INR model

the required bandwidth for MRC is for example $B = 8$ MHz and the total capacity is nearly 16.9 Mbps. The maximal achieved spectral efficiency is therefore 2.11 b/s/Hz.

7 Conclusion

This chapter focused on the radio resource dimensioning in a distributed OFDMA ad hoc network with an Aloha MAC protocol, we studied the impact of deploying advanced MIMO transceivers on the radio resource dimensioning. Two receiver models were envisaged, the bipolar and the independent nearest receiver model. We derived the individual and sub-medium outage and coverage probabilities for the two models under several MIMO antenna configurations. The coverage radii and the achieved total capacities were also studied. The radio dimensioning parameters include the required network bandwidth, the coverage radius in bipolar model, the density of the receivers in INR model and the achieved spectral efficiency. The results are based on the minimization of the sub-medium outage event that occurs when the number of RBs within a sub-medium is not sufficient to serve all nodes that randomly select this sub-medium. Analytical and numerical results showed the efficiency of the full diversity transmission modes in the optimization of the coverage radius-bandwidth tradeoff in the bipolar model and the receiver intensity-bandwidth tradeoff in INR model.

Appendix

5.A Proof of Lemma 5.1

The CDF of the maximal number of RBs in a non-empty sub-medium can be written as,

$$F^{(\mathrm{BP})}_{N^*_{\mathrm{RB}}}(r, n, N^*_m) = \mathrm{Prob}\{N^*_{\mathrm{RB}}(r, \tilde{\Phi}_k) \leq n \Big| \, |\Phi_k| > 0\} \tag{5.41}$$

Or equivalently,

$$F^{(\mathrm{BP})}_{N^*_{\mathrm{RB}}}(r, n, N^*_m) = \frac{\mathrm{Prob}\left\{(N^*_{\mathrm{RB}}(r, \tilde{\Phi}_k) \leq n) \cap (|\Phi_k| > 0)\right\}}{\mathrm{Prob}\{|\Phi_k| > 0\}}.$$

By averaging over all the possible non-empty pattern of Φ_k:

$$\begin{aligned}\mathrm{Prob}\left\{(N^*_{\mathrm{RB}}(r, \tilde{\Phi}_k) \leq n) \cap (|\Phi_k| > 0)\right\} &= \sum_{\ell=1}^{\infty} \left[F^{(\mathrm{BP})}_{N_{\mathrm{RB}}}(r, n, N^*_m)\right]^{\ell} \mathrm{Prob}\{|\Phi_k| = \ell\} \\ &= \sum_{\ell=0}^{\infty} \left[F^{(\mathrm{BP})}_{N_{\mathrm{RB}}}(r, n, N^*_m)\right]^{\ell} \mathrm{Prob}\{|\Phi_k| = \ell\} - \mathrm{Prob}\{|\Phi_k| = 0\}\end{aligned}$$

Knowing that Φ_k is a thinning of the PPP with intensity λp such that

$$\mathrm{Prob}\{|\Phi_k| = \ell\} = \frac{1}{\ell!} (\lambda p |\mathcal{R}|)^{\ell} \, e^{-\lambda p |\mathcal{R}|}$$

gives,

$$\sum_{\ell=0}^{\infty} \left[F^{(\mathrm{BP})}_{N_{\mathrm{RB}}}(r, n, N^*_m)\right]^{\ell} \mathrm{Prob}\{|\Phi_k| = \ell\} = \exp\left(- \lambda p |\mathcal{R}| \left(1 - F^{(\mathrm{BP})}_{N_{\mathrm{RB}}}(r, n, N^*_m)\right)\right)$$

and

$$\mathrm{Prob}\{|\Phi_k| > 0\} = 1 - \mathrm{Prob}\{|\Phi_k| = 0\}.$$

with $\mathrm{Prob}\{|\Phi_k| = 0\} = \exp(-\lambda p |\mathcal{R}|)$. The CDF of the maximum value in (5.11) in the non-empty sub-medium is deduced consequently.

5.B Proof of Lemma 5.2

The expansion of $\Xi_i(s) = \mathbb{E}\left[s^i(W+I)^i e^{-s(W+I)}\right]$ gives

$$\Xi_i(s) = \frac{1}{i!}\sum_{j=0}^{i} s^i \binom{i}{j} \mathbb{E}\left[W^j I^{i-j} e^{-s(W+I)}\right]. \tag{5.42}$$

Due to the independence of W and I,

$$\Xi_i(s) = \frac{1}{i!}\sum_{j=0}^{i} s^i \binom{i}{j} \mathbb{E}\left[W^j e^{-sW}\right]\mathbb{E}\left[I^{i-j} e^{-sI}\right]. \tag{5.43}$$

To find the expression of $\Xi_i(s)$ in Lemma 5.2, we use the following result:

Lemma 5.4 (Relationship between $\mathbb{E}\{X^k e^{-sX}\}$ and $\mathcal{L}_X(s)$). *For a given random variable X, we have:*

$$\mathbb{E}\left[X^k \exp(-sX)\right] = (-1)^k \frac{\partial^k}{\partial^k s}\left(\mathcal{L}_X(s)\right).$$

The proof of this lemma follows from the definition of the Laplacian:

$$\begin{aligned}\frac{\partial^k}{\partial^k s}\left(\mathcal{L}_X(s)\right) &= \frac{\partial^k}{\partial^k s}\left[\int_{\mathbb{R}} e^{-sx} p_X(x)dx\right] \\ &= (-1)^k\, \mathbb{E}[X^k e^{-sX}]\end{aligned}$$

6 Conclusion

This chapter aims in a first phase to summarize the achieved work and our major contributions detailed in the above dissertation. In a second phase we present an overview on the potential further orientations conceivable following this thesis.

1 Contributions

This thesis focused on the conception of a MANET formed within a hierarchical naval fleet isolated on the high seas. The mobile nodes are equipped with LTE radio devices and the network can be supported by a satellite backhaul via USAT installed on certain nodes referred as hybrid stations. Our global purpose was to provide statistical tools to help a network designer to set up a reliable hybrid Satellite-MANET and to provide the network with an accurate amount of radio resources to ensure a certain QoS within the MANET. To this purpose the average statistical behavior of the network was considered and we investigated the topology design of the network first, then we emphasis on the radio resource dimensioning in both a centralized and a distributed access scheme with Aloha MAC protocol.

To this intent we first tackled the topology design in a maritime hybrid Satellite-MANET, we provided an efficient solution for a network designer to characterise the required equipment characteristics and network parameters such that the antenna configuration, the power at the transmitter, the bandwidth, the routing protocol and the gain induced by the satellite component. We first focused on the network partitioning into clusters through HMC algorithm. We then developed a statistical model to evaluate the required inter-cluster and intra-cluster coverage radii to ensure fully connected clusters and thus full connection in the network. The centralized case where all staff-ships have to be situated at one hop from their respective cluster head and the distributed access scheme where pairwise communications are enabled the intermediate nodes acting as amplify and forward relays, have been envisaged. We introduced an analytical solution to derive the upper-bounds on the coverage radii and an exhaustive algorithm was proposed.

Additionally, end-to-end communications delays were studied, we proposed several path discovery protocol and showed that for the distributed access the protocol optimizing the nodes distribution in the network is the progressive search with π-spread angle as it is the one with the closest performance to the optimal shortest path algorithm one. Finally we introduced a strategy for optimizing the number of hybrid stations and to determine when the satellite backhaul optimizes the end-to-end communications delays. We considered three types of satellite backhauls: LEO, MEO and GEO, and showed that the propagation delays with the two latter are too long and thus terrestrial communications links are sufficient for intra-network communications. With the LEO satellite backhaul, we demonstrated that the end-to-end delays can be efficiently reduced by the deployment of HSs. The end-to-end delays distributions in function of the number of HSs in the network were computed, enabling the network designer to perceive a trade-off between the cost and the contributions of these structures.

Then we emphasis on the radio resource outage probability in a circular cluster of a centralized MANET. We provided an analytical model to enable a network designer to estimate properly the required total bandwidth in the network. To this purpose, we investigated advanced stochastic geometry tools and derived an upper-bound on the probability of the event that arises when the RRM entity has no more radio resources to serve all the active users. We envisaged two antenna configurations the SISO and the 2×2 MIMO extracting diversity and multiplexing gain. By setting up a tolerated threshold on the radio resource outage probability we were enable to estimate the required bandwidth and the average achieved spectral efficiency in a typical cluster. Moreover we considered both cases where all active users target the same/different QoS class. Numerical results showed that our analytical approach provides an accurate estimation of the required bandwidth. The impact of the maritime context was also studied and introduced a fast linear model enabling the tuning of the allocated bandwidth in function of the attenuation/amplification of the path-loss. A comparative study was lead with straightforward computation where the developed linear model appeared to be an efficient tool to foresee this fluctuation impact on the MANET dimensioning.

Finally we focused on the radio resource dimensioning in a distributed OFDMA ad hoc network with an Aloha MAC protocol, we studied the impact of deploying advanced MIMO transceivers on the radio resource dimensioning. We derived the individual and sub-medium outage and coverage probabilities for the two models under several MIMO antenna configurations. The coverage radii and the achieved total capacities were also studied. Two receiver models were envisaged, the bipolar and the independent nearest receiver model. The radio dimensioning parameters include the required network bandwidth, the coverage radius in bipolar model, the density of the receivers in INR model and the achieved spectral efficiency. The results are based on the minimization of the sub-medium outage event that occurs when the number of RBs within a sub-medium is not sufficient to serve all nodes that randomly select this sub-medium. Analytical and numerical results showed the efficiency of the full diversity transmission modes in the optimization of the coverage radius-bandwidth tradeoff in the bipolar model and the receiver intensity-bandwidth tradeoff in INR model.

2 Perspectives

In the following, we suggest the possible directions for future work keeping with our studies:

— Chapter 3 focused on the topology design of the network considering its average statistical behavior. We developed a statistical model based on stochastic geometry and graph theory to evaluate the required coverage radii leading to a fully connected network. Besides, from algebraic topology, simplicial homology is also a useful tool to characterize the topology of a wireless ad hoc network using simplicial complexes. It enables to study the coverage and connectivity matters. When stochastic geometry and graph theory help to identify connected or isolated components in the network, simplicial homology can be applied to detect the coverage holes [80, 81] in a given simulation area. Moreover, once the network topology is characterized, several applications to the optimize the network design can be derived. For instance, authors in [82] provide a tool for the frequency planning and authors in [83, 84] establish energy saving algorithms using this framework. In our case, a future work can be to apply this method to the specific mobile ad hoc networks in order to identify the coverage holes in a more dense network and also to optimize the power consumption and other key parameters.

— In Chapter 5 we tackled the dimensioning matter for a distributed OFDMA network with Aloha MAC protocol. However, several other protocols are available in literature as Carrier Sense Multiple Access "CSMA" which is a probabilistic MAC protocol, in which nodes "sense" the spectrum availability before transmitting. The main challenge of this protocol is to schedule the transmissions in order to prevent nodes which are close to transmit simultaneously. The neighbors of a node are the nodes situated in its contention domain. The contention domain of a node x regroups the nodes which receive a power from x above a certain threshold. Each node in the same domain should transmit only if it senses an idle medium. Moreover, the nodes do not transmit immediately after sensing an idle medium as this behavior does not preclude simultaneous transmission. Indeed, each node keeps a timer, if the medium is occupied it pauses its timer, else the node decreases its timer by one unit per time slot and transmits when the timer expires. The set of nodes which transmit simultaneously in the same medium can also be analytically modeled. Nodes can still be considered as distributed following an homogeneous P.P.P. Φ, however the set of nodes accessing the medium cannot be obtained by an independent thinning of Φ as in the Aloha protocol. Baccelli et al. [9] propose to represent the individuality of transmission by a Matérn hard-core model. This model is useful to derive closed form expressions of the density of nodes accessing the shared medium and the probability that two nodes transmit over the channel at a given time slot.

Bibliography

[1] T. Camp, J. Boleng, and V. Davies, "A survey of mobility models for ad hoc network research," *Wireless Communications and Mobile Computing*, vol. 2, no. 5, pp. 483–502, 2002.

[2] I. Communications, "https://www.iridium.com,"

[3] ITU-R, "Method for point-to-area predictions for terrestrial services in the frequency range 30 mhz to 3 000 mhz," 2014.

[4] 3GPP, "Ts 36.213 evolved universal terrestrial radio access (e-utra)," 2013.

[5] L. Ippolito, *Satellite Communications Systems Engineering: Atmospheric Effects, Satellite Link Design and System Performance*. Wireless Communications and Mobile Computing, Wiley, 2008.

[6] D. Tse and P. Viswanath, *Fundamentals of Wireless Communication*. New York, NY, USA: Cambridge University Press, 2005.

[7] L. J. Ippolito, *Satellite Communications Systems Engineering: Atmospheric Effects, Satellite Link Design and System Performance (Wireless Communications and Mobile Computing)*. Wiley Publishing, 2008.

[8] F. Baccelli and B. Błaszczyszyn, "Stochastic geometry and wireless networks: Volume i theory," *Foundations and Trends® in Networking*, vol. 3, no. 3–4, pp. 249–449, 2008.

[9] F. Baccelli and B. Błaszczyszyn, "Stochastic geometry and wireless networks: Volume ii applications," *Foundations and Trends® in Networking*, vol. 4, no. 1–2, pp. 1–312, 2009.

[10] L. Decreusefond, E. Ferraz, P. Martins, and T.-T. Vu, "Robust methods for LTE and WiMAX dimensioning,"

[11] M. Haenggi, "On distances in uniformly random networks," *IEEE Transactions on Information Theory*, vol. 51, pp. 3584–3586, Oct 2005.

[12] M. Haenggi and R. K. Ganti, "Interference in large wireless networks," *Found. Trends Netw.*, vol. 3, pp. 127–248, Feb. 2009.

[13] I. S. F. Ingelrest, D. Simplot-Ryl, "Optimal transmission radius for energy efficient broadcasting protocols in ad-hoc sensor networks," *Parallel and Distributed Systems*, vol. vol. 17, pp. 536–547, jun 2006.

[14] M. P. P. L. Y. Fang, "Cooperative communication aware link scheduling for cognitive vehicular networks," *Selected Areas in Communications*, vol. vol.30, pp. 760–768, may 2012.

[15] A. Amis, R. Prakash, T. Vuong, and D. Huynh, "Max-min d-cluster formation in wireless ad hoc networks," in *INFOCOM 2000. Nineteenth Annual Joint Conference of the IEEE Computer and Communications Societies. Proceedings. IEEE*, vol. 1, pp. 32–41 vol.1, 2000.

[16] M. Marina and S. Das, "On-demand multipath distance vector routing in ad hoc networks," pp. 14–23, Nov 2001.

[17] M. Marina and S. Das, "On-demand multipath distance vector routing in ad hoc networks," pp. 14–23, Nov 2001.

[18] P. U. 7561024, "Ad hoc network routing protocol including the use of forward and reverse multi-point relay spanning trees,"

[19] L. Mroueh, A. Kessab, P. Martins, S. Hethuin, and I. Bucaille, "Topology design of fully connected hierarchical mobile ad hoc networks," in *International Symposium on Wireless Communication Systems*, 2016.

[20] A. Kessab, L. Mroueh, P. Martins, and I. Bucaille, "Optimizing end-to-end propagation delays in hybrid satellite-maritime mobile ad hoc networks," in *submitted to the Software Telecommunications and Computer Networks*, 2016.

[21] D. Arthur and S. Vassilvitskii, "K-means++: The advantages of careful seeding," in *Proceedings of the Eighteenth Annual ACM-SIAM Symposium on Discrete Algorithms*, SODA '07, (Philadelphia, PA, USA), pp. 1027–1035, Society for Industrial and Applied Mathematics, 2007.

[22] S. Leng, Y. Zhang, H.-H. Chen, L. Zhang, and K. Liu, "A novel k-hop compound metric based clustering scheme for ad hoc wireless networks," *Wireless Communications, IEEE Transactions on*, vol. 8, pp. 367–375, Jan 2009.

[23] M. Haenggi, "On distances in uniformly random networks," *IEEE Transactions on Information Theory*, vol. 51, pp. 3584–3586, Oct 2005.

[24] B. Liu, S.-H. Choo, S.-L. Lok, S.-M. Leong, S.-C. Lee, F.-P. Poon, and H.-H. Tan, "Finding the shortest route using cases, knowledge, and djikstra's algorithm," *IEEE Expert*, vol. 9, pp. 7–11, Oct 1994.

[25] L. Mroueh, A. Kessab, P. Martins, S. Hethuin, and E. Vivier, "Radio resource dimensioning in a centralized ad-hoc maritime mimo lte network," in *Sarnoff Symposium, 2015 36th IEEE*, pp. 128–133, Sept 2015.

[26] A. Kessab, L. Mroueh, P. Martins, and S. Hethuin, "Impact of the itu-r maritime propagation on the dimensioning of a centralized lte manet," in *IEEE Wireless Communications and Networking Conference 2016*, 2016.

[27] P. Mohapatra and S. Krishnamurthy, *AD HOC NETWORKS: Technologies and Protocols*. Springer Publishing Company, Incorporated, 1st ed., 2010.

[28] F. E. Decreusefond L. and M. P., "Upper Bound of Loss probability for the dimensioning of OFDMA systems with multi class randomly located users," 2009.

[29] B. A. C. Roberto Carlos Hincapie and L. Ospina, "Survey on clustering techniques for mobile ad hoc networks," 2006.

[30] P. E. 1559280, "Method and device for establishing communication links with parallel scheduling operations in a communication system,"

[31] P. E. 1942614, "Data-path dynamic link maintenance in mobile ad hoc networks,"

[32] P. E. 1499989, "Reactive routing on demand in mobile network,"

[33] P. E. 1500287, "Wireless ad-hoc network and method for performing reactive routing therein,"

[34] P. E. 1473889, "Predictive routing in a mobile ad hoc network,"

[35] TEKEVER, "https://sites.google.com/a/tekever.com/monet/," 2010.

[36] I. B. G. Iapichino C. Bonnet O. del Rio Herrero C. Baudoin, "A mobile ad-hoc satellite and wireless mesh networking approach for public safety communications," *Signal Processing for Space Communications*, oct 2008.

[37] Y. B. W. D. Z. M. C. S. Y. Zhou, "Emergency communication system by heterogeneous wireless networking," *Wireless Communications, Networking and Information Security (WCNIS)*, pp. 488–492, jun 2010.

[38] X. Lagrange, P. Godlewski, and S. Tabbane, *Réseaux GSM : des principes à la norme*. Paris: Hermès Science, 5ème édition ed., 2000.

[39] 3GPP, "Universal mobile telecommunications system (umts);ue radio access capabilities(3gpp ts 25.306 version 8.12.0 release 8)," 2011.

[40] J. Proakis, *Digital Communications*. McGraw-Hill series in electrical and computer engineering : communications and signal processing, McGraw-Hill, 2001.

[41] H. G. Myung and D. J. Goodman, *Single Carrier FDMA: A New Air Interface for Long Term Evolution*. Wiley Publishing, 2008.

[42] "4g lte/lte-advanced for mobile broadband," pp. i – iii, Oxford: Academic Press, 2011.

[43] A. Lo and I. Niemegeers, "Multi-hop relay architectures for 3gpp lte-advanced," in *Communications (MICC), 2009 IEEE 9th Malaysia International Conference on*, pp. 123–127, Dec 2009.

[44] ITU-R, "M.1636 : Basic reference models and performance parameters of internet protocol packet network transmission in the mobile-satellite service," 2010.

[45] M. Hatay, "Empirical formula for propagation loss in land mobile radio services," *Vehicular Technology, IEEE Transactions on*, vol. 29, pp. 317–325, Aug 1980.

[46] K. Yang, T. Ekman, T. Roste, and F. Bekkadal, "A quasi-deterministic path loss propagation model for the open sea environment," in *Wireless Personal Multimedia Communications (WPMC), 2011 14th International Symposium on*, pp. 1–5, Oct 2011.

[47] K. Yang, A. Molisch, T. Ekman, and T. Roste, "A deterministic round earth loss model for open-sea radio propagation," pp. 1–5, June 2013.

[48] S. O. Rice, "Statistical properties of a sine wave plus random noise," *The Bell System Technical Journal*, vol. 27, pp. 109–157, Jan 1948.

[49] G. Watson, *A Treatise on the Theory of Bessel Functions*. Cambridge Mathematical Library, Cambridge University Press, 1995.

[50] A. Doukas and G. Kalivas, "Rician k factor estimation for wireless communication systems," in *Wireless and Mobile Communications, 2006. ICWMC '06. International Conference on*, pp. 69–69, July 2006.

[51] B. Sklar, "Rayleigh fading channels in mobile digital communication systems .i. characterization," *IEEE Communications Magazine*, vol. 35, pp. 90–100, Jul 1997.

[52] B. Clerckx and C. Oestges, *MIMO Wireless Networks: Channels, Techniques and Standards for Multi-Antenna, Multi-User and Multi-Cell Systems*. Academic Press, 2nd ed., 2013.

[53] A. Gorokhov, D. Gore, and A. Paulraj, "Receive antenna selection for mimo flat-fading channels: theory and algorithms," *IEEE Transactions on Information Theory*, vol. 49, pp. 2687–2696, Oct 2003.

[54] D. A. Gore, R. U. Nabar, and A. Paulraj, "Selecting an optimal set of transmit antennas for a low rank matrix channel," in *Acoustics, Speech, and Signal Processing, 2000. ICASSP '00. Proceedings. 2000 IEEE International Conference on*, vol. 5, pp. 2785–2788 vol.5, 2000.

[55] A. Gorokhov, D. Gore, and A. Paulraj, "Performance bounds for antenna selection in mimo systems," in *Communications, 2003. ICC '03. IEEE International Conference on*, vol. 5, pp. 3021–3025 vol.5, May 2003.

[56] A. Gorokhov, D. Gore, and A. Paulraj, "Receive antenna selection for mimo flat-fading channels: theory and algorithms," *IEEE Transactions on Information Theory*, vol. 49, pp. 2687–2696, Oct 2003.

[57] R. S. Blum and J. H. Winters, "On optimum mimo with antenna selection," in *Communications, 2002. ICC 2002. IEEE International Conference on*, vol. 1, pp. 386–390, 2002.

[58] D. G. Brennan, "Linear diversity combining techniques," *Proceedings of the IEEE*, vol. 91, pp. 331–356, Feb 2003.

[59] T. Eng, N. Kong, and L. B. Milstein, "Comparison of diversity combining techniques for rayleigh-fading channels," *IEEE Transactions on Communications*, vol. 44, pp. 1117–1129, Sep 1996.

[60] M. Kang and M. S. Alouini, "Largest eigenvalue of complex wishart matrices and performance analysis of mimo mrc systems," *IEEE Journal on Selected Areas in Communications*, vol. 21, pp. 418–426, Apr 2003.

[61] S. Thoen, L. V. der Perre, B. Gyselinckx, and M. Engels, "Performance analysis of combined transmit-sc/receive-mrc," *IEEE Transactions on Communications*, vol. 49, pp. 5–8, Jan 2001.

[62] G. J. Foschini, "Layered space-time architecture for wireless communication in a fading environment when using multi-element antennas," *Bell Labs Technical Journal*, vol. 1, pp. 41–59, Autumn 1996.

[63] Z. Bai, J. Berkmann, C. Spiegel, T. Scholand, G. Bruck, C. Drewes, B. Gunzelmann, and P. Jung, "On mimo with successive interference cancellation applied to utra lte," pp. 1009–1013, March 2008.

[64] S. P. Weber, J. G. Andrews, X. Yang, and G. de Veciana, "Transmission capacity of wireless ad hoc networks with successive interference cancellation," *IEEE Transactions on Information Theory*, vol. 53, pp. 2799–2814, Aug 2007.

[65] B. Blaszczyszyn and P. Muhlethaler, "Stochastic analysis of non-slotted aloha in wireless ad-hoc networks," in *INFOCOM, 2010 Proceedings IEEE*, pp. 1–9, March 2010.

[66] H. L. Lebesgue, "Intégrale, longueur, aire.," 1902.

[67] A. Papoulis and S. Pillai, *Probability, random variables, and stochastic processes*. McGraw-Hill electrical and electronic engineering series, McGraw-Hill, 2002.

[68] G. Bennett, "Probability inequalities for the sum of independent random variables," *Journal of the American Statistical Association*, vol. 57, no. 297, pp. 33–45, 1962.

[69] U. von Luxburg, "A tutorial on spectral clustering," *CoRR*, vol. abs/0711.0189, 2007.

[70] K. Wu, Prof., "Handbook of engineering electromagnetics, edited by rajeev bansal, marcel dekker, inc. 2004, 720 pages, $116.96, isbn: 0-8247-5628-2: Book review," *Int. J. RF Microw. Comput.-Aided Eng.*, vol. 16, pp. 635–636, Nov. 2006.

[71] A. S., "A simple transmit diversity technique for wireless communications," *IEEE Journal*, vol. vol.16, pp. 1451,1458, oct 1998.

[72] G. Bennett, "Probability inequalities for the sum of independent random variables," *Journal of the American Statistical Association*, vol. 57, no. 297, pp. 33–45, 1962.

[73] N. Abramson, "The aloha system: Another alternative for computer communications," in *Proceedings of the November 17-19, 1970, Fall Joint Computer Conference*, AFIPS '70 (Fall), (New York, NY, USA), pp. 281–285, ACM, 1970.

[74] L. G. Roberts, "Aloha packet system with and without slots and capture," *SIGCOMM Comput. Commun. Rev.*, vol. 5, pp. 28–42, Apr. 1975.

[75] F. Z. Kaddour, P. Martins, L. Decreusefond, E. Vivier, and L. Mroueh, "Outage probability upper bound for multi-class qos in the uplink of lte networks," 2013.

[76] R. Giacomelli, R. K. Ganti, and M. Haenggi, "Outage probability of general ad hoc networks in the high-reliability regime," *IEEE/ACM Transactions on Networking*, vol. 19, pp. 1151–1163, Aug 2011.

[77] M. Haenggi, "Outage, local throughput, and capacity of random wireless networks," *IEEE Transactions on Wireless Communications*, vol. 8, pp. 4350–4359, August 2009.

[78] S. Weber, J. G. Andrews, and N. Jindal, "An overview of the transmission capacity of wireless networks," *IEEE Transactions on Communications*, vol. 58, pp. 3593–3604, December 2010.

[79] S. P. Weber, X. Yang, J. G. Andrews, and G. de Veciana, "Transmission capacity of wireless ad hoc networks with outage constraints," *IEEE Transactions on Information Theory*, vol. 51, pp. 4091–4102, Dec 2005.

[80] F. Yan, A. Vergne, P. Martins, and L. Decreusefond, "Homology-based distributed coverage hole detection in wireless sensor networks," *IEEE/ACM Transactions on Networking*, vol. 23, pp. 1705–1718, Dec 2015.

[81] A. Vergne, L. Decreusefond, and P. Martins, "Reduction algorithm for simplicial complexes," in *INFOCOM, 2013 Proceedings IEEE*, pp. 475–479, April 2013.

[82] A. Vergne, L. Decreusefond, and P. Martins, "Simplicial homology for future cellular networks," *IEEE Transactions on Mobile Computing*, vol. 14, pp. 1712–1725, Aug 2015.

[83] N. K. Le, P. Martins, L. Decreusefond, and A. Vergne, "Construction of the generalized czech complex," in *2015 IEEE 81st Vehicular Technology Conference (VTC Spring)*, pp. 1–5, May 2015.

[84] N. K. Le, P. Martins, L. Decreusefond, and A. Vergne, "Simplicial homology based energy saving algorithms for wireless networks," in *2015 IEEE International Conference on Communication Workshop (ICCW)*, pp. 166–172, June 2015.